Asia Pacific Workshop On Time & Frequency (ATF2006)

Proceedings

New Delhi, India
11-13, December 2006

Organized by
National Physical Laboratory, India

Cosponsored by
NICT, Japan

Convenor of ATF 2006

P.Banerjee, NPLI, India

Scientific Organizing Committee (SOC) for ATF2006

Takao Morikawa, NICT, Japan Chairman,
M. Imae, NMIJ/AIST, Japan
H.S. Lee, KRISS, Korea,
Gao Xiao Xun, NIM, China
M. Hosokawa, NICT, Japan
P. Banerjee, NPLI, India
R. Bruce Warrington, NMI, Australia
Chia-shu Liao, TL, Taiwan

Author Index

A Digital Time Data Service Via Telephone Line With Some Unique Features Initiated By NPLI

P.Banerjee and A.K.Suri

National Physical Laboratory, New Delhi, India

Abstract

Time service via telephone line, in the name of Teleclock Service, with some unique features, has been started by NPLI. This paper describes this time service elaborating its special advantages.

Introduction

Various techniques to disseminate local time of a country the users, differ essentially by the accuracy, coverage area, and the maintenance cost of the service and by the ease and the cost of accessibility of the service to the users. For users who demand the time with a low accuracy (say of order of few seconds), the service via telephone line is very useful. This type of service has already been initiated in many developed countries. For example, USNO in USA gives voice announcement of time via telephone and one may also get time announcement by dialing 174 in Delhi. The automated Computer Time Service (ACTS) [1] NIST, USA and NPL TRUETIME by NPL, UK [2] are the time services via telephone line to synchronize the computer clocks to correct time. These services are accessible by a computer only.

National Physical Laboratory, India (NPLI) has developed and initiated an innovative system for transmission of digital time data via telephone line as Teleclock service. This unique time service may not only be accessed by a computer but also by a very inexpensive system called TELECLOCK Receiver, developed by NPLI. This paper describes the functional detail of the system and elaborates its special advantages.

Description of the Scheme

NPL has already started transmission of digital data of current time of Indian Standard Time (IST) through Telephone line. The Teleclock data format generator (TDFG) is directly fed by the second pulse from the cesium clock, through which IST is maintained. TDFG generates the digital data of hour, minute and second corresponding to the current values of IST.

These data are continuously transmitted through RS232 protocol at 1200-baud rate in a well-planned sequence continuously (Fig.1). The transmitted data is linked to a Standard Telephone Modem through RS232 port. The output of the modem is connected to one telephone line, which is dedicated for this service. MODEM operates in V.22 mode. The baud rate is chosen to be 1200 as the optimum so that it is not too slow but also not too

fast to become less immune to noise. Five sets of data are sent every second so that at the receiving end there is enough provision to confirm the correctness of the data.

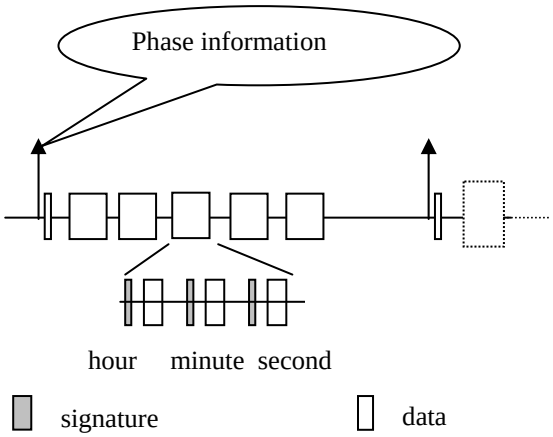

Fig.1. Data Format of Teleclock Service

The data sets also carry phase information of the second pulse through a special character so that the synchronization of second pulse of the receiver's clock may be achieved, if desired. This special character may also to be used to take into account of the propagation delay. In a special experiment, the jitter in the round trip propagation delay has been found to be around 2ms by the use of this special character.

The data corresponding to the each set of hour, minute and second is preceded by a particular "signature-character" respectively so that the corresponding data is confidently identified. The signature-character and sequence are so chosen that the possibility of false identification of signature-character becomes remote.

To access this time service it is not essential or necessary that one needs a computer. NPL has developed a Teleclock receiver for this purpose [3]. This receiver should remain connected to any direct telephone line. It may be noted that it does not disturb the normal usage of the telephone line. Teleclock receiver has an in-built clock run by a crystal oscillator. The receiver has the provision of dialing the telephone number of the line dedicated for this service manually by pressing a switch or automatically at a pre-programmed time. The frequency of automatic dialing is normally once in a day but may be increased or decreased on the user's demand. Through dialing, the receiver receives the data corresponding to the IST, sets its own time accordingly and disconnects itself from the telephone line. The frequency of the crystal oscillator is so accurate that by dialing once in a day, the receiver may maintain the time within few seconds of IST always.

Extension of the Range of Teleclock Service through Local Exchange

Many institutional complexes have number of clocks scattered over a large area of the respective complex. It is desirable that all these clocks show the same time. They should be linked to some standard time (say IST in India) within an accuracy of few seconds. It is not essential that all these clocks should be linked directly to the Teleclock service. A very convenient solution for linking these clocks to IST utilizing the Teleclock services has been introduced as shown in Fig.2. This scheme requires the availability of local telephone network through the Private Automatic Exchange (like PAX/EPABX) in the complex. In this proposal there is requirement of one specially designed Teleclock receiver which may be directly linked to the Teleclock Service of NPL through the MODEM marked I. Modem I can only dials the number of the telephone line to connect to NPL directly. In this Teleclock Receiver there is another MODEM marked II. The Modem II is connected to the one special line of local telephone network. The time data output from the Teleclock receiver is transmitted out through Modem II to the local network.

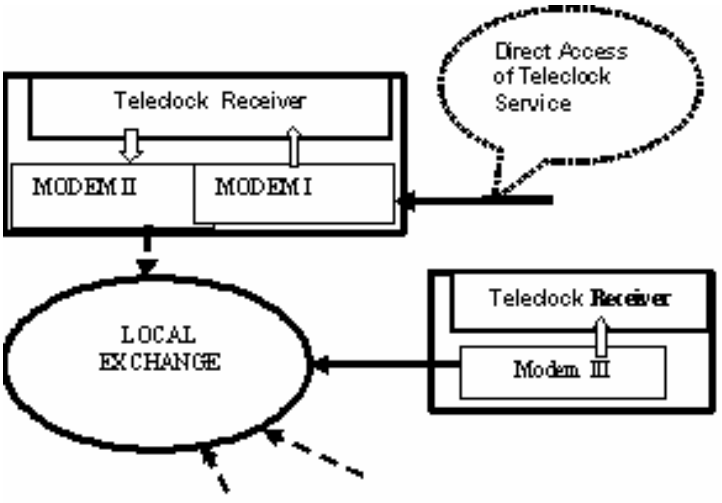

Fig.2. Extension of Teleclock Service via Local Telephone Exchange

To have access of the time through the local telephone one needs one normal Teleclock receiver with a simple difference that it dials the special number of the local network through the modem III instead of the number of the Teleclock service directly from NPL. Thus all clocks of the complex may be synchronized with respect to the master clock in the complex which has direct access of the IST maintained by NPL. There is no need of additional cable laying over the entire complex to link the slave clocks to its master clock as it is done in the conventional master slave clock system.

This type of arrangement for synchronizing clocks scattered over a large area has already been implemented in NPL premises and are to be soon set up in many other institutions and complexes.

Concluding Remarks

The Teleclock time service may not only be accessed by a computer but also by a very inexpensive system called TELECLOCK Receiver, developed by NPL. This very unique and novel feature makes this technology special and different from what have been started by the developed countries elsewhere. Further, transmission system to initiate this similar time service via telephone line in any country requires very small amount of investment. These are very encouraging issues for developing and under developed countries to initiate similar time service in the respective countries. Encouraged by these features, SASO of Saudi Arabia and NBSM of Nepal have already started the similar services with help of NPLI–developed equipment.

In this service, propagation delay may also be corrected with a jitter of 2ms leading to a better time accuracy.

Through this technique, one may have the master-slave system without the need of the laying of cables. This very attractive feature is an important advantage particularly when a complex is spread over few kilometers.

References

[1] "Set Your Computer's Clock via the Telephone: NIST Automated Computer Time Service (ACTS)", *Website: http://tf.nist.gov/service/acts.htm*

[2] J. Laverty, "NPL TRUETIME: setting your PC to the UK national Time scale", *Circular, 9August 1996, NPL, U.K.*

[3] P.Banerjee, "A device useful as master/slave clock for transmitting standard time over telephone network and a telephone network incorporating the device for transmitting and receiving standard time", *Patent in India 2472/DEL/95 dt. 29.12.95, Patent in USA No. 6,091,804 dt. July 18, 2000 and Patent in Europe (Germany, France, U.K., Italy and Sweden) No. EP 851324 dt. July 01, 1998.*

Absolute Frequency Measurement of a Cesium D2 Transition Line by Using Multi-mode Injection Locking Technique

[1,2]Eok Bong Kim*, [1]Sang Eon Park, [1]Won-Kyu Lee, [1]Dae-Su Yee, [1]Chang Yong Park, [1]Taeg Yong Kwon, and [1]Ho Seong Lee

[1]*Korea Research Institute of Standards and Science*
1 Doryong-Dong, Yuseong-gu, Daejeon 305-340, Korea

[2]Hyuck Cho

[2]*Department of Physics, Chungnam National University*
220 Gung-dong, Yuseong-Gu, Daejeon 305-764, Korea

Abstract

We have performed amplification of selected optical frequency comb (OFC) in near infrared area and remote absolute frequency measurement of $F = 4 \rightarrow F' = 5$ transition of cesium D2 line using optical and microwave signal of the amplified OFC. In order to amplify the OFC in near infrared region base on phase stabilized 1 GHz femtosecond mode-locked laser to hydrogen maser, we used anti-reflect coated diode laser at 850 nm with injection seed technique. For remote measurement, we have transferred the amplified OFC to remote site through the polarization maintain fiber. The measured averaging frequency of $F = 4 \rightarrow F' = 5$ transition of cesium D2 line was 351 721 960 525.51 kHz, which only consider a statistical uncertainty.

1. Introduction

Broadband optical frequency combs (OFC) based on femtosecond mode-locked laser (FML) and nonlinear optical fiber with very narrow line widths optical modes and precise absolute frequency values have expanded new horizon in the field of optical frequency metrology, high resolution spectroscopy, and optical communication, an so on,(Udem et al. 1999, Gerginov et al. 2004, Holzwarth et al. 2000, Jiang et al. 2005). And recently an experiment on distributing optical comb to remote site was performed by other group which has importance in that optical comb can transfer microwave and optical signal at the same time (Holman et al. 2004). Compared to conventional GPS using time transfer method optical fiber can provide more isolated environment for optical signal transfer so that it will make us construct better clock network especially in short term stability in local area. However, typical average power of the OFC components directly out of the oscillator ranges in hundreds of nW, which is insufficient power for such as long distance transfer through the optical fiber in near infrared, visible area and saturated absorption spectroscopy requiring high power and power stability. To solve optical power problem, the OFC should be amplified by tapered semiconductor amplifiers (TSA) (Cruz et al. 2006) or anti-reflect (AR) coated diode laser (Fortier et al. 2006) or distribute-Bragg-reflector (DBR) diode laser with injection locking technique (Park et al. 2006) or a single-mode continuous-wave (cw) laser by using the well-established phase-locking technique (Udem

*ubkim@kriss.re.kr

et al. 1999). For simultaneously using of optical and RF reference signal, TSA is best way because that provide large gains ($\geq$ 20 dB) but expensive and hard to use. On the other hand, AR coated diode laser is cost-effective and easy to handle.

In this experiment, we demonstrated the optical absolute frequency measurement of a laser in remote site as an practical use of optical and microwave signal transfer in the form of the OFC which is locked to hydrogen maser which was being compared with UTC. In this kinds of experiment sending cw laser from a remote site to optical comb system is more typical. However the configuration shown in this experiment can be useful in the case that cw laser power have not enough or there is a need for RF reference signal in remote site. We have performed selective amplification of the OFC in near infrared region by using AR coated diode laser at 850 nm with injection seed and transfer the amplified OFC to remote site through the polarization maintained optical fiber.

2. Experimental setup

In order to amplify the OFC in near infrared and remote frequency measurement, we composed experiment setup with phase stabilized the FML system to hydrogen maser, AR coated diode laser at 850 nm, frequency stabilized external cavity diode laser (ECDL) to cesium D2 transition line and RF divided system as shown Fig 1. The FML is operated with center frequency of about 850 nm with 50 nm spectral width and 1 GHz repetition rate (f_{rep}). The repetition rate of the FML is stabilized by controlling the laser cavity length with a piezoelectric transducer (PZT) and the carrier envelope offset frequency (f_{ceo}) of the FML is phase locked to hydrogen maser by controlling the intensity of the pump-laser beam with an acousto-optic modulator (AOM).

The output of the FML is divided into two beams by a pellicle splitter. The transmitted pulse get into PCF to generate an octave broaden comb to be used for offset frequency in f-to-2f interferometer. And the reflected beam is couple into the AR coated diode laser, of which gain band-width is about 810 nm $\sim$ 880 nm and temperature variation is stabilized within 1 mK. Before the reflected comb get into the diode laser it pass through a interference filter with 10 nm 3 dB bandwidth at 850 nm including cesium D2 transition frequency. This filtering enlarge input pulse width prevents AR coated diode laser from damage by high intense pulse. After passing through the interference filter, the total power of the OFC was about 1 mW and the number of transmitted modes was approximately 4000 for the FML having 1 GHz repetition rate. In order to improve the coupling efficiency, we were adjusted beam profile and polarization of incident comb by using two cylinder lens and half-wave plate.

A part of amplified pulse is coupled with optical fiber to transfer of the amplified OFC to remote site at 100 m distance in same building. We used single mode polarization maintain (PM) fiber in order to minimize power fluctuation caused by polarization rotating. 5 mW of OFC is coupled into fiber with 50 % coupling efficiency and output power was about 2 mW at remote site. We had 20 % loss during fiber transfer mainly caused by Rayleigh scattering.

In remote site optical comb output is divided into two paths by a dichroic beam splitter. The pulse rate of reflected beam is picked up by fast photodiode to construct reference frequency of remote site. Signal to noise (S/N) ratio of measured f_{rep} was typically more than 60 dB at a 300 kHz bandwidth. This detected signal of f_{rep} is divided by 16 by using home-made low noise digital divider and converted to 10 MHz radio frequency with commercial direct digital synthesizer (DDS). Transmitted beam from the dichroic beam splitter is overlapped with a external cavity diode laser (ECLD) with beam splitter to measure absolute frequency of the laser. The ECDL was stabilized to $F = 4 \rightarrow F' = 5$ transition of cesium D_2 line with modulation transfer spectroscope technique (MTS). The heterodyne beat (f_{beat}) between the amplified OFC and ECDL is picked up by photo-

diode, filtered and amplified. We measured the final signal by frequency counter which was phase-locked to external 10 MHz reference from the above DDS having traceability to UTC.

3. Results and discussion

Figure 2 shows the spectrum of the amplified OFC in near infrared region, which based on phase stabilized femtosecond mode-locked laser to a hydrogen maser with an instability of about 2×10^{-13} at 1s averaging time. Square symbol represent free running output of diode laser and then output power is about 1 mW. Circle line and triangle line represent spectrum of the amplified OFC by optical injection seed technique and for various center wavelength of the inference filter. When the power of injection seed beam of the OFC is about 1 mW, which correspond to 0.1 μW power per mode, and injection current of AR coated diode laser is about 120 mA, then the power of amplified comb is measured about 10 mW that correspond to about 1.3 μW power per mode and amplification rate is about 10 dB. Amplification of any selected the OFC with AR coated diode laser, in this case, it has more advantage for long term absolute frequency measurement with high S/N ratio compare to amplification method of selected single mode of the OFC because amplified comb is unaffected by various locking range caused by various current and temperature etc. Amplification efficiency of the selected OFC could be various by polarization and intensity of injection seed comb components and injection current of diode laser and mode matching condition.

We tested the frequency stabilities of the amplified OFC with the heterodyne beat measurement method. The instability of amplified OFC in original site by sampling time of 1 s was 5.0×10^{-14} and that of transferred OFC through the fiber link is 1.4×10^{-13}. This degradation is caused by group delay variation, vibration and temperature variation etc. Instability of divided signal with home made divide system and 10 MHz signal made by DDS are 2.3×10^{-13}, 8.6×10^{-13} at 1 s averaging time, respectively. Even through we didn't compensate for phase noise introduced by fiber link, microwave signal of the OFC have enough instability to use RF reference signal.

At first with optical and RF signal of unamplified OFC in remote site, we measured the frequency of the ECDL stabilized to $F = 4 \rightarrow F' = 5$ transition of cesium D_2 line. The S/N ratio of the beat frequency (f_{beat}) between the OFC and the ECLD was about 20 dB at 300 kHz resolution bandwidth which is insufficient directly frequency measurement with frequency counter. The same measurement with amplified OFC gave over 15 dB higher S/N ratio than with unamplified OFC. This f_{beat} is measured by frequency counter, which had frequency reference at 10 MHz signal from DDS as is described the above. With the measured f_{beat}, the absolute frequency of the stabilized ECDL can be calculated in the formula of $f_{\mathrm{ECDL}} = n \times f_{\mathrm{rep}} \pm f_{\mathrm{ceo}} \pm f_{\mathrm{beat}}$, where n is a integer chosen properly with the help of the known value of f_{ECDL} (Gerginov et al. 2004, Udem et al. 2000) without any ambiguity. Also we could exactly know the value of f_{rep} and f_{ceo} when optical frequency comb is stabilized to hydrogen maser at original site. Hence if these values are given to the remote site absolute value of laser frequency to be measured can be calculated with the same equation. Figure 3 shows the results of our absolute frequency measurements. The y-axis is the frequency deviation of each frequency measurement from the average frequency (f_{ave}). Each measurement point is an average of more than 200 data and for each data frequency counter averaged for 1 s. The error bars contains statistical uncertainty of $1/\sqrt{N}$, where N is the number of sample points and that has about $\pm$ 0.1 kHz. The total of measured frequencies has a standard deviation of $\pm$ 2.7 kHz, which corresponds to a relative statistical uncertainty of 9.3×10^{-12}. The average frequency is 351 721 960 525.45 kHz. This result have several ten kHz lower than previous reported value (Gerginov et al. 2004, Udem et al. 2000). Considered short term and long term

instability of amplified OFC, transferred OFC, and the offset of hydrogen maser, the total uncertainty of measurement system is about < 100 Hz. From this we could confirm that the average frequency offset and drift of each measurement result was caused by frequency stabilized system of ECDL, for example, Zeeman shift, the pressure shift, the line shape asymmetry, and the ac Stark shift etc.

4. Conclusion

We have amplified optical comb in near infrared region,which was phase stabilized to hydrogen maser, by using AR coated diode laser, and also we performed the remote measurement of absolute frequency of $F = 4 \rightarrow F' = 5$ transition of cesium D_2 transition line with transmitted amplified comb through polarization maintain fiber. Finally we have proved that distribution of optical frequency and microwave frequency to remote site has practicality and believe that simultaneous multi-sites distribution also is possible, where have applications like multi wavelength interference experiment, absolute distance measurement and optical communication base on fiber network etc..

References

Th. Udem., et al., 1999, Phys. Rev. Lett. **82**, 3569.

V. Gerginov, et al., 2004, Phys. Rev. A, **70**, 042505-1.

R. Holzwarth, et al., 2000, Phys. Rev. Lett., **85**, 2264.

J. Jiang, et al., 2005, Opt. Exp., **13**, 1958.

K. W. Holman, et al., 2004, Opt. Lett., **29**, 1554.

F. C. Cruz, et al., 2006, Opt. Lett., **30**, 1337.

T. M. Fortier, et al., 2006, Phys. Rev. Lett., **97**, 163905-1.

S. E. Park, et al., 2006, Opt. Lett., **31**, 3594.

Th. Udem, et al., 1999, Opt. Lett., **24**, 881.

Th. Udem, et al., 2000, Phys. Rev. A, **62**, 031801.

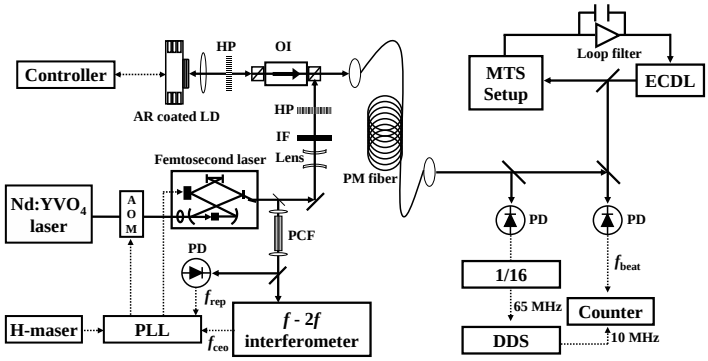

Figure 1. Schematic diagram for amplification of selected optical frequency comb in infrared area and for the absolute frequency measurement of the $F = 4 \rightarrow F' = 5$ transition of cesium D_2 line with amplified optical frequency comb.(PCF: photonic crystal fiber, HP: half-wave plate, OI: optical isolator, IF: interference filter, PD: photo detector).

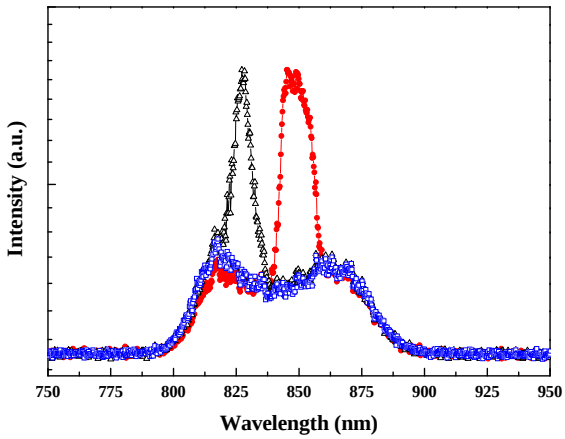

Figure 2. **Spectrum of optical frequency comb amplified by AR coated diode laser. Square symbol represent free running output of diode laser. Circle and triangle represent spectrum of amplified comb for various of center wavelength of used interference filter.**

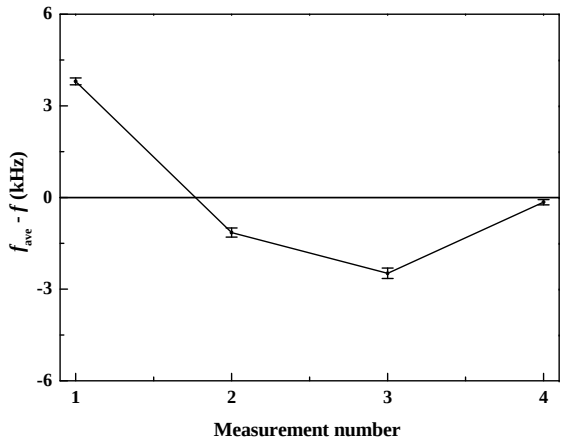

Figure 3. **Result of absolute frequency measurement of the $F = 4 \rightarrow F' = 5$ transition line in cesium vapor cell with transmitted optical frequency comb. Average frequency is $f_{\mathrm{ave}} = 351\ 721\ 960\ 525.45$ kHz.**

CHARACTERISTICS OF COHERENT POPULATION TRAPPING SIGNALS OF Cs-D_1 AND Cs-D_2 LINES

Ken-ichi Watabe[1], Toru Hirayama[2], Takeshi Ikegami[1], Ken Hagimoto[1], Shin-ichi Ohshima[1], Masato Yoshida[2], Masataka Nakazawa[2]

[1] *National Metrology Institute of Japan (NMIJ), AIST Tsukuba 305-8563, Japan*

[2] *Research Institute of Electrical Communication, Tohoku University, 2-1-1 Katahira, Aoba-ku, Sendai 980-8577, Japan*

Abstract

We have measured the properties of coherent population trapping (CPT) signals in Cs-D_1 line as a function of laser intensity. The three types of Cs cell were used through the measurements with varying buffer gas pressures. We observed a minimum linewidth as narrow as 200 Hz for the cell with a buffer gas pressure of 10 Torr.

1. Introduction

Coherent population trapping[1)] (CPT) has been applied to the development of small stable clocks with observed fractional frequency stability of better than 10^{-11} for averaging times around 100 s.[2,3)] CPT clocks have potential advantages relative to traditional intensity optical pumping clocks (which typically employ an optical and microwave double-resonance technique)[4)] including the possibility of substantial miniaturization without degradation of performance.[5)] In NMIJ, AIST and Tohoku University research has started on the atomic clock using CPT. As a first step, we observed the CPT signals for Cs-D_1 lines using an extended cavity diode laser (ECDL) as a light source and a waveguide-type electro-optic modulator (EOM) as an external phase modulator in order to produce two phase-coherent lights whose frequency difference is 9.2 GHz.

2. Experiment

Figure 1 shows the configuration of the experimental setup. We derived the two optical fields needed for the CPT signals by phase modulating the output from an ECDL in the vicinity of the D_1 line of Cs ($6^2S_{1/2} \rightarrow 6^2P_{1/2}$, $\lambda \approx 894$ nm). An EOM phase modulated the optical field at half of the ground-state hyperfine frequency of cesium (9 192 631 770 Hz). Zeeman energy levels degeneracy in the ground state is lifted by the application of a magnetic field. Three Cs cells, 25 mm in diameter and 25 mm long, were used in the measurements; without buffer gas, with nitrogen buffer gas at 5 Torr and 10 Torr. The buffer gas cancels the first order Doppler broadening (Lamb-Dicke regime) and increases the atomic transit time in the light beams. The laser power incident on the cell was regulated by a power control servo comprising of a photodetector, an acousto-optic modulator (AOM), an rf-synthesizer, a voltage controlled attenuator and control electronics. The $\lambda/4$ plate was used to circularly polarize the laser radiation. The transmitted power was detected with a Si photodiode as the modulation frequency was scanned over the hyperfine resonance.

Figure 2 shows the Cs hyperfine resonance line as observed in a cell as a function of laser intensity. We observed a minimum linewidth as narrow as 200 Hz for a buffer gas pressure at 10

Torr. The contrast is plotted against laser intensity in Fig. 3. The contrast is defined as the CPT signal intensity divided by the background instensity.

3. Conclusion

We measured the properties of coherent population trapping (CPT) signals in Cs-D_1 line as a function of laser intensity. We observed a minimum linewidth as narrow as 200 Hz for a buffer gas pressure of 10 Torr. The contrast was observed to reach a maximum contrast versus laser intensity in the cell without buffer gas and also in the cell with 5 Torr of buffer gas.

References

1) E. Arimondo: Prog. Opt. **35** (1996) 257.
2) M. Merimaa, T. Lindvall, I. Tittonen and E. Ikonen: J. Opt. Soc. Am. B **20** (2003) 273.
3) J. Vanier: Appl. Phys. B **81** (2005) 421.
4) J. Vanier, M. W. Levine, D. Janssen and M. J. Delaney: IEEE Trans. Instrum. Meas. **52** (2003) 822.
5) J. Kitching, S. Knappe and L. Hollberg: Appl. Phys. Lett. **81** (2002) 553.

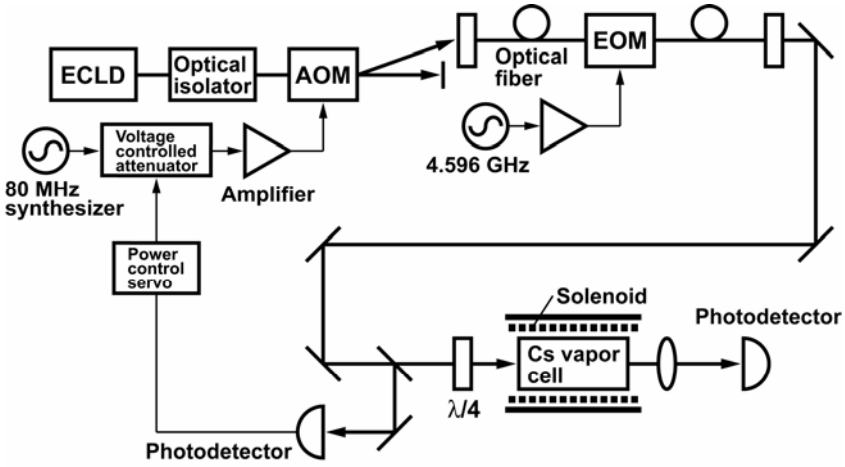

Fig. 1. Experimental arrangement used to observe the CPT phenomenon.

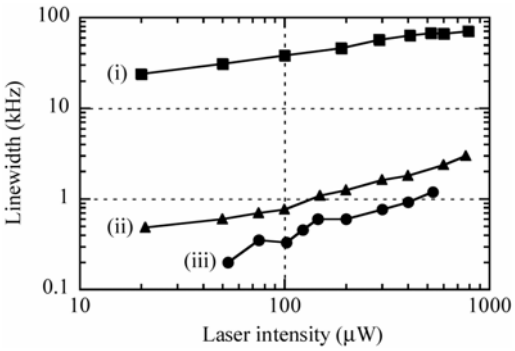

Fig. 2. CPT linewidth in a cell as a function of laser intensity. (i) represents results without buffer gas. (ii) and (iii) represent results with nitrogen buffer gas at 5 Torr and 10 Torr, respectively.

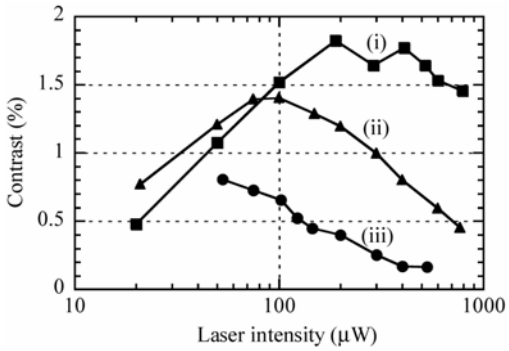

Fig. 3. CPT contrast in a cell as a function of laser intensity. (i) represents results without buffer gas. (ii) and (iii) represent results with nitrogen buffer gas at 5 Torr and 10 Torr, respectively.

DEVELOPMENT OF A FREQUNECY TRACEAVILITY SYSTEM USING GPS COMMON-VIEW METHOD FOR GENERAL USERS

Michito Imae, Yasuhisa Fujii, Tomonari Suzuyama, and Masaki Amemiya

Time and Frequency Division

National Metrological Institute of Japan (NMIJ), AIST

Tsukuba, Ibaraki, 305-8563, Japan

Abstract

NMIJ has started the remote frequency calibration service since January, 2005, based on GPS common-view method and Internet. This system was developed as part of the "e-trace project" which is consignment research fund of NEDO (New Energy and Industrial Technology Development Organization). As the clients of this system were mainly the calibration laboratories which are the first layer of the traceability system, so we can expect the technical experts in the organizations. The basic concept of this system was reported at the previous ATF workshop.

The system described in this paper is aimed for users in wider fields. It should be easy to use because we can expect no expert at the user site and be available at a popular price to generalize the remote calibration system.

The main functions of this system are :

i) it can receive L1 C/A code of GPS satellite for time transfer and store the data using CGGTTS format,

ii) Rb or TCXO is used for internal oscillator, and it can be synchronized to UTC(NMIJ) using the GPS receiving data at the NMIJ,

iii) it can provide own time transfer data in CGGTTS format to NMIJ or calibration laboratory to realize the traceability,

iv) the output signals of the system are two ports of 10 MHz, 5 MHz, 1MHz, and 1 pps.

The GPS receiving module has 12 channels of the data processing. NMIJ's GPS data is available through the web site and it is updated every hour and such data is used to control the internal oscillator. The function item iii) can realize to issue the calibration certification.

We are planning to develop proto-type ones of this system by the end of March 2007, and to start the demonstration experiments at the early time of 2007.

1. Introduction

We have been providing the frequency calibration service to the calibration laboratories using the "in house method". It means the client should bring their "Device Under Test" (DUT) to NMIJ for the calibration, and it has inconveniences, such as absence of the standard at the client site, transportation of the DUT, estimation of the uncertainty of the DUT after the calibration due to the aging effect. Therefore, the request and the expectation from the client site concerning a remote calibration service were very large.
We, NMIJ, have been developing the remote frequency calibration system using GPS common-view [1] method for several years to contribute to the industry.
This paper describes the MNIJ's remote frequency calibration system between NMIJ and calibration laboratories briefly, and then presents the device which is under development for the general users.

2. e-trace project and remote frequency calibration system between NMIJ and calibration laboratories

A project called "e-trace" has started at National Metrology Institute of Japan (NMIJ) and a few collaborating organizations since 2001. This project is financially supported by the New Energy and Industrial Technology Development Organization (NEDO). Figure 1 shows the concept of e-trace project.
Its purpose is to develop the remote calibration system for the traceability from the national standard kept at NMIJ in Tsukuba to the clients in each field, such as frequency, length, electricity, quantum radiation, dimensional standards, flow, temperature and pressure.
As the frequency standard is closely related to another standard, such as length and electricity, and easily realized its remote calibration system compared to another ones, then the remote calibration system of frequency is considered as one of the most important items in the e-trace project.
Our frequency remote calibration system uses the GPS common-view method and the system between NMIN and the calibration laboratories were presented at the ATF2002 and ATF2004 [3]. The system at the client site consists of a GPS time transfer receiver, a PC for data down load and transmission. Figure 2 shows an example of the client site system.
The GPS time transfer receiver which can output the comparison results in the CGGTTS format is used for this system and SMTP method is used for the data transmission from the client site to the NMIJ's data server computer. The obtained data at the client site is transmitted to NMIJ's data server computer once a day and the calibration certification is provided to the client once a month. The uncertainty of the system depends on the baseline length between NMIJ and the client and the GPS receiver used at the client site, and table 1 shows the typical ones using L1 C/A code multi-channel receiver.
We started this service since 2005 and we have 7 contracts with 6 clients at present.

3. Basic concept of the remote frequency calibration system for the general users

The remote frequency calibration system between NMIJ and calibration laboratory needs a special person for the supporting operation at the client site to meet the ISO/IEC17025's demands. However, in the case of the general user, it is difficult to expect a person who is familiar to the remote frequency calibration system. Therefore the system for the general users should be easily operated, and also have a good cost-performance for being widely accepted. In addition, GPS disciplined oscillator (GPS DO) has widely used for the reference signal source which is synchronized to UTC within some range, and there is a possibility to be accepted to keep the traceability by using GPSDO in future. But even if it will be acceptable, there are several problems, such as issuing the certification, the uncertainty limit and so on.
Considering the situation described above, we have started to develop a terminal device of remote frequency calibration for the general user. We named this device "GCET" and the concepts of this device are followings:

(1) Easy operation

(2) Highly good cost/performance

The basic specification is described in table 2. The device consists of Rb. oscillator or OCXO, GPS receiver module, CPU module, and 2 ports of reference signal output.

(3) Synchronization to UTC(NMIJ)

The internal oscillator can be synchronized to UTC(NMIJ) by monitoring the NMIJ's web site.

(4) Calibration certification

By sending the received results to NMIJ or calibration laboratories through the internet, the client can obtain the calibration certification by making the contract with NMIJ or calibration laboratories.

Figure 3 shows the whole diagram of remote frequency calibration system.

4. Performance and development schedule

The main specification of the device is described in table 2. Additional descriptions for several items are described below.

(1) GPS receiver and mounted oscillator

This device uses a GPS module which has 12 channel of L1 C/A code. It can also receive the SBAS signal for the positioning.

A Rb oscillator or an OCXO is installed in the device. It has 10 MHz of output reference signal and is synchronized to UTC(NMIJ) as described in (2).

(2) Synchronization to UNC(NMIJ)

We are providing our GPS data by the CGGTTS format in our web site, and it is updated every hour. The device access our web site to down load our data and make the common-view data processing to control the internal oscillator to synchronize to UTC(NMIJ).

(3) Data transmission

The device uses the HTTPS protocol to report it received data in CGGTTS format to the data server computer of the NMIJ or the calibration laboratory.

The proto-type one will be available by the end of 2006 and it will be commercially available around April of 2007. Figure 4 shows the outside and inside of the proto-type of GCET.

5. Conclusions

We have reported the basic concept and specifications about the remote frequency calibration system for the general users using GPS common-view method. This device will provide a very convenient frequency reference fully traceable to the national standard in Japan with a good cost-performance.

References

[1] D. W. Allan, M. A. Weiss, “Accurate Time and Frequency Transfer During Common-View of a GPS Satellite”, 34th Annual Frequency Control Symposium, pp.334-346, May 1980.

[2] D.W.Allan and C.Thomas, “Technical directives for standardization of GPS time receiver software”, Metrologia, Vol.31, pp.69-79, 1994.

[3] Y. Shibuya, Y. Fukuyama, M. Imae, M. Amemiya, T. Ikegami, and S. Ohshima, "Development and Application of the Frequency Remote Calibration System in Japan," Proceedings of ATF2004, pp298-302, 2005.

Table 1. Main specifications of the device

Baseline length between NMIJ and client site	CMC ($k=2$)
50 km	1.1 $\times 10^{-13}$ for averaging time of one day
500 km	1.4 $\times 10^{-13}$ for averaging time of one day
1,600 km	4.9 $\times 10^{-13}$ for averaging time of one day

Table 2. Main specifications of the device

GPS receiver	Signal	L1(1574.42 MHz), C/A code
	Number of channels	12 channels
	Sensitivity	< -135 dBm
	Positioning	< 5 m
	Data acquisition interval	1 second
Reference signal	Input (optional)	(option) 10 MHz
		(option) 1 pps
	Output	10 MHz: 2 ports +13 dBm ±3 dBm
		5 MHz: 2 ports +13 dBm ±3 dBm
		1 MHz: 2 ports +13 dBm ±3 dBm
		1 pps: 2 ports
Time transfer	Data format	CGGTTS format
	Uncertainty	< 5 ns : outside antenna
		< 20 ns : window-side antenna
	Time and Frequency synchronization.	Synchronize to UTC(NMIJ) using NMIJ's data from NMIJ's web site, otherwise synchronize to GPS time
	Data transfer	HTTPS protocol
Reference Oscillator (Synchronized to UTC(NMIJ))	Rb-type	< 1×10^{-13} @ 1 day (provisional) < 3×10^{-11} @ 1 s (provisional)
	OCXO-type	< 5×10^{-12} @ 1 day (provisional) < 1×10^{-10} @ 1 s (provisional)

Communication interface	Ethernet (10/100 BASE-T) RS-232C
Power	AC90 ~ 240V (50 ~ 60 Hz)

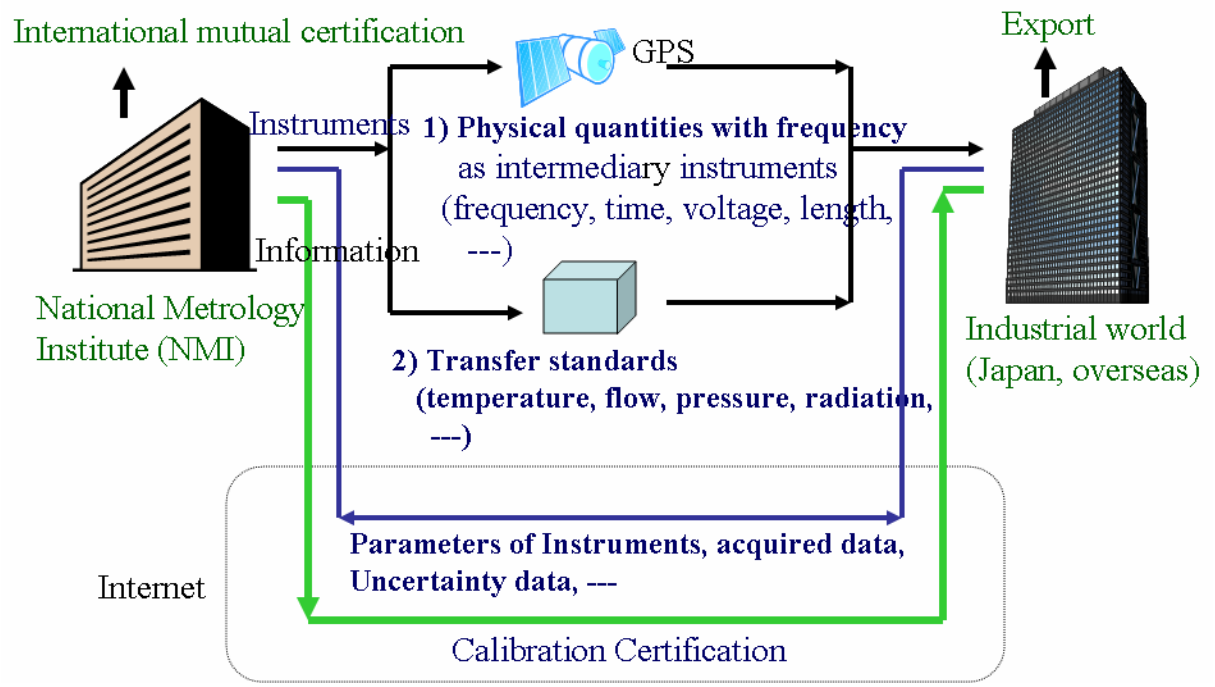

Figure 1. Concept of "e-trace"

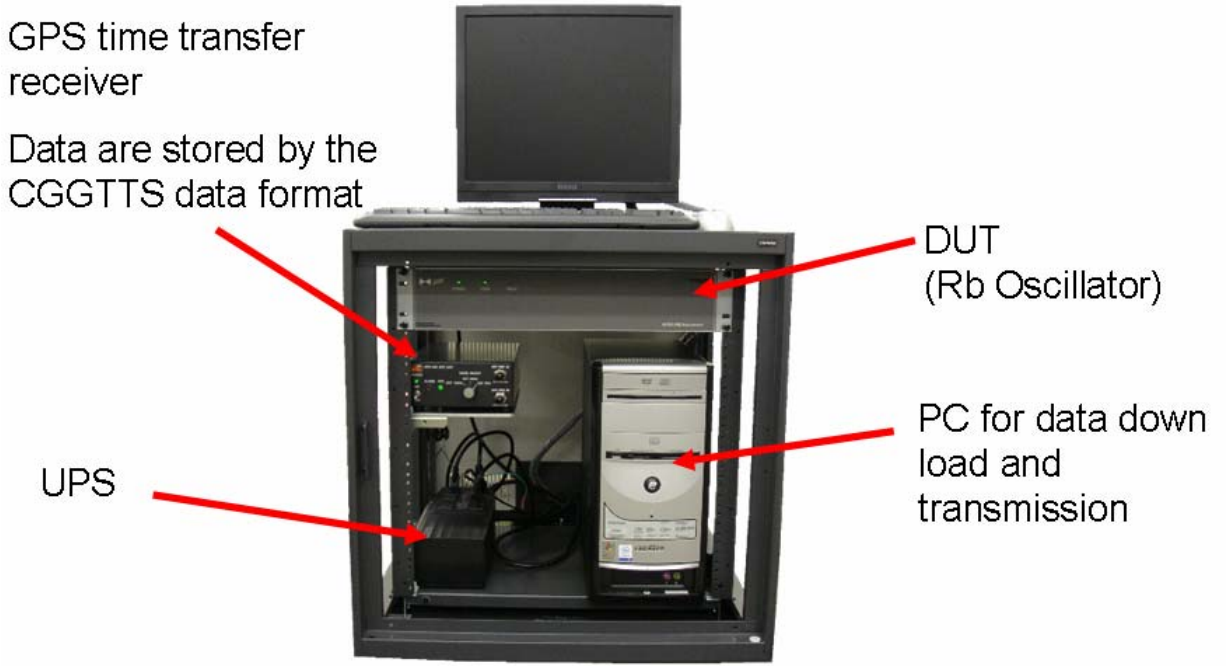

Figure 2. Example of the remote frequency calibration equipments for the calibration laboratories

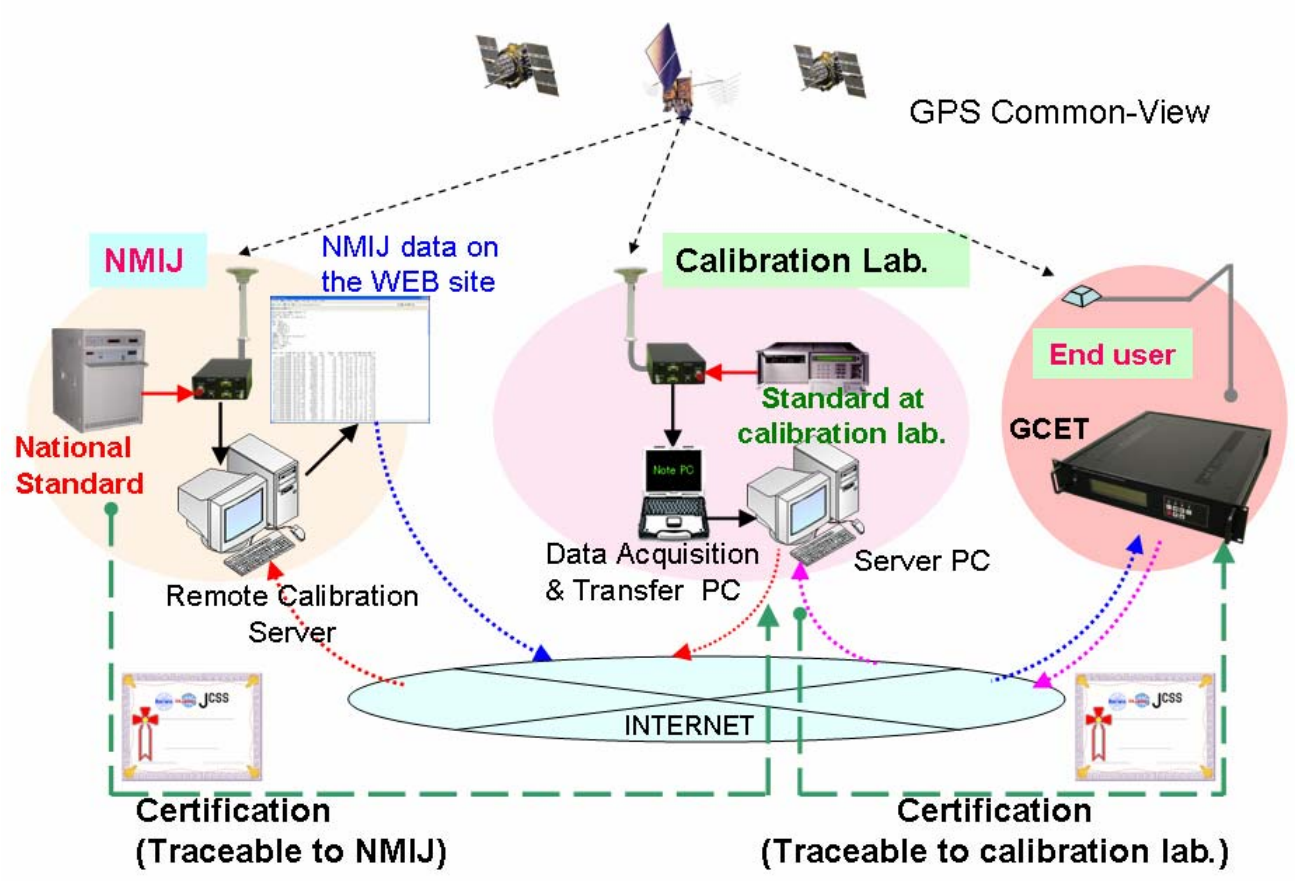

Figure 3. Schematic diagram of the whole system (from national standard to user equipment) of the remote frequency calibration system

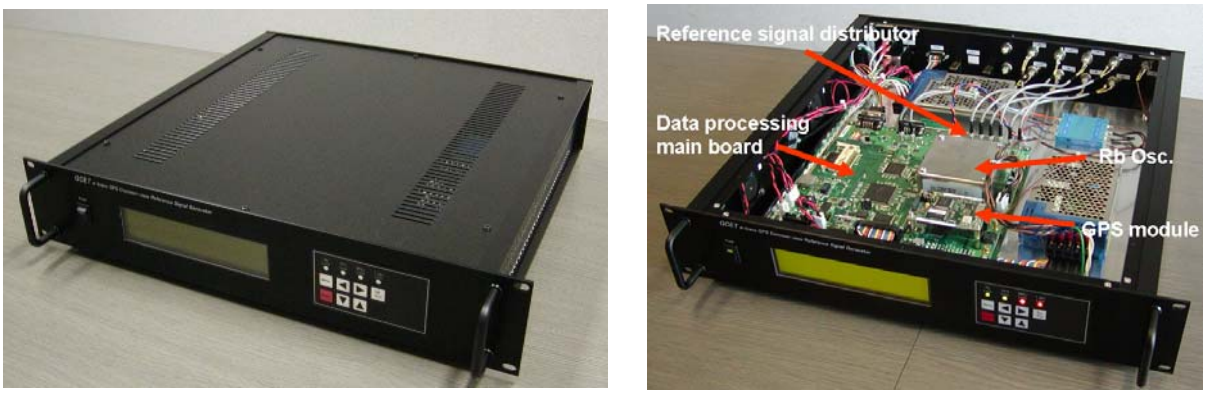

Out side view Inside of GCET

Figure 4. Photos of GCET

DEVELOPMENT OF A SINGLE CALCIUM ION OPTICAL FREQUENCY STANDARD IN NICT

Ying Li, Kensuke Matsubara, Hiroyuki Ito, Shigeo Nagano, Masatoshi Kajita, Kyoya Fukuda, and Mizuhiko Hosokawa

National Institute of Information and Communications Technology

Abstract

We are developing an optical frequency standard based on the $4s^2S_{1/2}$-$3d^2D_{5/2}$ quadrupole transition of a single Ca^+ ion. Three strategic researches are simultaneously in progress for developing the optical frequency standard. The first one is the development of a narrow linewidth clock laser system for the quadrupole transition. The second is trapping and confining a single Ca^+ ion to the Lamb-Dicke regime. The last one is the construction of an optical frequency comb for determining absolute frequency of the quadrupole transition. In this paper, we introduce recent progress of these studies.

1. Introduction

Novel frequency standards based on narrow optical transition frequencies of trapped single ion or neutral atoms have been proposed, as the frequency uncertainty can theoreticallybe reduced down to 10^{-18}[1]. Successful results have been obtained using $^{199}Hg^+$, $^{171}Yb^+$ ions [2-3] and Ca neutral atom and Sr neutral atoms in the optical lattice [4-7]. It is also useful to develop the optical frequency standards based on the $^2S_{1/2} - ^2D_{5/2}$ electric quadrupole transitions of a single Sr^+ [8] or Ca^+ ion confined to the Lamb-Dicke regime. One of advantages is fundamental waves of compact and robust diode lasers (LD) are available for a whole process of the cooling, repumping and probing.

We are proceeding to develop an optical frequency standard based on the quadrupole transition (729 nm) of a single $^{40}Ca^+$ ion [9, 10] in an RF trap, because of a long lifetime of the $^2D_{5/2}$ state (natural linewidth ~0.13 Hz). Three strategic researches are simultaneously in progress. Ⅰ. Development of a narrow linewidth and tunable frequency clock laser system; Ⅱ. Trapping and confinement of a single $^{40}Ca^+$ ion to the Lamb-Dicke regime; Ⅲ. Construction of an optical frequency comb for measuring the accuracy and stability of the clock laser system. For this optical frequency standard, an uncertainty of ~ 1 x 10^{-15} is expected.

2. Narrow Linewidth 729 nm Clock Laser System

The schematic diagram of a 729nm clock laser system is shown in Fig. 1. There are two procedures of the development: the first process reduces the linewidth of a diode laser (master laser); the second is frequency tuning by offset locking a diode laser (slave laser) to the stabilized master laser.

The master laser system is based on a 5 mW, antireflective coated (AR) laser diode with a center wavelength at 730 nm. The free running linewidth of the solitary laser is substantially reduced by

employing an extended cavity diode laser (ECDL) setup in Littman-Metcalf configuration [11]. In order to compress the spectral linewidth extremely and to suppress frequency drift of the ECDL, the laser is actively stabilized to an ultrahigh-finesse ultra-low expansion glass (ULE) Fabry Perot reference cavity by employing a frequency modulation (FM) sideband technique [12]. We choose an ULE reference cavity (Research Electro-Optics) whose free spectral range is 1 GHz and finesse is 6×10^4 (it corresponds to a 17 kHz spectral linewidth). It is very important to isolate the ULE reference cavity against acoustic, thermal and mechanical perturbation. We set the ULE optical cavity into a constant temperature vacuum chamber and the vacuum chamber is put on a vibration isolation platform (Nano-k 250BM-3 type) with an acoustic isolation box.

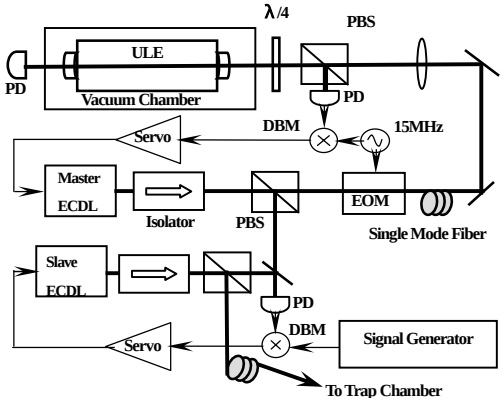

Figure 1 Experimental configuration of a laser frequency stabilization system: linewidth reduction by a constant temperature ultra low expansion glass (ULE) cavity, frequency tuning by offset locking to the master laser. The paths of the laser beams and the electric signals are distinguished as thick lines and thin lines, respectively. Photodiode (PD), double-balanced mixer (DBM), polarization-beam splitter (PBS), electro-optic modulator (EOM), extended cavity diode laser (ECDL).

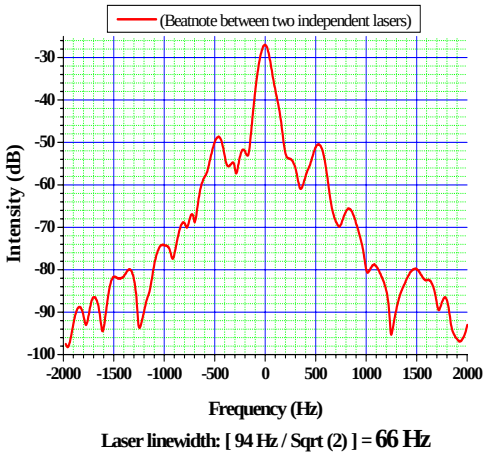

Figure 2 Spectrum of the beatnote between two laser beams stabilized to two independent ULE reference cavities. The measuring time is 3 s. The resolution bandwidth of the spectrum analyzer is 1 Hz. The linewidth of 66 Hz for one laser is estimated from the spectrum.

The laser light is coupled to a polarization maintaining single mode fiber (Fujikura) to obtain a single spacial TEM_{00} mode. Then the laser beam is mode matched to the ULE reference cavity. The reflected light from the cavity is detected by a Si PIN Photodiode (PD). After demodulation of the photocurrent by using a double-balanced mixer (DBM), the low-frequency component is amplified, integrated, and fed back to the ECDL (master laser) via two channels of the electrical servo circuit. A slow feedback loop (~ several hundreds Hz) - driving the PZT of the ECDL mirror – adjusts the laser frequency to a reference cavity resonance. Fast frequency fluctuations are compensated by superimposing the feedback current signal onto the laser cathode, obtaining a 1 MHz total servo bandwidth. The master laser is stabilized to the ULE optical cavity.

For an evaluation of the linewidth of the master laser, we measured the heterodyne beatnote between two narrow linewidth master lasers, individually stabilized to two independent ULE reference cavities. Figure 2 shows a beatnote signal of the stabilized lasers. Its linewidth is 94 Hz, which corresponds a 66 Hz linewidth for each laser, assuming the same linewidths.

For the frequency fixed master laser, the frequency of the slave laser is set with an arbitrary RF frequency difference using an optical phase-locked loop [13]. A beatnote between the master and the slave laser is detected by a fast photodiode and an RF frequency is set by a signal generator. The phase difference between the beatnote and the local oscillator is demodulated and feedback to the slave laser. The offset frequency is tunable relative to the fixed-frequency of the master laser system in a whole free spectral range of the 1 GHz. The feedback method is similar to that of the master laser.

An experimental result of a beatnote signal between the stabilized master laser and the offset locked slave laser at 729 nm with a 50 MHz offset frequency is shown in Fig. 3. The -3dB full linewidth (FWHM) of the beatnote seen from Fig. 3(A) is 1.3 Hz. The value is close to the resolution of spectrum analyzer (1 Hz, 8560E Hewlett Packard). In Fig. 3(B), the servo bandwidth of the phase-locked loop is 1.7 MHz. This result shows the linewidth of the slave laser is practically identical with that of the master laser. A ±500 MHz offset locking has also been confirmed. As mentioned above, the free spectral range is 1 GHz for our ULE reference cavity. It shows that the frequency tuning range covers the whole free spectral range of the ULE reference cavity.

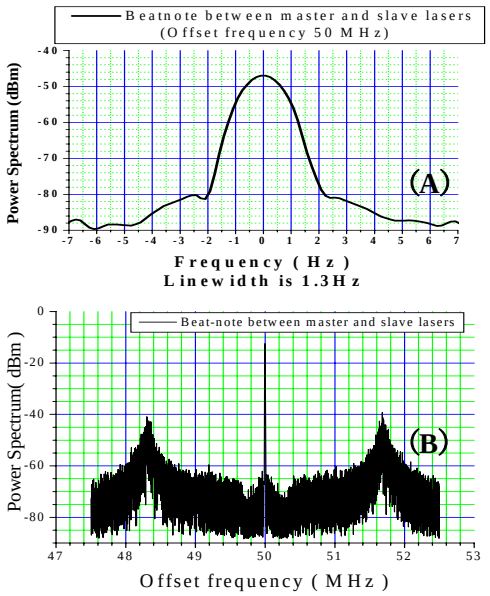

Figure 3 Measured beat-note between a stabilized master laser and an offset locked slave laser at 729 nm with ranges 14 Hz (A) and 6 MHz (B): The offset frequency is 50MHz. (A) shows that the -3dB full line-width of the beat-note is 1.3 Hz, closed to the resolution of spectrum analyzer (1 Hz). (B) shows that the bandwidth of the phase-locked loop is 1.7 MHz.

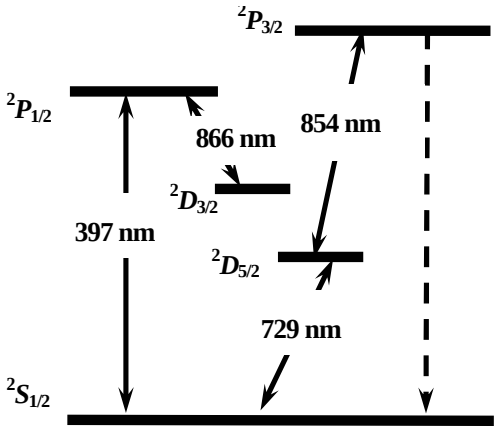

Figure 4 Partial term energies of Ca^+

3. Single Ca^+ Ion Trap

Partial term energies of Ca^+ are shown in Fig. 4. The $^2S_{1/2}$ –$^2P_{1/2}$ transition (397nm) is used for laser cooling, and the $^2P_{1/2}$ –$^2D_{3/2}$ transition (866nm) is used for repumping the ion to the laser cooling. The $^2S_{1/2}$ –$^2D_{5/2}$ electric quadrupole transition is the clock transition (729nm), that has a high line-Q (~10^{15}) due to long lifetime of the $^2D_{5/2}$ state (natural linewidth ~0.13 Hz). The $^2D_{5/2}$–$^2P_{3/2}$ transition (854nm) is used for repumping the laser cooling cycles. The lasers are ECDLs stabilized with scanning transfer cavities [14]. This method is suitable for a simultaneous frequency stabilization of multiple lasers because of its simple configuration. The control signal for the ECDL frequency is processed from the ratio of the space between transmission peaks of ECDL from the cavity scanning its length to those of the reference He-Ne laser. The signal is fed back to the PZT to control the cavity length. The frequency drifts of the ECDLs are measured to be less than 200 kHz for 1 hour and the frequency stabilities are found to be around 1×10^{-10} at 10^3 s in the Allan deviation. These performances are enough for the laser-cooling of an ion to the temperature of Doppler limit.

The laser-cooled single $^{40}Ca^+$ ion must be confined into a region smaller than the wavelength of the clock laser (729 nm, Lamb-Dicke regime) in the trap, to eliminate the Doppler linewidth broadening from the spectrum of the clock transition. A radio-frequency (RF) Paul trap consisting of two 1.0 mm-diameter rod electrodes and a 0.5-mm-radius ring electrode is equipped for trapping $^{40}Ca^+$ ions. Two additional electrodes are used for compensating the stray electric field. An RF voltage of 300 V at 19 MHz is applied to ring electrode. The ion trap apparatus is put in a stainless-steel chamber evacuated to a pressure below 5 x 10^{-8} Pa.

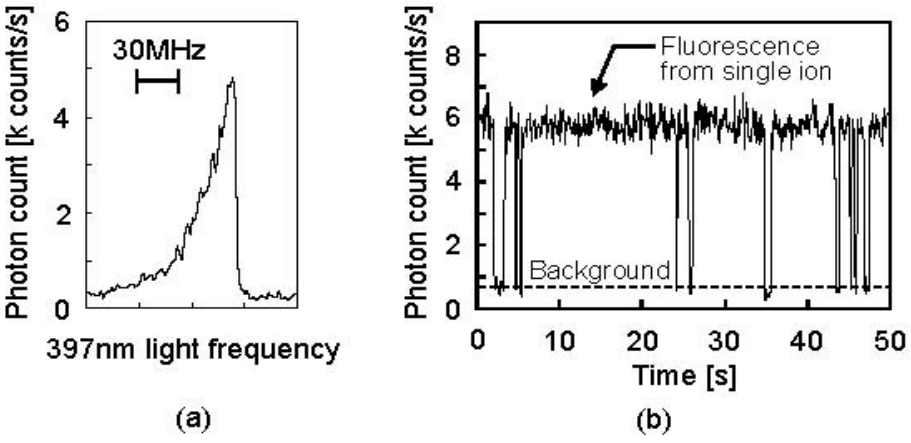

Figure 5 (a) Spectrum of the laser-cooled single $^{40}Ca^+$. (b) Quantum jumps accompanied with the clock transition.

The frequency of the 397-nm LD is fixed to ~ 100 MHz below the resonance center of $^{40}Ca^+$ ions and that

of the 866-nm LD is tuned to just resonance. After turning on the Ca oven and the photo-ionizing lasers for ~40 seconds, we scanned the 397-nm frequency to observe spectrum of the trapped Ca^+ ions. When we trapped multiple ions (photon numbers much larger than 7000 / s), the 397-nm LD is tuned to a higher frequency than the resonance center for several seconds so as to decrease number of the trapped ions. After confirming the single ion trap, we performed the micromotion compensation to cancel the electric stray field, which causes a large ionic oscillation. A typical spectrum of the single $^{40}Ca^+$ ion is shown in Fig. 5 (a). We measured the linewidth at several powers of 397 nm laser light to estimate the residual Doppler broadening. The temperature of the single $^{40}Ca^+$ ion is estimated to be below 10 mK.

After observing the laser-cooling spectrum, we fixed the 397-nm frequency at several MHz below the resonance frequency and observed the fluorescence intensity from a single $^{40}Ca^+$ ion. Then, the 729-nm light was focused into the trap and we observed the quantum jumps accompanied with the clock transition. A typical measurement result is shown in Fig. 5 (b). When the single $^{40}Ca^+$ ion is pumped into the metastable $^2D_{5/2}$ state by 729-nm light, fluorescence with the $^2S_{1/2} - {}^2P_{1/2}$ transition is extinguished completely.

For measuring spectrum profile of the clock transition, we measured the probability of the quantum jumps dependent on the 729-nm light frequency. The power of the 729-nm laser is fixed to ~ 30 μW. To prevent the power broadening caused by the cooling laser, the 397-nm light and the 729-nm light are applied to the ion alternatively with interval time of 25 ms. The 854-nm light was applied for 50 ms with intervals of 950 ms. When the 854-nm light is absorbed by the ion populating the $^2D_{3/2}$ state, the ion is returned to the laser cooling cycle. The transition probability is counted from the number of the quantum jumps during 1 minute at each 729-nm frequency. We measured the spectrum in an external magnetic field of ~ 5 G, and one Zeeman component is shown in Fig. 6. In this spectrum we observed the motional sidebands with a radial secular motion of ~1.6 MHz. The measured linewidth is the order of 600 kHz. It seems to be suffered by the residual Doppler broadening and the power broadening caused by the 729-nm laser radiation.

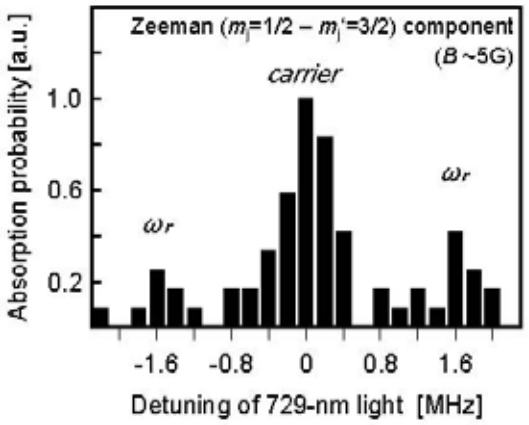

Figure 6 Electric quadrupole transition spectrum of $^{40}Ca^+$ ions. This is a Zeeman component measured in an external magnetic field.

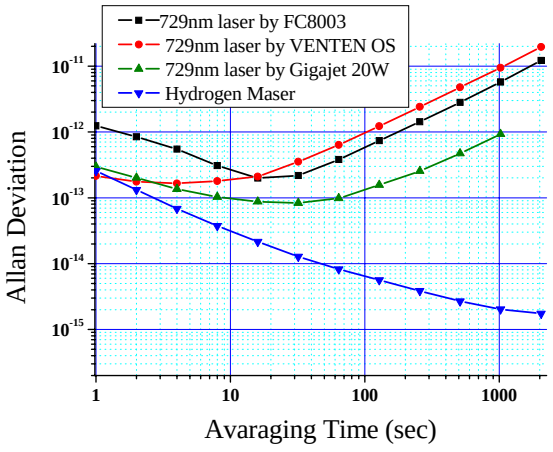

Figure 7 Measured frequency instabilities as given by the Allan deviation for a 729 nm clock laser stabilized to an optical cavity (red, black, and green curves). A hydrogen maser is used as frequency reference for FC8003, Venteon OS, and Gigajet 20W optical combs (blue curve).

4. Femtosecond Laser Optical Frequency Combs

An optical frequency comb generated from the femtosecond pulse mode-locked laser has made a revolution, since the end of the last century, the precise frequency metrology in optical region and enabled us to directly connect the optical frequency to the microwave frequency with high accuracy. It could be drastically improved the measurement accuracy of the optical frequency [15].

The periodic pulse train of a mode-locked laser can be described in the frequency domain as a comb of equidistant modes. The frequency of a mode with the number n of the comb is given as follows:

$$f_n = n f_{rep} + f_{ceo}, \qquad (1)$$

where f_{rep} and f_{ceo} represents repetition frequency and carrier-envelope offset frequency respectively. If the comb of the mode-locked laser pulse contains a full optical octave, employing a self-referencing technique, we can determine f_{ceo} from beatnote frequency between second-harmonics of the nth mode and the $2n$th mode. This can be described as following equation.

$$2(n f_{rep} + f_{ceo}) - (2n f_{rep} + f_{ceo}) = f_{ceo}. \qquad (2)$$

We are operating a commercial femtosecond optical frequency comb (FC8003). A photonic crystal optical fiber is employed as a nonlinear optics for the production of the spectrum more than an octave of bandwidth. There are some disadvantages for using it. The coupling the light into the fiber is sensitive alignment and tends to degrade with time because of the small core of the fiber. This will be a critical problem for a frequency standard required the stable long-term operation. In addition, excess phase noise is reported to appear in the light transmitted through the fiber [16, 17].

The mode-locked lasers directly emitting the broadband spectrum are excellent devices to overcome the disadvantages concerned with the photonic fiber. We are developing two other combs based on the different femtosecond mode-locked Ti:sapphire lasers with broadband spectrum: Venteon OS (Nanolayers GmbH) and Gigajet 20W (Gigaoptics GmbH) [18]. These optical frequency combs are required for the measurement precision of 10^{-16} for the absolute frequency of single frequency lasers in addition to the stable operation sufficient for the highly reproducible measurement.

Venteon OS is based on a Kerr-lens-mode-locked Ti:sapphire laser. It generates femtosecond pulses with the repetition frequency of 200 MHz and the output spectrum spanning a full octave. The average output power was measured to be 200 mW, when the laser was pumped by a frequency doubled Nd:YVO_4 laser with an output power of 5.7 W at 532 nm in wavelength (Coherent, Verdi-V 8). The frequency stabilization of f_{ceo} is achieved by a phase-locked loop (PLL) technique. The f_{ceo} is detected by a beatnote frequency of the 570 nm and 1140 nm light. The phase locking of the f_{ceo} is obtained by feeding the error signal to an acousto-optical modulator placed in the pump beam. When the f_{ceo} is locked, its frequency fluctuation is less than 1 mHz in an averaging time of 1 s, which is equivalent to the measurement accuracy of $>10^{-16}$. The f_{rep} is phase locked to a frequency reference of 200 MHz for the stabilization of the pulse repetition rate. The reference frequency is directly created from a 100 MHz output of the hydrogen maser by electrically

frequency doubling to reduce the excess phase noise. The control signal is obtained after the down-converting process by using a double-balanced mixer (DBM). The signal was fed back to a slow and fast PZT attached to the laser mirrors for controlling the cavity length.

Gigajet 20W is a Kerr-lens-mode-locked femtosecond Ti:sapphire laser with a repetition rate of 1 GHz. Its average output power was 800 mW at the pumping power of 8.5 W. The high repetition rate and high output power will give us the benefit of the strong heterodyne signal and good beat-signal separation. The f_{ceo} is obtained by using complex second and third harmonics (640 nm and 960 nm) self-referencing interferometer, since the output spectrum of the laser is spreaded by two-thirds of an octave. The phase locking methods of the f_{ceo} and the f_{rep} are similar to the Venteon OS optical comb system.

For the evaluation of the performance of the stabilized clock laser system, we used three femtosecond laser frequency combs, namely a commercial FC8003, Venteon OS, and Gigajet 20W frequency combs. We measured beatnote frequencies between the laser beam and the each frequency combs. The square root of the Allan variance of the measured beatnote frequencies are shown in Fig.7. The black line shows the measured frequency stability for the 729 nm laser with the commercial FC8003 comb. The short term stability is 1.5×10^{-12} in Allan deviation at an averaging time of 1 s. The red line and the green line show the measured results with the Venteon OS and Gigajet 20W frequency combs. These measurements show the frequency stability of 2×10^{-13} in Allan deviation at an averaging time of 1 s. The performance of the Venteon OS, and Gigajet 20W optical combs are more excellent than FC8003. The present measurement precision is limited by the stability of the hydrogen maser used as the frequency reference. The measurements are conducted in different days, because the output power of the clock laser is insufficient for the simultaneous measurement with good precision. There exist the discrepancies of the frequency stability at the long averaging times between each measurement. These are caused by the thermal expansion of the ULE reference cavity, which are appeared as the long-term frequency drift of 1~2 Hz per second. This will be decreased further by the improvement of the thermal stability system for the ULE reference cavity.

5. Conclusions

In NICT, an optical frequency standard is being developed, which is based on the $^2S_{1/2}-{}^2D_{5/2}$ quadrupole transition (729 nm) of a single $^{40}Ca^+$ ion. The frequency of the clock laser with the wavelength of 729 nm has been highly stabilized to the resonant frequency of the high finesse ULE Fabry-Perot reference cavity. The linewidth of 66 Hz is measured by a heterodyne beatnote between two independent diode laser systems. The laser frequency is continuously tunable on the whole free spectral range of the ULE reference cavity. Using this clock laser and the ion trap system, the quantum jump signal of the clock transition has successfully been observed. Its linewidth is less than 600 kHz together with the ionic motional sidebands, limited by the residual Doppler broadening and the power broadening caused by the clock laser radiation. The Venteon OS, and Gigajet 20W optical combs are being developed. The performances are more excellent than FC8003. The present measurement precision is limited by the stability of the hydrogen maser used as the frequency reference. Development of a high precision optical frequency standard is progressing in NICT.

Reference

[1] H. Dehmelt, et al. 1982, *IEEE Trans. Instrum. Meas.*, vol. 31, 83

[2] W. H. Oskay, et al. 2006, *Phys. Rev. Lett.*, vol. 97, 020801

[3] T. Schneider, et al. 2005, *Phys. Rev. Lett.*, vol. 94, 230801

[4] G. Wilpers, et al. 2006, Appl. Phys. B vol. 85, 31

[5] M. M. Boyd, et al. 2006, is submitted to *Phys. Rev. Lett.*

[6] M. takamoto et al. 2006, *J. Phys. Soc. Jpn.* vol. 75, 104302

[7] R. L. Targat, et al. 2006, *Phys. Rev. Lett.*, vol. 97, 130801

[8] H. S. Margolis, et al. 2004, *Science*, vol. 306, 1355

[9] K. Matsubara et al. Proc. Precise Time and Time Interval Systems and Applications Meeting, Vancouver, August, 2005, 616.

[10] M. Kajita, et al. 2005, *Phys. Rev.* A, vol. 72, 043404.

[11] M. G. Littman, al. 1978, *Appl. Opt.*, vol. 17, 2224

[12] R. W. P. Drever, et al. 1983, *Appl. Phys. B*, vol. 31, 97

[13] L. Ricci, et al. 1995, *Opt. Commum.* Vol. 117, 541.

[14] K. Matsubara et al. 2005, *Jpn. J. Appl. Phys.*, vol.44, 229

[15] Th.Udem, et al. 2002, *Nature*, vol. 416, 233

[16] L. Hollberg, et al. 2001, *IEEE J. Quantum Electron*, vol. 37, 1502

[17] L. Matos, et al. 2004, *Opt.Lett.*, vol. 29, 1683

[18] H. Ito, et al. 2006, Proc. 11th European Conference on Networks and Optical Communications, Berlin, 314

Development of the Precise Time Transfer Software Analyzing GPS Carrier Phase with Common-View Method

Yasuhisa Fujii [1,2], Michito Imae [1,2]

1:National Metrology Institute of Japan/AIST
Tsukuba Central 3, Umezono 1-1-1, Tsukuba, Ibaraki,305-8563 / JAPAN

2: CREST, Japan Science and Technology Agency
4-1-8 Honcho Kawaguchi, Saitama, Japan

Abstract

Optical frequency standards, such as optical lattice clock, have been developed rapidly and have a possibility to realize better uncertainty than the micro-wave primary frequency standards. NMIJ has been making collaboration with Prof. Katori of the University of Tokyo to evaluate the optical lattice clock located in Tokyo.

The University of Tokyo is about 50 km away from NMIJ at Tsukuba, and we selected GPS carrier phase common-view technique for the purpose of doing it precisely against the national standard, UTC(NMIJ). By measuring the frequency of the source oscillator placed at Tokyo in the precision of the order of $5x10^{-15}$ at the averaging time of 10^4 seconds, the frequency against SI second of the optical lattice clock can be evaluated.

So we developed the analysis software tool, which can get the time transfer result in real time.

Our final goal is to provide a reference signal with the higher stability being steered of the source oscillator placed at Tokyo by using the result analyzed with this software.

In this paper, we will show some analysis results close to that of using GIPSY software, and both results show a very good agreement for the actual observed data from the GPS dual frequency carrier phase receivers.

1. Introduction

The time and frequency standard is the most accurate, highest stability, and also smallest uncertainty than any other standards. But, by the progress of laser techniques and/or of specifications of laser instruments, it is getting to be expected that the frequency standard generated from optical instruments will show the more high accuracy and short term stability than usual microwave frequency standard.

Recently, in the Consultative Committee of Time and Frequency (CCTF) of the international metrology committee, a new working group named “WG-Secondary representation of the second” was organized for its purpose.

And also another new organization was organized, for the purpose of consideration about the more advanced time transfer techniques, for such as the above needs.

In this context, the joint team of H.Katori et.al.(Engineering Research Institute, The University of Tokyo) and F.L.Hong et.al.(National Metrology Institute of Japan/National Institute of Advanced Industrial Science and Technology) achieved to measure the absolute frequency of the Sr Lattice Clock in a small uncertainty.

* yasuhisa-fujii@aist.go.jp

The estimated frequency showed extremely good agreement with other two oversea groups, and it is the most lest uncertainty in the three results. Therefore, its value was adopted as one of the 4 kinds of optical clocks of “secondary representations of the second”, for the first time in Sep. 2006, by CCTF[1)].

In this experiment, the optical frequency from the Sr lattice clock was measured by using an Optical Frequency Comb set at the laboratory of University of Tokyo, but its local frequency should be linked against the microwave standard frequency in Japan which is kept at Tsukuba, 50km north from Tokyo.

Therefore, we brought one of our H-Maser standards into the laboratory at Tokyo for using this as the local frequency of the optical comb. Whole of the measurement system were kept in a still condition as long as possible, and we evaluated the maser frequency by using GPS carrier-phase measurement method. We set two systems at each sites, and two systems consist from two different types of receiver (one used Ashtech Z-12T and another used Javad Lexon-GGD). For this situation (about 50km baseline length), precise point positioning analysis was performed by using the famous analyzing software GIPSY-OASYS II (GOAII), and estimated the clock parameter [2),3),4)].

We are planning to provide our UTC(NMIJ) to the laboratory at Tokyo almost in real time (5x10^-15@10^4), instead of carrying our maser for long evaluation, in near future. For this purpose, we should prepare the BVA crystal oscillator at the laboratory at Tokyo and adjust it in short time with the time transfer results evaluated by analyzing GPS carrier phase.

Though, it is difficult to use GOAII for the purpose of above from two but important reasons. One is that it needs to get both the IGS precise orbit data and the IGS clock data for getting the precise time transfer results.

IGS data is precise but it took some time to get it. We need to evaluate the time transfer result almost in a real time, so we should use the broadcast data. Theoretically, orbital error caused from using the broadcasted ephemeris instead of using IGS precise ephemeris will be negligible in the small baseline length case by using the common view method. And another is for the reason of the performance of GOAII, which can output the estimated clock result for 300 seconds resolution. As we want to calculate time transfer result and adjust BVA within a short time, it is desirable to set the clock estimation period for voluntary.

For this reason, we develop the GPS carrier phase analyzing software especially for our use, the precise frequency transfer. We made the prototype software as the first step, and got good results compared to the time transfer results evaluated by GOAII. In this paper, we report about these results.

2. Outline of our software

We developed the GPS Carrier phase Analyzing Software for Time transfer (GCAST) to overcome some restriction using GIPSY-OASIS II (GOAII) on the base of the Matlab application;

(1) It use the broadcast ephemeris
(2) It uses an observation model based on the GPS common view method
(3) It can output the result for the voluntary time resolution
(4) It can sequentially process data with the GUI base

We used GOAII to calculate time difference between two receivers as follows. First we estimate the precise position by using precise point positioning strategy for each station,

second we evaluate each receiver clock as a time dependant parameter, and finally, we get the time transfer result by subtracting each other, just like the calculation “all-in-view” method.

On the other hand, the point that our GCAST calculates direct difference of two station’s clock bias is quite different. It extracts the GPS common view first, and makes single difference, then estimates some integer biases. The specifications of GCAST are shown in Table2.

3. System Configuration

Time transfer system configuration is showed in Figure3. There are two receivers for each site, one is Ashtech Z-12T and the other is Javad Lexon-GGD.

4. Compared results of GCAST against to the GOAII

Test data were used for evaluate our GCAST, that is acquired under the configuration mentioned in Table4.

Evaluation results of zero baseline length case and 50km baseline length case are shown in figure4.1 and 4.2.

In the case of zero baseline length (Figure4.1), the result of GCAST is 1.5 times better than that of GOAII for the averaging time of longer than 1200 seconds, which means the GPS common view estimation method is more effective than the “all-in-view” method in the zero baseline case. And it is clear from the time series estimation results that the algorithm of GCAST has higher calculation stability for bad data than that of GOAII.

While, in the case of 50km baseline length (Figure4.2), GCAST result is 2 times inferior than GOAII result for the averaging time of shorter than 5x10^4 seconds, and it shows the 1/tau trend for the period of 1 second to 2x10^4 seconds.

The baseline length dependency of stability evaluation will come from difference of the tropospheric delay calculation algorithm between the two software packages.

It means that the observation model is reasonable but that the calculation algorithm is not adequate for the case of 50 km baseline length which is good for zero baseline case.

GOAII uses Kalman filter method for filtering of 300 seconds. On the other hand, GCAST uses least squares method which is iterative calculation of the range estimation to converge the residuals after fitting, for the both reasons of easier coding and of easier development. As a result, the difference of estimation precision for 1 point between GCAST and GOAII causes the difference of the stability. We are planning to change the algorithm to use Kalman filter to improve 50 km baseline length result.

Then, our developed software will have a potential equally to the GOAII and it is enough to get the first target to achieve the estimation stability of 5x10^-15 at the averaging time of 1x10^4 seconds.

5. Summary

We developed the GPS carrier phase analyzing software especially for short baseline length precise time and frequency transfer, which results shows the good performance

compared to GOAII.
This is the first step to provide our national frequency standard UTC(NMIJ) via GPS to the laboratory at University of Tokyo, 50 km apart from NMIJ at Tsukuba. In near future, we will construct the BVA steering system almost in real time using this software, which is located at the laboratory at Tokyo.
Furthermore, to improve the result of the baseline length of 50km, the calculation algorithm will be changed from the least squares method into the method of using Kalman filter, for the purpose of getting the nearly equal performance to GOAII.

Acknowledgments

The authors are grateful to Prof. Katori of University of Tokyo, Dr. F.L.Hong of NMIJ, and their co-workers for the joint working supported from the Strategic Information and Communications R&D Promotion Program (SCOPE) of the Ministry of Internal Affairs and Communications of Japan. We thank to Dr. R. Ohtani of Geological Survey of Japan, AIST, for his helpful discussions about the GIPSY, and also gratefully acknowledge to the Jet Propulsion Laboratory with the use of the GIPSY software.

References

1) M. Takamoto, F.-L. Hong, R. Higashi, Y. Fujii, M. Imae, and H. Katori, J. Phys. Soc. Jpn. 75, 104302 (2006).
2) T Gregorius, Department of Geomatics, University of.Newcastle upon Tyne, “GIPSY-OASIS II How it works…” (1996)
3) W. Lewandowski, J. Azoubib, and W. J. Klepczynski, “GPS: Primary tool for time transfer,” Proc. IEEE 87, 163-172 (1999).
4) K. M. Larson and J. Levine, “Carrier-phase time transfer,” IEEE Trans. Ultrason., Ferroelect., Freq. Contr. 46, 1001-1012 (1999).

Table2. GCAST specifications

Target	To achieve the time transfer stability evaluation of 5x10^-15 at the averaging time of 1x10^4 seconds
Observation Data	L1/L2 Carrier-Phase and Pseudo-Ranges (CA/P1/P2) in RINEX format
Navigation Data	Broadcast Ephemeris in RINEX format
Estimation Parameters	Co-station Position (position of reference station is fixed) Zenith Delay of tropospheric wet component, Ambiguity of Carrier Phases, Receiver Clock Difference
Observation Model	Single Difference of two Carrier Phases and Iono-Free Pseudo-Ranges
Estimation Method	Least Squares Method
Estimation Period	Equals to the Resolution of RINEX data
Base Application	Matlab

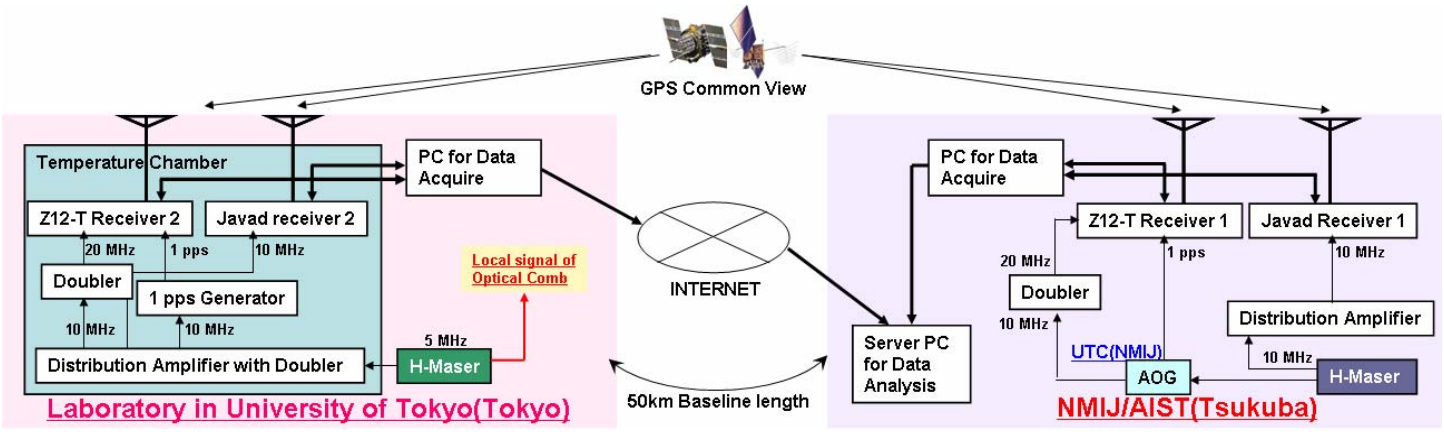

Figure 3. Schematic Figure of the System Configuration for evaluation.

Table4. Configuration of the data acquisition

Reference Station (Receiver)	NMIJ@Tsukuba(JAVAD)
Estimation Point (Receiver)	University of Tokyo@Toky(JAVAD)
Receiver Local	
of Reference Station	UTC(NMIJ) : H-Maser steered by AOG
of Estimation Station	H-Maser Free Running
Baseline Length	51 km
Observation Data	L1/L2 Carrier-Phase and Pseudo-Ranges(CA/P1/P2) in RINEX format
Navigation Data	Broadcast Ephemeris in RINEX format for GCAST IGS Precise Ephemeris in SP3 format with High Rate Clock Data for GOAII
Elevation Masks	15 degrees
Estimate Resolution	30 sec (RINEX format)
Observation Period	2006/04/18 - 04/26(9 days) and 2006/06/22 - 07/05(14 days)

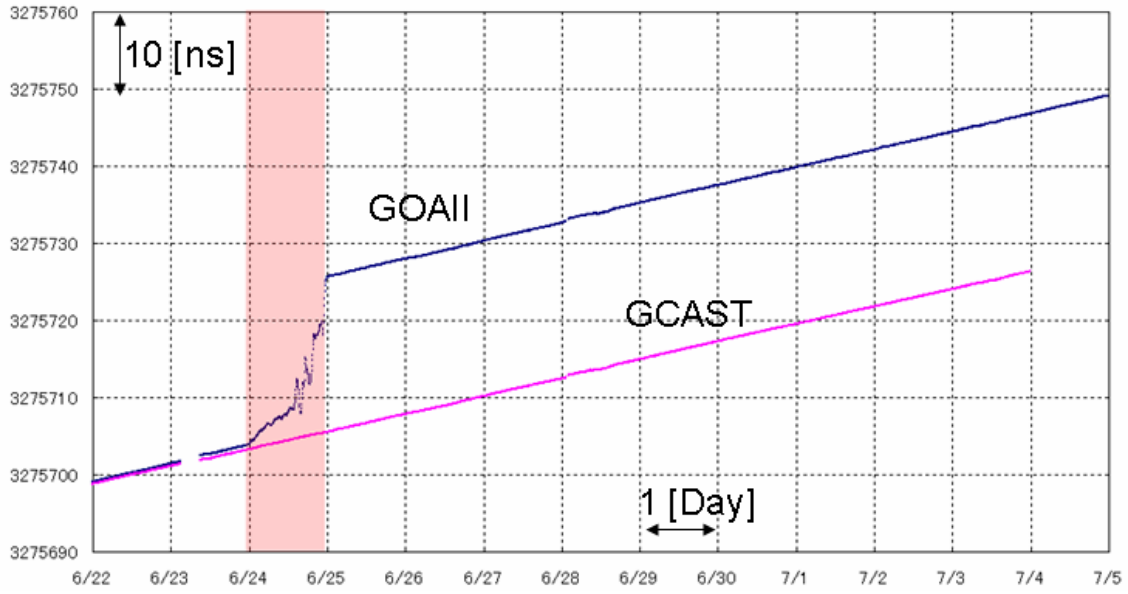

Figure 4.1(a) **Estimated result of time series for the case of the zero baseline length.**

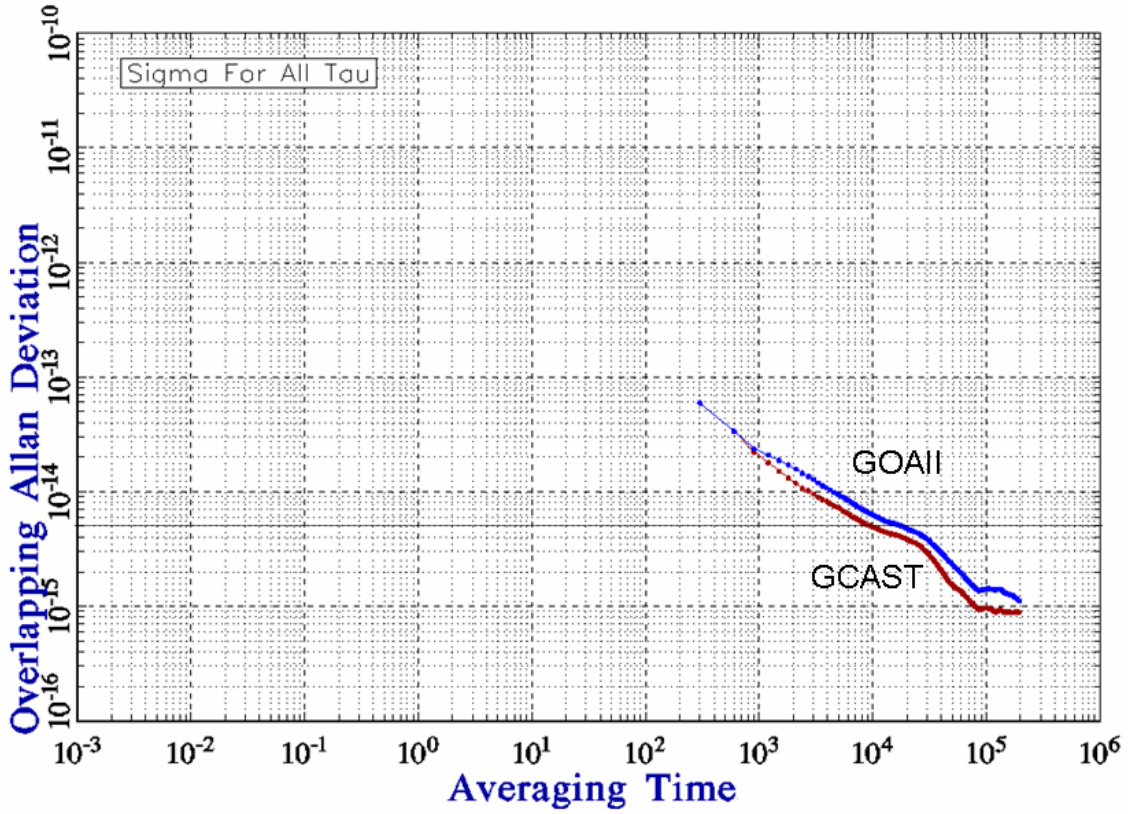

Figure 4.1(b) **Estimated result of stability for the case of the zero baseline length.**

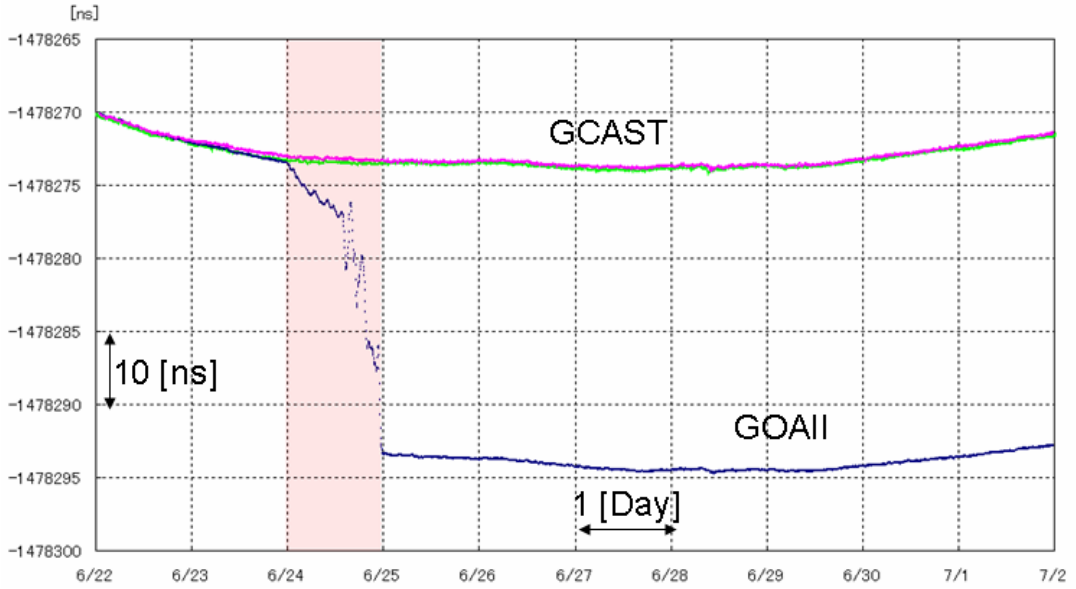

Figure 4.2(a) **Estimated result of time series for the case of the 50 km baseline length.**

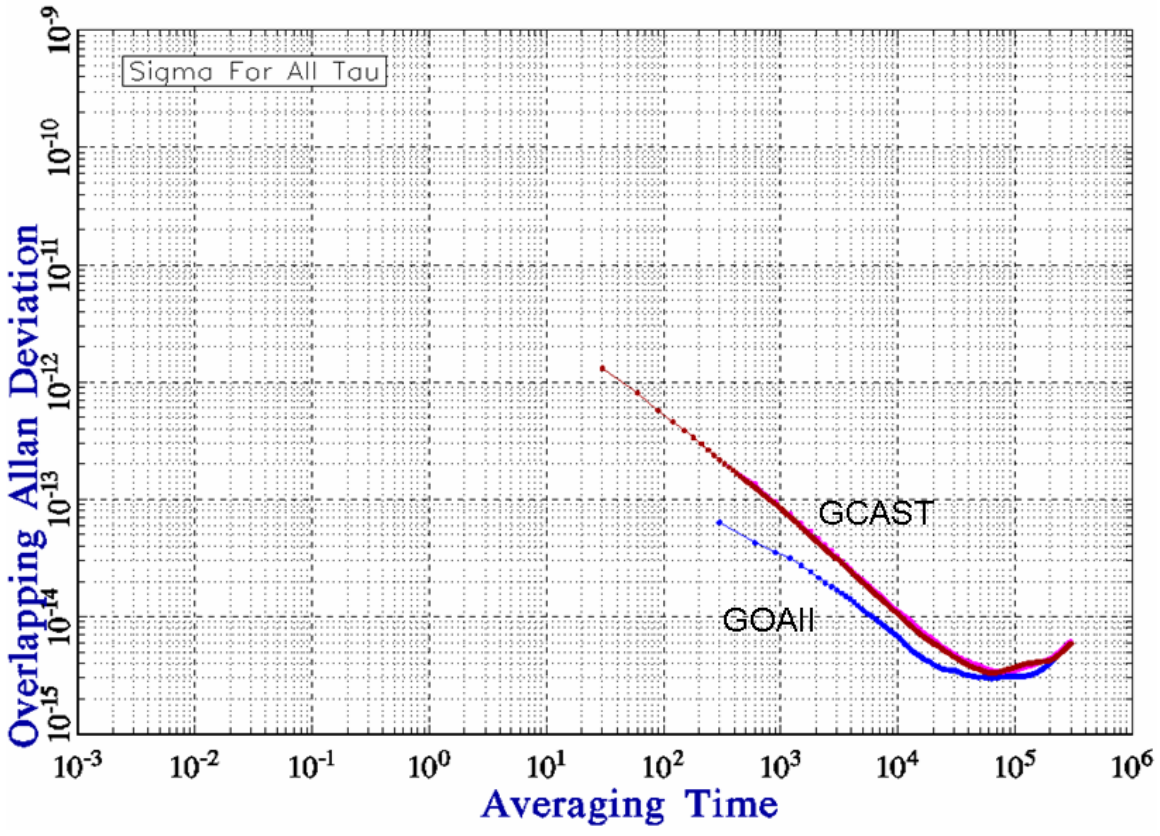

Figure 4.2(b) **Estimated result of stability for the case of the 50 km baseline length.**

Development of the Stopwatch/Timer Calibration System at National Metrology Laboratory, Malaysia.

A. Sahar Omar[#], Dr M. Nasir Z. Abidin, A. Rashid Z. Abidin and Md Noor Md Chik

National Metrology Laboratory (NML),SIRIM Berhad, Sepang, Malaysia.

([#]Email: ahmads@sirim.my)

Abstract

The National Metrology Laboratory of SIRIM Berhad has developed a straightforward and but effective measurement system that can do both stopwatch and timer measurement and calibration and traceable to the National Frequency Standard. The calibrator has been designed to work with a universal counter using a time interval measurement method. This paper will give an explanation on the system description, measurement algorithm and tests carried out to verify its performance.

1. Introduction

In support of the Legal Metrology framework in the country, the equipment used, to validate devices that are employed to charge customer according to the unit associated with the devices, are themselves required to be certified. In the field of time, we have developed a measurement and calibration facility to certify stopwatch and timer used to check parking meter and other similar devices.

Previous measurement capability for stopwatch and timer calibration at the National Metrology Laboratory of SIRIM Berhad was from one minute (sixty seconds) to any specified amount of time. It relies on images which brings a storage memory problems and difficulties to capture images for high-resolution stopwatch and timer (less than 0.1 second). However, most users use stopwatch and timer for the period of less than one minute. This limit the capability of the system.

In 2004, we designed and developed a stopwatch/timer calibrator that is reliable and simple to operate together with our existing time interval calibration system. The calibrator uses 3 timers to set Start, Stop and Range. The basic measuring principle of the calibrator is to make a simultaneous triggering, to start and stop the counting circuitry of both Standard and Device Under Test (DUT), and measuring and comparing the time interval between the events. The standard we used is Agilent 53131A connected to a 5 MHz external reference derived from a Caesium Frequency Standard. The system is capable to do measurement and calibration range of 1 to 100000 seconds for stopwatch and 0.01 to 100000 seconds for timer.

2. Measurement Set-up and Measurement Algorithm

The measurement is performed in a laboratory environment condition of $(23\pm2)^0$C and (55± 10)%RH. Figure 1 is the block diagram of the measurement system. The system consists of stopwatch/timer calibrator, universal counter controlled by PERL script running on a Linux workstation and a calibration jig. Simultaneous measurement for more than one stopwatches can be made by making a parallel connection between start/stop terminal of stopwatches and calibrator control lines using a calibration jig. For the Device Under Test (DUT) without the external start/stop terminal, a minor modification is needed as shown in Figure 2.

Figure 3 shows the measurement algorithm and the basic equation of error for stopwatch and timer calibration. During the evaluation of system performance, we found that there was a trigger delay (in microsecond) between the Calibrator and Device Under Test (DUT) and the Standard. This delay must be measured, verified and applied as a correction in the calibration

analysis. For the stopwatch calibration, the calibrator trigger delay consists of both start and stop trigger delays, whereas for the timer calibration only the start trigger delay shall be included.

3. Analysis and Calculation of Trigger Delay

The measurement set-up to determine the calibrator tigger delay is shown in Figure 5. The equipment and script used in this trigger delay measurement are the same as in Figure 1. For every single pulses triggered by the stopwatch/timer calibrator, the PERL scipt running on a Linux workstation will capture and record the time differences between the Channel 1 and Channel 2 of Agilent 53131A Universal Counter. The measurement recorded at 100 readings, which are taken as a set and repeated for six sets. An oscilloscope is used to visually verify the start and stop during the measurement sequence. Figure 6 and Figure 7 shows the waveform of the delay between the start and stop output pulses, and signal on DUT control lines, the amplitude and rise time of each signal are also recorded.

The mathematical model of this process can be given as :

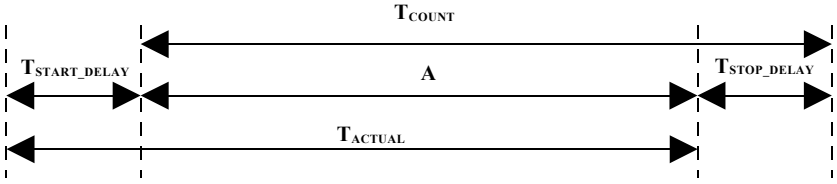

Figure 4 : Mathematical model to determine the calibrator trigger delay

Where

T_{COUNT} = Universal counter readings.
T_{START_DELAY} = Delay between the calibrator start output pulse and corresponding signal on the DUT control line.
T_{STOP_DELAY} = Delay between the calibrator stop output pulse and corresponding signal on the DUT control line.

From the Figure 4, the measurement equation is given as :

$$T_{START\_DELAY} = T_{ACTUAL} - A \quad (1)$$

$$T_{STOP\_DELAY} = T_{COUNT} - A \quad (2)$$

By subtract equation (1) and (2) :

$$T_{START\_DELAY} - T_{STOP\_DELAY} = T_{ACTUAL} - T_{COUNT} \quad (3)$$

$$T_{ACTUAL} = T_{COUNT} + T_{START\_DELAY} - T_{STOP\_DELAY}, \quad (4)$$

$$\mathbf{T_{ACTUAL} = T_{COUNT} + T_{CLT}} \quad (5)$$

Where

$$T_{CLT} = T_{START\_DELAY} - T_{STOP\_DELAY}$$

From the measurement rawdata, the mean and experimental standard deviation of the mean was calculated, and the results are as shown in Table 1. We combined both of these trigger delays to estimate the mean of calibrator trigger delay and its uncertainties.

	Mean	**Experimental Standard Deviation of the Mean (ESDM)**
Start Trigger Delay	6.84×10^{-5}	2.2×10^{-7}
Stop Trigger Delay	6.10×10^{-7}	2.3×10^{-8}

Table 1: Trigger delay measurement results

Table 1 shows that the calibrator trigger delay and its stability were dominated by the start triggering delay. This may be due to interconnection problems. The delay can be reduced by making the start and stop the delay as same as possible. We believe that we can overcome this problem by improving the connecting wires between the electronic components by using a high quality printed circuit board.

4. Conclusion

Based on the measurement results on trigger delay and its output signal waveform, basically it can be concluded that the calibrator is practically capable to directly compare the stopwatch readings and the time interval counter. In principles, this calibrator can work together with any time interval counter from different manufacturer. Further improvement is needed at the calibrator triggering signal especially in rise time and signal-to-noise ratio.

In 2005, the stopwatch and timer calibration services using this method was reviewed against the requirements of ISO/IEC 17025 by technical peer from National Measurement Institute, Australia. Corrective actions for non-conformance raised during peer review have been made to calibration procedures and the calculation of uncertainties, and also this service has been included into NML Malaysia CMC table.

Acknowledgements

We would like to thank Dr. Bruce Warrington of National Measurement Institute Australia, who has carefully reviewed the calibration services of the Time and Frequency Laboratory, NML, SIRIM Malaysia.

Reference

Guide to the Expression of Uncertainty in Measurement 1993, first edition, ISO, Geneva.

R. E. Bently. Uncertainty in Measurement : The ISO Guide. Publication TIP P1337 CSIRO, Sydney, Monograph 1 : NML technology Transfer Series, 2003.

Fundamentals of Time Interval Measurements, Application Note 200-3, Hewlett Packard Co.

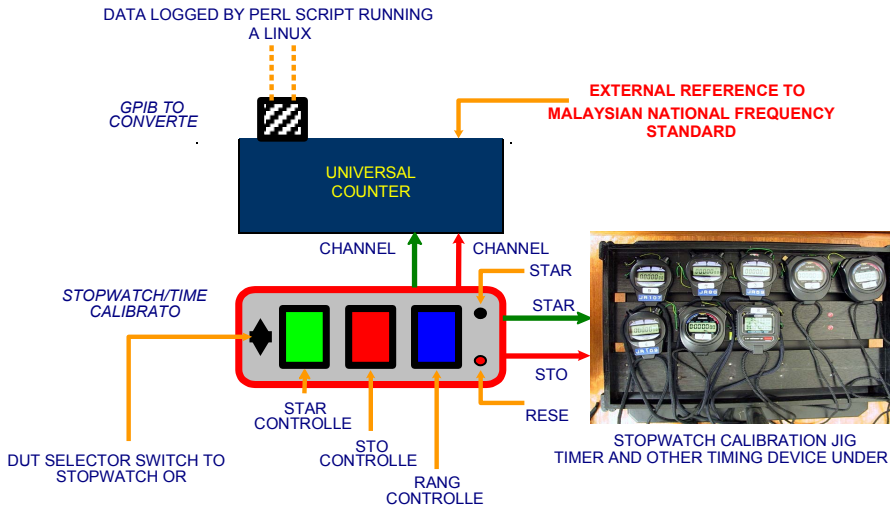

Figure 1 : Block diagram for time interval measurement and calibration of stopwatch and timer.

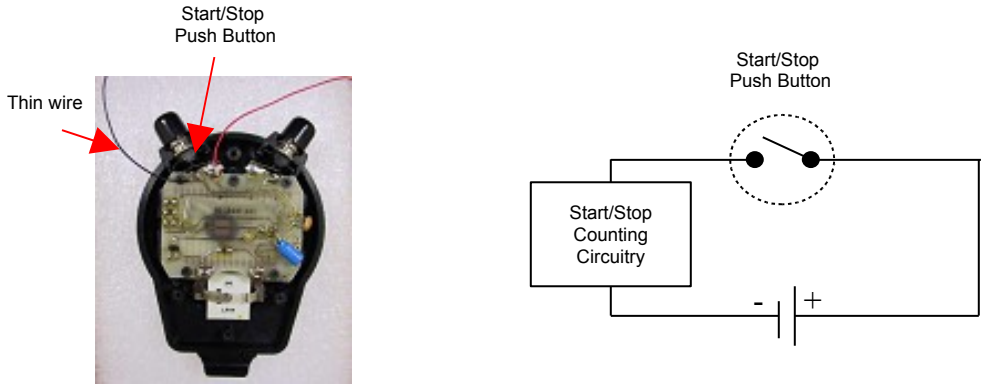

Figure 2 : Equivalent simplified diagram of stopwatch start/stop push Button.

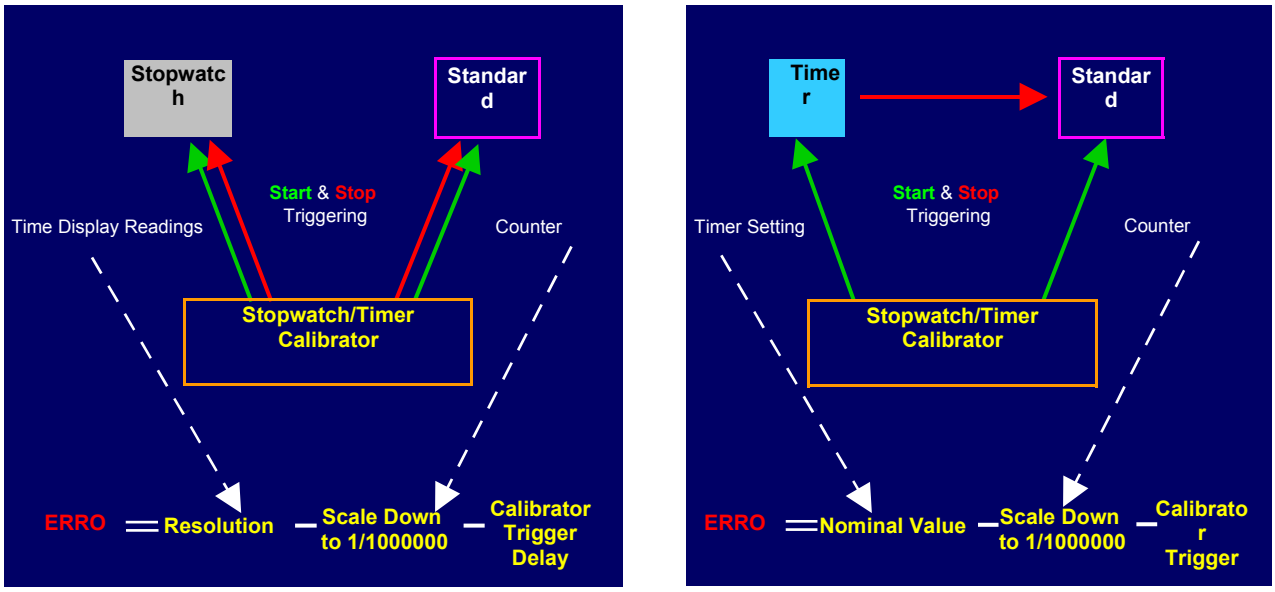

Figure 3 : Diagram of Measurement Algorithm.

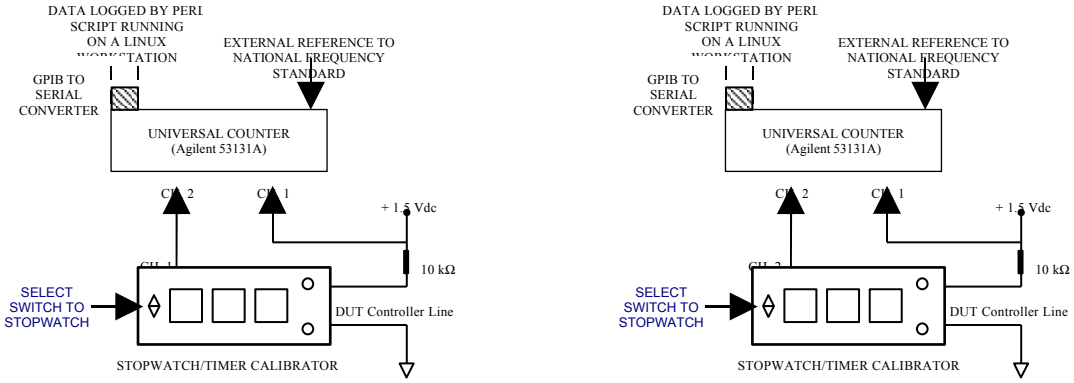

Figure 5 : Measurement set-up to determine the start trigger delay (left side) and the stop trigger delay (right side).

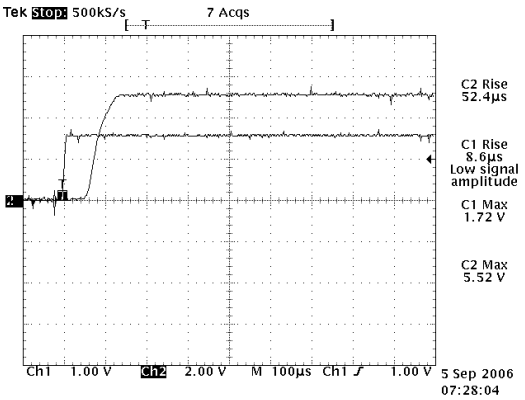

Figure 6 : Waveform captured shows the delay between the calibrator start output pulse (as C2) and the signal on the DUT control line (as C1).

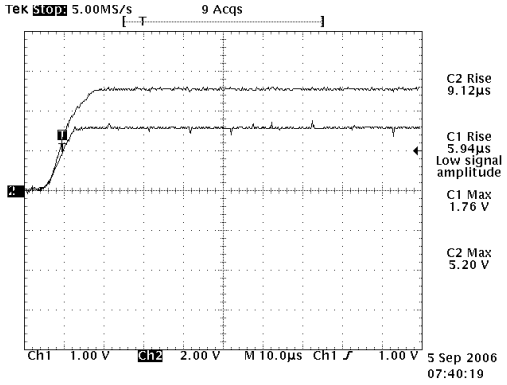

Figure 7 : Waveform captured shows the delay between the calibrator stop output pulse (as C2) and the signal on the DUT control line (as C1).

GPS-based precise time transfer by use of hybrid estimation strategy

*Seung Woo Lee, Chang Bok Lee, Sung Hoon Yang, Young Kyu Lee, Ji Ae Han

Department of Physical Metrology, Korea Research Institute of Standards and Science (KRISS)

1 Doryong-dong, Yuseong-gu, Daejeon 305-340 Republic of Korea

Abstract

Application of the hybrid estimation strategy to the GPS precise time transfer between KRISS and other NMI's was conducted. Since GPS provides temporally dense tracking data, it is possible to accommodate the effects of the stochastic parameters involved in the GPS time transfer tightly, without worrying about filter divergence due to insufficient data. To carry out the study a hybrid time transfer software system that utilizes the GPS carrier phase and code measurements were developed. Emphasis in this study is placed on the stochastic treatment of tropospheric wet delay and relative frequency fluctuation in the time comparison solution. The performance of the hybrid time transfer solution was assessed by use of the various measures such as comparison between the time transfer solutions and that from with that obtained from the GIPSY OASIS II. In order to guard against the measurement errors that might exist only in GPS, an independent time transfer solution obtained from TWSTWT was compared to the hybrid time transfer solution also. Finally the modified Allan deviation was computed with respect to each time transfer solution in order to evaluate the resultant frequency stability and some conclusions on the hybrid estimation strategy and relative performances of various time transfer solutions were drawn.

Keywords: GPS, Time Transfer, hybrid estimation strategy.

1. Introduction

Among various time transfer methods, GPS has unique advantages of providing global tracking data with high precision, which enables continuous international time transfer. The GPS time transfer is routinely conducted against other metrology institutes in KRISS and time transfer methods such as the Two Way Satellite Time and Frequency Transfer (TWSTFT) system are utilized also. Currently the GPS CV time transfer using the ionosphere-free P code or P3 code is officially utilized by BIPM, while time transfer by carrier phase still needs more research. Since the precision that carrier phase measurements can provide is much higher than that of P code, some effects that could be safely ignored in P-code time transfer should be accounted for in order to fully utilize the precision of the carrier phase measurements. Such effects may include antenna offset of the GPS satellites, temporal variation of the receiver coordinates and tropospheric wet delay. One way to accommodate such effects is called a hybrid estimation strategy where deterministic, dynamic parameters are computed by the batch estimation and the stochastic parameters are

* Corresponding author. Tel: +82 42 868 5280, Email: swlee@kriss.re.kr (S.W.Lee)

calculated by the sequential estimation. In this paper the GPS CV time transfer using GPS carrier phase measurements was conducted to achieve a high precision GPS time transfer and the hybrid estimation technique was employed. The performance of the time transfer was investigated through actual time transfer experiments between KRISS and NMIJ in Japan. Assessment of the performance was conducted by comparing the solution time series with other solutions computed from other time transfer techniques such as TWSTFT and P3, and other GPS software packages, which is selected to be GIPSY OASIS II by JPL in this study. Emphasis in this paper is placed on the stochastic treatment on the tropospheric wet delay and frequency fluctuation.

2. Models and Strategy

The Ashtech Z12T GPS receiver that is a multi-channel, dual frequency receiver was used and Z12T is a modified version of the Ashtech Z12 and it is altered to be connected to an external oscillator such as atomic clocks. From the dual frequency measurements of Z12T the ionosphere-free pseudorange and carrier phase can be formed and Eq. (1) shows the single differenced (SD) observation equation for a receiver A and a receiver B.

$$\begin{bmatrix} \Psi_{AB} \\ \Phi_{AB} \end{bmatrix} = \begin{bmatrix} \Psi_{IF,A} - \Psi_{IF,B} \\ \Phi_{IF,A} - \Phi_{IF,B} \end{bmatrix} + \begin{bmatrix} \varepsilon_{\Psi,AB} \\ \varepsilon_{\Phi,AB} \end{bmatrix}, \quad \begin{bmatrix} \Psi_{IF} \\ \Phi_{IF} \end{bmatrix} = \begin{bmatrix} \rho + T \cdot m(el) + c \cdot (\delta t_R - \delta t^S) \\ \rho + T \cdot m(el) + \lambda N + c \cdot (\delta t_R - \delta t^S) \end{bmatrix} + \begin{bmatrix} \varepsilon_{\Psi} \\ \varepsilon_{\Phi} \end{bmatrix} \quad (1)$$

In Eq. (1) the SD geometric range term, the SD integer ambiguity and part of tropospheric delay which remains constant in a data batch were considered as deterministic parameters so they are estimated in the weighted least squre estimation, while the time-varying tropospheric wet delay and frequency fluctuation are considered as stochastic parameters. The stochastic parameters listed in the above are modeled by use of the random walk process, which can be written as

$$\begin{aligned} T_{AB}(t) &= T_{AB}(t-\tau) + w_1(t) \\ \frac{dt^j_{AB}}{\tau}(t) &= \frac{dt^j_{AB}}{\tau}(t-\tau) + p_0 + w_2(t) \end{aligned} \quad (2)$$

Eq.(2) is used for stochastic modeling and the other models utilized in the study are summarized in Table 1.

3. Results

The GPS data of six days from 06/01/20 to 06/01/26 were selected to form single-differenced measurements between KRISS and NMIJ. As a relative measure of acuracy a comparison with other GPS time transfer solutions such as GIPSY OASIS II developed by NASA JPL was conducted. Six 1-day arcs of data were generated with 30 seconds

spacing and processed with each software package and the solutions were plotted together. As shown in Table 1, the IGS finalized GPS orbits were used as data in orbit interpolating. The noise statistics was determined based on the stability of the batch time transfer solution.

Table 1 Summary of GPS Models

Models	
Troposphere	MTT model
Ionosphere	Dual frequency correction applied
Integer Ambiguity	Estimated
Relativistic Correction	Applied
Phase Wrap-Around	Applied
GPS Orbits	Interpolated to IGS finalized orbits
Troposphere	Random Walk
Frequency Noise	Random Walk

It can be observed in Fig. 1 that overall trend of time transfers solutions agrees well with each other. Table 2 summarize the bias and RMS of time difference between each time transfer solutions. As can be in Table 2 the agreement between GIPSY and GV4 is better than 0.1 ns in an RMS sense, which is a good agreement taking into account that the noise level of the carrier phase is thought to be about 0.03 ns.

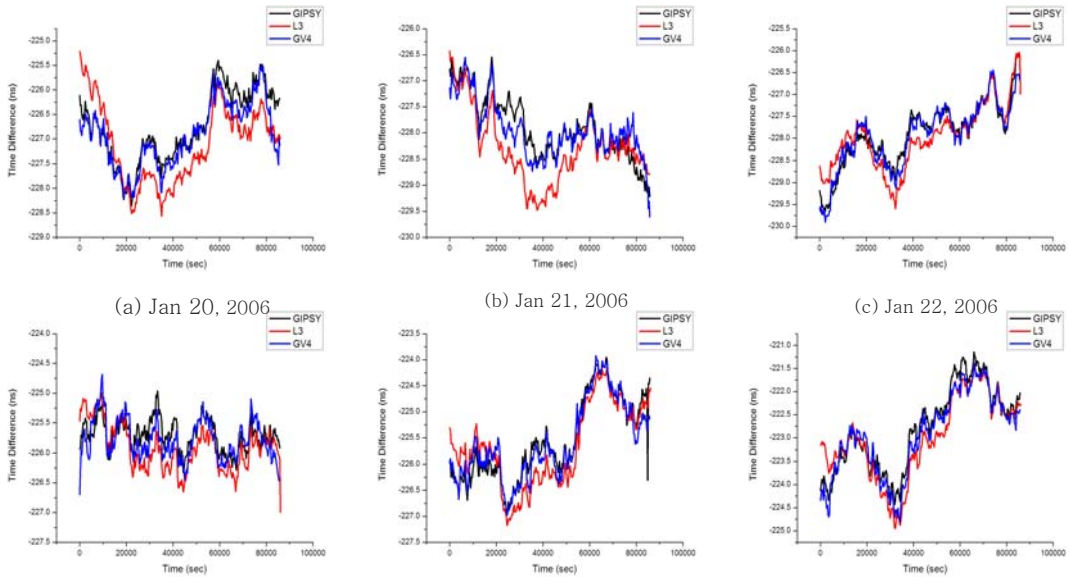

(a) Jan 20, 2006 (b) Jan 21, 2006 (c) Jan 22, 2006

(d) Jan 23, 2006 (e) Jan 24, 2006 (f) Jan 25, 2006

Fig. 1 A comparison of the KRISS-NMIJ time transfer solutions for Jan 20, 2006 to Jan 25, 2006.

Table 2 Statistics of difference between time transfer solutions

	2006/01/20		2006/01/21		2006/01/22		2006/01/23		2006/01/24		2006/01/25	
	Bias	RMS	Bias	RMS	Bias	RMS	Bias	RMS	Bias	RMS	Bias	RMS
GIPSY-L3	0.34	0.27	0.40	0.20	0.07	0.14	0.20	0.08	0.11	0.14	0.20	0.12
GIPSY-GV4	0.17	0.05	0.06	0.07	0.03	0.03	0.07	0.05	0.03	0.05	0.13	0.03
L3-GV4	0.18	0.25	0.34	0.11	0.04	0.13	0.13	0.09	0.08	0.09	0.07	0.10

Fig. 2 (a) and (b) shows results of 10-day time transfer between KRISS and NMIJ. The clock solutions obtained from GIPSY, TWSTFT and GPS P3 are plotted together for the purpose of comparison. Since TWSTFT utilizes a different transfer media from GPS it provides a independent time information and can serve as a measure to assess the performance of the GPS time transfer. It can be observed in Fig. 2 (a) that overall trend for clock solutions generally agrees well with each others. The clock solutions obtained from the GPS carrier phase generally coincide with that from TWSTFT. The clock solution obtained from GPS P3 looks noisier compared with the other solutions. Fig. 2 (b) shows the modified Allan deviation of each clock solution. It can be seen in Fig.2 (b) that noisy signature of the GPS P3 results in the highest level of the modified Allan deviation particularly for the time up to t=30000 sec. This is consistent with the notion of the Allan deviation, since the Allan deviation reflects frequency stability of a signal in the time domain, As time approaches to the end of the data span all four clock solutions seem converged to the nearly same point. Also the rate of convergence of the Allan deviation curves for GIPSY and TWSTFT looks almost same while that of GV4 becomes stabilized somewhat faster.

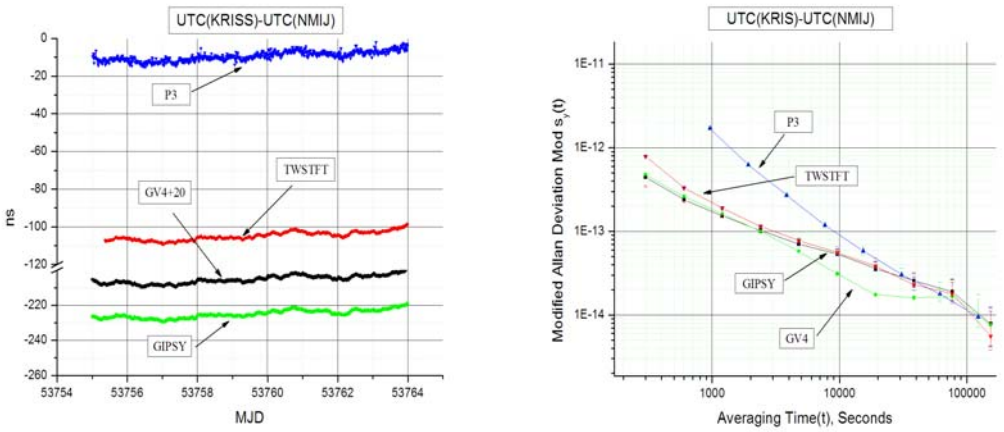

(a) (b)

Fig. 2 Results of 10-day time transfer between KRISS and NMIJ

4. Conclusions

Based on the results of actual time transfer between KRISS and NMIJ, the GPS time transfer using carrier phase measurements and hybrid estimation strategy is shown to be able to provide an accuracy and stability which are comparable to those of TWSTFT. While the TWSTFT data can be sparse sometimes and even a data outage can happen, the GPS data provide continuous, temporally dense tracking data, which makes GPS a cost-effective time transfer solution with high precision. The GV4 transfer solution agrees with GIPSY solution at the level of 0.03~0.07 ns, which is a good agreement taking into account that the inherent noise level of carrier phase signal. Based on the modified Allan deviation plot of the time transfer solution, the rate of convergence of the Allan deviation curves obtained from GIPSY and TWSTFT looks almost same while that of GV4 becomes stabilized somewhat faster, particularly in the mid-term region, while in the long-term region all the stability curves converge to the same point.

Reference

1. P. Misra, P. Enge, *Global Positioning System: Signals, Measurements, and Performance*, 2nd Ed., MA, Ganga-Jamuna Press, 2006.
2. D. W. Allan, M. A. Weiss, “Accurate Time and Frequency Transfer during Common-View of a GPS satellite,” in Proceedings of the 34th Annual Symposium on Frequency and Control, 1980, pp. 344-346.
3. C. Thomas, “Real-time Restitutioon of GPS Time Through a Kalman Estimation,” Metrologia, Vo. 29, 1992, pp. 397-414.
4. E. D. Kaplan, C. J. Hegarty, *Understanding GPS: Principles and Applications*, MA, Artech House, Inc., 2006.

HIGHLIGHTS OF 2006 ACTIVITIES OF THE NATIONAL TIME AND FREQUENCY STANDARD LABORATORY OF THE TELECOMMUNICATION LABORATORIES, CHT CO. LTD., TAIWAN

H. T. LIN, W. H. TSENG, S. Y. LIN, C. C. LIN, P. C. CHANG, and C. S. LIAO

ABSTRACT

Telecommunication Laboratories (TL) operates the Quality System in accordance with ISO 17025(since 2001) and ISO 9001(since 2000). The accreditation bodies are TAF CNLA (Chinese National Laboratory Accreditation of Taiwan Accreditation Foundation) and RWTÜV (Taiwan), respectively. TL has undergone peer assessment in 2001 and the technical assessors were from NML, Australia and CRL, Japan. On October 2004, TL passed the audit of TAF CNLA to continue the ISO17025 certification and the technical assessor was from NIST, USA.

This report covers four major activities on Time and Frequency area undertaken in TL, Taiwan:

- Reference Clocks and Time scales
  a. Reference clocks
  b. UTC(TL) and TA(TL)
- Time transfer
  a. GPS time transfer by carrier phase observables and smoothed P3
  b. Two-way satellite time and frequency time transfer (TWSTFT)
- Time Dissemination
  a. Speaking clock service
  b. Taiwan's computer time service (TCTS)
  c. Network time protocol (NTP) service
- Other activities
  a. Phase noise measurement
  b. Software radio design in frequency offset and phase noise measurements
  c. Planning of hybrid trust time stamping service
  d. Frequency proficiency test
  e. Research on intelligent RTC clock

1. Clocks and Time scales

1.1 Reference clocks

We have actually:

9- HP(Agilent)-5071A high performance cesium clocks

2- active H-masers CH1-75(Tuned).

2 AOG-110 micro-phase-steppers are used for generating the UTC(TL) and TA(TL)

1.2 UTC(TL) & TA(TL)

UTC (TL) has been derived from Cs#1712 until October 2004. In November 2004, we published an local atomic time scale TA(TL) and used this time scale with the Circular T monthly report to calibrate a hydrogen maser/micro-phase-stepper system to be our local coordinated time scale UTC(TL). In order to get the best long term stability, the TA(TL) is base on a 7~9 high-performance Agilent-5071A cesium clock ensemble, so that the UTC(TL) will follow the short-term stability of hydrogen maser and the long-term stability of cesium clock ensemble.

We compared the UTC(TL) with other Time Labs using GPSCP to verify the short-term and long-term stability of our new system, the short-term stability can achieve 4.5E-13 (τ = 300 sec) and the long-term stability can achieve 2E-15 (τ = 10 days) when compared with USNO. We also compared the frequency stability of UTC(TL) with UTC from 2001 to July, 2006 and the stability plot are demonstrated in Figure 1.

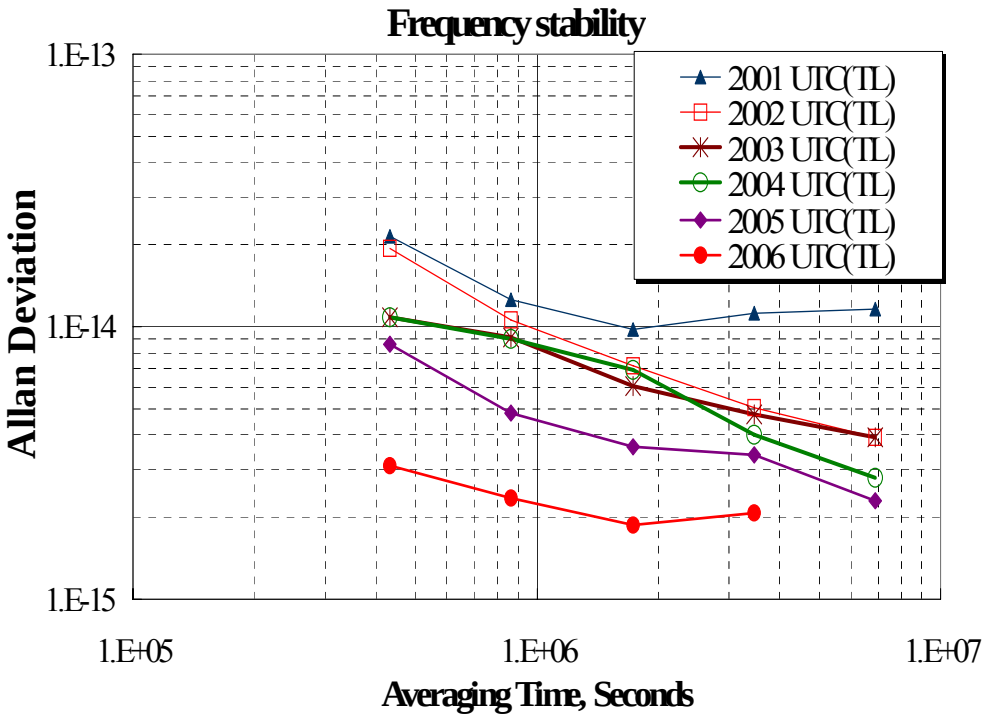

Figure 1 Stability of UTC(TL) from 2001 to July 2006

2. Time Transfer

2.1 GPS time transfer by carrier phase observables and smoothed P3

Due to clocks have become more precisely and accurately, the timing community is continuously seeking more precise and accurate systems to help them with synchronization. Global positioning system (GPS) is not only a navigation system, but also a reliable time-transfer system.

A GPS receiver can be programmed to display the difference between the local clock and the GPS time. GPS can easily provide the capability to allow synchronization of clocks to better than 100 ns in time.

In the technique of GPS common view, two GPS receivers (known as GPS time transfer units) simultaneously observe the same GPS satellite. Two clocks located at different sites can compare with each other by means of the GPS time derived by the two GPS receivers. Since the GPS time is common, the difference between the outputs of those two GPS receivers, programmed as mentioned above, is simply the difference between the two clocks. The technique known as GPS common view can be used to synchronize clocks over a large geographical area with uncertainty as good as 3-5 ns.

For the routine international collaboration, the Topcon/NML GPS multi-channel common-view system is operating in TL. Dual frequency data are adopted in this system and the ionospheric delay could be obtained to reduce the uncertainty of common-view comparison. Two Ashtech Z12T GPS receivers were set for the research of IGS/BIPM pilot project, and their raw observation data are sent to IGS global data center CDDIS. We also joined the BIPM-TAIP3 project. All the GPS observation data are available on TL's ftp site：**ftp://ftp.stdtime.gov.tw/pub/gps/**

We investigate the effectiveness of GPSAV and CV methods with SP3 code observables for improving the performance of time comparison. IGS products can determine and eliminate the satellite clock offset, atmospheric delays and ephemeris error. The common clock stability analysis of GPS CV method with P3 and SP3 codes are evaluated to understand the noise level. The GPS AV and CV with SP3 for middle, long and very long distant baseline laboratories were compared to calculate the effect of the stability for averaging times more than one day. The transfer noise of the GPS AV and CV with P3 and SP3 code could be determined by comparing distant laboratories with good time references.

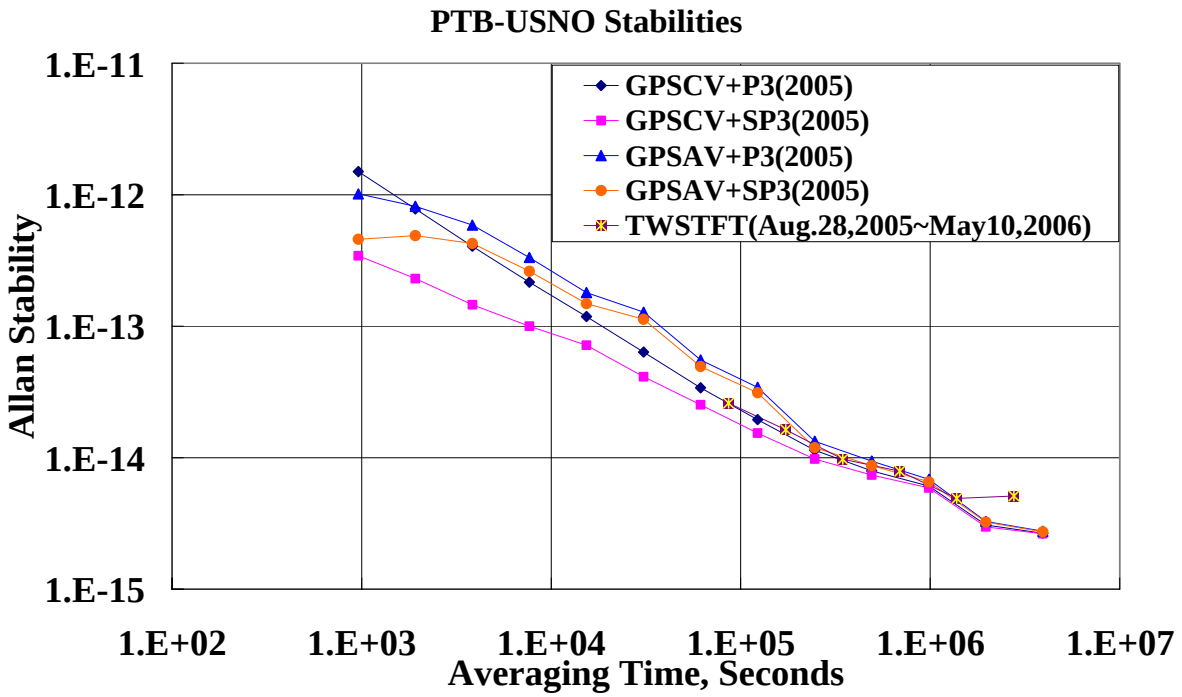

Figure 2 Calculation results of USNO-PTB by using different time transfer methods

2.2 Two-way satellite time and frequency transfer (TWSTFT)

TL has four TWSTFT earth stations. The TL-01 earth station, which point to the PAS-8 satellite, was used in NICT-TL (Dec 2002-Jun 2005) and NMIA-TL (Dec 2002-Jan 2005) links. Now the TWSTFT links through the PAS-8 is paused, and the station is currently used in the study of calibration system.

The TL-02 earth station, which point to the JCSAT-1B satellite, is used in the regular Asia-Pacific TWSTFT measurements. The data of the NICT-TL link has contributed to the computation of TAI since January 2002. From July 2005, a multi-channel NICT modem has replaced the Atlantis modem in the Asia-Pacific TWSTFT network, and TL can directly extend its TWSTFT links to NMIJ, NTSC, KRISS and SG. The NICT modem is remotely controlled by the NICT, and TL can dispense with the work of operation.

The TL-03 earth station, which point to the PAS-4 satellite, is used in the Asia- Europe TWSTFT link. The regular TL-VSL sessions (two times per week) has been performed from March 2003. In 2005, both VSL and TL have completed the automation of their TWSTFT system, and so the daily sessions have been adopted for this link. Currently, this link is paused, because the vacant space (Asia to Europe) of PAS-4 transponder was sold out and the capacity for occasional use is not available.

TL also makes much effort to extend the TWSTFT link towards North American in recent years. The C-band TWSTFT links to NMIA and NIST (WWV site in Fort Collins) had been performed from September 2002 to April 2003. The TL-04 earth station, which has 4.6 m diameter antenna and point to the NSS-5 satellite, was used for the C-band links.

However, the link was then stop for the reason of poor performance. Recently, a project of Asia-USA TWSTFT links through the earth station on Hawaii is under planning. TL will cooperate with NICT, NIST and USNO on this TWSTFT project, and it can be expected that a global TWSTFT links will be established in the near future.

TL is actively studying the delay stability of the TWSTFT earth stations. All the 70 MHz coaxial cables of our earth stations have been replaced by the phase stabilized Andrew cable this year. A calibration system with the satellite simulator has been successfully installed on one of our earth stations. The calibration system has the capability of measuring the delay variation of the earth station through a series of calibration loops. All the calibration loops with the resolution of 0.2 ns could be completed within 15 minutes. Thus, the calibration system will be helpful to improve the delay stability of the TWSTFT earth stations. In 2006, the measurements of earth station delay using a satellite simulator, including the data of using 2.5 MHz and 20 MHz chip rate coded signals is studied. The results showed that the effect of the temperature factor is obviously presented on the delay fluctuations, but the short-term and long-term temperature variations may contribute different degree of influence. A method for analyzing the correlation between the delay and temperature was proposed.

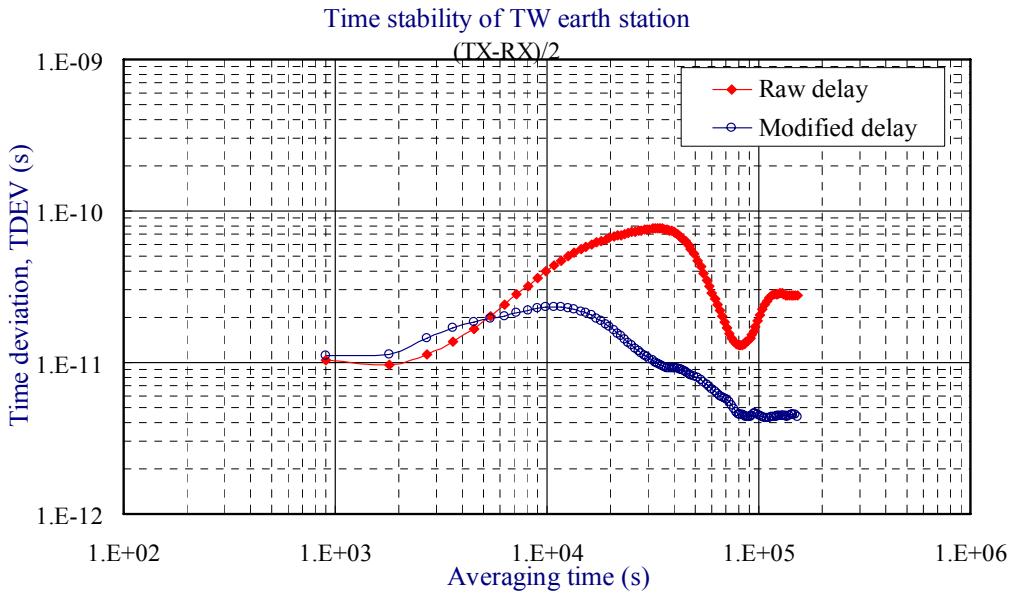

Figure 3 Correlation between the delay and temperature

3. Dissemination

3.1Speaking Clock Service

We had designed and setup a public voice time service station; it was called as 117 time service (the dialing number is 117). This system can provide accurate voice time signal to public users, and the time difference between voice time signal and UTC (TL) is less than 10 ms all over Taiwan. We use an industrial based personal computer (IPC) to develop our time synchronized speaking clock (TSSC) system. The system can trace to UTC (TL) via IRIG-B code and broadcast through PSTN automatically 24 hours a day.

3.2 TCTS Service

We had developed the Taiwan's Computer Time Service (TCTS) system, an ACTS-like telephone line service system. It is synchronized to UTC (TL) with IRIG-B time code. The "European Telephone Code" was modified into TCTS time format to match our needs, such as Lunar Calendar especially. Two modes, One-way and Loop-back, are operated. The propagation delay was measured precisely and compensated by Loop-back mode, which accuracy can reach the range of 1 ms around Taiwan island. Up to now, we have launched 2 TCTS systems with 8 lines, 5 speeds via the telephone line for public since 1998.

3.3 NTP Service

One of the most important time synchronization services we provided for the populace is the Network Time Synchronization Service. This Service uses Network Time Protocol (NTP) to synchronize clocks of computers in the Internet with national standard time. NTP builds a time tracking system in a hierarchical structure. The NTP timeserver with lower hierarchy is synchronized to that with higher one. NTP can estimate the network propagation delay and compensate the effect of delay for adjusting the local computer clock. In the Internet, the accuracy of NTP is about a few tens of milliseconds. Thus, it can provide an accurate time source for most information applications, including the Time Stamp Authority (TSA) application.

TL has begun to provide the Network Time Synchronization Service since June 1998. We installed multiple NTP timeservers in our Lab. and revised a friendly client program implementing Simple Network Time Protocol (SNTP) for Windows OS environments. In addition, the monitoring system was designed to monitor our NTP services and the monitoring program was used to count the number of NTP access to our NTP timeservers. Up to July 2006, the number of NTP requests was more than 1 hundred million (100,000,000) connections per day. NTP provides an authentication option to implement the security function. However, the present version client program does not implement any authentication function. To design a powerful authentication mechanism for our NTP

system is under running.

Figure 4 real-time NTP request monitoring

4 Other Research Activities

4.1. Phase noise measurement

We have done a few works to reveal that FFT sampling may induce some unreasonable ADEV values while the numerical integration is used for the T&F conversion. These ADEV errors occur because parts of the FFT sampling have no contributions to the ADEV calculation for some τ. We have also found such errors in the commercialized software. In order to solve this problem and not to purposely skip certain values of τ, we try to change the original FFT sampling in several ways, like dividing the sampling spaces into narrower ones or shifting the FFT sampling frequency a small amount, etc. An interposition skill is used for related calculations. According to our tests, the FFT sampling with logarithmic frequency space excels the others at improving the ADEV errors.

In the analysis of spurs effects, we see that spectral density with spurs is likely to double or triple the ADEV calculated from spectral density with spurs removed, so it is important and meaningful for laboratories to reduce ac power and other periodical noises in their own environment. The power-law processes can also perform the T&F conversion with the advantage to identify different noise types in spectral density.

4.2. Software radio design in frequency offset and phase noise measurements

In the proposed system, the analog-to-digital converter (ADC) utilized a Hydrogen maser frequency standard as the clock reference, and sampled the signal of the device under test (DUT). The digital signal processor (DSP) averaged each ADC's sample to represent one of the DUT's measurements in the gate time. The DSP could average the samples and record the measurements in each gate time interval, ranging from 1 microsecond to 1 second, and could therefore measure continuous samples of the DUT. The measurement noise could be decreased, thus improving the measurement resolution, by averaging the samples. According to the measurements, the frequency difference between DUT and frequency standard could be evaluated. Because the resolution in the proposed design was inversely proportional to both the gate time and the square of the number of the samples for averaging, it was better than that of standard counters when using long gate times. Additionally, the proposed measurement system could measure a frequency stability of below one second. Since the samples could be transferred to the phase measurement, the system could measure the phase noise of the DUT. The proposed system adopts the power spectrum to analyze the phase measurement transferred from the ADC sampling data. The DSP in the proposed system could run the power spectrum 1000 times to increase the phase noise measurement resolution.

4.3. Planning of hybrid trust time stamping service

A new design of a hybrid trusted time stamping source for time stamping authority and synchronization network was planned. The proposed design will easily trace to the national metrology institute whenever needed. It is a secure trusted third party time source in IETF framework, and is also a reliable frequency source for ITU-T G.811 recommendation.

4.4. Frequency proficiency test

In order to meet the requirements of ISO 17025 and the demand of TAF (Taiwan Accreditation Body) on calibration laboratories for inter-laboratory comparisons, TL has performed the proficiency testing activities of frequency calibration laboratories in June and July of this year. A HP 8662 frequency synthesizer was used as the DUT with aging of 5E-10/day and temperature coefficient of 1.1E-10/^{o}C. The DUT was transferred to each participating laboratory together with our calibration system according to the predetermined schedule, and was measured by the lab's calibration system and ours simultaneously. Results from both systems were then compared and analyzed. There were 12 laboratories participated in this activities, including 11 accredited laboratories and one under accreditation. The "En" value was used to assess a lab's ability to calibrate equipment within its accredited level of measurement uncertainty. According to the calculation results, the absolute value of each lab's "En" is smaller than 1, which means their calibration abilities are all qualified.

4.5. Research on intelligent RTC clock

Traditionally, a computer system has a real-time clock (RTC) for its timekeeping, but the RTC cannot synchronize automatically to external time standard, and does not have self-compensated mechanism for its time draft adjustment either. Aimed at the disadvantage of the RTC clock mentioned above, we designed an intelligent RTC clock to improve its performance. A design sketch of our IRTC constructed entirely of functional blocks is shown in figure 5. Basically, it consists of two modules: the tracking module and the timekeeping module. The tracking module tracks the reference time signal derived from the Taiwan's ACTS system. Its signal is available over the telephone line. The output of the tracking module splits two directions : one is added to the loop 1 (labeled from a1 to a5) mixed with the output of the *time accumulator* at the node Σ1 which resulted in a value called time difference ; The other one is added to the loop 2 (labeled from b1 to b3) and mixed with the output of the *slop timer* at the node Σ2 which resulted in a value called drift rate. The controller calculates both values using a specific algorithm to characterize the performance of the system oscillator and then uses this characterization to estimate optimal correction values feeding to the *programmable divider*. The programmable divider produces three types of pulse: *offset, offset-interval, and slop-interval*. The offset-interval and slop-interval seriate pulses flow individually to the stuff/swallow counter. Both offset and offset-interval pulses are used timely to modify the time difference, and the slop-interval pulse is used to modify the drift rate. The stuff/swallow counter deletes or stuffs a single pulse among the pulse train generated from the *pre-scalar*. The time accumulators take the output of the pre-scalar's pulse train as its time-base to accumulate *time* and *date*.

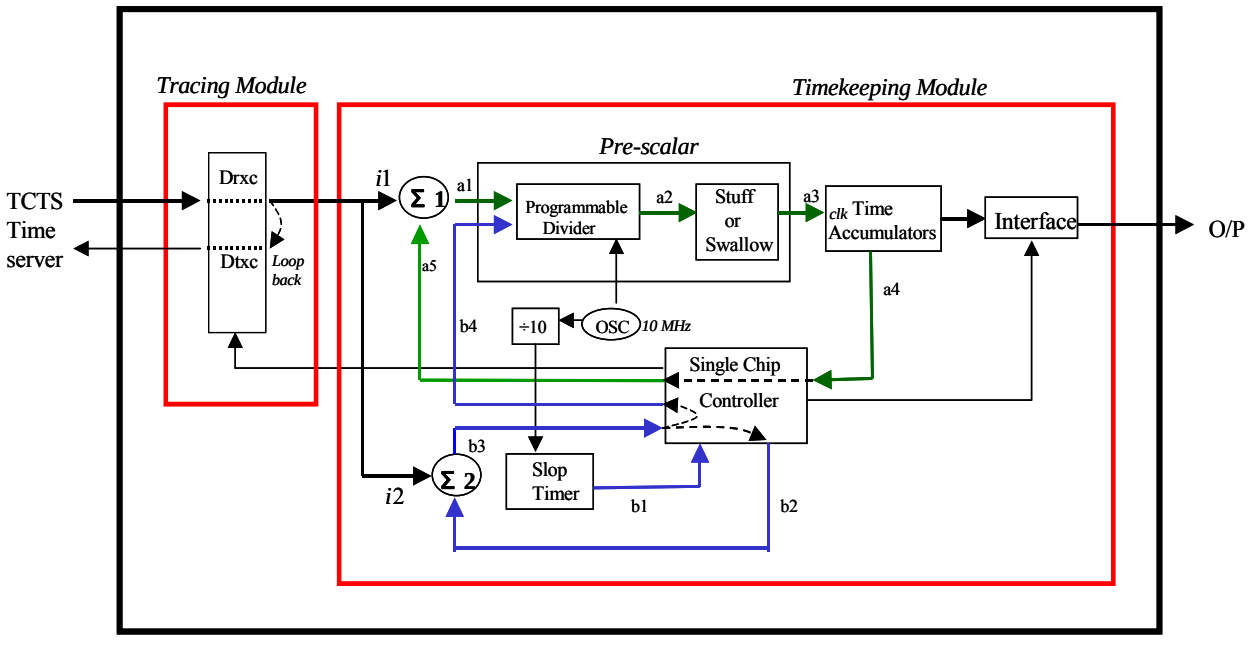

Figure 5 Block diagram of intelligent RTC clock

Improvements in Optically Pumped Cesium Beam Clock

Young-Ho Park, SooHeyong Lee, Sang Eon Park, Ho Seong Lee, and Taeg Yong Kwon*

Korea Research Institute of Standards and Science
1Doryong, Yuseong, Daejeon, 305-340 Korea

Abstract

Several key components of the atomic beam tube of KRISS-1 [1, 2] such as Ramsey cavity, fluorescence collector, Cs oven, and C-field rods have been recently redesigned to improve signal to noise ratio of Ramsey spectrum. The modified pump laser now outputs $\pi+\sigma^{\pm}$ polarized light which is frequency stabilized to F=4 to F'=3 transition line using the modulation transfer spectroscopy. Currently, short term frequency stability of KRISS-1 shows Allan deviation of $8.7\times10^{-13}\,\tau^{-1/2}$. And long term stability is limited to 5.5×10^{-15} at a sampling time of 3×10^{4} s. Enhanced magnetic field homogeneity along the drift region reduced the uncertainty in quadratic Zeeman shift to less than 10^{-15}. Aside from the hardware improvements, we have developed an alternative regularization method [3] to accurately obtain velocity distribution of Cs atoms and to measure Rabi frequency within uncertainty of 0.02%. We plan to reduce the combined standard uncertainty of KRISS-1 down to 1×10^{-14}.

1. Enhanced Atomic Beam Tube Design

We have made several modifications on the cavity design of KRISS-1. Length of the redesigned Ramsey cavity is still 36cm from one end of the interaction region (each 1cm in length) to the other (see Fig. 1). Nevertheless the length dimension of the cutoff waveguide is now increased from 15 to 30 mm while a graphite shield pipe has been installed along the drift region to decrease light scattering and unwanted interference with microwave field. The fluorescence collector unit consists of two concave mirrors (see Fig. 2), and grooves have been carved on the inner part of the graphite spacers to reduce internal light scattering.

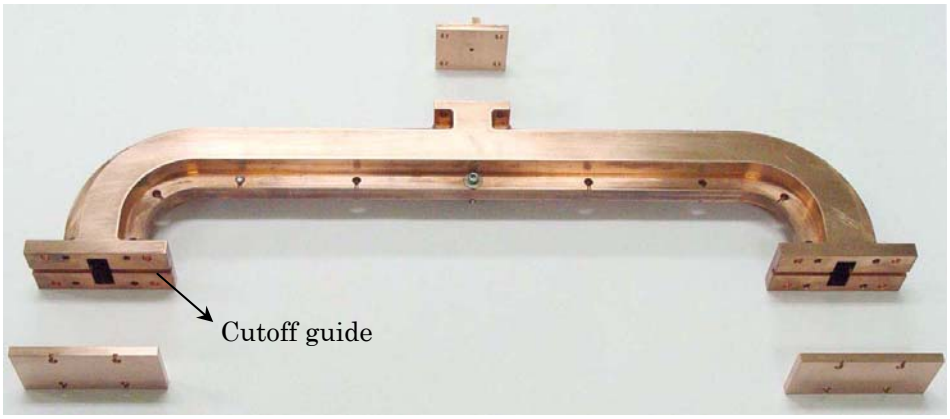

Fig. 1. Ramsey cavity of KRISS-1. The cutoff guide is lengthened to 30 mm from 15 mm.

*E-mail: tykwon@kriss.re.kr; Tel. +82-42-868-5141; Fax. +82-42-868-5287.

Fig. 2.
Fluorescence collector. The concave mirrors are made of copper. The graphite spacer has grooves on inner surface in order to reduce scattered light.

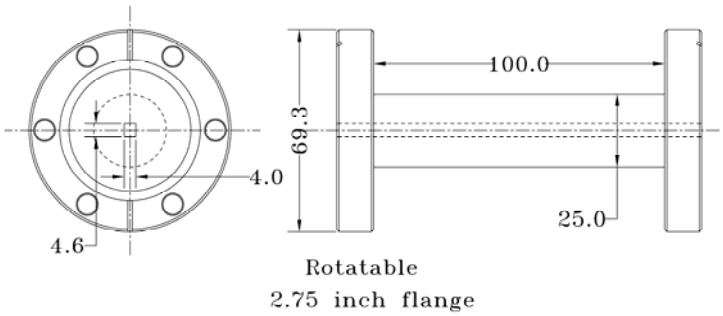

Fig. 3.
The cesium beam collimator with a 10-cm long rectangular hole.

Figure 3 shows the schematics of the Cs oven collimator that delivers the Cs atoms from the reservoir into the cavity. The cross-section of the collimator is 4 by 4.6 mm^2 and it is 10 cm in length. Under normal operation, the temperature of the reservoir is maintained at 100 ^oC while the collimator is kept at about 120 ^oC. Shape of the electric current pole is also redesigned to enhance the magnetic field homogeneity. Figure 4 shows the magnetic field distribution along the drift region before and after the installation of the modified pole. Figure 5 shows the Ramsey spectrum for m=3 transition. These comparisons show that the magnetic inhomogeneity is reduced from 1 % to below 0.1 % and, in result, the center of the Ramsey spectrum now coincides with center of the pedestal. The frequency shift due to the inhomogeneity in magnetic field is less than 10^{-15}.

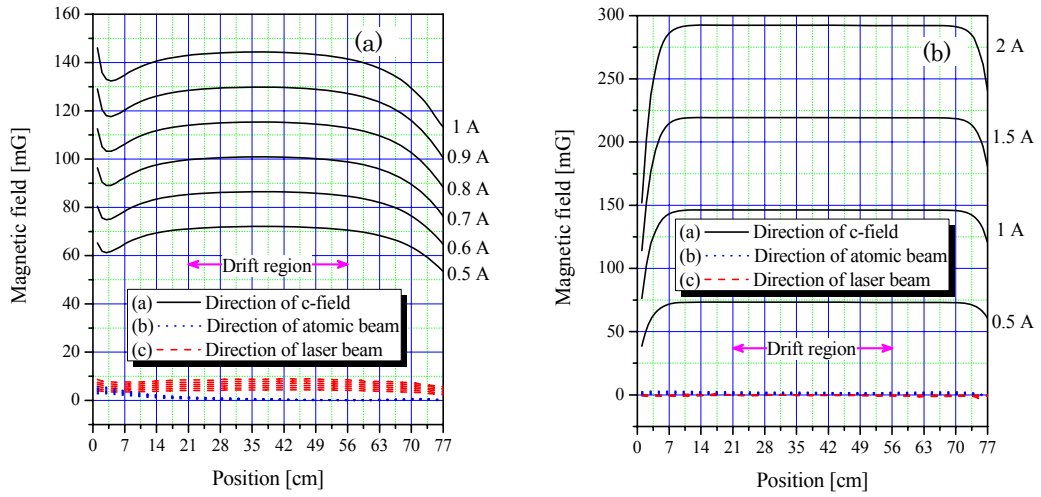

Fig. 4. Measured c-filed strength (a) before and (b) after reducing the magnetic field inhomogeneity.

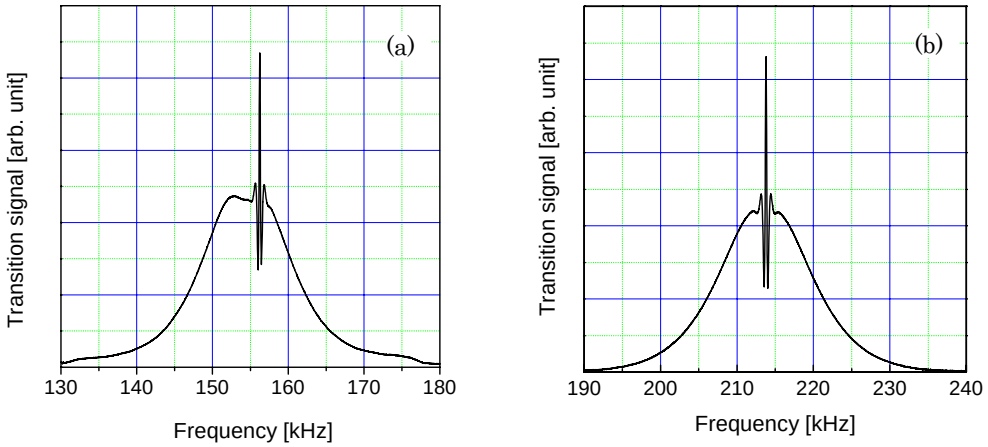

Fig. 5. Rabi-Ramsey spectrum of m = 3 transition (a) before and (b) after reducing the magnetic field inhomogeneity.

2. Regularized inverse for determining the atomic velocity distribution and the Rabi frequency

Ala'a Makdissi et al [3] adopted an inverse approach to obtain atomic velocity distribution inside a Ramsey cavity. In this method, given an accurate Rabi frequency value, the velocity distribution is calculated from single Ramsey spectrum. Shirley et al [4] took a different approach where he measured Ramsey spectrums at several different microwave powers and calculated the velocity distribution and the Rabi frequency by taking weighted average. In our work, we have developed an alternative method to deduce atomic velocity distribution and Rabi frequency simultaneously by applying regularized inverse method to Ramsey spectrums measured at two different microwave powers. In the numerical simulation, uncertainty in the calculated Rabi frequency is about 0.02 %. However, in actual experiment, the uncertainty is limited due to leveling instability of the frequency synthesizer.

Using the regularized inverse method, velocity distributions at 4 different transitions (m = 0, 1, 2, 3) of KRISS-1 are obtained (See Fig. 6). Different areas under different distribution curves implies that there are significant variations in density of Cs atoms that resides at each Zeeman sublevels. The transit time distributions from neighboring Ramsey spectrums enable us to obtain correct shape of Rabi-pedestals of neighboring transitions and calculate Rabi pulling shift.

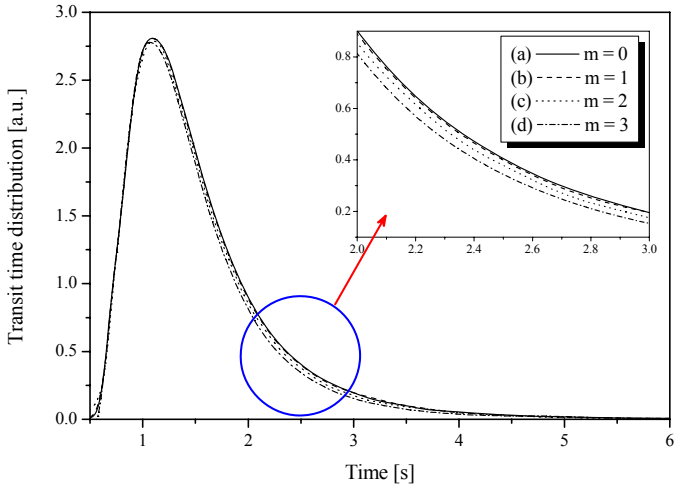

Fig. 6.
Transit time distributions for the clock transition and the neighboring transitions.

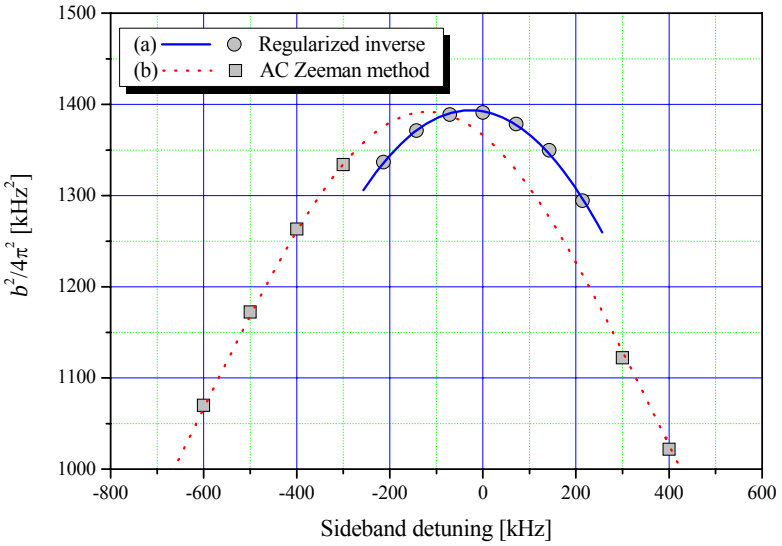

Fig. 7.
Cavity response function measured from
(a) regularized inverse and
(b) ac Zeeman method.

Figure 7 shows the cavity response function respect to the input microwave frequency. (a) is the response function obtained from a set of 7 Rabi frequencies at each transition of m=0, ±1, ±2, and ±3. Each Rabi frequency value obtained from our regularized inverse method is divided by relative transition strength of each transition and plotted against the corresponding frequency to obtain the shape of the response curve. (b) is the response function obtained from AC Zeeman method by injecting off-resonant microwave into Ramsey cavity [5, 6]. Slight shift of center frequencies in these two measurements is due to ambient temperature difference at the time of the experiments. We note that AC Zeeman method requires an extra frequency synthesizer to make the measurement. Most importantly, only the off-resonant frequency components can be measured by AC Zeeman method. On the other hand, the regularized inverse approach only requires Ramsey spectrums. And thus, continuous monitoring of the cavity response is possible while the atomic clock is under operation.

3. Frequency instability and systematic uncertainties

Figure 8 shows relative frequency instability of KRISS-1 when hydrogen maser was used as the reference frequency source. Short term stability at a sampling time of 1 second is 8.7×10^{-13}, which is about 4 times better than previous the measurement made prior to the modification. The long term stability is about 5.5×10^{-15} at a sampling time of 3×10^{4} s.

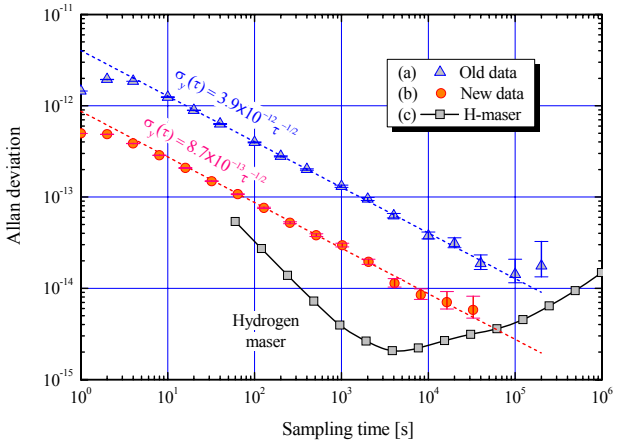

Fig. 8.
Frequency instability of KRISS-1 relative to hydrogen maser (a) before and (b) after the improvements.

Table I displays the uncertainty evaluation result for KRISS-1. There are certainly improvements due to redesigned hardware such as C-field inhomogeneity and light scattering. However, more importantly, considerable improvements are made in shift parameters that depend on accurate deduction of Rabi frequency values and atomic velocity distributions. At current state, most significant sources of frequency shifts are cavity phase and light scattering, which limit the combined systematic uncertainty of KRISS-1 to 1.2×10^{-14}.

Table I. Relative frequency biases and their uncertainties (preliminary results).

Physical Effect	Shift × 10^{14}	Uncertainty × 10^{14}
Quadratic Zeeman effect	46837.5	0.1
C-field inhomogeneity in drift region	1.48 → 0	0.1 → **0.042**
Resonance inhomogeneity*	0	0.23 → < **0.1**
Quadratic Doppler effect*	-31.1	0.28 → **0.05**
Cavity pulling*	0	0.52
Bloch-Siegert shift*	0.35	0.04 → **0.0002**
Rabi pulling*	0	0.2 → < **0.05**
Gravitational shift	0.95	0.1
Blackbody radiation	-1.64	0.02
End-to-end cavity phase*	406.5	2.4 → **0.7**
Fluorescent light shift*	-	< 0.3
Scattered light shift*	7.8	3.5 → **0.8**
Combined type B uncertainty		4.3 → **1.2**

*: bias depending on the transit time distribution and the Rabi frequency.

4. Conclusion

Atomic beam tube and Ramsey cavity of KRISS-1 have been redesigned and reassembled recently. Homogeneity of the static magnetic field was increased by reshaping the rods for c-field current. Several components such as graphite shields and spacers were added to reduce light scattering. Cs oven now consists of an I-nipple with a 10cm long rectangular hole, an elbow, and a pinch-off tube. Furthermore, we developed a method, regularized inverse approach, to derive the atomic velocity distribution and Rabi frequency of the atomic clock much more accurately. The regularized inverse approach offers a diagnostic tool for measuring cavity response and atomic population in Zeeman sublevels, which are essential for calculating the cavity pulling and Rabi pulling shifts. In overall, both type-A (statistical) and type-B (systematic) uncertainties were reduced by hardware and software improvements. We expect to lower the combined uncertainty of KRISS-1 down to less than 1.0×10^{-14} in near future.

References

[1] H. S. Lee, S. H. Yang, J. O. Kim, Y. B. Kim, K. J. Baek, C. H. Oh and P. S. Kim, Metrologia, 1998, **35**: 25-31.

[2] H. S. Lee, K. J. Baek, T. Y. Kwon, and S. H. Yang, IEEE Trans. Instrum. Meas., 1999, **48**: 492-495.

[3] Ala'a Makdissi and Emeric de Clercq, IEEE Trans. Ultrason. Ferroelectr. Freq. Control, 1997, **44**: 637-642.

[4] Jon H. Shirley, IEEE Trans. Instrum. Meas., 1997, **46**: 117-121.

[5] C. Fertig and K. Gibble, IEEE Trans. Instrum. Meas., 1999, **48**: 520-523.

[6] Young-Ho Park, Cha-Hwan Oh, Pill-Soo Kim, Taeg Yong Kwon, Sang Eon Park, Sang-Kyung Choi, and Ho Seong Lee, IEEE Trans. Instrum. Meas., 2005, **54**: 780-782.

MAGNETO-OPTICL TRAP OF YTTERBIUM ATOM FOR AN OTPICAL LATTICE CLOCK

Chang Yong Park*, Sang Eon Park, Taeg Yong Kwon, Eok Bong Kim, and Ho Suhng Suh

Korea Research Institute of Standards and Science 1Doryong, Yuseong, Daejeon, 305-340 Korea

Abstract

We report on ultra high vacuum and a cost-effective magneto-optical trap (MOT) of ytterbium atom by using diode lasers as a pre-step for an optical lattice clock [1]. For the lasers of Zeeman slower, magneto-optical trap, and probe, we have built several GaN external cavity diode laser (ECDL), which has output power of 10 mW at a wavelength of 399 nm. We have trapped 5×10^6 atoms for ^{174}Yb and 2×10^6 atoms for ^{171}Yb respectively with 1.2 ~1.5 mK of cloud temperature. Our future works are discussed in order to further decrease the trapping temperature for loading in optical lattice.

1. Introduction

Recently single ion trap and neutral atoms optical lattice trap are examined as the most probable environments for realizing most precise optical and RF frequency standards. Optical lattice made with magic wavelength has the merit in providing ensemble of millions of quantum absorber with compensated ac Stark shift for clock transition [1], while it has shorter lifetime (usually 1 s) than single ion trap does (several month), because of shallow potential depth to resist against collisions between trapped atoms and molecules in vacuum chamber. This lifetime affects to the coherence time of atoms trapped in lattice, which limits the uncertainty of measurement. Thus it is sure that long-lived optical lattice will be one of critical factors in near future.

The first condition to achieve long lifetime is to make ultra-high vacuum at least below the pressure of 10^{-9} torr. However usual trap system has a conflict in that to load atom to trap potential it needs a little high atomic flux but to keep it long time it needs extremely low pressure. To solve this problem several creative trap systems are developed, for example double MOT and magnetic transport. They are really good systems except for their complexity. In this paper we introduce even conventional magneto-optical trap system equipped with oven and Zeeman slower can be kept in UHV pressure of 10^{-9} torr just with careful design. We reported the increase of trap lifetime with new design compared to the lifetime of our former trap system [2].

The transition frequencies of Ytterbium atoms (399 nm, 556 nm, 578 nm) are difficult to obtain in a cheap way. Thereby we introduce our cost-effective laser systems in this report. Especially GaN diode laser system for laser cooling and trapping of ytterbium atom is stabilized in robust system.

2. Experiment setup

For magneto-optical trap equipment of ytterbium atoms we followed the conventional design composed of an oven and nozzle for making collimated thermal atomic beam, a Zeeman slower

to decelerate thermal atoms below the capture velocity, and a chamber for optical trapping.

In designing oven and nozzle the main object was reducing the oven temperature as low as possible. For that, well collimated atomic beam and well isolated chamber for oven are the key points. We made nozzle from a stainless steel screw bolt to have 25 holes with diameter 0.5 mm and 40 mm length by discharge drilling, as the result, the divergence angle of thermal atoms is only 0.8 degree. When atoms reach trapped region the cross section area did not exceed 1 cm^2 which is smaller than cross section area for trapping lights, by which the number of atoms that don't participate in trapping process could be minimized. The nozzle was coupled to oven by the screw on it which makes the oven chamber blocked from a next chamber except the holes on the nozzle, so that ytterbium atoms can be recycled until they go out through the nozzle. With those small considerations we could reduce the minimum temperature of oven to 350 $^{\circ}C$ to capture sufficient number of ytterbium atoms. This temperature was almost 40 $^{\circ}C$ lower than previous experiment with our old system. Because the atomic flux of chamber increases rapidly around this temperature, this reducing temperature will contribute to lower the operating pressure of MOT. The temperature of main chamber during cold oven goes down to 5×10^{-10} torr and it is becoming better as time goes on.

Zeeman slower played an important role as a component differential pumping between the trapping main chamber and the oven side chamber. Coil of Zeeman slower was wound on a 400 mm long stainless pipe having 10 mm inner diameter. The conductance for molecular flow was calculated as small as 0.2 l/s. Both sides were pumped with ion pumps. We located the ion pump for trapping chamber to face with the atomic beam flux to make atoms directly go into the ion pump without remaining in trapping chamber after passing through the trapping region. Finally, we could achieve the operating pressure of $1\sim2\times10^{-9}$ torr for trap chamber. The pressure before Zeeman slower was 5×10^{-8} torr at 350 $^{\circ}C$ and the pressure inside the oven maybe is much higher. In the previous experiment the operating pressure was $6\sim9\times10^{-9}$ torr, consequently we could reduce the pressure by almost factor 5.

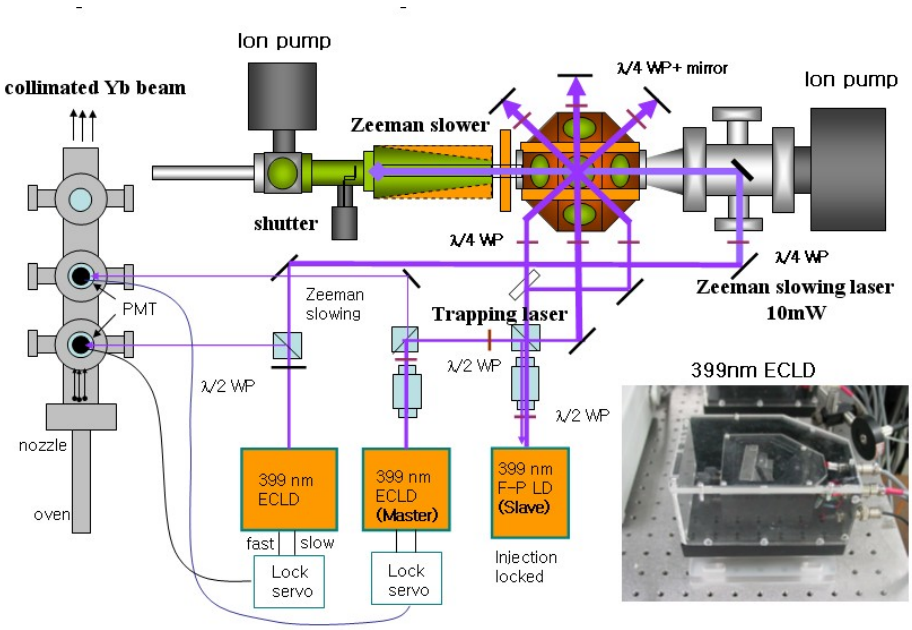

Fig 1. Magneto-optical trap system.

Zeeman slower of 40 cm length had 7 steps coil winding which gave magnetic field gradient according to σ^--configuration for Zeeman slowing where magnetic field increased along with the atomic beam direction. In this configuration filed intensity has maximum value at the exit of

the slower. In order to eliminate an extending field in the region of trap center we added another coil wound reverse direction and connected in series electrically with the slowing coil. Thus the residual field was smaller than 1 gauss.

A GaN based violet diode laser with 10 mW powers was used for Zeeman slowing light after frequency stabilizing and reducing by grating feedback. The laser was aligned to propagate counter to atomic flow and focused to have wider cross section in the exit of slower, which will compensate the momentum diffusion of atoms and help to keep the light intensity along with the slower. The frequency of the laser was locked to Doppler-free resonance signal from another collimated atomic beam. The detuning of the laser was controlled by tilting the incident angle with atomic beam. Because there exist 7 isotopes in ytterbium and the isotopes separation are several hundred MHz, we could easily found appropriate locking signals for optimal detuning of slowing laser.

Trapping chamber has 18 windows with standard 2.75 inch CF flange. On surface of the chamber there are two slots (depth 25 mm, width 20 mm) to wind anti-Helmholtz coil pair. The magnetic field gradient near the center of MOT was 30 G/ cm at 3 A coil current. Also 2 pairs of additional coils were wound over the chamber to move zero filed point to the crossover area of 6 trapping lights.

The trapping laser is the same kinds of laser used for Zeeman slowing and its frequency detuning was controlled with the same. However a small part of the laser power was amplified with the injection locking of a F-P diode laser with 20 mW, thus we could obtain 30 mW power for MOT. However the final intensity of trapping light were 2 mW/cm^2 because of loss from mirror and several optics for alignment. For keeping the injection locking status in optimal we controlled the temperature of slave laser not to change within 1 mk. Our trapping laser system is very cost-effective and reliable.

3. Experiment result & Discussion

We measured atomic flux passing the main chamber depending on temperature of oven by fluorescence detection of $^1S_0$-$^1P_1$ transition of ^{174}Yb (natural abundance 31.4 %). By rough calculation the flux of ^{174}Yb had 1×10^{10} /s at 350 $^\circ$C. The number increased to 6×10^{10} /s at 390 $^\circ$C. However the pressure of chamber increased slowly for this temperature variation, from 2×10^{-9} torr to 3×10^{-9} torr, which means our design for vacuum was successful. And by inserting smaller orifice at the entrance or exit of the slower the pressure will be reduced more.

Performance of Zeeman slower was tested by changing the frequency detuning of slowing laser and magnetic field flux. The velocity distribution of the atoms could be measured by scanning the frequency of a probe laser which crossed atomic beam with 45 degree incident angle. The final velocity of atoms could be controlled by detuning of slowing laser from almost zero to near a hundred m/s. However the measured slowing range (200 m/s) was disappointing one because it was just 60 % of our expectation from a simulation (340 m/s). This result is caused by slowing laser intensity ($I / I_s = 0.1$) being attenuated inside chamber and imperfection of the magnetic field gradient control. By amplification of slowing laser with injection locking and by adding offset magnetic field coil on 7 steps gradient coil we can improve the efficiency. If the efficiency of slowing becomes better, the temperature of oven can be lowered.

In this experiment we tried to trap ^{174}Yb, ^{171}Yb isotopes among its 7 isotopes because our interesting is focused on those two isotopes for optical lattice clock experiment. We measured the lifetime and the number and the temperature of trapped atoms. For measuring number of trapped atom we used roughly calibrated PMT during the previous experiment on which fluorescence from the atom cloud was imagined by a couple of lens set. We have trapped 5×10^6 atoms for ^{174}Yb and 2×10^6 atoms for ^{171}Yb respectively.

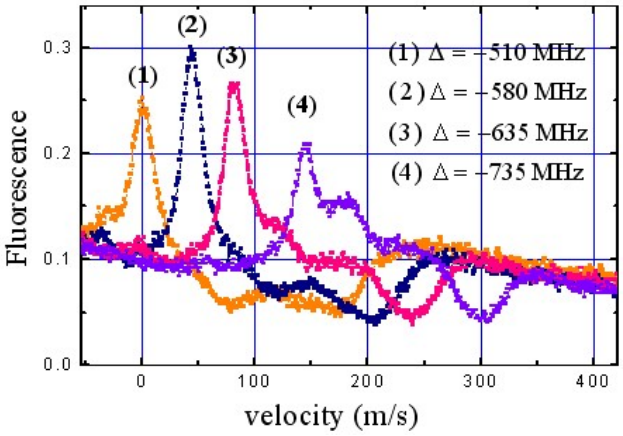

Fig. 2. Velocity distribution of slowed atoms depending on slowing laser detuning

The temperature was measured by release and recapture method where one of horizontal axis of trapping lights is turn off for 10 ms, during that time trapped atoms expand according to 1-dimensional Boltzman velocity distribution. After trapping light is turned on we can straightforwardly obtain the temperature with the ratio of remaining atom number. The measured temperature was 1.5 mK for ^{171} Yb and 1.2 mK for ^{174} Yb. This data was summarized on table 1. The decay lifetime of trapping process measured by on and off of the atomic beam shutter and Zeeman slowing laser by which we can block the loading of atoms to MOT. Consequently, we can found the decay lifetime has 1.6 s for both isotopes. In former experiment the decay time was 1.0 s for ^{174}Yb and 0.6 s for ^{171} Yb. This increase of decay time is due to the reduction of molecular collision in improved vacuum condition. Another loss process is collision between trapped atoms depending square of atom number. However measured decay time for smaller trapped atom number didn't show notable change. This loss process will be dominant for several order higher trap density. A remaining loss process is that ytterbium atom has another transition branching to $^1P_1$ - ^3D_j - $^3P_{2,0}$. Because the life times of $^3P_{2,0}$ is 20 s, if the ytterbium atom go into those states, they will fall down by gravity and finally escape from trapping potential. For Yb MOT using $^1S_0$-$^3P_1$ transition the lifetime will be limited by this process. However that kind of loss disappears in the trapping potential using $^1S_0$-$^3P_1$ transition because this transition is pure two-level system.

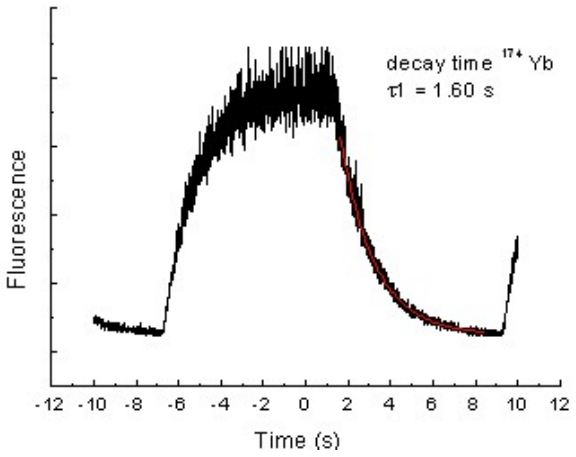

Fig. 3. Decay time measurement of Yb MOT

In our future works trapping with $^1S_0$-$^3P_1$ transition (556 nm, Doppler temperature limit ~4 μK)

is necessary in other reason. Because the potential depth of optical lattice we can make with our usable laser is just around 50~100 μK, with the cooling process using $^1S_0$-$^1P_1$ ytterbium can be loaded to lattice potential. We will make 556 nm laser form frequency doubling of 1112 nm diode laser (output power ~ 200 mW).

Table. 1. Summary of Yb MOT experiment

Isotope	Natural Abundance %	Number of trapped atom	Temperature	Lifetime	Lifetime
171	**14.3**	**2×10^6**	**1.5mK**	**1.6 s**	**0.6 s**
174	**31.8**	**5×10^6**	**1.2 mK**	**1.6 S**	**1.0 s**

3. Other future works for optical lattice clock

We are working on linewidth narrowing of diode laser with super-cavity which will be used for clock laser in future.

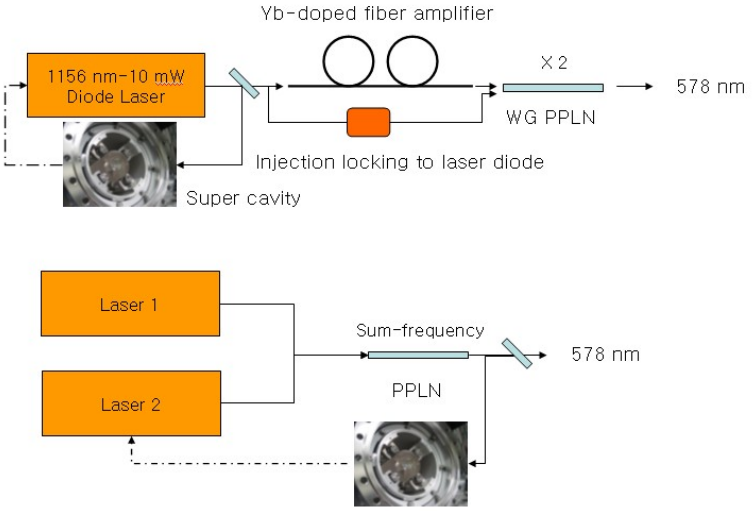

Fig. 4. Plans for building a clock laser system

4. Conclusion

We constructed a conventional magneto-optical trap system with Zeeman slower for ytterbium optical lattice clock. The lifetime of trapping process was increased from 50 % to 150 % just by careful design of oven and nozzle, Zeeman slower, vacuum system for effective differential pumping. With additional minor modifications we believe the pressure will fall down below 10^{-9} torr. We constructed cost-effective trapping laser system by using diode lasers with grating feedback and injection locking which will make ytterbium optical clock system compatible with other system based on other elements like strontium and calcium.

References

[1] H. Katori, M. TaKamoto, V. G. Pal'chkov, and V. D.Oviannikov, Phys. Rev. Lett. **91**, 173005 (2003)

[2] Chang Yong Park and Tai Hyun Yoon, Phys. Rev. A. **68**, 055401 (2003)

The New Generation System of JAPAN Standard Time at NICT

Yuko Hanado, Kuniyasu Imamura, Noboru Kotake, Fumimaru Nakagawa, Yoshiyuki Shimizu, Ryo Tabuchi, Lam Quoc Tung, Yukio Takahashi, Mizuhiko Hosokawa and Takao Morikawa

National Institute of Information and Communications Technology
4-2-1 Nukui-Kitamachi, Koganei, Tokyo 184-8795, Japan
Tel: 81-42-327-7624 Fax: 81-42-327-6694 E-mail: (yuko@nict.go.jp)

Abstract

NICT has completed a new generation system of Japan Standard Time (New JST system). There are various renewals in this system. One of the big changes is an introduction of hydrogen masers as signal sources of UTC(NICT) instead of Cs atomic clocks. This greatly improves the short-term stability of UTC(NICT). Another big change is an introduction of a newly developed 24ch dual-mixer-time-difference system (DMTD) as the main tool for measurements. A reliability of the system is also improved by enhanced redundancy and monitoring system. The New JST system has started the regular operation since February 7 in 2006, and since then UTC(NICT) is synchronized with UTC within 10ns.

1. Introduction

Japan Standard Time (JST) is generated by the National Institute of Information and Communications Technology (NICT). JST is defined as UTC(NICT) + 9 hours. UTC(NICT) is the local timescale maintained by NICT to trace UTC. NICT generates UTC(NICT) from atomic clocks at the Koganei headquarters by using a system with high measurement precision and high reliability. The first generation system of JST became operational in 1976. Since then, JST and UTC(NICT) have been maintained without large changes in the systems [1].

In 2004, a new building for time and frequency facilities was built, and on this occasion, we developed a new generation system. This system, the fifth generation, adopts various renewals in the whole system. For example, the hydrogen masers were introduced as the source clock, and the 24-ch dual-mixer-time-difference (DMTD) systems were newly developed for the highly precise measurements. Especially, it is the first experience for us to use the hydrogen masers in the JST system. The high redundancy, new monitoring system, and the modern building with various securities contribute to enhance the systems' reliability.

The project of developing a new JST system was started in 2002. In the first two years we investigated the system construction and checked the performances of devices; mainly the newly developed DMTDs. After the new building was completed in 2004, we started a development of the new system at the new building while a regular operation of UTC(NICT) was continued at the old building. In the beginning of 2006 we finished all performance check and operational tests, and the regular operation of the new JST system was started on February 7, 2006. We aimed to the synchronization with UTC within 10 ns, and it has been generally achieved since the operation started.

We presented the outline and the development status of the new JST system at the ATF2004 [2]. In this paper, we introduce the additional detail of data processing and the data in a regular operation. The principle of UTC(NICT) generation is outlined in Section 2 and the detail of new JST system is described in Section 3. The result of the regular operation is introduced in Section 4.

2. How is JST generated?

Figure 1 shows a generation procedure of JST at the NICT Koganei Headquarters. The basis of JST is the average atomic time (now it is called as "TA(NICT)") calculated from an ensemble of Cs atomic clocks [3]. TA(NICT) is calculated based on the time differences between Cs atomic clocks. Since TA(NICT) is merely a paper-clock, an oscillator is required as the source of actual signals. As this oscillator, we use the output of an atomic lock (we call it "source clock") steered by Symmetricom's Auxiliary Output Generator (AOG-110). . The 5-MHz carrier signal and 1pps signal from the AOG are used as the actual UTC(NICT) signals. The AOG is regularly steered (current interval is one day) so that UTC(NICT) traces TA(NICT). The AOG is also adjusted occasionally if the time difference between UTC(NICT) and UTC becomes large. The time difference of UTC(NICT) from UTC is measured by using GPS common-view or TWSTFT (two-way satellite time and frequency transfer) methods [4] [5]. The values of UTC - UTC(NICT) every 5 days are published in the Circular-T monthly by BIPM.

3. New JST system

The block diagram of the new JST system is shown in figure 2. Its construction is based on the configuration described in Section 2 and similar with the former JST system [1], however, various improvements are adopted in the new system as follows.

3-1. Clocks, TA(NICT) and UTC(NICT)

We have 18 Cs atomic clocks (5071A with high performance tube) and 4 hydrogen masers (RH401A, Anritsu Corp.). These hydrogen masers have auto-tuning function and show the following characteristics of the frequency stability; $\sigma_y(1\ s) \leqq 4 \times 10^{-13}$ (non-auto-tune mode), $\sigma_y(10^3 - 10^4\ s) \leqq 2 \times 10^{-15}$, and $\sigma_y(1\ day) \leqq 2 \times 10^{-15}$ (auto-tuning mode). These hydrogen masers are used as the source clock of UTC(NICT) instead of Cs atomic clocks. This change improves a short-term frequency stability of UTC(NICT) more than 10 times. The frequency stabilities of Anritsu hydrogen masers measured by the new system are shown in figure 3.

TA(NICT) is calculated from only the Cs atomic clocks. Hydrogen masers are not included in this calculation yet. The timescale algorithm is almost same as that of the former system [1]; it is based on a weighted averaging method with various parameters. We estimate the rate of a Cs atomic clock from the latest 30 days, and define the weight by the normalized reciprocal of $\sigma_y(\tau = 10\ days)$ calculated from the latest 30 days' CS-TA(NICT). Calculation interval of TA(NICT) is one hour. These parameters such as 10 days, 30days, and one hour are easily changeable.

Based on TA(NICT), we generate a real-time timescale UTC(NICT). The signals of UTC(NICT) are generated from the AOG whose source clock is one hydrogen maser. The rate of this hydrogen maser is estimated from the latest 5days' data. We adjust the AOG frequency once a day at UTC 1:20 so that UTC(NICT) traces the TA(NICT). Occasionally some offset is added to keep UTC(NICT) close to UTC.

3-2. Measurement system

In the former system, clocks' time differences were measured by a time-interval -counter [1]. The 1pps signals of the clocks were serially switched for the inputs of the counter, and their time intervals were obtained by one shot measurement. This method is, however, not adequate for the highly precise measurement of hydrogen masers.

In the new system, a newly developed 24ch-DMTD system (Japan Communication

Equipment Co., Ltd.) is a main tool for this measurement [6]. It measures the time intervals between the reference 5MHz from a hydrogen maser and the 5MHz from 24 clocks simultaneously. These 5MHz signals are down-converted into 1kHz in the DMTD to improve a phase resolution. The block diagram is shown in figure 4. Though a DMTD measures the clocks' time differences every second, we use the hourly representative value obtained by a linear fitting of 2 hours' data. The gate time and precision in each second are 100ms and 0.2ps, respectively. It is confirmed that the DMTD's system noise is lower than the hydrogen maser's frequency stability in figure 5.

Though the precisions of 5MHz measurements by DMTD are very high, it sometimes causes a phase discontinuity if the cycles are miscounted. This miscounting may occur after a data loss of a long term. In order to avoid this problem, we use 1pps measurement at a time-interval-counter together with the DMTD measurement. We adopt counter's result to define the initial phases of clocks, and accumulate the frequency obtained from the DMTD's results after that. This method is effective to obtain a high measurement precision and a reliability of the phases.

3-3. Redundancy in a system construction and a data processing

While the former JST system equipped with double redundancy in its main units [1], the new JST system has triple redundancy. The UTC(NICT) output is selected from the outputs of three AOGs. The selected AOG and its source clock are called as a master unit. If some trouble occurs in the master unit, the UTC(NICT) output is quickly switched to one of other two units. An automatic switching is technically possible, but for safety we designed the system so that human decision is required in the switching process of the main unit.

The measurement unit consists of three equivalent DMTDs and one time-interval -counter for redundancy. They make the same measurements, so their results should be equal in a normal situation. If one of them is collapsed, its result becomes different from others. The wrong device is identified by comparing these three results. This judgment and bad data removing are automatically carried out by the following procedure.

As described in section 3-2, we obtain the hourly phase data in each clock measured by DMTDs. First we calculate the frequency from the slope of two data with one hour interval.

$$f(t_2) = \{\phi(t_2) - \phi(t_1)\} / (t_2 - t_1), \qquad t_2 - t_1 = 3600s. \qquad (1)$$

Here $\phi(t_2)$ and $\phi(t_1)$ are the phase data. We get this frequency from each DMTD; f_A, f_B, f_C.(A,B,C express each DMTD). This frequency is also calculated from the data of the time-interval-counter; f_T. Next, we calculate the following value S which shows the sum of the differential from other systems.

$$\begin{aligned} S_A &= |f_A - f_B| + |f_A - f_C| + |f_A - f_T|, \\ S_B &= |f_B - f_C| + |f_B - f_T| + |f_B - f_A|, \\ S_C &= |f_C - f_T| + |f_C - f_A| + |f_C - f_B|, \\ S_T &= |f_T - f_A| + |f_T - f_B| + |f_T - f_C|, \end{aligned} \qquad (2)$$

We select the smallest two values among these four values. If DMTD-A has a trouble and its data go wrong, S_A becomes larger than other three values and will not be selected. If S_B and S_C are selected here, we adopt the average of f_B and f_C as the measurement data finally. When some trouble occurs and there is only one system's data, we adopt it as the measurement data. This method allows us to obtain a measurement result if at least one DMTD system or the time-interval-counter works correctly.

3-4. Computers, monitoring systems and environments

The various tasks are distributed to several PCs to avoid the concentration of the risks. We use Linux PCs as servers, and Windows PCs to control the devices. The measurement data and calculation results are managed by a database. The database server equips with a RAID system. The system clock is synchronized with UTC(NICT) by using NTP.

The system statuses such as room temperature and humidity, conditions of devices, and data acquisition processes, are regularly monitored and checked automatically. Check points are increased compared with the former system. Each abnormal status is notified by an alarm and an e-mail. The monitoring program working on a web browser was developed so that the system statuses are confirmed at multiple distant terminals when needed. Monitoring UTC(NICT) signals by oscilloscopes is newly introduced, which is very effective for a rapid detection of troubles.

There are four rooms for atomic clocks. The temperature and humidity in those rooms are kept at 24+/-0.5 degree and at 40+/-10% respectively. The new building equips with a dynamo and a large UPS to protect the system from sudden stop of the commercial power supply. All the electricities of the New JST system are supplied with this UPS. In addition there are also DC batteries for the atomic clocks and the main devices. They can supply the electricity to the system for several hours in the case of the building power supply stops. This building also has a high security against the invasion and a quake-absorbing structure for a high reliability.

4. Current operative situation

The new JST system started a regular operation since February 7, 2006. Figure 6 shows the time difference of UTC - UTC(NICT) reported by the circular-T. Our aim is to keep the synchronization with UTC within 10ns, and it has been achieved except one since the operation started. In the early period of this year, hydrogen masers were not so good condition. We had to change the master unit on February 27 because of a sudden breakdown of the master hydrogen maser. This change, however, did not affect UTC(NICT) and JST because the redundant units were well synchronized. The change of the master unit on March 29 was a planned one to return the system to the best situation. There was a large drift in UTC(NICT) in late June, and we added a frequency adjusting of -3×10^{-15} to trace UTC. This drift was caused by some Cs clocks' frequency changes. Additional adjusting of 1×10^{-15} was done on October 2, and now we keep UTC(NICT) almost flat against UTC.

5. Summary

The new JST system started the regular operation on February 7, 2006. in this system, various improvements are adopted. The hydrogen maser used as a source clock improves a short-term frequency stability of UTC(NICT), and the new developed DMTD system provides the highly precise measurement data. We use the 1pps measurements by a time-interval-counter together with the DMTD carrier signal measurements not to lose the phase continuity even though a system trouble occurs. The main units for generating UTC(NICT) equips with three equivalent units for redundancy. The measurements units are also constructed by three equivalent DMTD systems and one time-interval-counter. Their results are compared with each other and bad data is removed automatically. We obtain the measurement data if at least one of these four devices is correctly working. The monitoring system is improved to enhance both performance and convenience. Since the regular operation was started, UTC(NICT) keeps the synchronization with UTC within 10 ns, which satisfies the initial target of this system.

Acknowledgement

We deeply appreciate the staff effort made to maintain the UTC(NICT) generation system, and are grateful to many staff members for their helpful discussions with us.

References

[1] Y. Hanado et al, "Generating and Measurement System for Japan Standard Time", Special Issue of NICT Journal, vol.50, Number 1/2, pp.169-177, 2003
[2] Y. Hanado et al, "The New Generation System for Japan Standard Time", Proc. of ATF2004, pp.230-235, 2004
[3] Y. Hanado, K. Imamura and M. Imae, "Upgrading of UTC(CRL)", Proc. of the 2003 IEEE IFCS and 17th EFTF, pp.296-300, 2003
[4] T. Gotoh et al, "GPS Common View", Special Issue of NICT Journal, vol. 50, Number 1/2, pp.113-123, 2003
[5] M. Imae et al, "Two Way Satellite Time and Frequency Transfer", Special Issue of NICT Journal, vol.50, Number 1/2, pp.125-133, 2003
[6] F. Nakagawa, M. Imae, Y. Hanado and M. Aida : Development of Multi channel Dual Mixer Time Difference System to generate UTC (NICT)", IEEE Trans. Instrum. Meas., vol. 54, No.2, pp. 829-832, April, 2005.

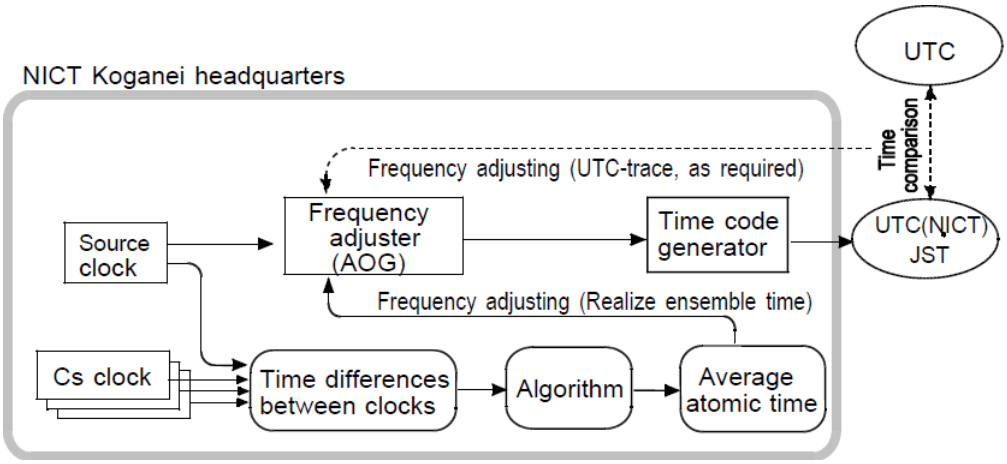

Figure 1. Generation procedure of JST.

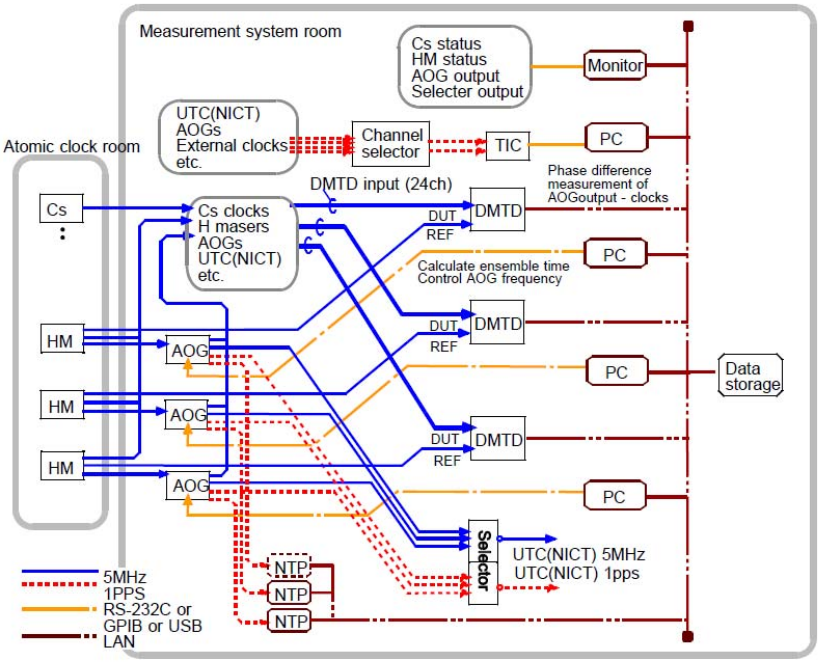

Figure 2. Block diagram of the new JST system.

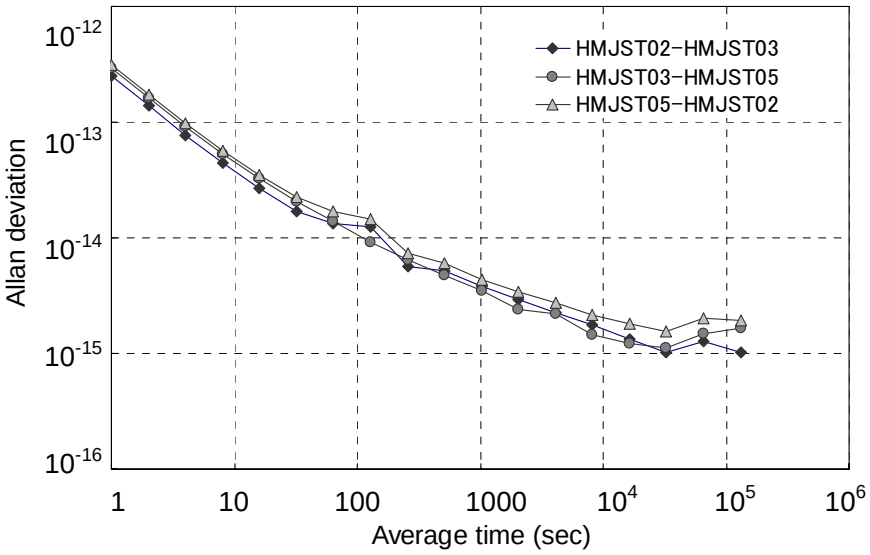

Figure 3. Frequency stability of Anritsu hydrogen masers.

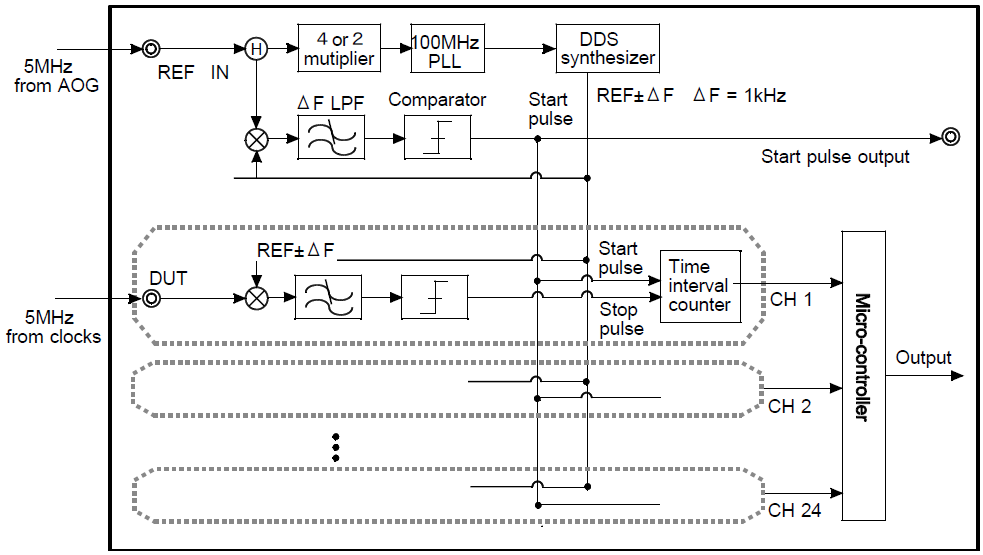

Figure 4. Block diagram of DMTD system.

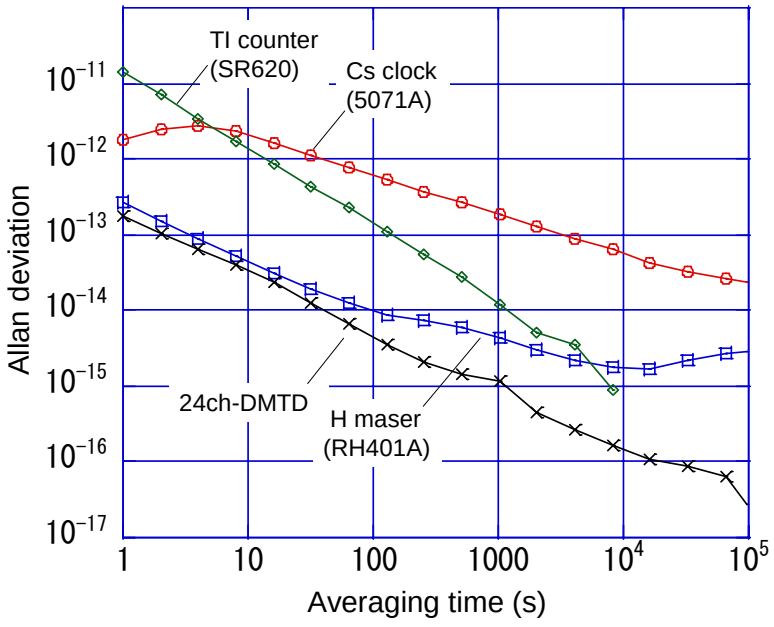

Figure 5. System noise of multi-channel DMTD system.

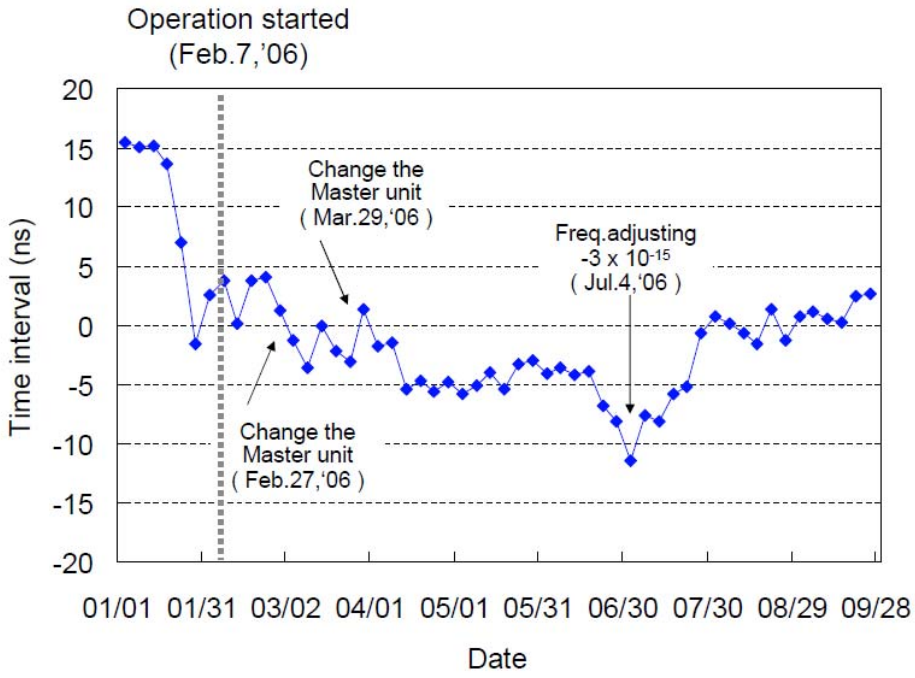

Figure 6. UTC - UTC(NICT)

NICT's Operational Atomic Fountain NICT-CsF1

Motohiro Kumagai, Hiroyuki Ito, Masatoshi Kajita and Mizuhiko Hosokawa

National Institute of Information and Communications Technology
4-2-1 Nukui-Kita, Koganei, Tokyo, 184-8795 JAPAN

Abstract

National Institute of Information and Communications Technology (NICT) has developed a cesium atomic fountain frequency standard to realize the definition of the SI time scale. Recently, we built a new atomic fountain NICT-CsF1. NICT-CsF1 has a frequency stability of $4 \times 10^{-13} / \tau^{1/2}$, and a frequency uncertainty of 2×10^{-15}.

1. Introduction

NICT has developed a Cs atomic fountain frequency standard to contribute to TAI and Japan Standard Time (JST). JST has been responsibly maintained for a long time by NICT. In 2002, we first succeeded to observe a Ramsey signal, which is narrower than 1Hz, and the preliminary results were shown in the previous workshop, ATF2002 [1]. Since then, we made several efforts to improve the SN ratio of the Ramsey signal. In 2004, we started to develop a newly designed atomic fountain frequency standard for stable practical operation. In the development, we constructed a compact and stable atomic fountain with making the most use of our experience and results with the first fountain. Furthermore, we improved the optical system and prepared stable microwave synthesizers by carefully reviewing the whole system. As a result, we have succeeded to observe the Ramsey fringes of narrower than 0.9Hz with high SN ratio [2]. We named the standard "NICT-CsF1". It has achieved frequency stability of $4 \times 10^{-13} / \tau^{1/2}$. Several frequency shifts due to the systematic effects have been evaluated. So far, the total uncertainty is estimated to be 2×10^{-15}.

In this paper, we describe the structure of NICT-CsF1 and the present status of the evaluation of its frequency shifts and the related uncertainties. And, we are preparing for a more complete and detailed paper of NICT-CsF1, which will be published somewhere.

2. System Description of NICT-CsF1

The picture and the structure of NICT-CsF1 are shown in Fig.1. NICT-CsF1 consists of three parts; a laser cooling region, a microwave interaction region and a detection region. The detection region is located between the laser cooling region and the microwave interaction region. A selection cavity, which pre-selects m_F=0 atoms, is installed just above the laser cooling region (about 8cm above the loading point). The laser cooling region consists of a trap chamber with several view ports and a pair of anti-Helmholtz coils, which produce a magnetic gradient of 100mT/m. The microwave interaction region has a C-field coil and a cylindrical microwave cavity. The cavity has a TE_{011} resonance mode, whose loaded quality factor is about 18000. The whole of this region is surrounded by three-layers magnetic shield, which produce the shielding of order 10^3. The detection chamber has three laser interaction areas where the detection beams are irradiated to the falling atoms. The highest and the lowest ports have spherical mirrors each to increase the fluorescence collection. The fluorescence light collected by each mirrors is focused on a photo detector via a light pipe. Ultra high vacuum ($<2\times10^{-7}$ Pa) for the whole system has been achieved by using two ion pumps and two NEG pumps.

Two extended-cavity diode lasers are used as master lasers. Both lasers are stabilized to

Cesium D_2 absorption by modulation transfer spectroscopy technique. Two 150mW laser diodes are injection-locked to the highly stabilized ECDL to amplify the laser power for the laser cooling. The frequency and the power of each laser beam are controlled with acousto-optics modulator (AOM). Each laser beam is delivered to the vacuum chamber through a polarization maintaining fiber (PMF). The diameters of the laser beams, which are circular-polarized, are 12mm for the vertical beams and 25mm for the horizontal beams with the power density of at least 10mW/cm^2. The other frequency-stabilized ECDL is used as repumper at the cooling and the detection.

As the source of 9.192GHz microwave interrogation, we use a synthesizer of Spectra Dynamics Incorporation (SDI CS-1). All VCXOs and DDS are phase-locked to the 5MHz of the hydrogen maser, which is linked to UTC(NICT). Controlling DDS by PC, we tune the microwave frequency with a resolution finer than 1μHz.

3. Data acquisition

Cs atoms are captured in a magneto-optical trap (MOT), and then cooled in the optical molasses. The atoms are launched upward by (0,0,1) moving molasses. After giving the launch velocity to the atoms, the launched atoms are post-cooled to about 2μK by the polarization gradient cooling (PGC). All the laser beams are turned off by AOM and extinguished by mechanical shutters after the launching. In the selection cavity, the m_F=0 components of the launched atoms (F=4) are pumped to the (F=3,m_F=0) state by the π-pulse microwave. The others in the F=4 state are blasted away by the radiation pressure of the downward beams in the vertical direction. The (F=3,m_F=0) atoms continue the ballistic flight into the Ramsey cavity. Two π/2-pulse microwave interactions at going upward and downward move the atom from the (F=3, m_F=0) state to the (F=4, m_F =0) state with following the transition probability due to the microwave frequency. To avoid the noise due to cycle-to-cycle fluctuation of the number of the launched atoms, the signal is normalized by measuring both the number of the F=4 atoms and the number of the F=3 atoms separately at the detection zone. The observed Ramsey pattern is shown in Fig.2.

To lock the microwave frequency to the narrow atomic resonance, we adopt the frequency modulation locking method, in which the microwave is toggled between f_0-Δν/2 and f_0+Δν/2, where f_0 is the microwave frequency, and Δν is the linewidth of the Ramsey fringe, at each cycle. By comparing the transition probabilities at the two frequencies, the centre frequency f_0 is steered to make the probabilities at the two frequencies equal. The amount of the steer is proportional to the probability difference. The error signal is fed back to the DDS in the 9.192GHz synthesizer. Fig.3 shows the allan deviation of the frequency difference between NICT-CsF1 and the hydrogen maser. The frequency stability of $4\times10^{-13}/\tau^{1/2}$ has been achieved, which is mainly limited by the phase noise of the hydrogen maser.

4. Systematic Frequency Shifts

The systematic shifts identified for NICT-CsF1 are evaluated with their uncertainties theoretically and experimentally. The preliminary results are summarized in Table1.

Second-order Zeeman shift

The magnetic field B in the interaction region is calculated by monitoring the (F = 4, m_F = 1) – (F = 3, m_F = 1) transition with linear dependence on B. This transition is also used to check the homogeneity of the magnetic field along the atomic trajectory. The map of the time-averaged magnetic field <B> over atomic path, from the Ramsey cavity through the apogee back to the cavity, is obtained by increasing the launching height with typical 7 mm step

(Fig. 4). The neighboring fringes adjacent to the central one are also measured to ensure its continuity. The C-field of NICT-CsF1 is typically 125 nT and the variance is 0.4 nT. The offset due to the magnetic inhomogeneity is of the order of 10^{-19}, which is negligible. The uncertainty of the second-order Zeeman shift is mainly caused by the temporal instability of *B*. In NICT-CsF1, the temporal variation of the monitored transition frequency is less than 0.5 Hz, leading to an uncertainty of less than 1×10^{-16}.

Collision Shift

The frequency shift due to collision between cold atoms is evaluated by extrapolating to zero density when amounts of the shift have a linear relation with the atomic number densities. To control the atomic density without changing the atomic cloud size, the parameters of MOT and launching are not touched at all. Only the intensity of the microwave fed to the selection cavity is controlled to vary the atomic density. In Fig.5, the map of the frequency of NICT-CsF1 against the hydrogen maser is shown by varying the atomic number density randomly from N = 0.01 to 0.55. N is the intensity of the photo detector. It is proportional to the atomic density. Linearity over a range from N = 0.01 to 0.55 has been confirmed. The slope between the fractional frequency and N is calculated as α= -32 with a variance of 7. NICT-CsF1 is typically operated at the density of N = 0.2; therefore, we estimate that a bias for the collision shift is -6.4×10^{-15} with an uncertainty of 1.4×10^{-15}. The acquisition of more data will reduce the uncertainty.

Microwave-power dependence shift

We found the microwave power dependence shift by changing the microwave field amplitude from $\pi/2$ to $9\pi/2$ (odd multiplies of $\pi/2$) in NICT-CsF1. An evaluation of the frequency shift associated with the microwave is not simple because it is related to the microwave spectral purity, the microwave leakage and the distributed cavity phase. We evaluate the shift based on Ref. 3&4, taking account for two contributions; a term proportional to the microwave power and an oscillating term proportional to the microwave amplitude. By the least square fitting, a bias for the microwave power dependence shift is estimated to be -1.3×10^{-15} with the uncertainty of 1.3×10^{-15}. As for the microwave power dependence shift, further investigation theoretically and experimentally is required.

The Other Corrected Shifts

The room for NICT-CsF1 is well temperature controlled at 297K (±0.1K). NICT-CsF1 is operated at 298K in equilibrium, and a bias due to the blackbody radiation is estimated to be -16.9×10^{-15}. Considering the thermal gradient and the thermal conductivity, we estimate an uncertainty of 0.4×10^{-15} corresponding to 2K.

The altitude of the microwave interaction region is measured as 114.7m in the GRS80 reference flame, which corresponds to 76.6m above the geoid surface. Here we used Japanese geoid model 'GSIGEO2000'[5]. The gravitational red shift is calculated to be 8.4×10^{-15}. Considering lunar and solar tidal displacement of the Earth's crust, the uncertainty in this shift is below 1×10^{-16}.

Uncorrected Shifts

The resonance frequency of the microwave cavity in NICT-CsF1 is closer (700kHz) to the clock transition. We estimate a bias for the cavity pulling shift is below 1×10^{-16}, which is negligible. From the population of m_F =0 and that of $m_F\neq0$ components, the Rabi pulling shift and the Ramsey pulling shift are calculated to be much less than 1×10^{-16}. The light shift is also negligibly small because all laser beams are blocked by some mechanical shutters during the Ramsey time. The frequency shift due to the background gas is estimated as 1×10^{-16}.

5. Summary

NICT has developed the cesium atomic fountain frequency standard NICT-CsF1. In this paper, the basic structure and the preliminary accuracy evaluation of NICT-CsF1 is reported. It has been achieved the frequency stability of $4\times10^{-13}/\tau^{1/2}$, which is mainly limited by the phase noise of the hydrogen maser. Several frequency shifts due to the systematic effects has been evaluated preliminarily. So far, the combined frequency uncertainty is estimated to be 2.0×10^{-15}.

References

[1] M. Kumagai et al. 2002, Proc. of ATF2002, 150
[2] M. Kumagai et al. 2005, Proc. of 19th EFTF, 278
[3] S. Weyers et al. 2006, to be published in Proc. of 20th EFTF
[4] K. Szymaniec et al. 2006, Metrologia, 43, L18
[5] H. Nakagawa et al. 2003, Bulletin of the Geographical Survey Institute 49, 1

Table 1. Systematic biases and their uncertainties of NICT-CsF1

Physical effect	Bias	Uncertainty
2nd Zeeman	71.3	<0.1
Collision	-6.4	1.4
Blackbody	-16.9	0.4
Gravity	8.4	<0.1
MW-power dependence	-1.3	1.3
Cavity-pulling	<0.1	<0.1
Rabi-pulling	<0.1	<0.1
Ramsey-pulling	<0.1	<0.1
Majorana	<0.1	<0.1
AC Stark	<0.1	<0.1
2nd Doppler	<0.1	<0.1
Background gas	0.1	<0.1
Total		2.0

Fig.1 Photo and structure of NICT-CsF1.

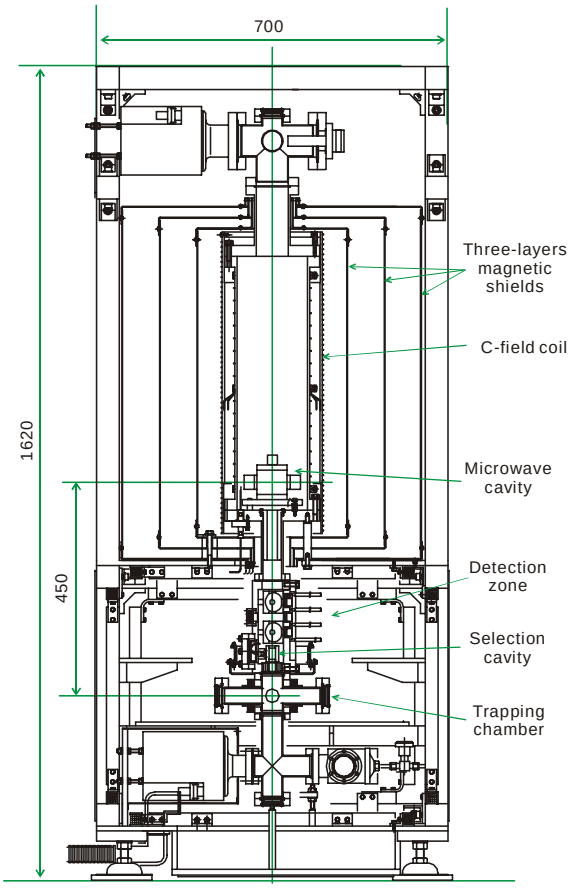

Fig. 2 Observed Ramsey fringes of NICT-CsF1. The linewidth of the central fringe is less than 0.9Hz.

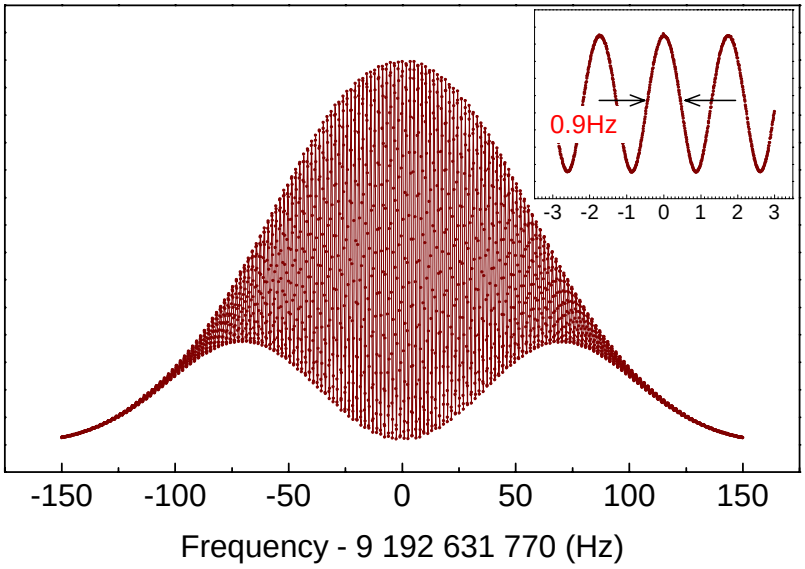

Fig. 3 Allan deviation of the frequency difference between NICT-CsF1 and the hydrogen maser. The short-term stability is limited by the phase noise of the hydrogen maser.

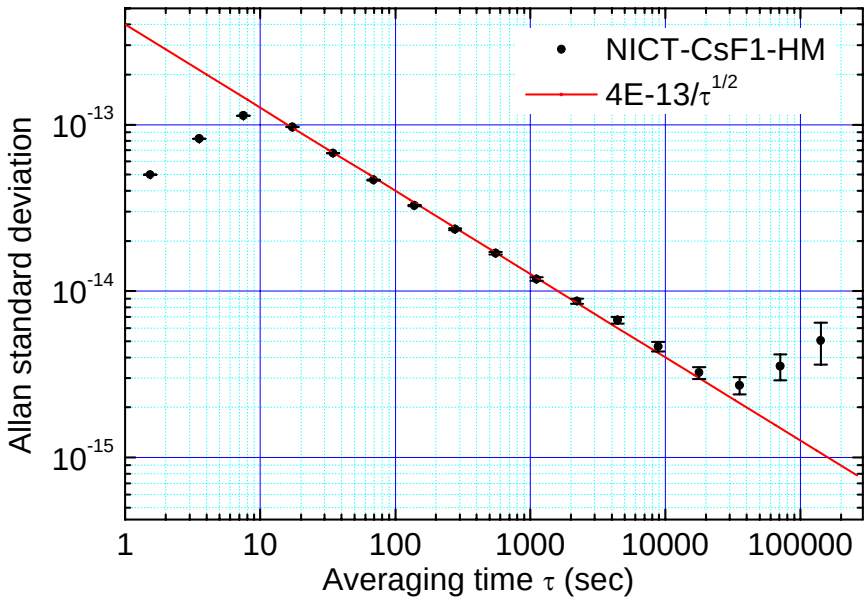

Fig. 4 Map of the time-averaged magnetic field over the atomic path with different heights. At the normal operation, the atoms are launched to a height of 39.9cm.

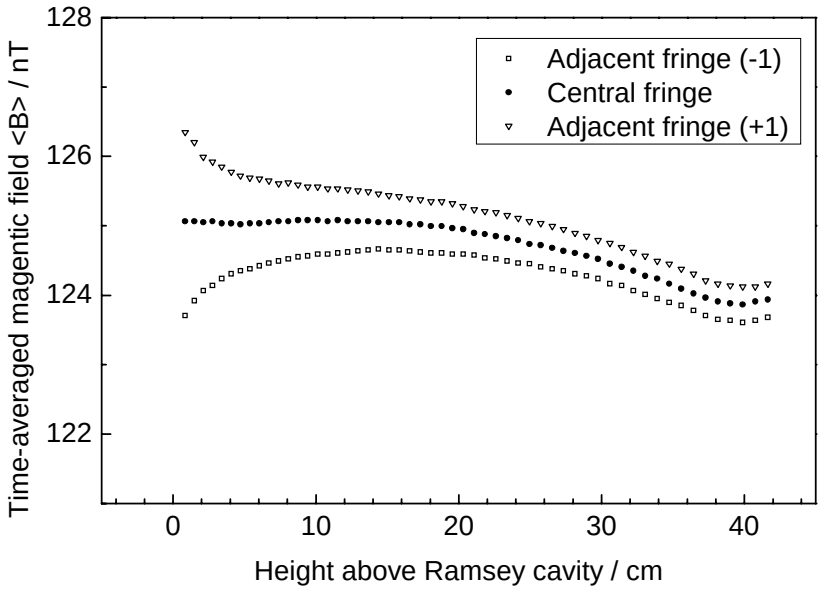

Fig. 5 The fractional frequency difference between NICT-CsF1 and the hydrogen maser as a function of the number of detected atoms. X-axis indicates the atomic number density in an arbitrary unit.

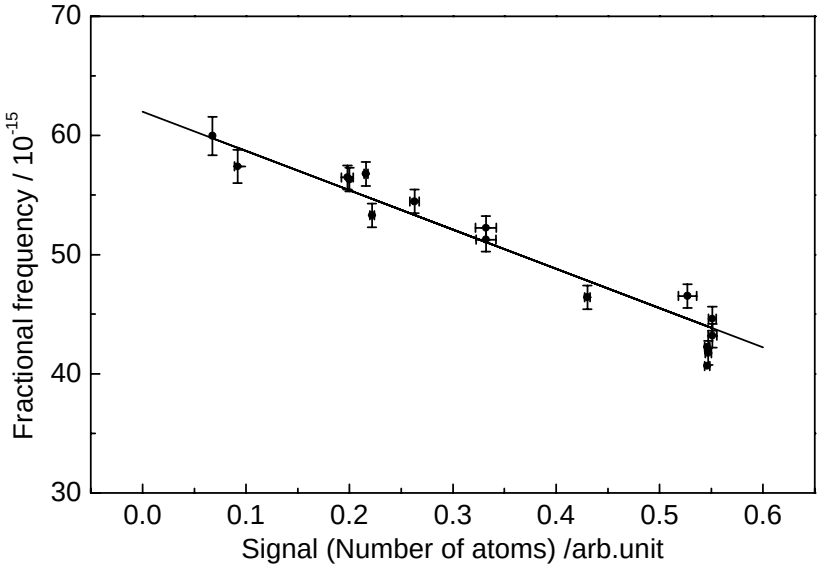

Optical Frequency Synthesis with a DBR Diode Laser Injection-Locked by Optical Frequency Comb

Sang Eon Park*, Eok Bong Kim, Young-Ho Park, Dae-Su Yee, Taeg Yong Kwon, Chang Yong Park, Han Seb Moon[1] and Tai Hyun Yoon[2]

Korea Research Institute of Standards and Science 1Doryong, Yuseong, Daejeon, 305-340 Korea

[1]*Department of Physics, Pusan National University, Busan 609-735, Korea*

[2]*Department of Physics, Korea University, Anam-Dong, Seongbuk-Gu, Seoul 136-713, Korea*

Abstract

A optical frequency synthesizer is realized by using a frequency-stabilized optical frequency comb and injection-locked distributed-Bragg-reflector (DBR) laser diode. The injection-locked DBR laser acts as a single-frequency filter and, simultaneously, a high-gain amplifier of the optical frequency comb. Frequency instability of the heterodyne beat signal between two independently injection-locked DBR lasers is measured to be 2.3×10^{-16} at 1 s averaging time. The output frequency of the sweep optical frequency synthesizer can be precisely tuned about 1 GHz and a saturated absorption spectrum of the Cs D2 line at 852 nm is recorded by the amplified single-mode DBR laser.

1. Introduction

Femtosecond laser frequency combs (FLFC) play very important roles in optical metrology.[1,2] FLFC enables the linking of a single-mode CW laser with the microwave frequency standard using an electrical phase-locking technique.[3] To do this, the signal-to-noise ratio of the heterodyne beat signal between the single-mode CW laser and the FLFC should be sufficiently high, and the frequency variation of the beat signal and the linewidth of the CW laser should be smaller than the electronic servo bandwidth. These issues can be addressed by adapting an optical injection-locking technique.[4] The amplification of the FLFC using a tapered amplifier has been demonstrated,[5] but the output spectrum was multi-mode. The optical injection-locking technique has been used for the generation of the millimeter-wave.[6]

In this report, a sweep optical frequency synthesizer using the diode laser optically injection-locked by the FLFC is realized without the use of electronics for a phase lock loop. In addition, an optical frequency of up to 1 GHz can be swept by controlling the repetition rate of a femtosecond laser. In this way, one component of the FLFC can be selected, amplified and swept while the spectral characteristics of the injection-locked laser is identical to that of the selected mode of the FLFC.[7,8]

* E-mail: parkse@kriss.re.kr; Tel. +82-42-868-5723; Fax. +82-42-868-5287

2. Experimental setup

The experimental setup of the sweep optical frequency synthesizer is shown in Fig. 1. A mode-locked Ti:Sapphire laser with a repetition rate of 1.05 GHz was used as a master laser. The center frequency and the full-width at half maximum of the FLFC spectrum were approximately 820 nm and 30 nm, respectively. The femtosecond laser was pumped by a 532 nm laser with an output power of 5.5 W. The maximum power of the femtosecond laser was approximately 700 mW. The output of the femtosecond laser was divided into two by a pellicle beamsplitter. One laser beam with a power of 60 mW was used for the optical injection-locking. The second laser beam was used to stabilize the carrier-envelope-offset-frequency (f_{ceo}) employing an *f*-to-2*f* interferometer, and the control of repetition rate frequency (f_{rep}).[1,9] A DBR (Distributed-Bragg Reflector) laser was used as a slave laser. The wavelength of the DBR laser was 852 nm, which corresponds to the frequency of the Cesium D2 line. The maximum output power of the DBR laser was 150 mW, according to the manufacturer's specifications, but it was typically operated under a power of 60 mW for this experiment. An 852.3-nm interference filter with a FWHM of 1.5 nm was used to inject the optical frequency comb near the Cesium D2 transitions and to avoid optical damage to the DBR laser. After passing through the interference filter, the power of the femtosecond laser was nearly 200 μW, which corresponds to 300 nW per mode, as the number of modes is approximately 600 within a 1.5-nm bandwidth. The injected optical power into the DBR laser was adjusted by rotating a help-wave plate. The spectrum of the injection-locked laser was analyzed by observing the transmitted signal of a high-finesse cavity. A setup of a saturated absorption spectroscopy in a cesium vapor cell was employed in order to analyze the injection-locking condition and to test the sweep optical frequency synthesizer.

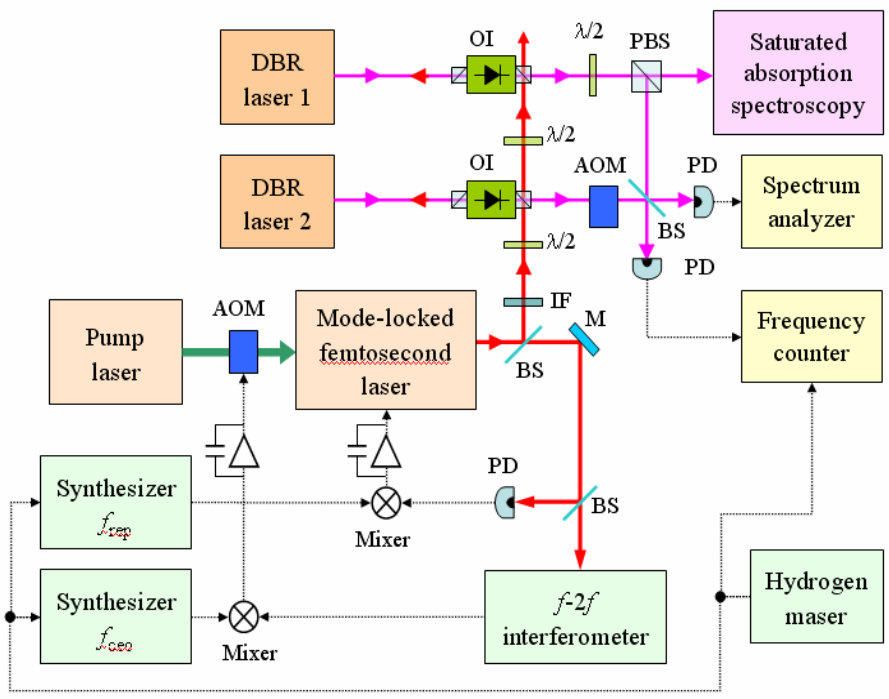

Fig. 1. Experimental setup. M; mirror: IF; Interference filter: L; lens: λ/2; half-wave plate: PP; anamorphic prism pair: OI; optical isolator: BS; beam splitter: FPC; confocal Fabry-Perot cavity: PD; photodetector.

3. Experimental results

Figure 2 shows the saturated absorption spectrum of the cesium D2 line observed by scanning the supply current of the DBR laser as the injected optical power was varied, and while the repetition rate and the carrier-envelope-offset frequency were stabilized using a microwave synthesizer referenced to a hydrogen maser. When the frequency of the free running DBR laser approached the frequency of the comb mode within a locking range, optical injection-locking is accomplished. Within a locking range, the saturated absorption signal remains unchanged, as the frequency of the slave laser is locked to one component of the optical comb. As the injection power increases, the locking range becomes wider, but an unwanted nearest side-mode is likely to be generated. Accordingly the generated side-mode intensity that depends on the injected power was investigated. Fig. 3 shows the side-mode suppression ratio separated by 1.05 GHz from the main mode as a function of the injected optical comb power by measuring the heterodyne beat power between the injection-locked DBR laser and an external cavity diode laser frequency locked to the F=4 → F'=5 transition of the cesium D2 line using modulation transfer spectroscopy. When the injected power is less than 50 μW, the relative side mode suppression is lower than -38 dB, which is not a critical level for most experimental needs single mode lasers. It is difficult to discern the coupling efficiency of injected power to a DBR laser; nonetheless, the injected power of Fig. 2 and Fig. 3 indicate the optical power of the femtosecond laser measured in front of the diode laser.

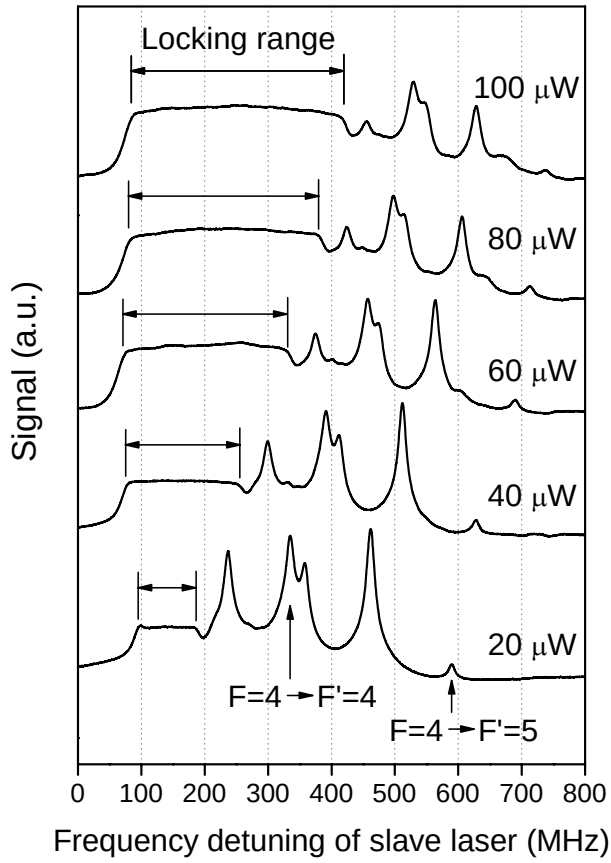

Fig. 2. The saturated absorption spectrum of the cesium D2 line as the injected optical power changes, as observed by scanning the supply current of the DBR laser while repetition rate of the femtosecond laser is stabilized. The locking range becomes wider as the injected power increases.

With a high-finesse cavity, the transmitted spectrum of a DBR laser is observed as a function of the cavity length as shown in Fig. 4. The full-width half maximum (FWHM) of the transmitted signal of the DBR laser without optical injection locking was measured to be 5 MHz, which corresponds to the linewidth of the DBR laser. When the DBR laser is optically injection-locked, the FWHM of the transmitted signal is 2 MHz, as it is limited by the finesse of the cavity. This indicates that the linewidth of the DBR laser is narrowed by optical injection locking, as the linewidth of individual comb line is narrower than 2 MHz.

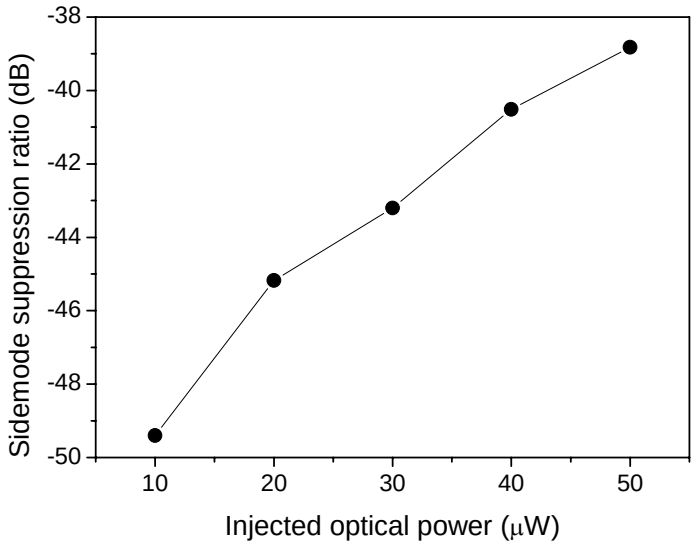

Fig. 3. Side-mode suppression ratio of the DBR laser under the injection-locked condition as a function of the injected power. The side-mode is separated by a frequency of 1.05 GHz from the main-mode.

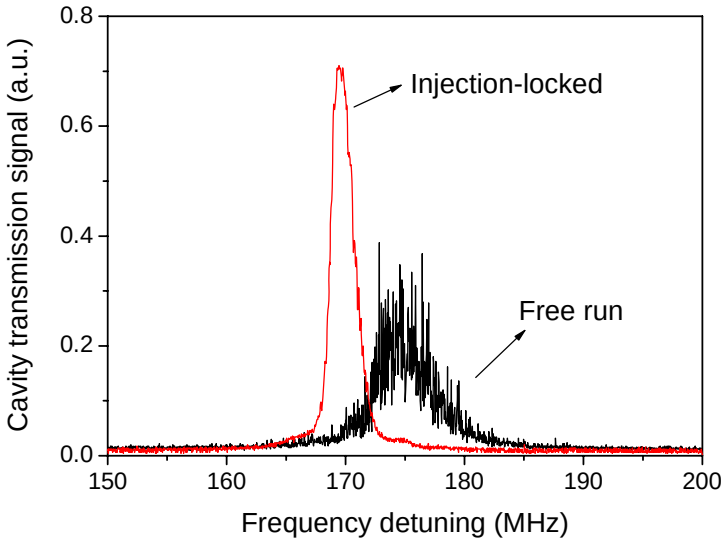

Fig. 4. The cavity transmission signal with and without (free run) optical injection-locking.

The frequency instability between two DBR diode lasers independently optical injection-locked with an identical mode of FLFC is investigated. In order to measure the heterodyne beat-note signal between two DBR lasers, the frequency of one DBR laser is shifted by 80 MHz using an acousto-optic modulator (AOM). Figure 5 shows the beat spectrum observed by an RF spectrum analyzer. The center frequency of the heterodyne beat spectrum is 80 MHz, which is identical to the driving frequency of the AOM. The measured bandwidth of the beat signal is limited by the resolution bandwidth of the spectrum analyzer. In addition, the beat frequency was measured using a frequency counter, and the Allan deviation was calculated by changing the gate time of the counter. This is shown in the inset of Fig. 5. The Allan deviation for a sampling time of 1 s is 2.3×10^{-16}, and has a $1/\tau$ dependence.

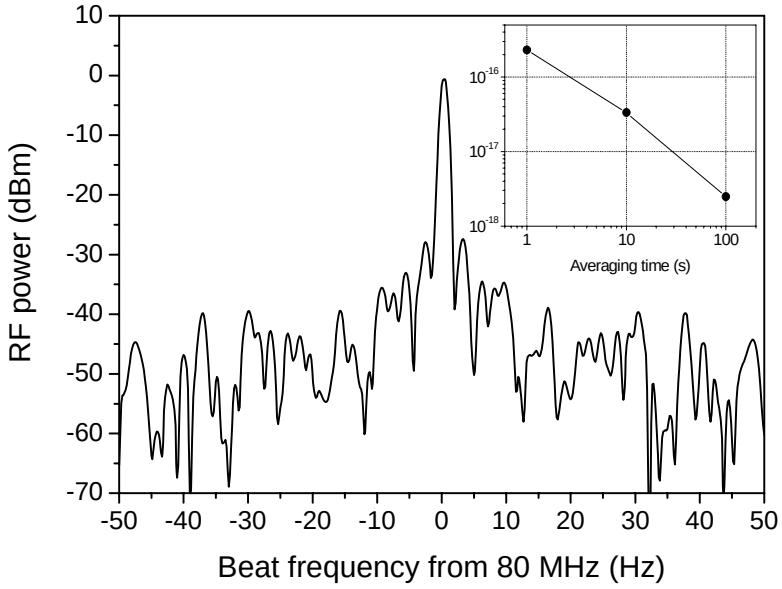

Fig. 5. The heterodyne beat spectrum and the frequency instability (inset) between two independently optical injection-locked DBR lasers with an identical mode of FLFC.

Figure 6 shows the saturated absorption signal of the cesium D2 transition observed through the use of the optical injection-locked DBR laser as a function of the repetition rate while the carrier-envelope-offset frequency is stabilized. The absolute optical frequency can be easily calculated by $f_{opt} = N \times f_{rep} + f_{ceo}$, where the integer number N is 340476, and the carrier-envelope-offset frequency is -182 MHz in this experiment. As the injection locking range is few hundred MHz, as shown in Fig. 2, the scan range over 1 GHz for the optical frequency cannot be accomplished. Thus, the supply current of the DBR laser is swept synchronously with the repetition rate in order to maintain the optical injection locking condition. The frequency interval of the repetition rate between data points is 2 Hz which corresponding to about 681 kHz in the optical frequency and each data point is the average of six samples. The acquisition time of each data point is approximately 0.3 s.

4. Conclusion

In summary, a sweep optical frequency synthesizer based on the optical injection-locking technique is demonstrated. The injection-locked DBR laser acts as a single frequency filter and amplifier. The characteristics of the injection-locked DBR laser are

analyzed. We anticipate that an injection-locked DBR laser with single frequency component of optical frequency comb generator would allow a precise measurement of optical frequency with high signal-to-noise ratio and would be used as an essential component of optical frequency synthesizer for the sub-kHz laser spectroscopy in the future optical lattice clock. Moreover, accurate optical frequency measurement and precision spectroscopy for a multi-level atomic system would be possible when two or more DBR lasers are optically injection-locked to the different components of one cavity-stabilized optical frequency comb.

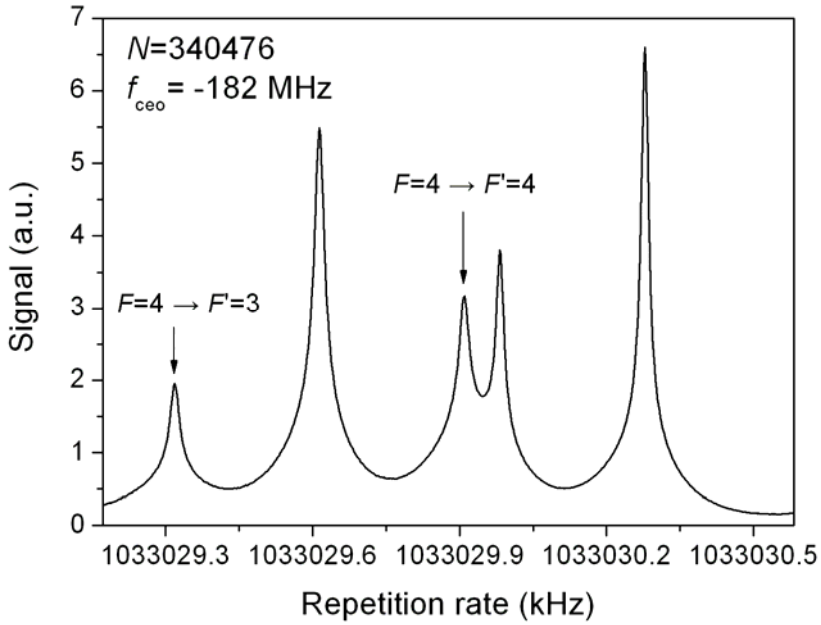

Fig. 6. The saturated absorption signal of the cesium D2 line observed by means of the injection-locked DBR laser as a function of the repetition rate, while the carrier-envelope-offset frequency is stabilized. The intensities of pump and probe beams are about 100 μW/cm^2 and 130 μW/cm^2, respectively.

References

[1] D. J. Jones, S. A. Diddams, J. K. Ranka, A. Stentz, R. S. Windeler, J. L. Hall, S. T. Cundiff, Science 288, 635 (2000).

[2] M. Niering, R. Holzwarth, J. Reichert, P. Pokasov, T. Udem, M. Weitz, T.W. Hänsch, P. Lemonde, G. Santarelli, M. Abgrall, P. Laurent, C. Salomon, and A. Clairon, Phys. Rev. Lett. 84, 5496 (2000).

[3] J. D. Jost, J. L. Hall, J. Ye, Opt. Express 10, 515 (2002).

[4] R. Lang, IEEE J. Quantum Electron. QE-18, 976 (1982).

[5] F. C. Cruz, M. C. Stowe, J. Ye, Opt. Lett. 31, 1337 (2006).

[6] S. Fukushima, C. F. C. Silva, Y. Muramoto, A. J. Seeds, J. Lightwave Technol. 21, 3043 (2003).

[7] S. E. Park, E. B. Kim, Y.-H. Park, D. S. Yee, T. Y. Kwon, C. Y. Park, H. S. Moon, and T. H. Yoon, Opt. Lett. Vol.31, 3594 (2006).

[8] H. S. Moon, E. B. Kim, S. E. Park, and C. Y. Park, Appl. Phys. Lett. 89, 181110 (2006).

[9] J. Reichert, R. Holtzwarth, T. Udem, and T. W. Hänsch, Opt. Commun. 172, 59 (1999).

PERFORMANCE ANALYSIS OF AN INTERNET BASED UTC (SG) DISSEMINATION SYSTEM

LIU YanYing

National Metrology Centre, SPRING Singapore,
1 Science Park Drive, Singapore 118221
E-mail: liu_yan_ying@spring.gov.sg

This paper gives an evaluation of the performance of SPRING Singapore's Network Time Service (NeTS) based on the statistical analysis of the data collected over a period of more than two years. The results showed that by incorporating an algorithm, the time server was able to disseminate the UTC (SG) time through internet to industry and the public at an uncertainty better than 0.01s, independent of the number of requests received.

1. Introduction

The National Metrology Centre (NMC), SPRING Singapore, has been providing a Network Time Service (NeTS) of the UTC (SG) since February 2001. The UTC (SG) is disseminated through internet by using a dedicated leased line with 128kbps network transmission speed provided by a local internet service provider.

NeTS is a service for users to synchronise their computer time to UTC (SG) through internet by means of three different protocols, namely, Time Protocol, Daytime Protocol and Network Time Protocol (NTP). All users need to do is to make a time request to the NeTS server, and the server would then response with the UTC (SG) information. The users' machine would adjust its system time to synchronise to UTC (SG) time signal.

The NeTS server calibrates itself against the Automatic Computer Time Service (ACTS) server. The calibration is done every 50 minutes through a dial-up to ACTS which provides the direct 1 PPS signal. This dialling interval was determined experimentally to give a good balance between prediction accuracy and telephone cost. The algorithm, which was developed by J.Levine [1], was used to measure the time difference between the machine time and UTC (SG) for each call, perform the calculation and then implement the incremental time adjustment. Through this method, the NeTS server system clock is continuously steered in order to prevent a sudden step change in system time.

There are two NeTS servers at SPRING. One is an active server (NeTS1) providing routine service while another (NeTS2) is a backup to prevent accidental system failure. Both are Compaq Alpha stations operating on the UNIX system, and their internal clock oscillators are very stable. During the period between December 2002 and January 2005, the daily number of requests received by SPRING dramatically tripled from about 110,000 to 350,000, which meant that the server had to process about 4 requests per second.

2. Statistical Analysis

As mentioned, to synchronise to the UTC (SG), the two NeTS servers calibrate their system times against the ACTS server through periodic dial-ups (every 50 minutes). At each dial-up,

the time difference between the NeTS and ACTS is measured. A total of 20,189 and 18,507 such records of dial-ups were collected for NeTS1 and NeTS2 respectively, between 2002 and 2005. The two data sets were analysed and the UTC (SG) dissemination uncertainty of each was computed.

For the NeTS1 server, the 20,189 time offset measurements at a span of 751 days were processed in terms of a time series. The mean of absolute values of all the time offsets was 1.5ms with a standard deviation of 1.1ms. It was found that about 97% of the total measurements were within ± 0.004s. About 3% were within the range between ± 0.004s and ± 0.008s. There were a few outliers scattered outside ±0.008s, but all were less than ±0.01s.

The Allan Deviation was calculated by Stable32[2] using the data collected on NeTS1 to identify the measurement system noise. It was found that both the short-term and long-term noise was characteristic of white phase noise. The other types of noise were removed when the server clock was controlled by the algorithm. The same analysis was applied to NeTS2 and similar results were obtained.

3. Conclusion

The statistical analysis showed that by using an algorithm, both controlled NeTS servers were able to keep their system times synchronised to the UTC (SG) to within 0.01s. The noise over short and long periods was dominated by white phase noise. The time difference between NeTS server and UTC (SG) was not affected by the increasing number of time requests received each day. The uncertainty of the UTC (SG) dissemination by internet was 0.01s.

Reference:

[1] J.Levine, “An algorithm to synchronize the time of a computer to universal time,” IEEE transaction on networking, vol. 3, No. 1, 1995

[2] Stable32, Frequency Stability Analysis, Version 1.3, Hamilton Technical Services

Precise Estimations of High-Speed Network Time-Transfer

Tsukasa Iwama* , Akihiro Kaneko, Akihiko Machizawa, and Hiroshi Toriyama

National Institute of Information and Communications Technology
4-2-1 Nukui-Kita, Koganei, Tokyo, 184-8795 JAPAN

Abstract

The Global Positioning System (GPS) common-view method is one of the main methods used for time-transfer to remote atomic clocks. This method gives accurate time, but it is difficult to set up and operate. Network Time Protocol (NTP) is widely used for time-transfer in network environments. However, it is difficult for simple NTP to receive accurate time because of the effects of cross-traffic and the interrupt requests of software processing.

We have recently developed the hardware for a Simple-NTP (SNTP) board that can measure a one-way delay time with ns-order accuracy. This SNTP board can be operated by an external atomic clock. Thus, we can compare precision time at remote sites through a network.

We have also developed a precise method for estimating network time-transfer that reduces the effects of cross-traffic by using data-filtering techniques. Using measured data, we estimated the performance of our method and found that it is almost as accurate as the GPS common-view method when the standard deviation (SD) is ≤ 2 μs.

1. Introduction

The demand for a high-speed and high-precision network time-transfer technique is increased in line with the development of the information and communications technology. The Global Positioning System (GPS) common-view method is usually used for time-transfer to remote atomic clocks. This method offers accurate time, but it is difficult to set up and operate, especially in Internet Data Centers (IDCs). Network Time Protocol (NTP) is widely used for time-transfer in network environments. Unfortunately, in the typical Internet environment, even on the same route, it is difficult for simple NTP to receive accurate time because of the effects of cross-traffic and the interrupt requests of software processing. Therefore, an estimate of actual transfer delays is needed to improve the accuracy of time distribution.

We have recently developed hardware in the form of a Simple-NTP (SNTP) board that can measure one-way delay time. It is applicable to Giga-bit Ethernet (GbE) connections and has a theoretical time resolution of 4 ns. By installing SNTP boards on both sides of a transfer path, we can immediately obtain the delay time of the path with a precision within 10 ns. However, this requires highly stable atomic clocks on both sides. Thus, we compare the precision time at remote sites through a network.

In this study, we also developed a precise method for estimating network time-transfer that reduces the effects of cross-traffic using data-filtering techniques. Using measured data, we estimated the performance of our method and found that it is almost as accurate as the GPS common-view method. From the comparison results, the network time-transfer method using data-filtering is practical and accurate when the standard deviation (SD) is ≤ 2 μs.

*iwama@nict.go.jp

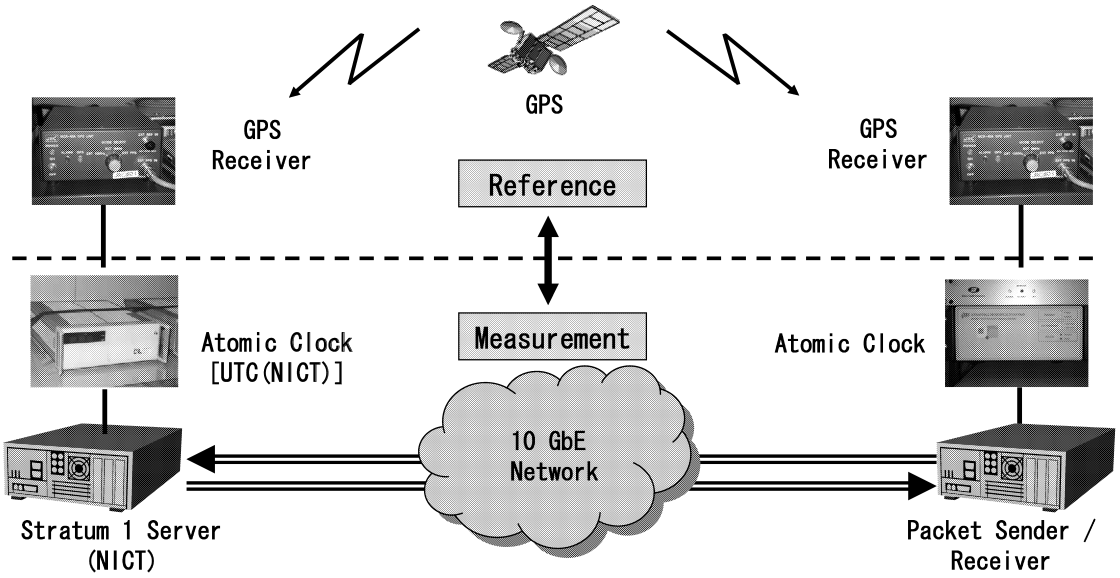

Figure 1. Block diagram of Network Time-Transfer System.

2. Network Time-Transfer System

In Fig. 1, a block diagram of the network time-transfer system used to measure real-time, one-way time delay in an Internet environment is shown.

The measurement systems included a packet sender/receiver (P-S/R), a packet responder (P-Res: stratum 1 server), atomic clocks, and a high speed ($\geq$ 1 GbE) network environment. The P-S/Rs and P-Res consist of Free-BSD-based PCs with a hardware SNTP board installed between the PCs and the network.

The hardware SNTP board automatically stamps an NTP-time on each packet as they pass through. Here, the time stamp is generated from signals sent from an atomic clock. In these measurements, the atomic clock on the P-Res was a UTC(NICT), based on Coordinated Universal Time, and on the P-S/Rs, it was a cesium atomic clock. Both time scales were compared using the GPS common-view method, and the time difference was recorded.

In these measurements, we used three P-S/Rs, the first was at Ohtemachi, which is in the center of Tokyo and about 30 km from NICT, the second was at Dohjima in the center of Osaka, about 400 km from NICT, and the other was at NICT, located in Koganei, in west Tokyo. At the NICT P-S/R, packets were carried via the Ohtemachi Network Node. Therefore, an NICT P-S/R and a P-Res were placed at different network-segments and connected through the Ohtemachi Network Node.

3. Time-Transfer Results

3.1. One-way delay data

NTP packets were sent from the P-S/R at the rate about 7 or 8 per second. In Fig. 2, samples of received one-way delay data are presented. Figure 2(a) indicates the one-way data from Ohtemachi to NICT received in one day. In this network environment,

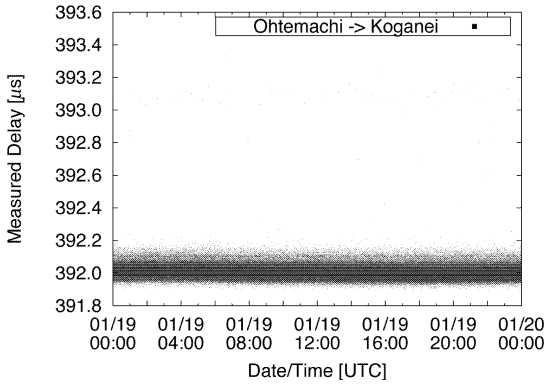

(a) Ohtemachi->Koganei

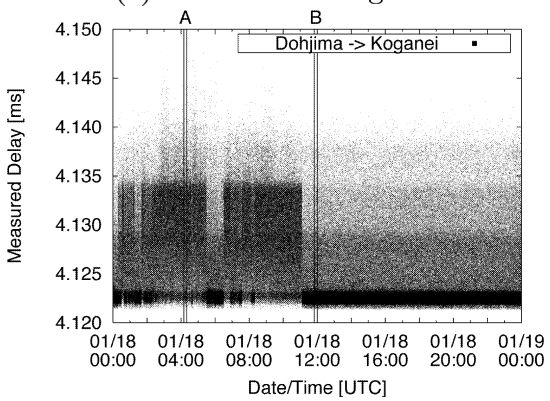

(b) Dohjima->Koganei

Figure 2. Samples of Received One-way Delay Data

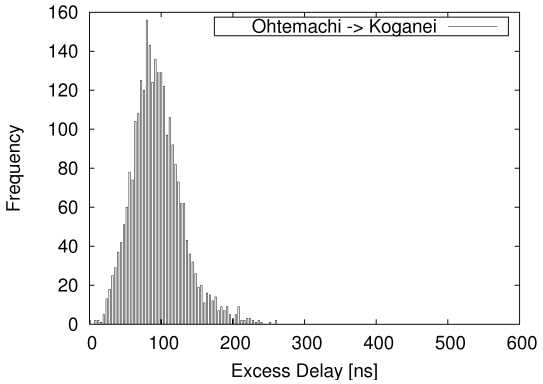

(a) Ohtemachi->Koganei

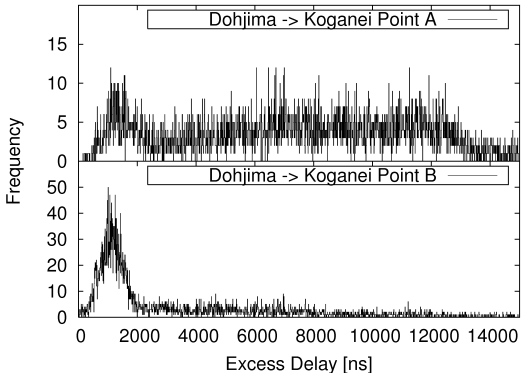

(b) Dohjima->Koganei

Figure 3. Histograms of Measured Excess Delay Data

cross-traffic is light, and the excess delay of one-way delay data was about 200 ns. Figure 2(b) is the one-way delay from Dohjima to NICT received in one day. In this network environment, there was heavy cross-traffic due to the large number of packets that flow between Tokyo and Osaka. Therefore, the excess delay was more than 18 μs in this route. From Fig. 2(b), it is clear that cross-traffic was most intense in the morning.

Figure 3 shows the histograms of received excess one-way delay data. In Fig. 3(a), the SD σ is about 40 ns, and 95% of the data are within the 160 ns from the minimum delay time. In Fig. 3(b), SD is about 3-4 μs in the morning and about 2 μs in the afternoon.

From Fig. 3, we can see that a forward domain of the delay profile forms a bell shape regardless of the traffic conditions. When there is heavy cross-traffic, data from a queueing delay domain increase, and data from a bell-shaped domain relatively decrease. In Fig. 3(b), the delay profile is different at point A and B, but the widths of the bell shapes are the same, at about 2 μs. This result indicates that the bell-shaped domain is independent of the cross-traffic.

By paying attention to this point, it is possible to estimate the actual transfer delays that are not easily affected by cross-traffic. That is, by filtering only the bell-shaped domain and extracting and averaging the data, we can provide more accurate measurement data.

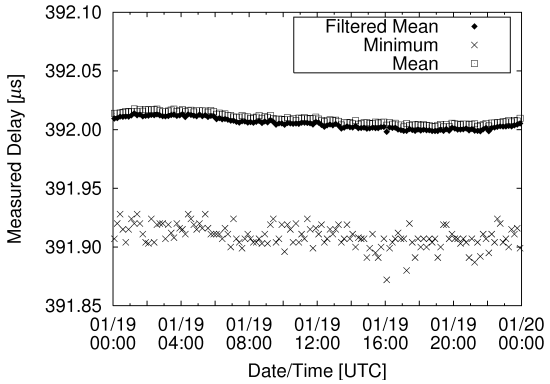

(a) Ohtemachi->Koganei

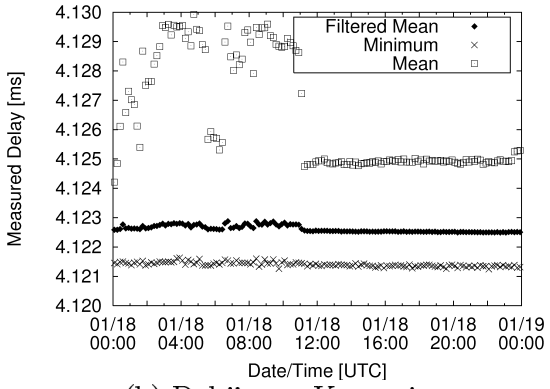

(b) Dohjima->Koganei

Figure 4. Samples of Calculated One-way Delay Data

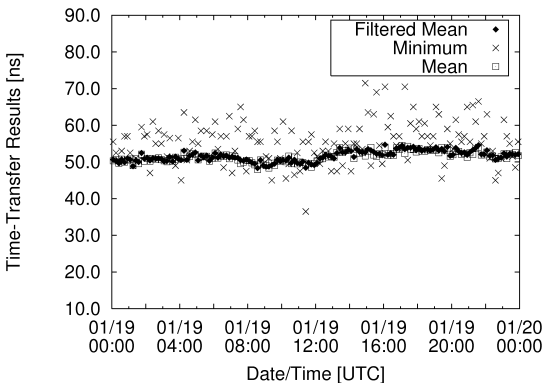

(a) Ohtemachi->Koganei

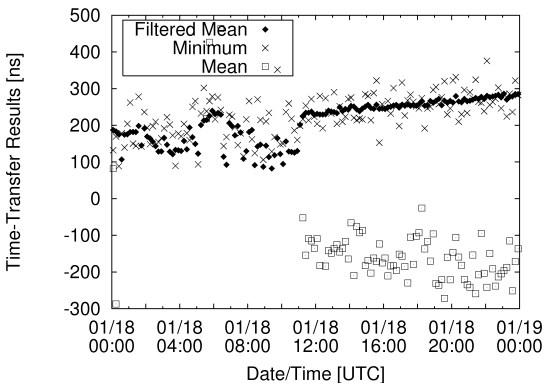

(b) Dohjima->Koganei

Figure 5. Samples of Network Time-Transfer Results

3.2. Data-filtering

To estimate the data accuracy, we need to compare the measurement data with GPS common-view data. Therefore, received data were filtered and averaged every 10 minutes in order to obtain the measurement data.

Figure 4 shows samples of the calculated results of one-way delay data. Source data are the same as in Fig.2. In Fig. 4, the mean of all-data and the minimum data in 10 minutes are plotted for comparison. Fig. 4(a) depicts the data in light cross-traffic, the data-filtered mean is almost the same as the all-data mean and has better stability than the minimum data. On the contrary, in condisions with heavy cross-traffic (b), the data-filtered mean has almost the same stability as the minimum data and much better stability than the all-data mean. These results demonstrate that the data-filtering method operates effectively.

To estimate the effect of the data-filtering method, we calculated the network time-transfer. Figure 5 shows samples of the results. Source data were also the same as in Fig.2. In Fig. 5, time-transfer results are not calibrated, but are half of the difference between the up-link and down-link.

In Fig. 5(a), SD is about 40 ns, and data stability is several ns in the data-filtered mean and all-data mean, and about 10-15 ns in the minimum data. At the left side of Fig. 5(b), SD is 3-4 mus, and data stability is 100-200 ns in the data-filtered mean and the minimum data, and about 200 ns with a 2-mus data offset in the all-data mean. At the right side of Fig. 5(b), SD is about 2 mus, and data stability is 10-20 ns in the

Table 1. Comparison of SD with data stability

SD	Data-filtered mean	Mean	Minimum
40 ns	several ns	several ns	10-15 ns
200 ns	10 ns	20 ns	40-50 ns
2 μs	10-20 ns	200 ns (offset -400 ns)	100 ns
3-4 μs	100-200 ns	200 ns (offset -2 μs)	100-200 ns
10 μs	100-200 ns	1 μs (offset -3 μs)	200 ns

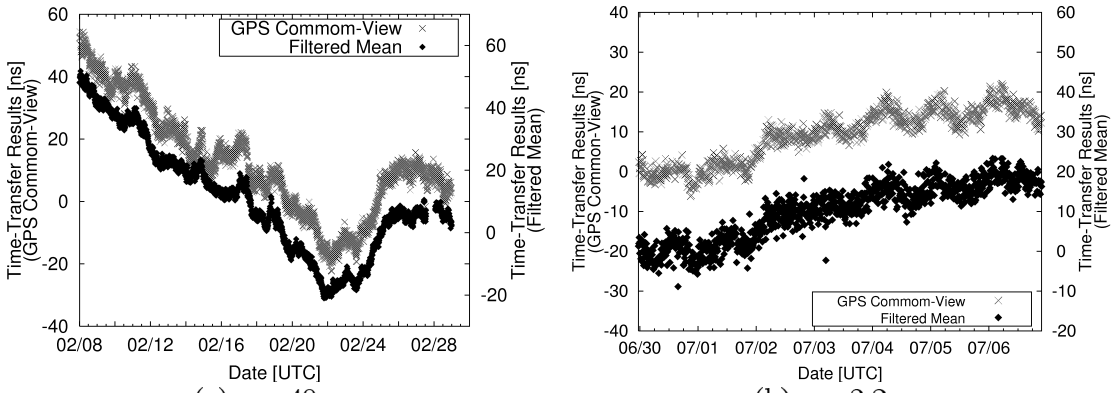

(a)$\sigma \approx 40$ ns (b)$\sigma \approx 2.2$ μs

Figure 6. Compare Data-filtered Mean with GPS Common-View

data-filtered mean, about 100 ns in the minimum data, and about 200 ns with a 400-ns data offset in the all-data mean.

Using a NICT-Ohtemachi-NICT network link with additional controlled cross-traffic, we estimated the relationship between SD and data stability. Table 1 presents this relationship. The superior results of the data-filtering method are evident in all the SDs listed in the table.

3.3. Compare with GPS common-view

Finally, to estimate the accuracy of the data-filtering method, we compared the data-filtered mean with GPS common-view data. Figure 6 shows the comparison results. In the figure, we adopted only highly precise data where the GPS altitude was more than 60 degrees. The data-filtered means were plotted with a 20-ns offset. Figure 6(a) shows that the accuracy of the data-filtered mean is less than 10 ns and is almost the same as the highly precise GPS common-view data when SD $\approx$ 40 ns. In heavy cross-traffic conditions, as in Fig. 6(b), accuracy of the data-filtered mean is 10-20 ns and corresponds to Table 1.

From these comparison results, it is evident that network time-transfer using data-filtering is a practical method with the accuracy listed in Table 1.

4. Conclusion

We have developed a hardware SNTP board that can measure a one-way delay time with ns-order accuracy. This SNTP board can be operated by an external atomic clock. We have also developed a precise method for estimating network time-transfer that reduces the effects of cross-traffic using data-filtering techniques. Using measured data, we estimated the performance of our method and found that it is almost as accurate as the GPS common-view method.

The comparison results indicate that network time-transfer using a data-filtering method is practical and accurate when the standard deviation $\leq 2\ \mu s$.

Acknowledgments

We would like to thank to Prof. Ito and Prof. Okada, the University of Electro-Communications for their useful comments and suggestions to this study.

References

Iwama, T., et al. 2004, Proc. ATF2004, 317.
Iwama, T., et al. 2006, IEICE Trans. vol. J89-D.

SIMPLE TIME AND FREQUENCY DISSEMINATION METHOD USING OPTICAL FIBER NETWORK

Masaki Amemiya, Michito Imae, Yasuhisa Fujii,
Tomonari Suzuyama, Shin-ichi Ohshima and Masaaki Susumu*

Frequency Measurement Systems Section, National Metrology Institute of Japan,
AIST, Tsukuba Central 3, Ibaraki, 305-8563 JAPAN
****GEO5 Co., LTD, 1-12-1 Harayama, Saitama, 336-0931 JAPAN***

Abstract

This paper describes a simple and cost effective frequency dissemination method. In the current digital communication networks, node clocks are hierarchically synchronized to the atomic master clock through fiber links. This synchronized network is used as an intermediate for remote calibration service. A prototype reference signal generator has been developed for recovering the communication timing signal and generating 10 MHz signal from it. The generator output frequency at the client site can be traced to UTC(NMIJ) in some uncertainty depending on stability of the node clocks and distance from the master clock. Stability performance of the generated reference signal has been tested at Okinawa the farthest prefecture from Tokyo where the master clock is located (1,500 kilometers in a beeline). The primary rate (1.544 MHz) for telecommunication service is chosen for 10 MHz signal generation in the experiment. Sinusoidal phase fluctuation with one day period is dominantly observed. It is mainly caused by fiber expansion and contraction with daily based temperature change. It degrades the stability (Allan deviation) to the level of 5×10^{-13} (τ = 40,000 s, almost half day), however the major part of the phase fluctuation can be canceled by all day averaging. Then the Allan deviation becomes 1×10^{-13} obtained at Okinawa in 10 consecutive days measurement. The worst relative frequency deviation (1 day averaging) is -6.3×10^{-13}. The results indicate the method is promising for the purpose with a better uncertainty of around 10^{-12} by all day averaging.

1. Introduction

They have to bring their standard-oscillators to National Metrology Institute of Japan (NMIJ) in the traditional calibration services. For overcoming this inconvenience, NMIJ has studied remote calibration service using optical fiber network [1]. Frequency end users need simple and economical frequency standard distribution. The uncertainty of around 10^{-12} is good enough for general frequency users. To meet the demands, we use synchronous optical fiber communication networks which are currently used. This paper shows the methods and the test results.

2. Economical and Simple Frequency Distribution Method

2.1 Configurations

Existing synchronous optical fiber communication networks are utilized to distribute standard frequency as simple and economical as possible. The network node clocks (Rubidium atomic oscillators) are hierarchically synchronized to the master clock (Cesium atomic oscillator) through fiber links as shown in the middle of Fig.1. End users obtain frequency source directly from the transmission clock. The obtained frequency can be traced to UTC (NMIJ) if the master clock of the telecommunication network is synchronized to UTC (NMIJ). This direct dissemination is an ideal method, however, some negotiations with telecommunication companies will be needed. On the other hand, it is easy to trace the frequency to UTC (NMIJ) by the common-view method as shown in Fig.1. The method is well used in the GPS satellite time transfer [2] [3]. At the user site, transmission clock signals extracted from the output signal of digital service units (DSU), which are transmission terminators, are used as a source for the generator to synthesize the 10 MHz reference signal as shown in Fig.2.

2.2 Analysis of frequency stability

Causes of phase fluctuation in the synchronous networks are accumulations of fluctuation in optical fiber transmission systems and the atomic oscillators. Here main factor induced by the transmission systems is examined in addition to the oscillator instability.

(A) Instability by jitter

Jitter is generated in regenerators and line terminals. There are two kinds of jitter, one is pattern jitter depending on bit patterns and the other is random jitter caused by noises in regeneration circuits. The standard deviation σ_x for the instantaneous phase $x(t)$ having the time dimension is expressed as follows when ϕ_{rms} is the effective value of the total jitter

$$\sigma_x = \frac{\phi_{rms}}{360} T_0 \qquad (1)$$

where T_0 is the period which is the reciprocal of the line clock frequency f_0. The Allan standard deviation σ_y is given by

$$\sigma_y(\tau) = \sqrt{3}\,\frac{\sigma_x}{\tau} \qquad (2)$$

which is well known relation.

Figure 3 shows calculated σ_y for the clock rate of 1 GHz and 10 GHz since the transmission speeds of 600 Mbps, 2.4 Gbps, 10 Gbps are typically used and also those are ITU-T standards. The jitter ϕ_{rms} is supposed as $3.5°rms$ which is accumulated value in a 122 regenerator line of a 5,000 km cable [4]. The stability of Rb oscillators generally degrades in the long term (**>** 10^3 s) as shown in Fig.3. Therefore, the PLL in the slave oscillator is set to lock to the master Cs oscillator in this region. Figure 3 shows the noise level of jitter is negligibly small compared to Cs oscillator in the long term. On the other hand, the noise level of jitter happens to be larger than Rb or Cs in the short term if the clock rate is as small as 1.5 MHz if the jitter is $0.1°rms$ as shown in Fig.3. This degradation should be considered especially in the access line.

(B) Instability by wander

Wander is slow phase fluctuation less than 10 Hz [5], mainly caused by temperature change of fiber and cable. The time delay Δt for a 1 km fiber with temperature change of 1 degree is given by (3) from the temperature coefficient for refraction and expansion of silica fiber.

$$\Delta t = 5\times10^3(ns/km)\times(6.7+0.55)\times10^{-6}(1/°C)$$

$$= 36ps/km/°C. \quad (3)$$

Sinusoidal phase fluctuation at the output of fiber is assumed for daily or yearly based wanders. Then the instantaneous phase $x(t)$ is simply expressed as follows

$$x(t) = A\sin(2\pi\frac{t}{T_1}) \quad (4)$$

where A is the amplitude (0-peak) and is T_1 the period. The Allan variance $\sigma_y^2(\tau)$ is given by the definition as follows

$$\sigma_y^2(\tau) = \left\langle \frac{(\bar{y}_{i+1} - \bar{y}_i)^2}{2} \right\rangle \quad (5)$$

where $\bar{y}_i$ is given by (6) using $x(t)$.

$$\bar{y}_i = \frac{x(t_i + \tau) - x(t_i)}{\tau}. \quad (6)$$

Then, the Allan variance for sinusoidal wander is derived by time averaging over the period for the right hand of (5) using (4) and (6). As a result

$$\sigma_y^2(\tau) = \frac{1}{T_1}\frac{A^2}{\tau^2}\int_0^{T_1}\{x(t) - 2x(t+\tau) + x(t+2\tau)\}^2 dt$$

$$= \frac{A^2}{\tau^2}(3 + \cos 4\pi\frac{\tau}{T_1} - 4\cos 2\pi\frac{\tau}{T_1}). \quad (7)$$

As an example, Δt becomes 18 ns (A is 9 ns) when the temperature of a 1,000 km fiber is changed by 0.5 ℃ in total per day from (3). Calculated stability results for the amplitudes of 5 ns and 10 ns using (7) are shown in Fig. 4. In short term the Allan deviation $\sigma_y(\tau)$ is proportionally degraded to τ. And it becomes maximum where τ is 30,000 ~ 40,000 s which is less than half day (=43,200 s). The peak value for A =10 ns for instance is 7.4×10^{-13}. For large τ, it is decreasing with oscillation. The peak values are proportional to $1/\tau$. Apparently, it becomes zero at 1 day and its multiple number since the phase fluctuation is cancelled under the assumption of sinusoidal wander.

In the same manner, $\sigma_y(\tau)$ for yearly wander with 10 ns o-p amplitude is about 2×10^{-15} where τ is around 1.5×10^7. These results are plotted in Fig.3.

3. Reference signal generator and its performance

Figure 5 shows the prototype reference signal generator, that is an Oscillator synchronizing to the Atomic clock Network (A-Net-Oscillator). Clock frequency becomes 1.544 MHz if we use the primary rate telecommunication services. The clock signal of 1.544 MHz is recovered from the DSU output signal with a high impedance circuit (more than 1 MΩ) so that telecommunication signal with 100 Ω impedance is no influenced. Then the recovered 1.544 MHz is used for generating 10 MHz reference signal by PLL (crystal oscillator).

The stability of the 1.544 MHz signal and generated 10 MHz signal is shown in Fig.6. There is no significant difference between them. It shows well synchronization to the atomic network while the stability of the output signal of a usual frequency counter (XO based internal time base) is degraded in the long term.

4. Stability test results at faraway region

Stability and relative frequency of the generated reference signal has been tested with a commercial Cs clock (high performance type) at Okinawa the farthest prefecture from Tokyo where the master clock is located (1,500 kilometers in a beeline). There are terrestrial systems (cables are laid in conduits) and the submarine system (905 km cable and 9 optical amplifier repeaters) [6] as shown in Fig.7. Another A-Net-Oscillator output signal has also been measured at the same time at NMIJ in Tsukuba about 50 kilometers away from Tokyo.

Stability results are shown in Fig.8. Long-term stability (around 1 day) for both Tsukuba and Okinawa are well below 10^{-12}, however short-term stability at Tsukuba is not good compared to one at Okinawa. The reason of the degradation is probably jitter performance of the switching equipment in the access line, as already described in 2.2.

Measured phase drift to the Cs clock at Okinawa is shown in Fig.9. Sinusoidal phase fluctuation with one day period is observed in straight 10 days measurement. It is mainly caused by fiber expansion at noon time and contraction at night time. This degrades the stability to the level of 5×10^{-13} (τ = 40,000 s, almost half day) as shown in Fig.10. Measured and calculated results in Fig.10 are clearly showing the major part of the phase fluctuation can be canceled by all day averaging as already discussed in 2.2. Then the Allan deviation becomes 1×10^{-13}. The worst relative frequency deviation (1 day averaging) at Okinawa is -6.3×10^{-13} as shown in Fig.11. The Cs clock was carried to Okinawa with electric power off. Measured relative frequencies of the clock to UTC(NMIJ) are 1.8×10^{-14} (expanded uncertainty is 6.1×10^{-14}) before carrying and -8.6×10^{-14} (expanded uncertainty is 6.3×10^{-14}) after carrying back to Tsukuba.

5. Summary

For satisfying the remote frequency-users' demands, simple and economical frequency dissemination method was considered. Current synchronous optical fiber communication networks were used in this method. The prototype reference signal generator synchronizing to the atomic clock network was developed. The stability of the generator was tested at the farthest region 1,500 kilometers in a beeline from the master clock. Good stability of 1×10^{-13} was obtained by all day averaging while the sinusoidal daily based wander degrades the performance. The results indicate the method is promising for the purpose with a better uncertainty of 10^{-12}.

Acknowledgments

The authors would like to thank K. Izumi and A. Mito at AIST for their support of this project. The authors would like to thank S. Aoyagi, Y. Takigawa and H. Fukuda at NTT laboratories, M. Kihara at Nihon University for their continued technical support. The authors would also like to thank T. Haneji at OITC for his great support and help in Okinawa.

References

[1] M. Amemiya, M. Imae, Y. Fujii, T. Suzuyama, S. Ohshima, S. Aoyagi, Y. Takigawa, and M. Kihara, "Time and frequency transfer and dissemination methods using optical fiber network", IEEJ Trans. FM, Vol.126, No.6, pp.458-463, 2006.

[2]D.W.Allan, M.A.Weiss, "Accurate Time and Frequency Transfer During Common-View of a GPS Satellite", 34th Annual Frequency Control Symposium, pp.334-346, May 1980.

[3] Y. Shibuya , Y. Fukuyama, M. Imae, M. Amemiya, T. Ikegami, and S. Ohshima, " Development and application of the frequency remote calibration system in Japan," ATF (Asia-Pacific Workshop on Time and Frequency) 2004, Beijing, pp. 298-302, October, 2004.

[4] M. Amemiya, M. Aiki, T. Matsuno, Y. Ichihashi and H. Shirakawa: "Jitter accumulation in a 5000km submarine optical repeatered line", Transactions of the IEICE, Vol. E 70, No.7, pp.605-607, (July, 1987).
[5] ITU-T Recommendation G.810.
[6] M.Amemiya, and Y. Sato: "FSA-10G large capacity submarine optical amplifier system and upgrade trials for the future", Pacific Telecommunication Council 1996 (PTC '96), January 14-18, 1996, Honolulu, pp.225-232.

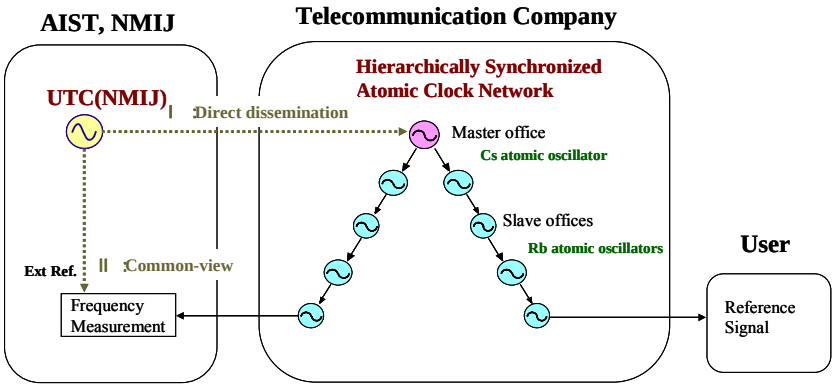

Fig.1. Simple frequency dissemination method using the existing synchronous optical fiber communication networks.

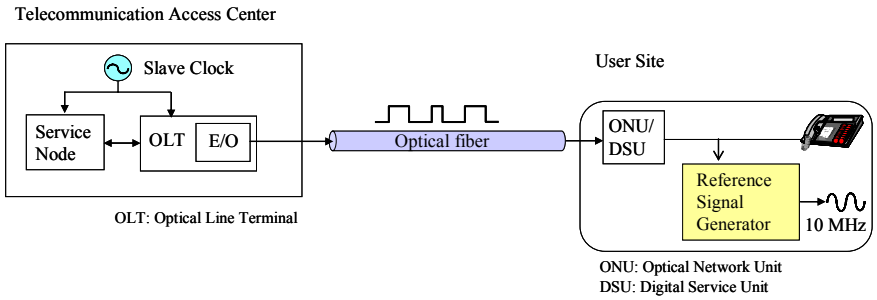

Fig.2. Example of access system configurations for frequency standard distribution.

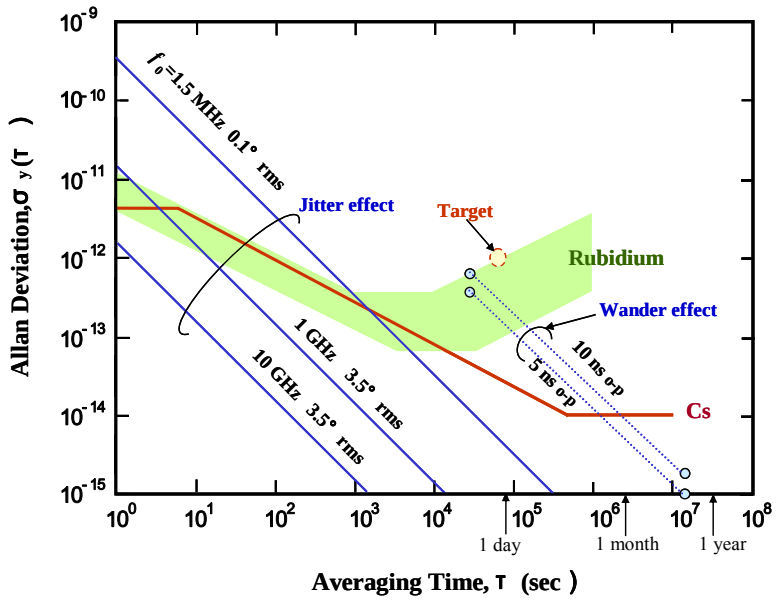

Fig.3. Estimated stability of optical fiber network for hierarchical synchronization.

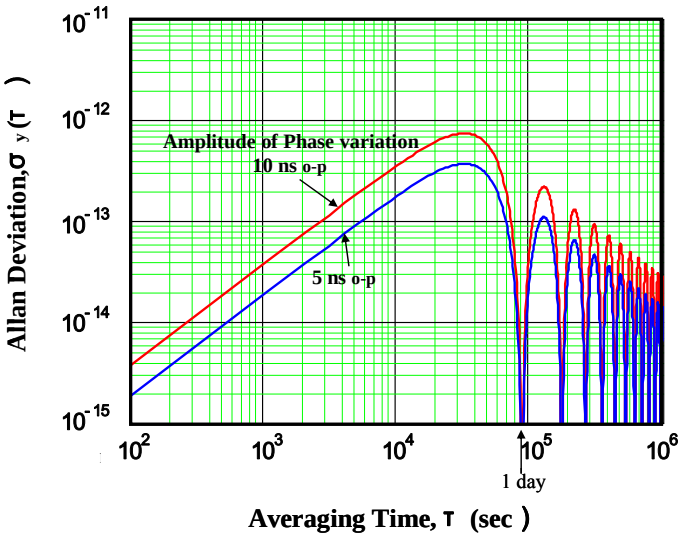

Fig.4. Calculated frequency stability for daily temperature change of fiber

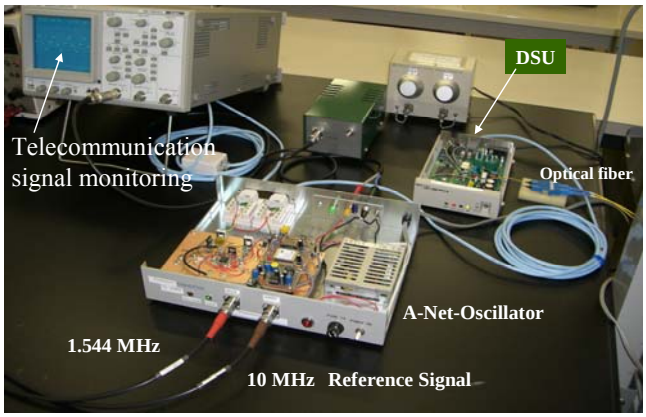

Fig.5. The prototype reference-signal-generator and measurement set.

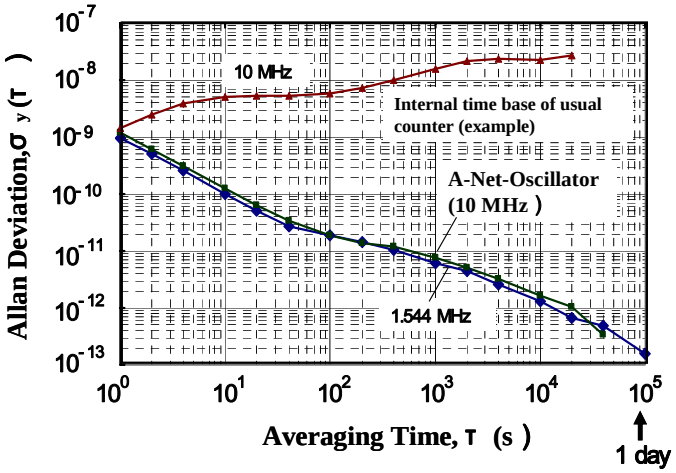

Fig.6. Measured frequency stability of the prototype generator output referred by UTC(NMIJ).

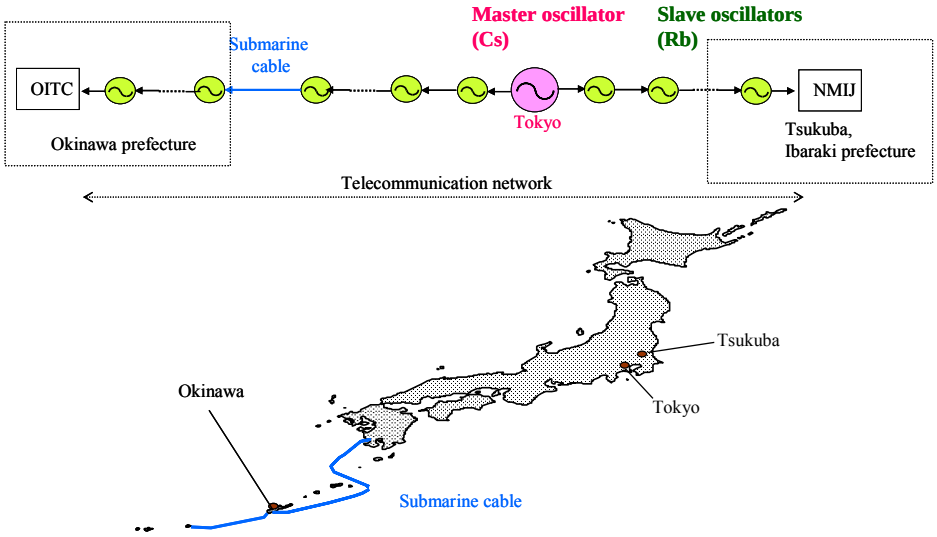

Fig. 7. Measurement configuration and location.

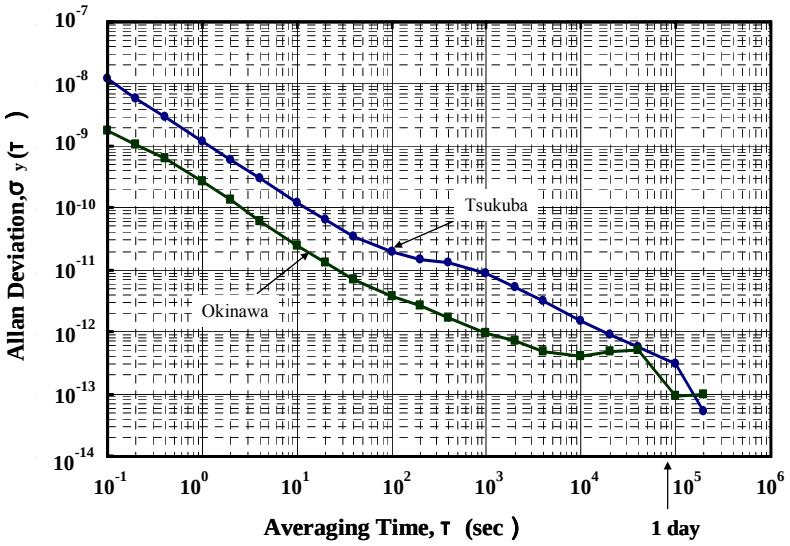

Fig. 8. Measurement frequency stability at Tsukuba and Okinawa.

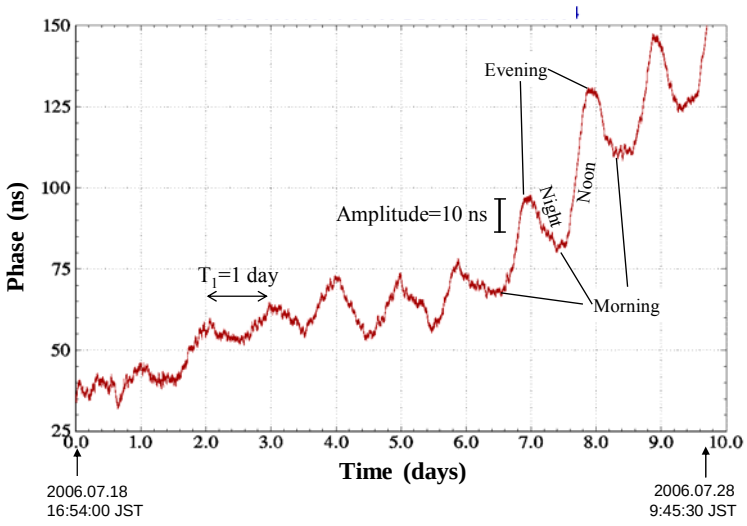

Fig. 9. Measurement phase drift at Okinawa.

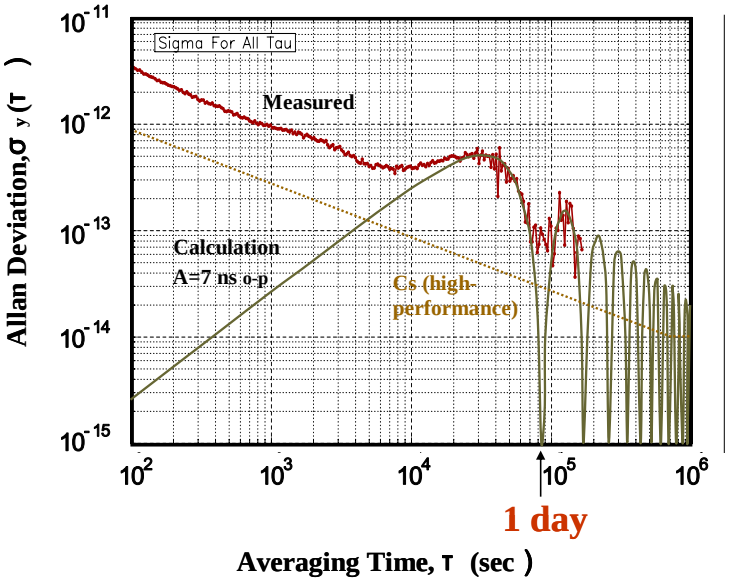

Fig. 10. Stability test result with calculation at Okinawa.

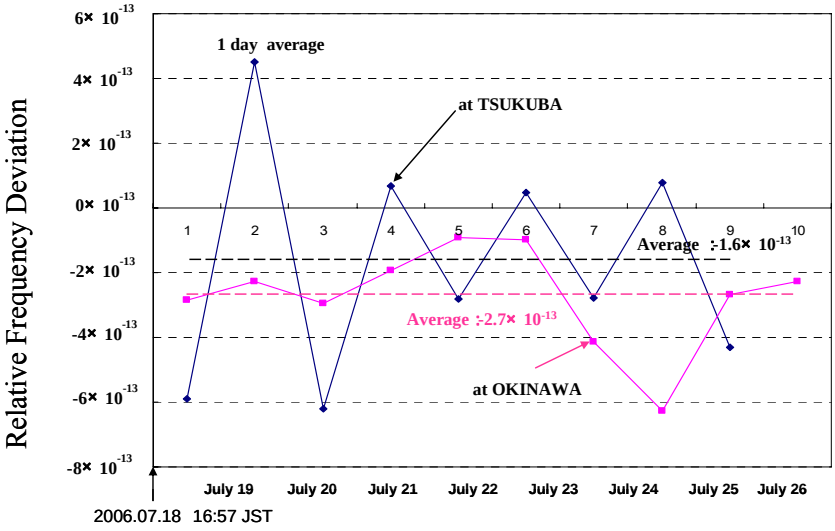

Fig. 11. Relative frequency deviation at Tsukuba and Okinawa.

STATUS REPORT OF TIME & FREQUENCY ACTIVITIES AT NMIJ/AIST

Shin-ichi Ohshima

Time and Frequency Division
National Metrology Institute of Japan, AIST
Tsukuba, Ibaraki 305-8563, Japan

During the two years since the last ATF we have put forward the developments and improvements of primary frequency standards, NMIJ-F1 and NRLM-4. The time scale of UTC(NMIJ) has been modernized by implementation of hydrogen masers, and calibration activities, such as remote calibrations, have been widely expanded. In the field of optical frequency, activities on new types of optical frequency standards, such as optical lattice clocks, have been enhanced. In addition progress was made in new technologies such as optical fiber combs.

1. Cs Atomic Fountain Frequency Standard, NMIJ-F1

In 2005, NMIJ started the operation of NMIJ-F1 as a primary frequency standard. The design, the basic performance and the preliminary evaluation of NMIJ-F1 are described in Ref.[1]. The resulting uncertainties are larger than the preliminary evaluation [1], because the operational conditions are different from previous experiments. The conditions will be improved and the uncertainty will be reduced in future.

The present evaluated uncertainties $\boldsymbol{u}_A$, $\boldsymbol{u}_{link/lab}$, $\boldsymbol{u}_B$ are briefly described in the following.

Type A uncertainty $\boldsymbol{u}_A$

The NMIJ-F1 uses an optical molasses to load the atoms, and its frequency stability, $\sigma_y(\tau)$, is about $1\times10^{-12}\tau^{-1/2}$. The measurement uncertainty based on the frequency instability is 1.1×10^{-15}, assuming white FM noise over the comparison period of 10 days.

Uncertainty of the link in the laboratory $\boldsymbol{u}_{link/lab}$

The uncertainty due to the link in the laboratory, $\boldsymbol{u}_{link/lab}$, consists of two factors as written in the following equation

$$u_{link\,/\,lab} = \sqrt{u_{dead\ time}{}^2 + u_{link\,/\,maser}{}^2}$$

where $\boldsymbol{u}_{link/maser}$ is the uncertainty due to the noise of the phase comparator between the fountain and the hydrogen maser, and $\boldsymbol{u}_{dead\ time}$ is the uncertainty due to the operational dead time of the fountain. The $\boldsymbol{u}_{link/maser}$ was 0.5×10^{-16} over a period of 10 days. NMIJ-F1 was operated almost continuously with an efficiency of over 90 %. The operation was occasionally interrupted due to earthquakes, electric power failures and so on. The $\boldsymbol{u}_{dead\ time}$ was approximately 10^{-16} for six frequency comparisons of TAI and NMIJ-F1.

Type B uncertainty $\boldsymbol{u}_B$

The following table shows typical uncertainty budgets that were used for the frequency comparison during

MJD 53589-54034. Type B uncertainty is contributed to by the following six factors [1,2,3] and totals 4.0×10^{-15}. It is mainly limited by the estimation of cold collisional frequency shift.

Source of uncertainty	Bias	Uncertainty
2nd order Zeeman	185.2	0.9
Black body radiation	-18.0	1.4
Gravitation	1.6	0.1
Cold collisions	0.0	3.3
Distributed Cavity Phase	0.0	1.2
Microwave power dependence	0.0	0.7
Total	**168.8**	3.9

In 2006 the microwave system for Ramsey interrogation was modified in order to improve its reliability. The frequency difference between the center of the Ramsey fringe and the hydrogen maser is estimated from the control record of the Direct Digital Synthesizer that is a part of the synthesis chain. A new pulse pattern generator was also introduced for sequential control of NMIJ-F1. With the new pulse pattern generator many parameters, such as launch height, sequence cycle in the fountain, and shutter timing, are easily changeable. The power dependence of microwave for Ramsey interrogation is being investigated.

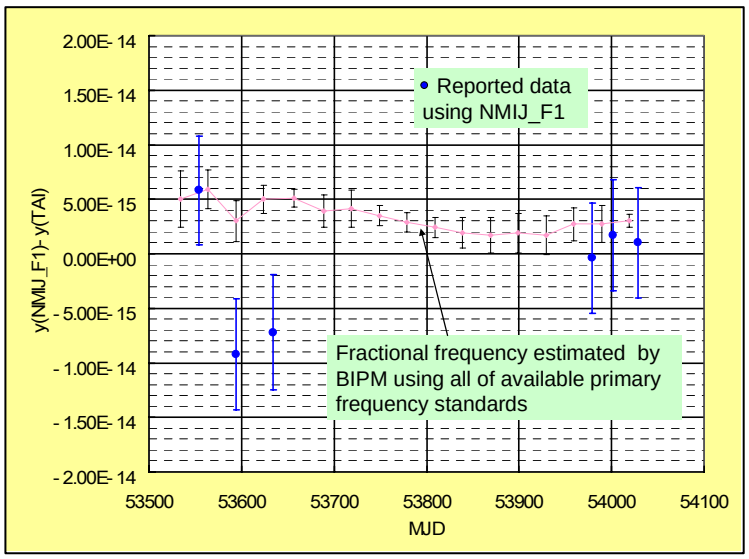

Figure 1. Frequencies of NMIJ-F1 published in Circular-T.

Figure 1 shows frequency comparison between NMIJ-F1 and TAI from MJD 53549(28/06/2005) to 54034(26/10/2006). The blue data points indicate frequency difference between NMIJ-F1 and TAI which were published in Circular-T. The six measurements were published in Circular T. Uncertainties of each measurement, including the uncertainty of a link to TAI, are estimated by a conventional method. The diamond-shaped data points show the frequency difference between PFS and TAI.

2. Optically Pumped Cs Beam Frequency Standard, NRLM-4

The optically pumped cesium beam frequency standard, NRLM-4, was operating as a primary frequency standard from February 1998 [4] to November, 2000. Its operation restarted this year. The previous uncertainty of 2.9×10^{-14} was due to the distributed cavity phase shift. In order to reduce this uncertainty, the Ramsey cavity was replaced with an H-bend ring cavity. In the H-bend cavity the direction of C-field and oscillating microwave field is perpendicular to the Cs beam propagation direction. The uncertainty, at a level

of 1×10^{-14}, is being reevaluated in order to restart the report to BIPM in a few months.

3. Cryogenic Sapphire Oscillator

Two cryogenic sapphire oscillators (CSO1 and CSO2) have been developed for use as a local oscillator for the Cs atomic fountain and as a reference signal for a femtosecond mode-locked laser. The CSOs employ a loop oscillator configuration, which is controlled by a Pound-type frequency stabilization scheme and a power control servo. These oscillators exhibited a fractional frequency stability of 1.1×10^{-15} at an averaging time of 1 s [5]. For averaging times between 2 s and 640 s the measured oscillator fractional frequency instability was below 10^{-15} with a minimum of 5.5×10^{-16} at an averaging time of 20 s as shown in Figure 2.

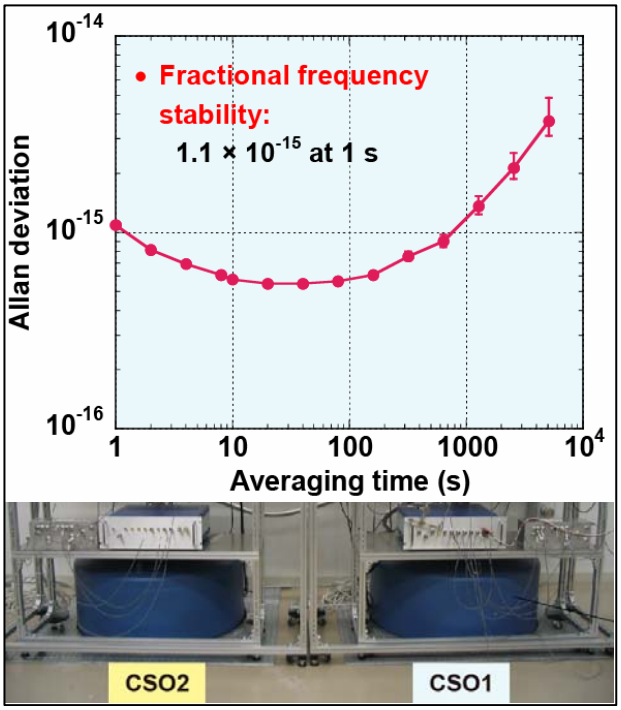

Figure 2. Two cryogenic sapphire oscillators and their frequency stability.

Optical frequency synthesis from a CSO has been implemented using a fiber-based frequency comb. The synthesized optical frequency exhibited an Allan deviation of $\sim6\times10^{-14}\tau^{-1/2}$ for averaging times between 1 s and 100 s. A minimum frequency instability of 3.0×10^{-15} at an averaging time of 1280 s was observed by comparing a rubidium two-photon stabilized laser. The short-term frequency stability was limited by the rubidium two-photon stabilized laser [6].

4. Time scale of NMIJ

UTC(NMIJ) was generated by the master clock method using one of the Cs clocks until May, 2004. From June, 2004 to February, 2006, the UTC(NMIJ) was steered using an AOG with a Cs clock as its source. In March, 2006, the Cs clock was replaced by a hydrogen maser as the source oscillator for the AOG to generate UTC(NMIJ) as shown in Figure 3. Accordingly, the short term stability and uncertainty of UTC(NMIJ) have been extremely improved. It is used for the evaluation of the primary frequency standards and optical frequency measurements, and as the reference signal for frequency traceability for industrial clients.

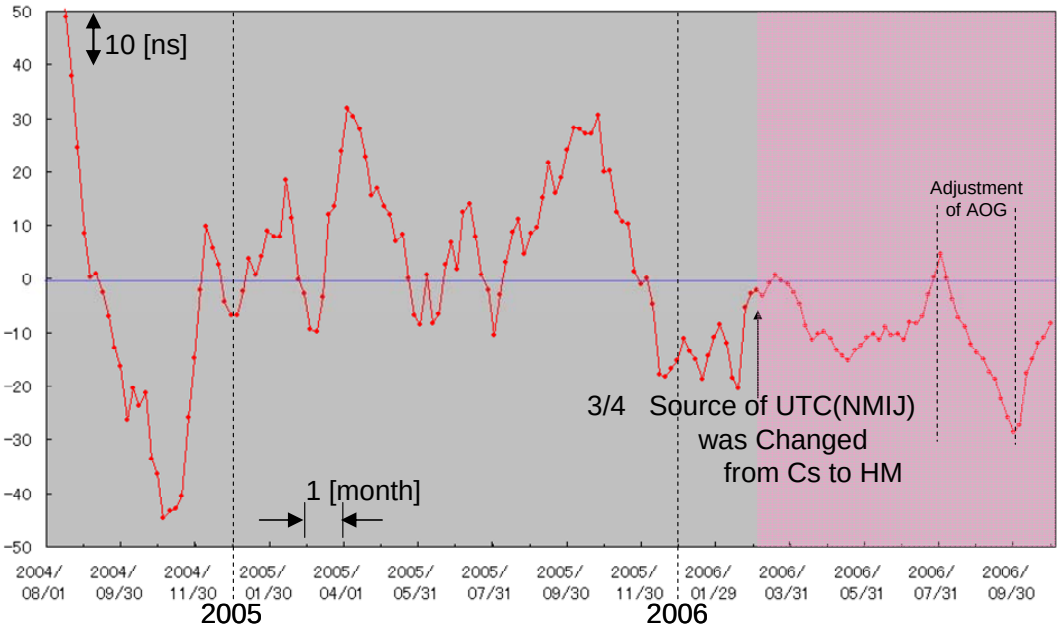

Figure 3. Recent status of UTC-UTC(NMIJ).

5. Time and frequency transfer

In order to contribute to the keeping of TAI, we have been using a Z12-T, a dual frequency GPS receiver, for global time and frequency transfer. We also have been participating in the two-way satellite time and frequency transfer link in Asia-Pacific region using JCSAT-1B and a multi-channel TWSTFT modem. For the two-way link to European institutes, we installed an earth station at NMIJ for the PAS-4 satellite as shown in Figure 4. It will be available in very near future.

Figure 4. Antennas for TWSTFT systems in NMIJ.

Two kinds of research activities are underway for highly precise time and frequency transfer. One of them is basic research on the TWSTFT using carrier phase for sub pico-second level time transfer, and for 10^{-16} – 10^{-17} level frequency transfer. The other activity is precise frequency transfer using an optical fiber network. We are developing a bi-directional fiber amplifier which can realize long distance frequency transfer using a

single optical fiber. Preliminary results obtained in the laboratory using 100 km optical fiber show the system noise to be better than 9×10^{-16} for an averaging time of 10,000 s as shown in Figure 5 [8].

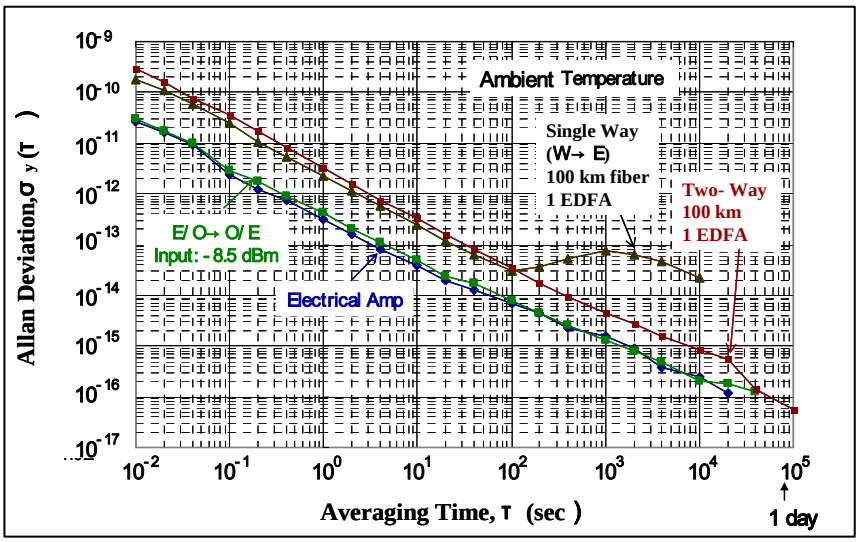

Figure 5. System noise of two-way 100-km fiber transmission with bi-directional amplifier.

6. Frequency calibration service

In January, 2005 frequency remote calibration service using GPS common-view method began, in addition to the in-house frequency calibration service [9]. Received data from the GPS common-view receivers at client sites is automatically transferred to the NMIJ data server everyday and monthly certifications are provided to the customers. We have seven customers including two Japanese-descended companies located at outside of Japan.

We are also studying the possibility of frequency dissemination using the clock signal of the public digital communication network. The preliminary results show the capability of frequency distribution to be 10^{-12} for the averaging time of 1 day [8].

7. Frequency measurement of Sr optical lattice clock

The Sr optical lattice clock was developed by the University of Tokyo, and NMIJ has collaborated to measure its absolute frequency. The university is about 50 km away from the NMIJ. The first measurement was carried out using a commercial Cs clock referenced to the SI second and the result was 429 228 004 229 952(15) Hz [10, 11]. Later JILA measured the frequency to be 429 228 004 229 869(19) Hz [12]. These two results have a poor agreement.

The University of Tokyo and NMIJ have performed an improved frequency measurement based on a hydrogen maser linked to UTC(NMIJ) using GPS carrier phase signals [13]. The Allan standard deviation of the Sr lattice clock was found to reach 2×10^{-15} at an averaging time of 1300 s. The newly obtained absolute frequency of the Sr lattice clock was 429,228,004,229,875 Hz, with an uncertainty of 4 Hz. This frequency value differs from our previous measurement by five times the combined uncertainty but falls within the uncertainty of the JILA value. The preliminary results of our improved frequency measurement were presented at the CLEO/QELS 2006 conference [14]. Later it was learned that the SYRTE group has posted

their measured frequency value of the Sr lattice clock as 429 228 004 229 879(5) Hz on the arXiv [15] during the CLEO/QELS conference. There is good agreement between the measurement results of the three groups as shown in Figure 6, and they were used to determine the recommended value, 429 228 004 229 877(6.4) Hz, for the secondary representation of second.

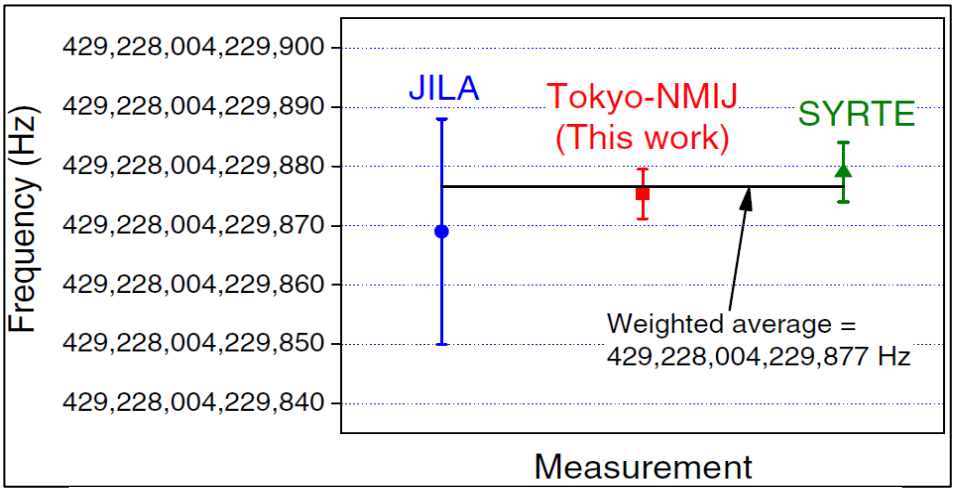

Figure 6. Three frequency measurements of Sr lattice clock.

8. Yb optical lattice clock

Development of an Yb optical lattice clock is in progress at NMIJ/AIST in cooperation with the University of Tokyo. The vacuum system, including the source oven, the Zeeman slower, and the magneto-optical trap (MOT) chamber have been constructed. The LD based 399 nm laser system for the Zeeman slower and the MOT has also been constructed. The violet MOT has been successfully built as shown in Figure 7. The fiber laser based 556 nm SHG system for the spin-forbidden MOT, and the 578 nm SFG laser system for the $^1S_0$-$^3P_0$ clock transition have been prepared.

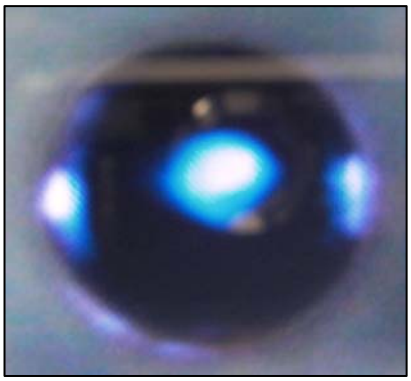

Figure 7. Violet MOT of Yb atoms.

9. Fiber frequency comb

A fiber-based frequency comb system has been developed. The system consists of a modified mode-locked fiber laser and a backward pumping amplifier, combined with a highly nonlinear fiber, which has a short zero-dispersion wavelength. As a result, the signal to noise ratio of the obtained carrier-envelope-offset frequency is larger than 45 dB at a bandwidth of 100 kHz. Using the fiber-based comb

system, frequency measurements of a 1542-nm acetylene-stabilized laser and a 532-nm iodine-stabilized Nd:YAG laser were taken over a continuous period of more than one week as shown in Figure 8. The long-term measurement revealed that the frequency stability of the iodine-stabilized laser was 5.7 x 10^{-15} at an averaging time of 100 000 s [16].

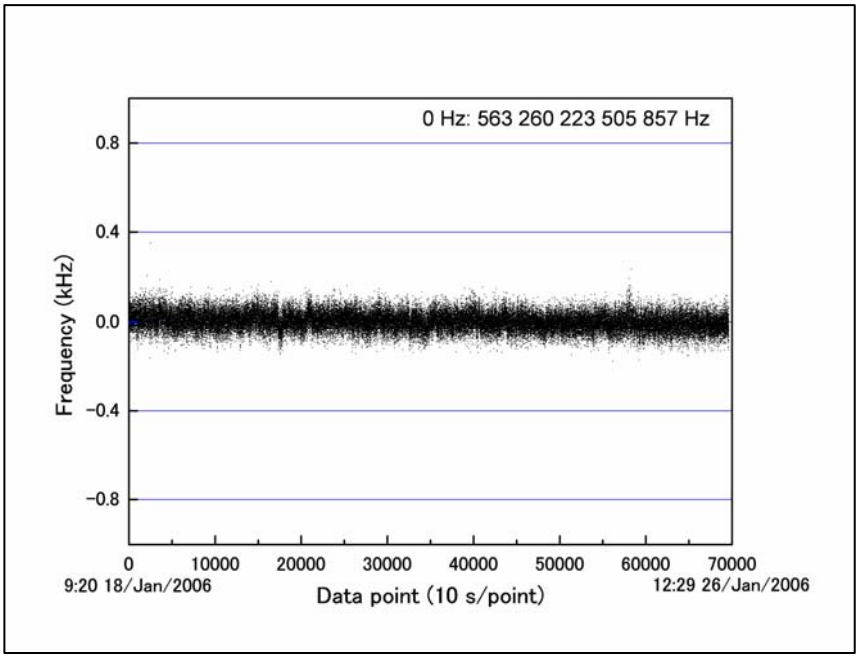

Figure 8. Long-term operation of fiber frequency comb. This example shows the frequency measurement of iodine stabilized Nd:YAG laser for one week.

References

[1] T.Kurosu, Y.Fukuyama, Y.Koga and K.Abe, “Preliminary evaluation of the Cs atomic fountain frequency standard at NMIJ/AIST.” IEEE Trans. Instrum. Meas. 53, pp. 466-471, 2004.

[2] T. Kurosu, Y. Fukuyama, K. Abe, S. Yanagimachi and Y. Koga, “Evaluation of the Cs atomic fountain frequency standard at NMIJ/AIST.” Proceedings of the joint meeting EFTF/FCS, Tampa, May 2003. pp. 68-71.

[3] S. Yanagimachi, Y. Fukuyama, T. Ikegami and T. Kurosu, "Numerical Simulation of Distributed Cavity Phase Shift in Atomic Fountain Standard." Jpn. J. Appl. Phys. 44, pp. 1468-1475, 2005.

[4] K.Hagimoto, S.Ohshima, Y.Nakadan, Y.Koga, “Accuracy evaluation of theoptically pumped Cs frequency standard at NRLM”, IEEE Trans. Instrum. Meas. 48, pp.496-499, 1999.

[5] K. Watabe, J. G. Hartnett, C. R. Locke, G. Santarelli, S. Yanagimachi, T. Ikegami, and S. Ohshima, “Progress in the development of cryogenic sapphire resonator oscillator at NMIJ/AIST”, to be published in Proc. 20th European Frequency and Time Forum.

[6] K. Watabe, H. Inaba, K. Okumura, F.-L. Hong, J. G. Hartnett, C. R. Locke, G. Santarelli, S. Yanagimachi, K. Minoshima, T. Ikegami, A. Onae, S. Ohshima, and H. Matsumoto, “Optical Frequency Synthesis from a Cryogenic Sapphire Oscillator Using a Fiber-Based Frequency Comb”, submitted to the CPEM 2006 special issue of the IEEE Transactions I&M.

[8] M. Amemiya, M. Imae, Y. Fujii, T. Suzuyama, S. Ohshima, S. Aoyagi, Y. Takigawa, and M. Kihara, “Time and frequency transfer and dissemination methods using optical fiber network”, IEEJ Trans. FM, Vol.126, No.6, pp.458-463, 2006.

[9] Y. Shibuya, Y. Fukuyama, M. Imae, M. Amemiya, T. Ikegami, and S. Ohshima, “Development and Application of the Frequency Remote Calibration System in Japan”, Proceedings of ATF2004, pp. 298-302, 2004.

[10] M. Takamoto, F.-L. Hong, R. Higashi, and H. Katori, “An optical lattice clock,” Nature 435, 321, 2005.

[11] F.-L. Hong, M. Takamoto, R. Higashi, Y. Fukuyama, J. Jiang, and H. Katori, “Frequency measurement of a Sr lattice clock using an SI-second-referenced optical frequency comb linked by a global positioning system (GPS),” Opt. Express 13, 5253, 2005.

[12] A. D. Ludlow, M. M. Boyd, T. Zelevinsky, S. M. Foreman, S. Blatt, M. Notcutt, T. Ido, and J. Ye, “Systematic study of the ^{87}Sr clock transition in an optical lattice,” Phys. Rev. Lett. 96, 033003, 2006.

[13] M. Takamoto, F.-L. Hong, R. Higashi, Y. Fujii, M. Imae, H. Katori, “Improved frequency measurement of a one-dimensional optical lattice clock with a spin-polarized fermionic ^{87}Sr isotope,” J. Phys. Soc. Jpn., 75, 104302, 2006..

[14] H. Katori, M. Takamoto, R. Higashi, and F.-L. Hong, “Optical Lattice Clock: Towards Frequency Measurement at 10^{-18} level (invited),” presented at the Quantum Electronics and Laser Science Conference 2006, Long Beach, CA, 21-26 May 2006.

[15] R. Le Targat, X. Baillard, M. Fouche, A. Brusch, O. Tcherbakoff, G. D. Rovera, and P. Lemonde, “An accurate optical lattice clock with ^{87}Sr atoms,” arXiv:physics/0605200.

[16] H. Inaba et al., “Long-term measurement of optical frequencies using a simple, robust and low-noise fibaer based frequency comb,” Opt. Express 14, pp.5223-5231, 2006.

Status Report of Time and Frequency Activities in NML–SIRIM, Malaysia

Dr. M. Nasir Z. Abidin*, A. Sahar Omar,
A. Rashid Z. Abidin and Md. Nor Md. Chik

National Metrology Laboratory (NML–SIRIM),
Lot PT 4803, Bandar Baru Salak Tinggi,
43900 Sepang, Malaysia

Abstract

This paper presents the current status of the time and frequency activities of NML–SIRIM. It also describes the development of new facilities and services which are required to the meet the demands of the government, industries and commercial e–initiatives.

1 Introduction

2 Performance Comparisons Study of GPS Common–View Location

Moving to a new location in Sepang from Shah Alam has provided us with an opportunity to investigate the quality of the GPS common–view data. Especially in relation to the GPS signal scatter and reflection caused by tall buildings in the vicinity of the GPS antenna on the roof of Building 8 in Shah Alam. In comparison the NML complex in Sepang is seen as having clear sight of the GPS signal and should in theory provide better quality data. Referring to Fig. 1, the RMS value in Shah Alam is lower due to a better technical performance GPS antenna. However the antenna's operating condition specifications indicate that it is not suitable for tropical climate, and soon developed a fault. The current GPS antenna employed is more apt to handle the humidity and temperature of a tropical climate, but the technical performance is not as good the previous antenna.

Fig. 1(b) and Fig. 2(b) show the effects caused by faulty antenna. Fig. 2 shows the improvement in the quality of the GPS data. The plots in red for Shah Alam and Sepang show the UTC difference corrected with modelled ionospheric delay, and it can be seen clearly that the daily data spread is much lower in Sepang. As for the plots in green where the UTC difference is corrected with measured ionospheric delay, the mean daily data scatter reduces from about 20 ns in Shah Alam to 10 ns in Sepang. One other factor that contributes to the improvement of the GPS data in Sepang is that the GPS antenna is rigidly mounted on a specially constructed platform that reduces vibrations.

3 Round 3 of the APMP GPS Intercomparison

APMP has been conducting an intercomparison of the internal delays of time transfer receivers at APMP laboratories. NML joined the intercomparison in Round 3, where a travelling receiver commissioned by TL Taiwan and developed at NMI Australia was shipped in the APMP region with ties made to calibrated receivers at the Observatoire de Paris and at NIST in Boulder. The receiver was hosted in October and the intercomparison lasted 10 days from late October to early November 2005, before the receiver was shipped to Paris. An interim report is currently under preparation by NMI Australia.

*Email:drnasir@sirim.my

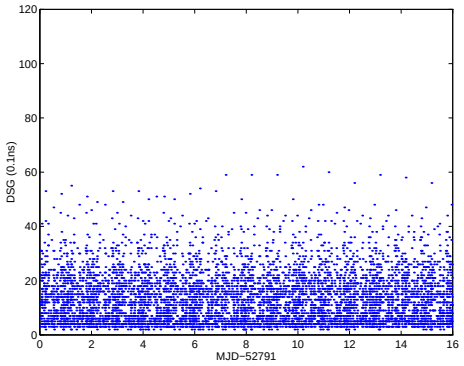

(a) Shah Alam – RMS 1.67 ns

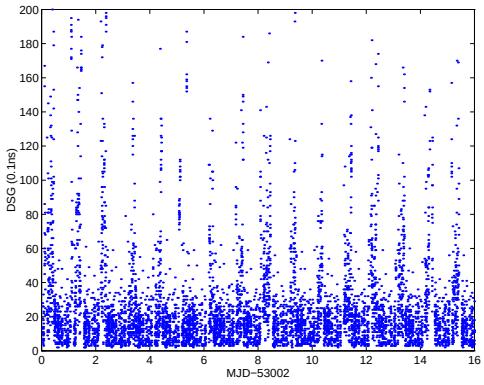

(b) Shah Alam – RMS 10.2 ns (faulty antenna)

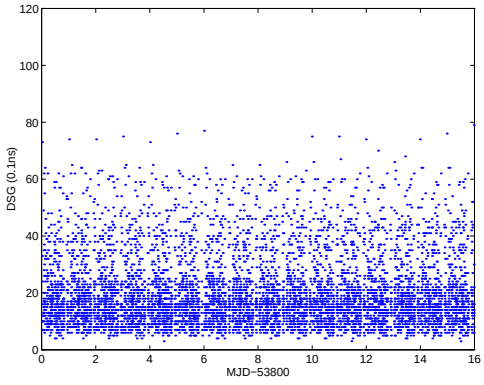

(c) Sepang – RMS 2.4 ns

Figure 1: RMS scatter of 1 s measurements of [REF–GPS] over a 13–minutes track over a 16–days study period.

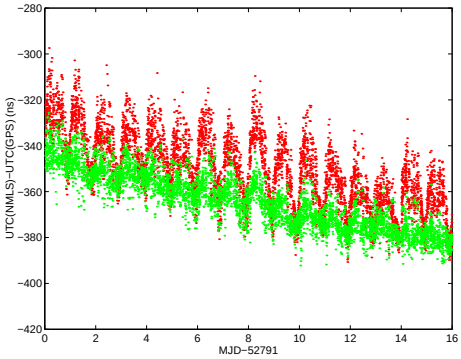

(a) Shah Alam – UTC(NMLS) not steered

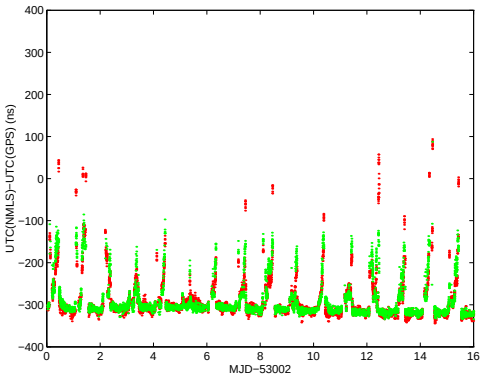

(b) Shah Alam – (faulty antenna)

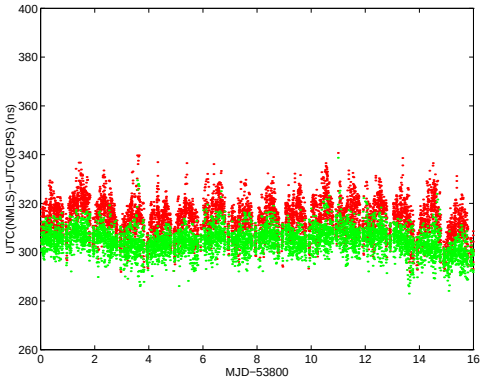

(c) Sepang – UTC(NMLS) steered

Figure 2: UTC(NMLS)–UTC(GPS) performance and comparisons between data using modelled and measured ionospheric corrections over a 16–days study period.

4 Laboratory ISO 17025 Certification and Peer Review

In 1999, the Global Mutual Recognition Agreement (MRA) was signed by the representatives of the national metrology institutions (NMIs) of the participating countries at the 21st Conference Generale des Poids et Mesures (CGPM) in Paris, France. NML, who signed the Metre Convention in September 2001 and the CIPM–MRA in October of the same year, responded to the participation in the CIPM–MRA by first, developing its quality system which will satisfied the ISO 17025 or the local DSM SAMM[1] S1 standards and second, by constructing a traceability system for all the physical measurement standards, as required for mutual international recognition. DSM certification of conformity in the ISO 17025 or DSM SAMM S1 standards for NML was partly acquired (not all NML's measurement and calibration activities were audited) in 2003. Summarizing,

- For time and frequency standards, the submission of the Global Positioning System (GPS) satellites common–view time transfer data to BIPM for the International Atomic Time (TAI) and Universal Coordinated Time (UTC) is considered as a CIPM key comparison. The contents of the publication of the regular time transfer results in *Circular–T* is registered to **Appendix B**.
- Thus, as part of the regional and global MRA, where the laboratory's developed set of calibration procedures, work instructions and associated infrastructures for quality management of device calibrations requiring accreditation as being compliant with ISO 17025 and DSM SAMM S1 standards, a peer review of the time and frequency laboratory was conducted in March, 2005. The peer review serves two purposes: one is related to the laboratory accreditation associated with DSM SAMM Scheme, and the other is related to the more critical issue of international recognition of the calibration certificates issued by NML. An issue that requires the submission and acceptance of NML time and frequency laboratory CMCs.
- Related to the Scope of Accreditation submitted for acceptance, where after the DSM reviewer reports and findings have been addressed and being made to comply, the laboratory has been awarded with the Certificate of Accreditation SAMM 261 by the DSM in February 2006.

5 Stopwatch and Timer Calibrator

Continuing from the success of SIRIM Berhad's Innovation Award, although only winning the consolation prize for the "HIGH ACCURACY IMAGING TECHNIQUE FOR THE CALIBRATION AND EVALUATION OF TIME RECORDERS, TIME DISPLAYS, TIMERS AND STOPWATCH" project in 2002, we seeked to improve the calibration facility to overcome a few shortcomings such as the minimum allowable time–interval, better uncertainty and direct traceability to the MNFS. Summarizing,

- DSM ISO 17025 Auditor in 2003 made a suggestion to look into time–interval calibration less than 1 minute, since most stopwatch applications are made less than a minute.
- Reliance on imaging have caused severe memory problem. And furthermore the technique is not able to calibrate timer directly, thus making long turnaround time for calibration.
- Therefore, we developed a new and cheap calibrator than can calibrate both stopwatch and timer, and provides a direct traceability to the MNFS.
- The "STOPWATCH/TIMER CALIBRATOR SYSTEM" developed won consolation prize of the SIRIM Berhad's Innovation Award 2004. Refer to Fig. 3 for picture and system description.
- The calibrator's measurement technique and its standard operating procedure and uncertainty evaluation was accepted and accredited by DSM auditor in the 2005 Peer Review exercise.

[1] Skim Akreditasi Makmal Malaysia (*Malaysia Laboratory Accreditation Scheme).*

(a) Stopwatch/timer calibrator

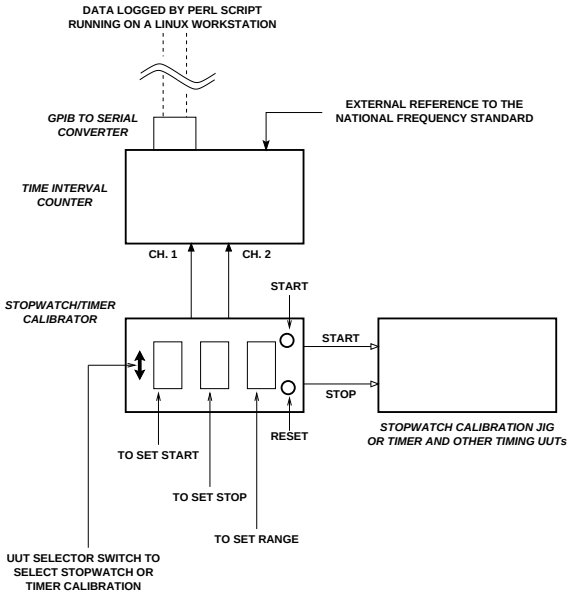

(b) Stopwatch/timer calibrator system description

Figure 3: NML–SIRIM's stopwatch/timer calibrator system. Winner of 2004 SIRIM Berhad's Innovation Award consolation prize technology category of electrical/electronic.

6 Web Time Display Project

The objective of this project is to create an animated web time display for Malaysian Standard Time. Summarizing,

- As the national timekeeper, the Time and Frequency Laboratory of National Metrology Laboratory, SIRIM Berhad, seeks to provide time services not only through automated telephone time code generator or network time protocol (NTP) servers, but also by displaying time directly on the Internet web page.
- The advantage of a web time display service is that it is accessible to the users who are connected to the Internet without any special software other than the use of HTML based browser. The accuracy of the time display will take into account the network delay between the user and the time server in SIRIM Berhad.
- There is a significant public relations benefit because it will raise public awareness of the activities of NML and SIRIM.

7 DSM Proficiency Test by Inter Laboratory Comparisons (ILC) for SAMM Scheme Programme PT1–4 Frequency

The ILC sole purpose is to assess the comparability of results issued by the laboratories accredited by DSM under the Skim Akreditasi Makmal Malaysia (SAMM) scheme. Most of the participants in this ILC are accredited by DSM with respect to their approved Scope of Accreditation. The identification code number for this programme is DSM PT1–4. This programme was coordinated by the National Metrology Laboratory (NML) SIRIM Berhad. Summarizing,

- This ILC programme is a proficiency testing programme organised by DSM, designed to gauge and evaluate whether the frequency calibration results obtained by accredited laboratories are in agreement with the reference laboratory results, and specified to be within their claimed uncertainties and with errors similarly treated. Participants are encouraged to use the method recommended by NML, but the methods which are practiced at their laboratories are allowed with the strict condition that the laboratories must present in details the actual method carried out.
- The artefact used is a Pendulum Timer/Counter/Analyzer Model CNT–90 internal quartz oscillator 10 MHz reference frequency source. The programme begun in June 2005 and completed in October 2005. A total of 9 accredited laboratories participated in this programme.
- The proficiency test by inter–laboratory comparisons confirmed that the results reported by the DSM accredited laboratories were generally in agreement either with the reference laboratory or with each other. Out of the nine laboratories only four were required to investigate the nature of their failure to get the $\mathrm{E_n}$ values to be within the limits dictated. One of the laboratories, although met the $\mathrm{E_n}$ criteria of < 1, its true measurement capability need to improve further.

8 Electronic Date/Time Authentication, Certification and Distribution System

The advent of Internet have made the progress towards an advanced information society gaining momentum, where the reliance on paper–based information is decreasing. In-line with the launched of Malaysian e–Government initiatives, digital data and information are beginning to be accepted into the social infrastructures. However, the current approach of only digitally signing the data, makes it very difficult to protect against fraudulent practices.

In handling electronically digitized documents or information which are simply bits and bytes, authoritative proof of who, what and when of an event that has occurred is vital. Problems such as spoofing,

alteration and repudiation (a phenomenon in which the existence of an event is denied after the fact, as the name implies) are abundant with digitized information. Electronic signature technology alone is inadequate to deal with such problems. Citing a few examples, it is difficult to prove the occurrence of an event such as transaction, issuance and reception without accurate time data; tampering by other or third party may be prevented but the sender can modify the description; and limitations to the effective term of the public key make it difficult to protect documents for long-term storage. These problems can be solved by having accurate and accredited electronic time stamp to the signature. On–line businesses are now seeing how vital it is to have a secure, authentic and auditable time stamp for transactions.

Summarizing,

- As a national organization, the National Metrology Laboratory, SIRIM Berhad (NML–SIRIM) already has a well established set of procedures for the maintenance and establishment of the Malaysian Standard Time (MST), the basis for the country legal and civilian time, which is directly traceable to the Coordinated Universal Time (UTC). However, NML–SIRIM only provided accurate time, but it has not accredited the time it provides. Recently, NML embarked on a project to use the time it has established as the primary reference for secure time distribution, and establishing an audit trail. Thus, providing a certified link to the UTC time - further enhancing the evidential value of time stamps created by electronic time stamping system.

- Given that local computer time is easy to change, standard NTP communications are insecure and even wireless transmissions are open to compromise, a secure and verifiable pathway to a trusted source of time is an essential prerequisite for business processes. To fulfill these NML–SIRIM recently acquired two time source master clock (TSMC) servers for the secured and authenticated time services. In using TSMC servers a solution that guarantees authenticity, security, and auditability, since it uses a combination of precision timing and Public Key Infrastructure (PKI) technology, is provided.

- The TSMC server uses a secure transport protocol, DS/NTP, to establish a secure link to a time stamping appliance or a lower clock. The linking process, which incorporates an automatic process of auditing and calibration to synchronise time, uses cryptographic keys to ensure that time values cannot be compromised in transit. At the end of the process the TSMC issues a signed certificate attesting to the calibration and traceability of the time. This certificate may form part of a chain of such certificates, held by a recognised time authority providing traceability of time used in a time stamping appliance time–stamp tokens to the national source of UTC, maintained by NML–SIRIM. The signing keys used in this process are protected by a FIPS 140–2 Level 3 HSM.

STATUS REPORT OF TIME AND FREQUENCY ACTIVITIES AT THE VIETNAM METROLOGY INSTITUTE

Nguyen Bang
Head of Time and Frequency Laboratory (TFL)
Vietnam Metrology Institute (VMI)
N^0 8, Hoang Quoc Viet Road, Caugiay District, Hanoi, Vietnam

Abstract

Laboratory of time and frequency is one of 10 laboratories belonging to VMI. Currently, main activities of VMI in the field of the time and frequency metrology are the maintenance of the national time scale, UTC(VMI) and its dissemination through calibrations and broadcasting services. This paper outlines some of the activities of the time and frequency laboratory of VMI and an update on some of the activities of the time & frequency of VMI since the most recent ATF meeting at Beijing in 2004.

1. Introduction

The main activities in time and frequency of Vietnam Metrology Institute include the maintenance of the national time scale, which is designated as UTC(VMI). Time and frequency services traceability UTC(VMI) provided to industrial and users through the calibration of frequency sources and measuring devices. The users can also access time-of-day information by Standard time (of the day) of VMI any time from the Website www.tcvn.gov.vn or through broadcast from the Radio the Voice of Vietnam at 6:00, 12:00, 18:00 and 21:00 everyday.

The corrected time of the day is then calculated and made available to users through Radio the Voice of Vietnam.

2. Clocks and UTC(VMI)

In time and frequency laboratory of VMI have two 5071A Cesium clocks, one of clocks with a high-performance tube. A dual mixer time - difference measurement system measures the time difference: TSC12030-110 made by Timing Solution Company. With the DMTD system, we can measure the time difference among up to 4 clocks at the same time, which is impossible with a time interval counter and a switch unit.

See Block diagram of the new Vietnam Standards system

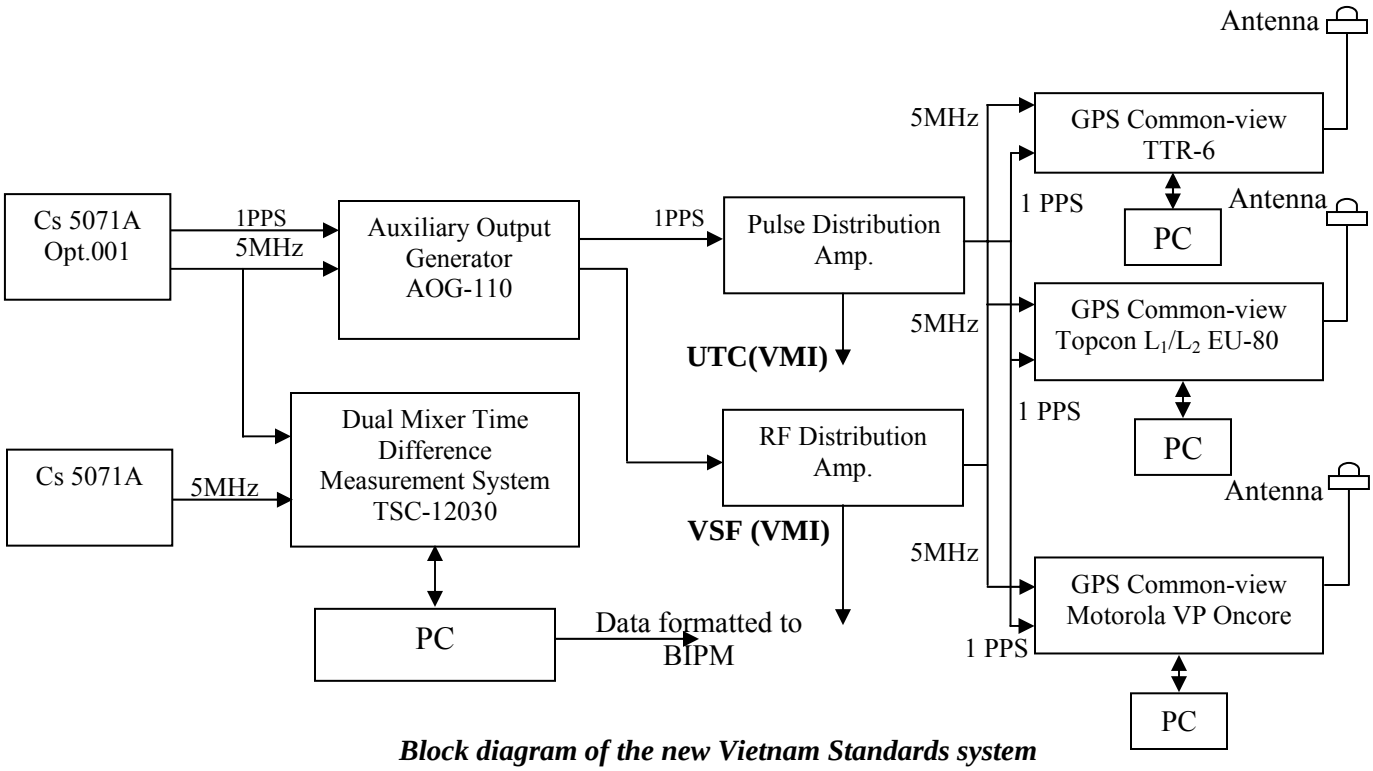

Block diagram of the new Vietnam Standards system

3. Maintenance of UTC (VMI)

UTC(VMI) is maintained with the help of high-performance 5071A Cesium clocks. It is generated by following BIPM tracking schedule for time comparisons via GPS common-view. For dissemination, it is maintained less than 1 μs of UTC. The Vietnam Standard Time is then defined as:

UTC(VMI) + 7h

4. Dissemination of time in Vietnam

The activities of time and frequency section of VMI involve the maintenance of time scale, UTC(VMI) standard time dissemination services, calibration services, research and development activities.

4.1.Calibration services:

Officially, time and frequency laboratory of VMI has been providing frequency calibration services for universal counters, signal generators, quartz oscillators, Rubidium frequency standards and the time interval from 0.01s, GPS receiver, Stop-watches, Tachometers…In house computer programs have been written for the various types of counters and frequency measuring equipments used.

4.2. Block diagram of Local clock vs. UTC(VMI) measurement

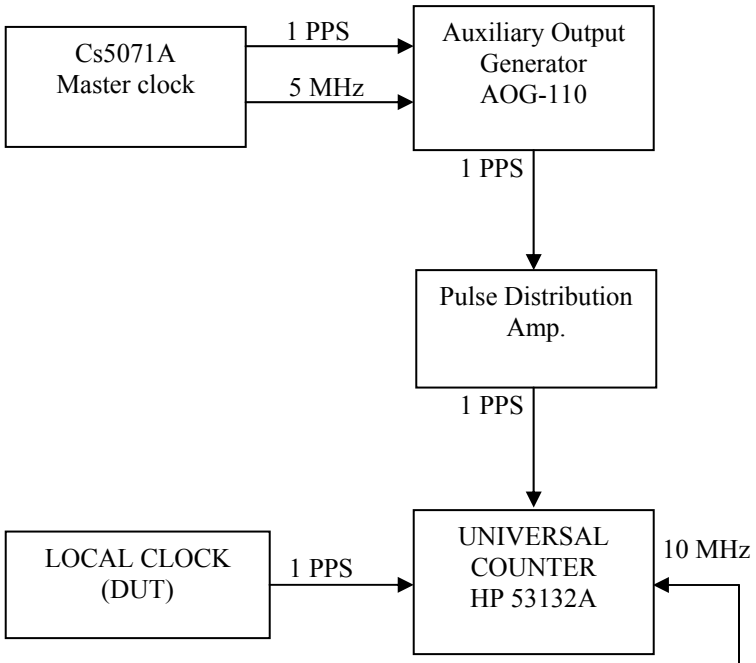

4.3. Block diagram of other measurements

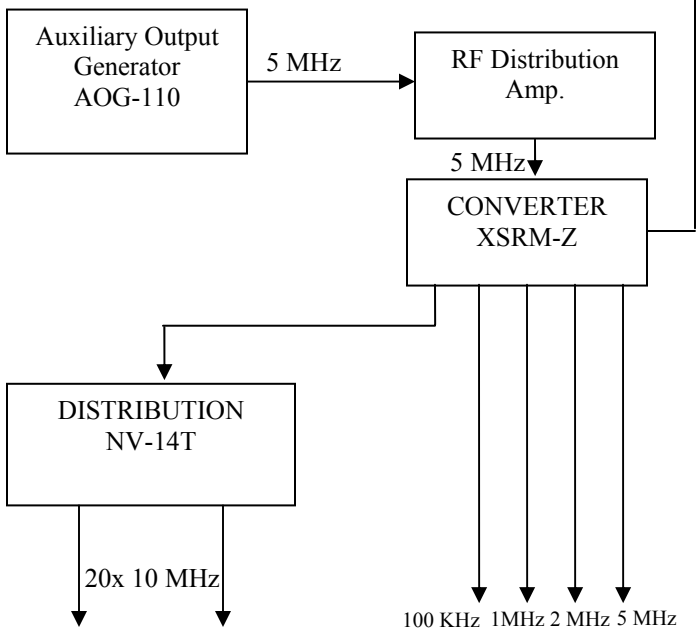

CALIBRATION INSTRUMENT

5. APMP GPS common-view time transfer experiment.

Now, we have three systems use to GPS common – view time transfer include TTR6, Topcon and Oncore systems.

Every month we download the data from APMP website and generated the reports for Topcon and Oncore systems. For examples:

The results from 1st to 15th October 2006 of the GPS common – view time transfer between UTC(VMI) and UTC(NMIA) used ONCORE receiver are shown in Fig 1

10/2006	MJD	(ΔF/F).E-13 (0000 UTC)	UTC_{VMI} -UTC_{NMIA} (0000 UTC) (ns)	σ (ns)	$\sigma/\sqrt{N}$ (ns)	N
1	54009	-0.6+/-1.3	162	22	3.1	50
2	54010	-2.5+/-1.4	158	23.8	3.2	54
3	54011	-2.5+/-1.4	146	25.3	3.3	57
4	54012	-1.6+/-1.3	140	24.6	3.3	57
5	54013	-2.6+/-1.3	132	23.4	3.1	57
6	54014	-1.2+/-1.5	127	27.5	3.6	57
7	54015	-3.4+/-1.4	114	25.3	3.4	57
8	54016	-3.4+/-1.2	93	22.8	3	57
9	54017	-2.8+/-1.3	77	23.3	3.1	57
10	54018	-3.2+/-1.4	64	26.4	3.5	57
11	54019	-2.5+/-1.2	51	21.9	2.9	57
12	54020	-2.4+/-1.2	40	21.5	2.8	57
13	54021	-2.4+/-1.2	29	22.5	3	57
14	54022	-2.5+/-1.3	20	24.1	3.2	56
15	54023	-2.4+/-1.3	12	24.4	3.3	54

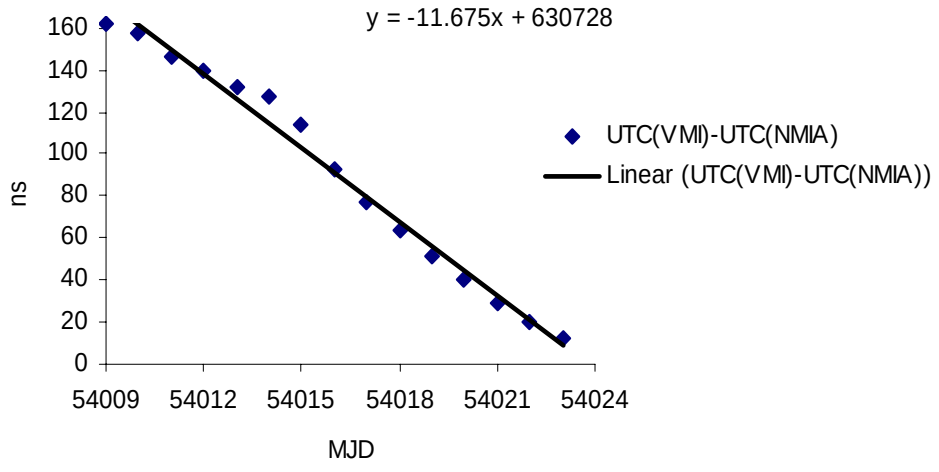

Fig1. The results from 1st to 15th October 2006 of the GPS common – view time transfer between UTC(VMI) and UTC(NMIA) used ONCORE receiver

From value y = -11.675 we can calculate to the difference frequency offset per day is -1.4 E-13.

The results from 1st to 15th October 2006 of the GPS common – view time transfer between UTC(VMI) and UTC(NMIA) used JAVAD EU-80 receiver are shown in Fig 2

10/2006	MJD	(ΔF/F).E-13 (0000 UTC)	UTC_{VMI} -UTC_{NMIA} (0000 UTC) (ns)	σ (ns)	$\sigma/\sqrt{N}$ (ns)	N
1	54009	-0.8+/-0.4	210	7.4	1.1	49
2	54010	-2.5+/-0.8	203	13.2	1.8	53
3	54011	-2.2+/-0.7	191	13.5	1.8	57
4	54012	-1.3+/-0.7	185	13.6	1.8	57
5	54013	-2.4+/-0.7	176	12.3	1.6	57
6	54014	-2.3+/-0.8	164	14.2	1.9	56
7	54015	-2.3+/-0.7	153	12.5	1.7	56
8	54016	-3.1+/-0.7	138	12.6	1.7	57
9	54017	-2.4+/-0.8	122	13.9	1.9	56
10	54018	-2.8+/-0.7	107	12.4	1.7	55
11	54019	-1.9+/-0.7	95	12.8	1.7	55
12	54020	-2.4+/-0.7	83	12.7	1.7	56
13	54021	-2.2+/-0.7	71	12.5	1.7	57
14	54022	-1.9+/-0.7	62	12.9	1.7	56
15	54023	-1.9+/-0.8	55	14.3	1.9	56

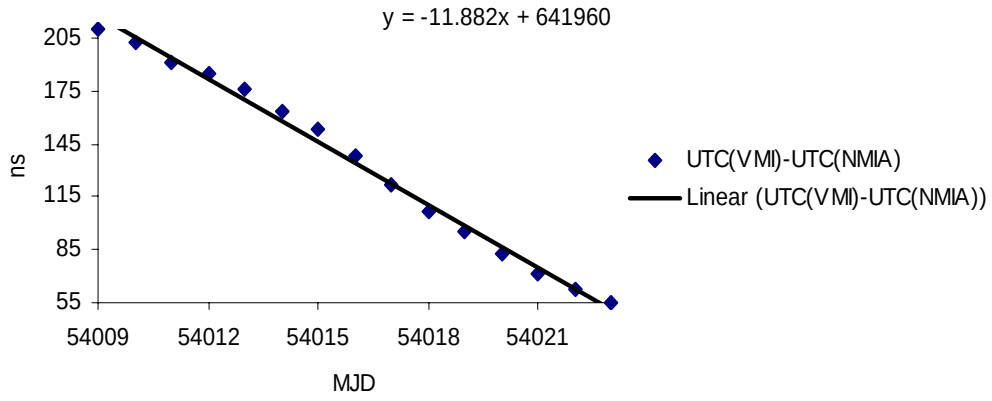

Fig 2. The result of the GPS common – view time transfer between UTC(VMI) and UTC(NMIA) used Javad EU-80 receiver

As a result, the measurement uncertainty between 10^{-13} to 10^{-14} had been reported from our laboratory.

6. Future development plan

The future plans for VMI time and frequency activities are summarized as follow:

- Continue disseminations of time on the Radio the Voice of Vietnam and researching about disseminations of time though NTP.
- Distribution time by NTP
- After the new Standards time system operating stable, we'll send the data from GPS common-view system and difference time UTC(VMI) – Clock (1,2) to BIPM.
- Submission of CMC for the regional and international MRAs

7. Acknowledgements

We would like to thank Dr. HosongLee and all colleges in Time and frequency Group of Korea Research Institute of Standards and Science (KRISS) helped us to build the new time and frequency standards system.

Dr. Peter Fisk of NMIA Australia and Dr BruceWarrington together with staff of the Time and Frequency Group have been providing and setting up the GPS common – view system at VMI Javad EU-80 L_1/L_2, and have sending two reports of the GPS common – view time transfer between UTC(VMI) and UTC(NMIA) used Javad EU-80 and Oncore receiver to us every weeks.

Reference

[1] Actives Time and Frequency in Vietnam Metrology Institute. (Proceeding of the fourth National Conference on Metrology – 11/2005-Nguyen Bang & Trieu Viet Phuong)

[2] Report of NML on GPS Common-view time and frequency transfer between NMIA and VMI, September 2006.

[3] APMP CCTF Data Plot, National Measurement Institute Australia

[4] Status report of Time & Frequency activities of KRISS, NIMT, NMIA, ATF 2004.

Status Report on Time and Frequency Activities at KRISS

Taeg Yong Kwon, Dai-Hyuk Yu, Sang Eon Park, SooHeyong Lee, Sung Hoon Yang, Chang Bok Lee, Young Kyu Lee, Seung Woo Lee, Chang Yong Park, Won-Kyu Lee, and Ho Seong Lee

Korea Research Institute of Standards and Science, 1 Doryong, Yuseong, Daejeon, 305-340 Korea

Abstract

We introduce the research activities being carried out at the Time and Frequency Laboratory of the Korea Research Institute of Standards and Science (KRISS). Research activities related to time and frequency and performed by other groups within the Division of Physical Metrology of KRISS are also introduced.

1. Introduction

Research activities in time and frequency field up to 2004 were described in a previous report at ATF2004[1]. In this paper, we briefly report recent progress and introduce research activities newly begun at KRISS.

At present, KRISS research activities in time and frequency involve the following;

- Maintenance and generation of UTC(KRIS) and TA(KRIS)
  - Time comparison system between commercial atomic clocks
  - Research on time scale algorithms
- Development of cesium atomic frequency standards
  - Cesium atomic fountain
  - Optically-pumped cesium beam frequency standard (KRISS-1)
  - Development of a multi-launched fountain system
- Development of optical frequency standards
  - Ytterbium optical lattice clock
  - Absolute optical frequency measurement with femtosecond comb
- Precise measurement and calibration
  - Development of a remote frequency calibration system
  - RF and optical frequency transfer over a fiber network
- Time comparison via satellites
  - GPS common-view time transfer system
  - Two-way satellite time transfer system
  - GPS carrier phase experiments
- Dissemination of standard time and frequency
  - Time service through the internet
  - HLA broadcasting station

2. Maintenance and generation of UTC(KRIS) and TA(KRIS)

The Korea Research Institute of Standards and Science (KRISS) is in the process of re-newing its traceability system in time and frequency (Figure 1.).

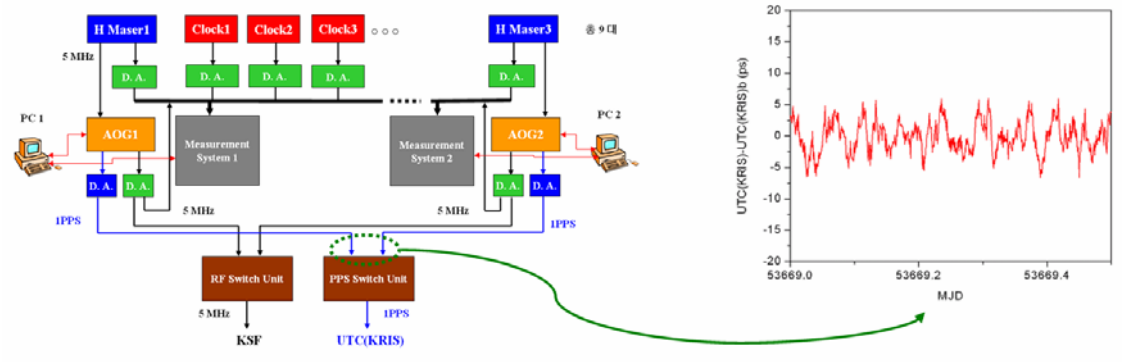

Fig. 1. Dual system to keep traceability to UTC.

We have five cesium clocks (HP5071A, four of them have high-performance beam tubes) and three hydrogen masers (Sigmatau and KVARZ) in the timescale-generating clock ensemble. One more hydrogen maser will be operational in 2007. To ensure reliability of UTC(KRIS) generation, we are building dual UTC(KRIS) generation system. Fig. 1 shows the block diagram of the dual system and its capability of time synchronization. Each system use different hydrogen maser as a reference and steer the frequency by using a phase microstepper (AOG110, Symmetricom). Resulting 1 PPS and 5 MHz signals are fed into the PPS and RF switch unit respectively. In case of sudden failure, the switch units automatically change the reference input to 1 PPS and 5 MHz output of another system in normal operation. As shown in Fig. 1, 1 PPS outputs from two UTC(KRIS) generation system can be synchronized within 10 ps. In the final operation status with each system maintained independently, the time difference between the two may need post-correction after the sudden input change. We are in the progress of moving all the atomic clocks into the stability chambers, which keep the temperature within 0.1 ^{o}C and relative humidity within 1 %. After the stabilization of clocks in the chambers, we will finalize the new set-up of UTC(KRIS) generation system.

3. Development of Cesium atomic frequency standards

We are developing a cesium atomic fountain frequency standard and a cesium atomic beam frequency standard at KRISS[2]. Here we briefly introduce the recent research results obtained from an optically-pumped cesium beam frequency standard(KRISS-1).

Several components of KRISS-1 have been redesigned and reassembled recently in order to increase magnetic field homogeneity and to reduce the light scattering. We developed an alternative method to derive the atomic velocity distribution and Rabi frequency much more accurately using a regularized inverse on two Ramsey spectra. This method offers a diagnostic tool for measuring cavity response and atomic population in Zeeman sublevels, which are essential for calculating the cavity pulling and Rabi pulling shifts. As shown in Fig. 2, the Allan deviation of KRISS-1 is reduced due to the improvements in hardware. The long term stability is about 5.5×10-15 at a sampling time of 3×104 s. Table I displays the uncertainty evaluation result

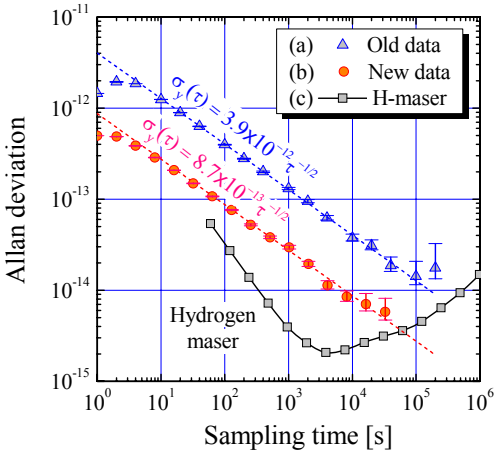

Fig. 2. Allan deviation of KRISS-1 relative to hydrogen maser (a) before and (b) after the improvements.

for KRISS-1. There are certainly improvements due to redesigned hardware such as C-field inhomogeneity and light scattering. However, more importantly, considerable improvements are made in shift parameters that depend on accurate deduction of atomic velocity distributions and Rabi frequency values. At current state, most significant sources of frequency shifts are cavity phase and light scattering, which limit the combined systematic uncertainty of KRISS-1 to 1.2×10-14. In overall, both type-A (statistical) and type-B (systematic) uncertainties were reduced by hardware and software improvements.

Table I. Relative frequency biases and their uncertainties (preliminary results).

Physical Effect	Shift × 10^{14}	Uncertainty × 10^{14}
Quadratic Zeeman effect	46837.5	0.1
C-field inhomogeneity in drift region	1.48 → 0	0.1 → **0.042**
Resonance inhomogeneity*	0	0.23 → < **0.1**
Quadratic Doppler effect*	-31.1	0.28 → **0.05**
Cavity pulling*	0	0.52
Bloch-Siegert shift*	0.35	0.04 → **0.0002**
Rabi pulling*	0	0.2 → < **0.05**
Gravitational shift	0.95	0.1
Blackbody radiation	-1.64	0.02
End-to-end cavity phase*	406.5	2.4 → **0.7**
Fluorescent light shift*	-	< 0.3
Scattered light shift*	7.8	3.5 → **0.8**
Combined type B uncertainty		4.3 → **1.2**

*: bias depending on the transit time distribution and the Rabi frequency.

4. Development of optical frequency standards

4.1. Ytterbium optical lattice clock

We are developing an optical lattice clock based on ^{171}Yb fermion isotope. The ultimate stability and accuracy of the Yb optical lattice clock are expected to be well below 10^{-15} (at 1 s) and 10^{-17}, respectively. The current research status is summarized as follows: 1) Previous magneto-optical trapping of Yb atoms using frequency-stabilized violet laser diodes has been improved with attached Zeeman slower, which increased the lifetime for trapping process. We are now working on decreasing the trap temperature of the Yb MOT below 0.1 mK in order to transfer Yb atoms effectively into the optical lattice potential formed by a single-mode Ti:sapphire laser at 759 nm. 2) We are developing a sub-Hz laser with 1156.8 nm diode laser locked to the high-finesse optical cavity. The laser will be frequency doubled to probe the clock transition at 578.4 nm. 3) We have constructed the optical frequency synthesizer based on 1 GHz ring Ti:sapphire femtosecond mode-locked laser. Tracking ability of the system will be measured by comparing the system with the previously developed 100 MHz based one. Details of the research can be found in [3].

4.2. Absolute optical frequency measurement with a femtosecond comb

We developed a optical comb injection-locking technique into a diode laser to increase the S/N ratio of the beat note signal when measuring the absolute optical frequency of a laser[4,5]. The injection-locked diode laser acts as a single-frequency filter and, simultaneously, a high-gain amplifier of the optical frequency comb. Using this method,

we measured the absolute frequency of an external cavity diode laser (ECDL) locked to F=4 → F'=5 transition of cesium D2 line with MTS (modulation transfer spectroscopy) technique[4,5], where the optical frequency synthesizer based on a 1 GHz femtosecond laser system linked to the hydrogen maser. The absolute frequency of an ECDL locked to F=4 → F'=5 transition of cesium D2 line, f_{ave}, is measured to be (351,721,960,559 ±39) kHz. Details of the research can be found in [6].

5. Precise measurement and calibration

5.1. Development of a remote frequency calibration system

We have developed a remote frequency calibration system(Fig. 3). The GPS common -view technique is adopted for remote calibration of frequency generators. The CMC of the remote frequency calibration was estimated to be 2.5×10^{-13}.

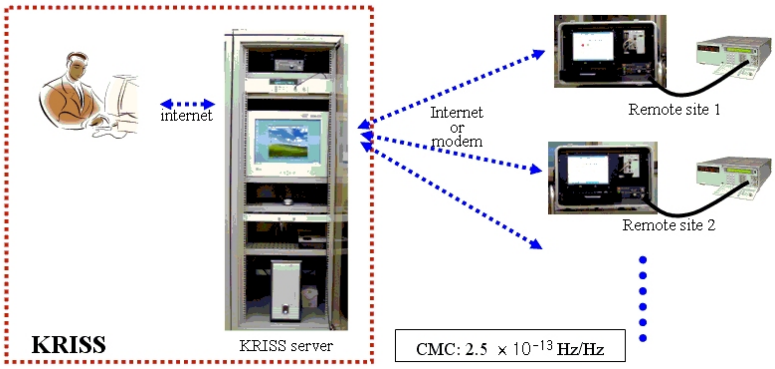

Fig. 3. Remote frequency calibration system.

5.2. RF and optical frequency transfer over a fiber network

We have installed an underground fiber network which connects two laboratory buildings in KRISS to deliver the optical frequency standards and the RF/microwave frequency standards between them. The fiber network has a length of 250 m and consists of 24 single mode fibers with five different fiber core sizes to cover the wavelength range from 400 nm to 1600 nm. We have transferred highly stable 100 MHz RF standard produced by a low noise synthesizer referenced to a hydrogen maser through a 23 km fiber network which is made up of the round-trip fiber network mentioned above and a 22.5 km fiber spool. The RF is transferred by the amplitude modulation of a 1550 nm DFB laser by a Mach-Zehnder modulator. The fiber-induced phase noise due to the vibration and the temperature fluctuation in the optical path is detected and is compensated by configuring a noise-canceling servo. The transfer instability was 6×10^{-14} at 1 s of averaging time and 2×10^{-17} at 10000 s of averaging time (Fig. 4). The single sideband phase noise was greatly reduced by more than 20 dB below the Fourier frequency of 1 kHz by this servo. The transferred RF has nearly the same stability as the original reference frequency. Also, we have transferred a narrow-linewidth 1.5 μm laser through a 525 m fiber network with excellent transfer stability. The fiber-induced optical phase noise during the fiber transmission is cancelled by configuring a noise-canceling servo utilizing an acousto-optic modulator. The standard deviation of the optical phase fluctuation was 0.21 rad and the transfer instability was 2×10^{-17} at 1 s of averaging time (Fig. 5).

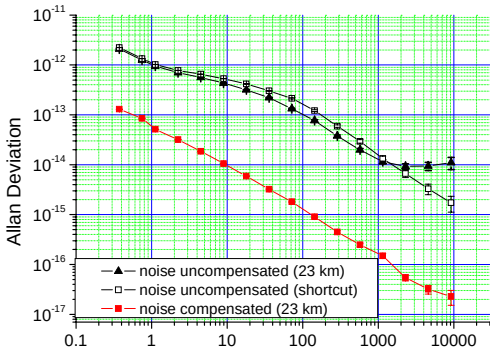

Fig. 4. RF (100 MHz) transfer instability when 23 km fiber was used.

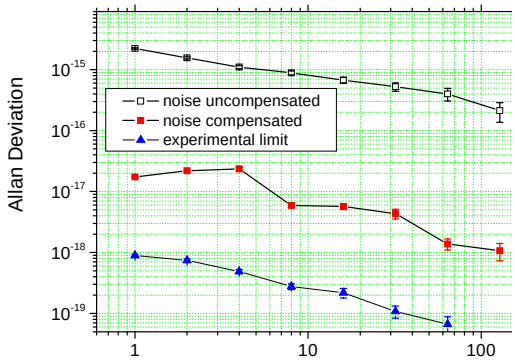

Fig. 5. Optical frequency transfer instability when 525 m fiber was used

6. Time comparison via satellites

At KRISS, three techniques of time comparisons were employed: one is the use of geodetic GPS receivers allowing the GPS P3 analysis to be achieved; another is TWSTFT; and the other is GPS carrier phase.

Three TWSTFT systems have been constructed at KRISS. One is for Asia link via JCSAT-1B which belongs to the JSAT communications satellites group, another for Oceania region via PAS-8 which is a member of the PanAmSat communications satellites, and the other for Europe link via PAS-4. We use multi-channel modems developed by the National Institute of Information and Communications Technology (NICT), which have capability of performing simultaneous two-way time transfer functions among a maximum of 7 stations. Fig. 6 shows the network connected to the TWSTFT modem at KRISS. For now, the time transfer experiments via JCSAT-1B have been accomplished by 6 institutes: NICT(Japan), National Metrology Institute of Japan (NMIJ, Japan), National Time Service Center (NTSC, China), Telecommunication Laboratories (TL, Taiwan), Standards, Productivity and Innovation Board (SPRING, Singapore) and KRISS (Korea). In this paper, the time difference data obtained from a subset of 4 laboratories (KRISS, NICT, TL and NMIJ) in such a network were used for the comparison between time transfer techniques by using GPS P3, GPS CP and multi-channel TWSTFT via JCSAT-1B.

The modem used for TWSTFT via JCSAT-1B is a multi-channel model based on the code division multiple access (CDMA) technique. Simultaneous time transfer among 7 institutes can be conducted by employing a single modem. It is observed that one extra channel in the modem is dedicated to measure the signal path delay in order to account for the temperature variations and unexpected events occurred during signal travel

For the GPS time comparison, geodetic receivers are generally used to measure pseudo-range and collect carrier phase measurements. Two geodetic receivers are now in operation at KRISS and are continuously retrieving code and phase measurements from all observable satellites at both L1 and L2 frequencies. The receivers are referred to 20 MHz and 1 pulse per second (PPS) signals from a hydrogen maser. The code and phase measurements recorded by the receivers are stored at every 30 seconds in Receiver INdependent EXchange (RINEX) format files. It is well known that some corrections to the time transfer measurements should be made in order to achieve a higher precision: for example, applying precise orbit data and eliminating ionospheric and tropospheric delays. A software developed by KRISS is used to analyze the GPS carrier phase data. The input data to the software for the GPS time comparison

are obtained from the RINEX files, and the GPS carrier phase and pseudo-range data are processed together with the precise GPS orbit information provided by the International Global Navigation Satellite System (GNSS) Service formerly known as International GPS Service (IGS). The effect of ionosphere delays is removed by applying the ionosphere-free combination of L1 and L2 carrier phase data, while that of tropospheric delays is removed by using Saastamoinen's model with the given standard atmosphere values of temperature, atmospheric pressure and vapor pressure coefficients. Using above methods, we can get the results that difference between P3 code and TWSTFT vs. carrier phase and TWSTFT after subtracting the average value from the data in Fig. 7.

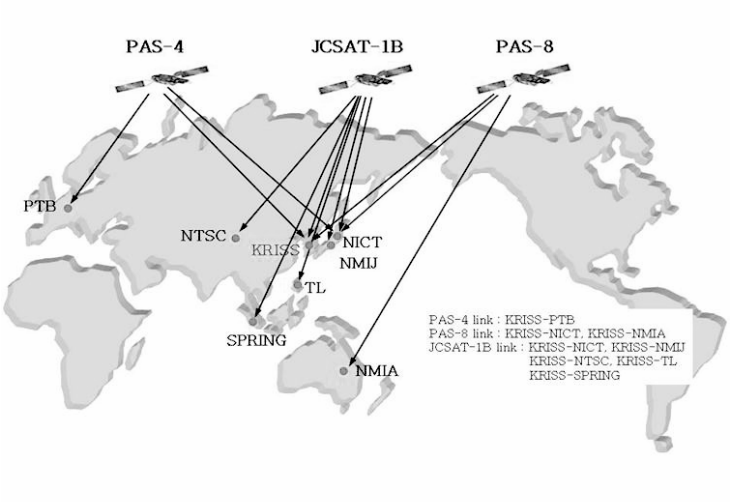

Fig. 6. Time transfer links at KRISS by means of TWSTFT method.

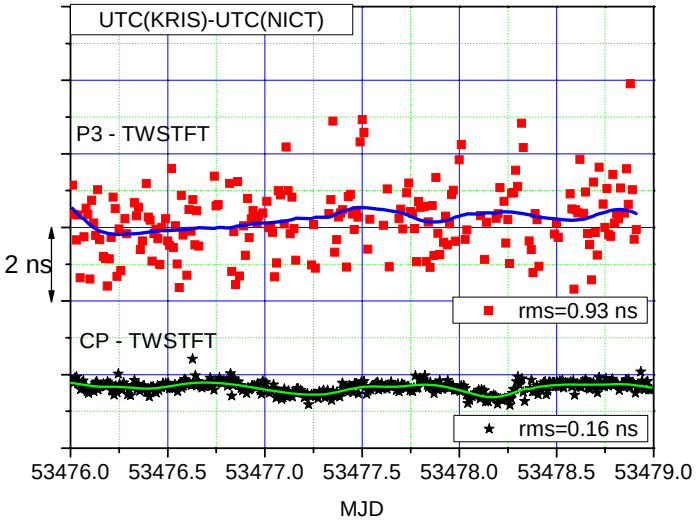

Fig. 7. Difference between P3 code and TWSTFT vs. carrier phase and TWSTFT after subtracting the average value from the data, and each difference was intentionally shifted for easy distinction.

7. Dissemination of standard time and frequency

We have upgraded our NTP service. Since 2005, three NTP servers have dealt with more than 15 million connections per day of internet standard time synchronization requests. Before this upgrade, three servers are located inside internal network of our institute. NTP services are sometimes open to a huge amount of connections and cause failure of internal network equipments such as the main firewall. If this happens, NTP service was also stopped. To solve the problems, we moved the logical location of the servers outside of the internal network. Users who wish to synchronize the computer clock can now connect to the server directly without passing through KRISS internal network. We also changed the servers from the computers with WIDOWS environment to the Linux based NTP servers as shown in Fig. 8. Two new servers are in operation for redundancy.

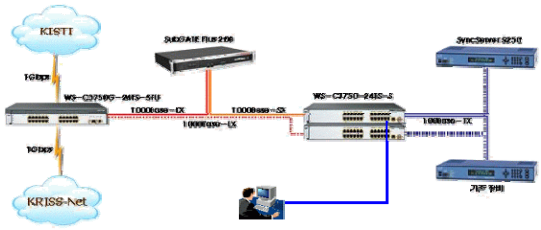

Year	Number of Time Servers	Users per day)	Hits (million/day)
2002	2	63,000	1.6
2003	3	100,000	6
2004	3	170,000	9
2005	3	250,000	15

Fig. 8. Upgrade of Korea Standard Time NTP service.

References

[1] T.Y. Kwon et al., 2004, Proc. ATF2004, pp. 72.
[2] H.S. Lee et al., 2004. J. Korean Phys. Soc., 45, 256.
[3] C.Y. Park at al., 2006, Proc. ATF2006, to be published.
[4] S.E. Park et al., 2006, Opt. Lett., 31, 3594.
[5] S.E. Park et al., 2006, Proc. ATF2006, to be published.
[6] E.B. Kim et al., 2006, Proc. ATF2006, to be published.

Status Report on Time and Frequency Standard Activities at ITDI[1]

Manuel M. Ruiz

Electricity, Time and Frequency Section, National Metrology Laboratory
Industrial Technology Development Institute, Manila, Philippines

This report discusses the time and frequency facilities and activities at the Industrial Technology Development Institute, Manila, Philippines. It describes the process for obtaining international traceability for its reference standard and the dissemination of traceable values through the calibration services it provides. It also describes its plans for the improvement of its capabilities and services.

Introduction

ITDI is mandated by law to maintain physical standards for basic units of measurement - time interval and its dimensional reciprocal, frequency included. Under the same law, PAGASA[2] tasked with maintaining Philippine standard time (of day). ITDI, in its mission to provide traceable time and frequency calibrations to industry, has also attained the capability to provide its own estimates of UTC – time of day.

Facility on Time and Frequency Standards at ITDI

ITDI presently maintains a lone HP 5071A Cesium Beam Frequency Standard as its standard for time and frequency. Through a cooperation with the National Measurement Institute of Australia (NMIA), the 1 pps output of this standard is continuously compared with the Australian national frequency standard through the GPS common view technique. The GPS receiver, computer hardware and software both for controlling the receiver and extracting and converting timing data into CCTF format were provided by NMIA under a project involving selected NMI's in the Asia-Pacific region. A block diagram for the comparison set-up is shown in Figure 1.

ITDI also maintains a commercial HP 58503A Multi-channel GPS Time and Frequency Reference Receiver as an independent back-up standard to its cesium system.

All frequency measurement and generation activities performed at the facility are directly referenced to the cesium standard ~~(through a distribution amplifier)~~.

Traceability of ITDI Time and Frequency Standards

The Philippines not being a member of the Meter Convention obtains traceability to UTC using timing data from a member state, i.e., Australia as follows:

$$\frac{\text{UTC} - \text{UTC}(\textit{Australia}) \quad \text{—— (1)}}{\text{ITDI Ref} - \text{UTC}(\textit{Australia}) \quad \text{—— (2)}} - \frac{}{\text{UTC} - \text{ITDI Ref}}$$

[1] ITDI – Industrial Technology Development Institute
[2] PAGASA – Philippine Atmospheric, Geophysical and Astronomical Services Administration, Department of Science and Technology (DOST)

Data needed for 1 is obtained from BIPM's Circular T Publication. Data needed for 2 on the other hand comes in part from timing equipment at ITDI which is compiled and processed into a weekly report by NMIA. The report gives the epoch difference and fractional frequency offset of ITDI's standard with respect to Coordinated Universal Time Australia, UTC*(AUS)* and the Australian National Frequency Standard, respectively.

Traceable Frequency Distribution at ITDI

Figure 2 shows the frequency distribution system provided by ITDI in the country.

Traceable frequency is disseminated to users in the form of calibration services. Time and frequency related instruments submitted for calibration at ITDI include:

- High Stability Frequency Oscillators and Generators
- Universal / Frequency Counters
- Time Interval Counters
- Stopwatches / Timers
- Tachometers / Stroboscopes

ITDI's time and frequency facility also provides traceable frequency for its other measurement activities in the low frequency Ac and RF fields.

Calibration and measurement activities are mostly computer aided to make work more efficient and convenient for the staff.

Official Philippine Standard Time Keeper

The Time Service Unit of the PAGASA, a sister organization of ITDI, is responsible for maintaning and disseminating Philippine Standard Time (PST). For this time keeing purpose, PAGASA has operated since 2004 a rubidium based common view GPS time transfer system developed by the NMIA (Figure 3). International traceability is acquired through a three way clock comparison with ITDI and NMIA (Figure 2).

The PAGASA timing system is capable of serving as a stratum 1 network time protocol server for disseminating time through the internet but this dissemination service is presently suspended due to network security concerns. Time of day dissemination is presently performed aurally by voice through the telephone to interested users.

Other Related Activities and Plans

- Training. ITDI participated in the ASEAN Seminar and Workshop on Measurement Standards in Bangkok which presented the "e-trace" Remote Time and Frequency Standard Calibration System using GPS CV Method developed by the AIST, Japan. This forum also provided the opportunity to compare calibration methods used in NIMT together with their evaluation and treatment of uncertainties in frequency measurements. This event also provided the occasion for comparing and validating results of ITDI's in-house developed Allan Variance calculator with the NIMT software.

- APMP Comparison. ITDI recently participated in the APMP GPS Receiver intercomparison. ITDI stands to benefit from the exercise by obtaining delay values for its CV GPS receiver and also better determination of its antenna coordinates as an end result of this activity.

- Proficiency Testing and Laboratory Accreditation. ITDI has started to provide local interlaboratory comparisons in various fields of measurement. This activity is in support of the Philippine Laboratory Accreditation Service as part of the assessment process of accrediting calibration laboratories. ITDI will organize and coordinate a calibration interlaboratory comparison of a frequency counter early 2007. ITDI will also act as the reference laboratory for this activity.

  ITDI also provides technical assessors for undertaking assessment activities for the Philippine Laboratory Accreditation Service.

- Short Term Collaborative Activities. ITDI has proposed a collaborative project with the Department of Science and Technology, Shanxi Province under the China – Philippines 13th protocol on Science and Technology. Proposed areas of cooperation are:
  - Standard time dissemination through a combination of voice and audio beeps. This activity seeks to investigate and establish accuracy of "as received" time signals at a particular reception point (by measurement of propagation delay). This will be a joint activity with PAGASA.
  - Design and development of interlaboratory comparison protocol on the calibration of frequency counters and frequency sources. This activity intends to include improving present measurement techniques and the identification and evaluation of error sources.

- Establishment of Quality System and Accreditation of Measurement Services. Facing pressure from industry and the Philippine Laboratory Accreditation Service for traceable time and frequency measurements, ITDI has started to document its activities and procedures. As an attendant activity, a more rigorous investigation and treatment of measurement uncertainties is being undertaken.

Challenges and Opportunities

Sourcing of funds for updating, upgrading and maintenance of equipment and facilities has always been challenge for the ITDI. Equipment are now relatively old and chances of failure grow with each passing day. Environmental conditioning and back up power supply for the laboratory also need to be addressed. The ITDI also faces the lack of trained personnel to staff the laboratory. In addition, cost would be a major constraint in its planned accreditation of its measurement services. ITDI however could take the opportunity of the demand placed by industry to provide internationally traceable measurement services. A recently passed metrology law will also enable ITDI to use funds generated from its calibration services for improvement of its facilities.

Conclusion

Aside from revenue remitted by its overseas manpower, the economy of the Philippines relies to a great extent on its top export earner, the electronics industry. Traceability of standards and measuring instruments used for quality control of products it exports is essential if not a requirement. ITDI being the primary supplier of measurement standards in the country continually strives (no matter how meager its resources may be) to provide traceability at uncertainty levels appropriate and required by its industry.

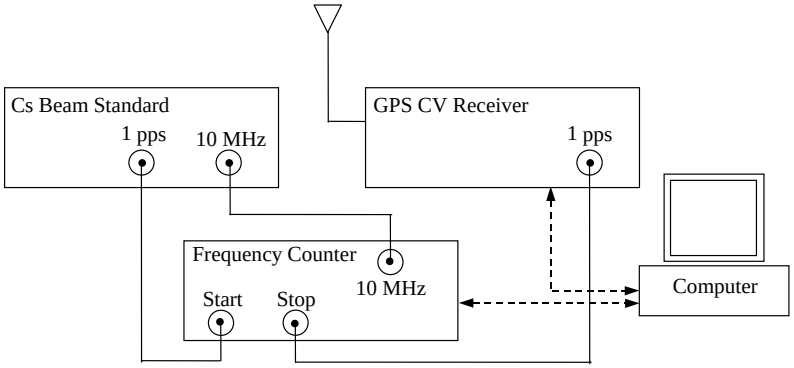

Figure 1. GPS Common View Comparison Set-up

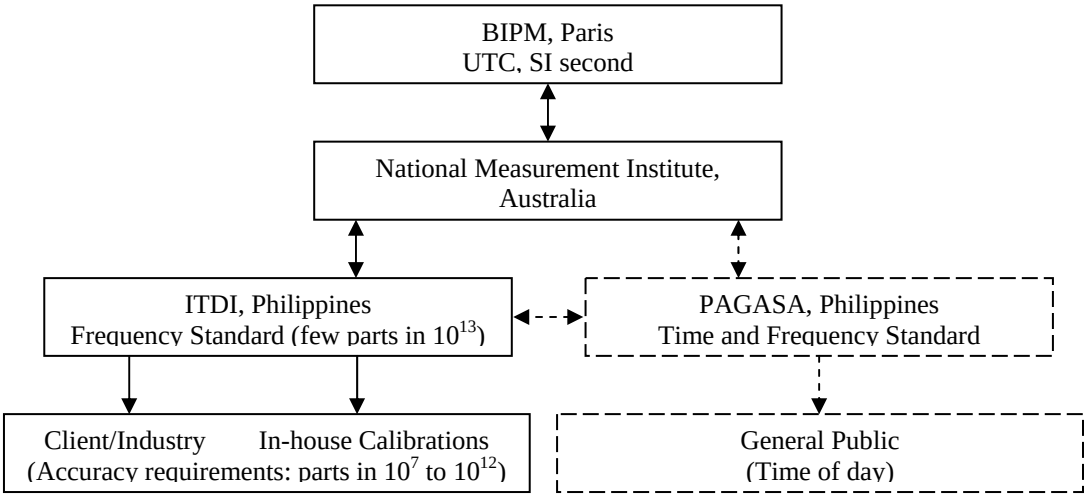

Figure 2. Traceable Frequency Distribution in the Philippines

Figure 3. PAGASA Rubidium based Common View GPS Time Transfer System

TIME AND FREQUENCY ACTIVITIES at the National Institute of Information and Communications Technology (NICT)

Mizuhiko Hosokawa, Kuniyasu Imamura, Yasuhiro Koyama, Hiroshi Toriyama, and Shin'ichi Hama
National Institute of Information and Communications Technology, Tokyo, Japan
4-2-1 Nukui-Kitamachi, Koganei, Tokyo 184-8795, Japan
e-mail matubara@nict.go.jp, fax +81-42-327-6694

Abstract

The time and frequency standards related groups in the National Institute of Information and Communications Technology (NICT), were integrated into one large group in April 2006. All the activities of the research and service such as Atomic frequency standards, time transfer and time keeping have been continued and in progress. In this paper, we will show the activities on time and frequency such as atomic frequency standards, time transfer and time keeping.

1. INTRODUCTION

The time and frequency standards groups, which consisted of the following 6 groups, Atomic Frequency Standards Group, Time and Frequency Measurements Group, Japan Standard Time, Quasi-Zenith Satellite System Group, Radio Astronomy Applications Group, and Time Stamp Platform Group in the National Institute of Information and Communications Technology (NICT) were integrated into one large group, Space-Time Standards Group with 4 subsidiary projects, Space-Time Applications Project, Time and Frequency Measurement Project, Next Generation Time and Frequency Standards Project, and Japan Standard Time Project in April 2006. All the activities of the research and service have been continued and progressed.

2. ATOMIC FREQUENCY STANDARDS

2.1. OPTICALLY PUMPED STANDARD, NICT-O1

The first optically pumped cesium primary frequency standard CRL-O1 changed its name to NICT-O1 in April 2004. NICT-O1 operated from April, 2000 to June, 2006. The data of the accuracy evaluation of TAI scale unit have been sent to BIPM twice a year on average. Type B uncertainty of the standard was estimated as 5.4×10^{-15}. In most cases during the evaluation period, the total uncertainties of the standard were less than 1×10^{-14}

Figure 1. Optically pumped cesium primary frequency standard (NICT-O1).

2.2. FOUNTAIN

NICT has conducted the development of a cesium atomic fountain primary frequency standard. We named it as NICT-CsF1. It has achieved a frequency stability better than $5 \times 10^{-13}/ t^{1/2}$. Several frequency shifts due to the systematic effects have been evaluated. So far, the combined frequency uncertainty has been estimated to be less than 2×10^{-15}. A paper on NICT fountain is shown by Kumagai et al. in ATF2006.

Figure 2. Cesium atomic fountain primary frequency standard (NICT-CsF1).

2.3. OPTICAL FREQUENCY STANDARD

NICT have developed an optical frequency standard using an electric quadrupole transition in single, laser-cooled, trapped Ca^+ ions [1, 2]. For a 729-nm clock laser system, we have obtained a laser linewidth of 66 Hz and a root Allan variance of 2×10^{-13} at 1s. The electric quadrupole transition of single $40Ca^+$ ions was detected by the shelving method, and we have measured the transition spectrum. For the optical-frequency measurement, a frequency comb system has been developed by using the broadband femtosecond-pulse laser.

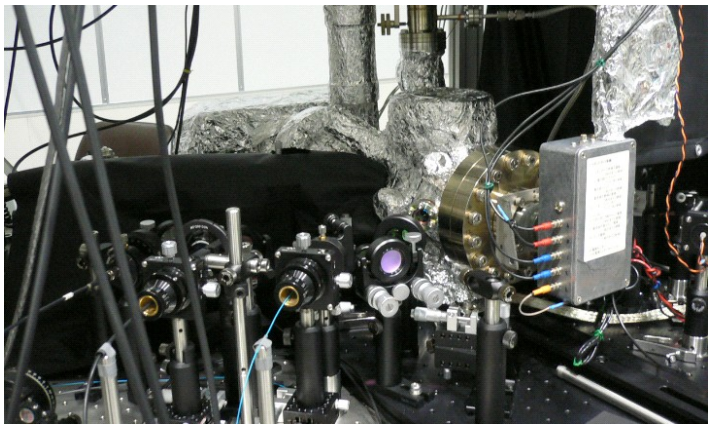

Figure 3. Optical frequency standard using an electric quadrupole transition in single, laser-cooled, trapped Ca+ ions.

3. TIME KEEPING

The generation system of Japan Standard Time (JST) has been largely renewed by using a occasion of moving the system to a new building. We have 4 hydrogen masers and 18 Cs atomic clocks. Hydrogen masers have been introduced into the JST system for the first time. The signal source of JST has been changed from a Cs atomic clock to a hydrogen maser, which improves a short-term frequency stability of both UTC(NICT) and JST. We developed a 24ch-DMTD system for the simultaneous measurements of time differences among the clocks [3]. The precision of measurements is about one hundred times better than that by a time interval counter in the previous system. The reliability of this system has been strengthened by the improved monitor functions and triple redundancy. The time scale algorithm of the system has been also improved [4]. This new JST system has been operating since February 7, 2006. UTC(NICT) generated by this system has been synchronized with UTC within around10ns since then.

4. PRECISE TIME TRANSFER

4.1. GPS

NICT has changed the P3 and Multi-Channel (MC) GPS receivers from ASHTECH Z-XII Metronome and Topcon Euro-80 to Septentrio PolaRX2, from Feb. 7, 2006. We have provided both P3 and MC CCTF data from the same receiver in order to avoid any errors caused by using different receivers [5].

We have also made a redundant system with three Septentrio receivers. These receivers are connected to the independent AOG signals, and as a consequence, the system is robust in the case that the receiver or the distribution system has a trouble. (Fig. 4.)

In addition, observation at IGS station of NICT (site name is KGN0) is finished on Apr. 1 2006. Our RINEX files are continuously available for the carrier phase time transfer as follows; http://www3.nict.go.jp/w/w114/data/GPS/rinex/.

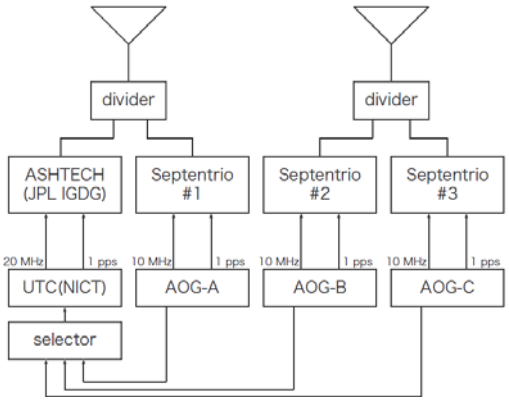

Figure 4. Interplay between time and frequency stability.

4.2. TWSTFT

NICT and major T&F institutes in the Asia-Pacific region, such as NMIJ in Japan, NMIA in Australia, NTSC in China, TL in Chinese Taipei, KRISS in Korea, and SPRING in Singapore, are cooperatively constructing a TWSTFT network in this region. To operate those links, we use multi-channel modem (NICT modem) developed by NICT. Time transfer is regularly performed and data/hour are reported to the BIPM. NICT carried out calibration trips by using a portable station between NICT and TL in February, 2006.

A TWSTFT link between NICT and PTB was established in July 2005. This link is connected by using the NICT modem. The time transfer is hourly performed and the data are also reported to the BIPM. The TWSTFT link to USA has experimentally started between NICT and USNO by using a SATRE modem via VDB from April 2006. Since the link is conducted in a very low elevation angle and the quality of the link is not enough, we plan to change the relay station to Hawaii.

Figure 5. TWSTFT: NICT multi-channel modem and portable station.

4.3. ETS VIII

NICT plan to conduct a precise time and frequency transfer experiment between a ground-reference clock and an atomic clock on the satellite ETS-8 (Engineering Test Satellite -8). ETS-8, which will be launched in late 2006, is a Japanese geostationary satellite equipped with cesium-beam frequency

standards. NICT developed an equipment to carry out two-way time transfer by using carrier phase measurement. It is also possible to calibrate internal delays and delay variations of the transmitting and receiving paths between the satellite and the ground station. By using this method, we expect to achieve precision of approximately 10 ps. We completed electrical test and environmental test of the equipment, and the ground stations are almost ready.

4.4. QZSS

Japan has started a project of Quasi-Zenith Satellite System (QZSS) from 2003. QZSS will be highly useful for supplement to the modernized GPS in urban canyon and mountainous area with its high visibility brought out by its inclined orbits. In this project, NICT is to develop a space-borne hydrogen maser (SHM) and time management system, and to carry out experiments by using them [6]. By conducting two-way time transfer between the on-board clock and the ground clock by using Ku-band link, the management of the QZSS system time, which links to UTC(NICT), is expected to achieve nano second level. The engineering models (EM) of those on-board equipments were developed and have been taken environmental tests. The first satellite is planned to be launched in 2010.

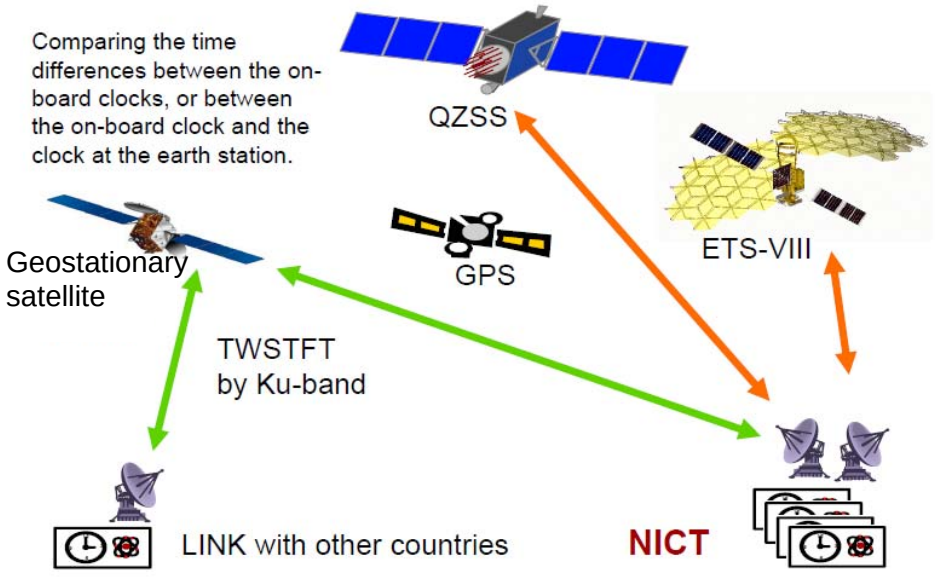

Figure 6. Time transfer systems at NICT.

5. DISSEMINATION

5.1. STANDARD-FREQUENCY AND TIME-SIGNAL EMMISIONS

NICT provides the dissemination service of standard-frequency and time-signal via LF band, as shown in Fig.7. The signals from the two LF stations, namely Ohtakadoya-yama station and Hagane-yama station, cover whole Japan. Table 1 shows the characteristics of the stations, Both stations operate 24 hours a day. A market of radio controlled watch and clock have been developed.

5.2. FREQUENCY CALIBRATION SYSTEM FOR TRACEABILITY

NICT have been conducting a frequency calibration service referenced to UTC(NICT). In order to fulfill the requirements of global MRA, NICT have established a quality system for the frequency calibration service, which was assembled by the accreditation body, National Institute of Technology and Evaluation. The conformity to ISO17025 was certified at the end of March 2001. BMC of the system is 1×10^{-13}.

Table 1. characteristics of LF stations

	Ohtakadoya-yama	Hagane-yama
Frequency	40 kHz	60 kHz
E.I.R.P	13 kW	23 kW
Antenna	250 m height	200 m height
Latitude	37°22' N	33°28' N
Longitude	140°51' E	130°11' E

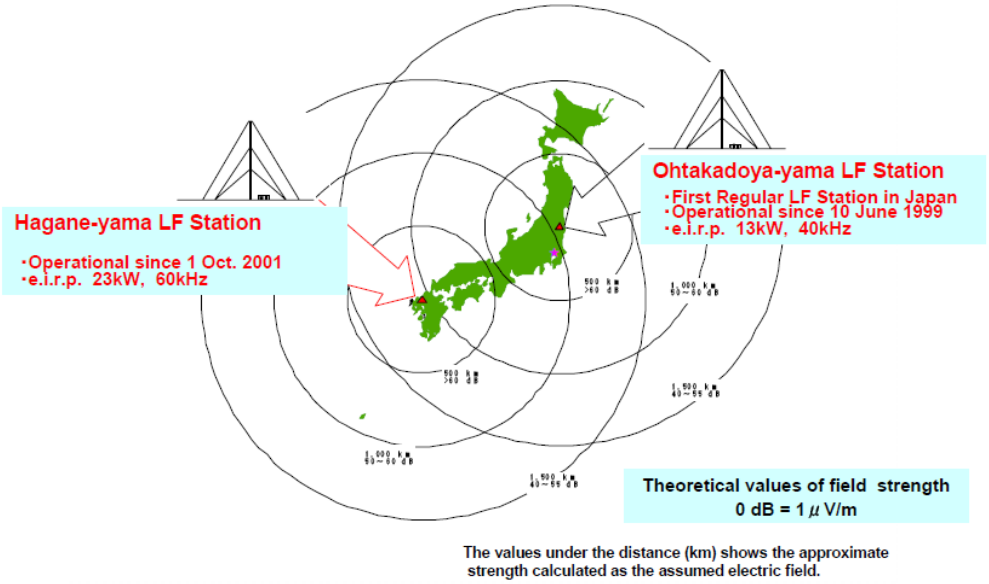

Figure 7. LF time and frequency service stations in Japan.
The values under the distance (km) shows the approximate strength calculated as the assumed electric field.

5.3. PUBLIC NETWORK TIME PROTOCOL SERVICE

NICT has developed a new hardware SNTP server which can handle with a million request per second. By using this server, we have started the public NTP service since June this year.

6. TRUSTED TIME STAMPING

Accurate and trusted time is required for safe use of electronic commerce or other important information exchanges. NICT has developed the time stamping platform systems for verifying new techniques under actual operation environment. Following experiments have been conducted in collaboration with time stamping service providers:

(1) using two different time stamping methods at the same time for making stronger against compromise of encryption algorithm
(2) new time transfer technique to ensure the time traceability
(3) validity term extension method with re-time-stamping
(4) validity term extension method with hysteresis signature techniques.

7. SPACE MEASUREMENTS AND OTHER ACTIVITIES

Very Long Baseline Interferometer (VLBI) technology has been developed in Kashima branch of the NICT [7]. Since this spring, this team has been a part of the space-time standards group. Recent topics on this field is the development of the e-VLBI system and the measurement of the positions of spacecrafts such as Nozomi and Hayabusa [8].

REFERENCES

[1] K. Matsubara, Y. Li, M. Kajita, K. Hayasaka, S.Urabe, M. Hosokawa, 2005, " *Single Ca^+ ion trapping toward precise frequency measurement of the 4 $^2S_{1/2}$ - 3 $^2D_{5/2}$ Transition*" The joint conference between the Frequency Control Symposium and the Precise Time and Time Interval Systems Applications Meeting , pp. 616-622.

[2] M. Kajita, Y. Li, K. Matsubara, K. Hayasaka, M. Hosokawa, 2005, " *Prospect of optical frequency standard based on a $^{43}Ca^+$ ion*" PHYSICAL REVIEW A, Vol. 72, No. 43404, pp. 1-7,

[3] F. Nakagawa, M. Imae, Y. Hanado, M. Aida, 2005, " *Development of Multichannel Dual-Mixer Time Difference System to generate UTC (NICT)* " IEEE TRANSACTIONS ON INSTRUMENTATION AND MEASUREMENT, Vol. 54, No. 2, pp. 829-832

[4] Y. Hanado, M. Hosokawa, K. Imamura, N. Kotake, 2006, " *Improvement of frequency Cange at Japan Standard Time*" Electric Engineering in Japan, Vol. 157, No. 1, pp. 1236-1243.

[5] T. Gotoh" *Improvement GPS time link in Asia with all in view*" IFCS & PTTI 2005, pp. 707-711.

[6] Y. Takahashi, J. Amagai, M. Fujieda, S. Yokota, K. Kimura, S. Hama, I. Kohno, I. Kouno, S. Kogure, 2005, " *Concept Design of the Time Management System for Satellite Positioning System using Quasi-zenith Satellites*" 2005 International Symposium on GPS/GNSS, 11B-6.

[7] H. Takeuchi, T. kondo, Y. Koyama, R. Ichikawa, 2005," *A VLBI Correlator with Internet-based Distributed Computing*" URSI GA2005, J06.10(0886)

[8] M. Sekido,R. Ichikawa, H. Takeuchi, Y. Koyama, E. Kawai, T. Kondo, M. Yoshikawa, N. Mochizuki, Y.Murata, and R. Kato, 2005, "*VLBI observation of spacecraft for navigation –Approaches with group delay and phase delay*", XXVIIIth General Assembly of International Union of Radio Science(URSI), J06-P.7, (0859)

Time Management System of QZSS

Shin'ichi Hama[1*], Yasuhiro Takahashi[1], Jun Amagai[1], Miho Fujieda[1], and Kazuhiro Kimura[1]

[1] *National Institute of Information and Communications Technology (NICT)*
4-2-1 Nukuikita-machi, Koganei, Tokyo, 184-8795 JAPAN

Abstract

Japanese Quasi-Zenith Satellite System (QZSS) project has changed to have a positioning/navigation mission only (without the communications and broadcasting mission) since March, 2006. NICT is in charge of the time management system of QZSS. We developed the engineering model of the on-board equipments and are testing them in a space environment. The ground system, consisting of time management stations and monitor stations, is being designed in detail. The first QZSS satellite will be launched in 2010 and be used for experiments.

1. Introduction

Japan has started the Quasi-Zenith Satellite System (QZSS) project since FY2003. QZSS will consist of three satellites and improve the visibility of the satellites greatly in mid-latitude area such as Japan. Government sector, consisting of four ministries and their relating research institutes, is working for a complement and augmentation system to GPS[1]. A private sector was originally in charge of communications and broadcasting mission, but drew off from their mission on March 2006. The first satellite, which bears only positioning/navigation mission, is planned to be launched in 2010 followed by some experiments, and the consequent schedule will be decided later by the government. The current orbit design assumes that three satellites be placed on 45 degree inclined geosynchronous orbit (GSO) planes with ascending node intervals of 120 degrees each other. The orbits have an eccentricity of 0.1 to weight its service over Japan. In Tokyo, for example, where the maximum elevation for a GSO satellite is 48 degrees, at least one Quasi-Zenith Satellite (QZS) is visible with elevation higher than 78 degrees. This characteristic is very useful particularly in urban canyons or mountainous area. The positioning and navigation mission aims to establish the technology of satellite positioning system which can work as complement and augmentation of the modernized GPS.

The Japan Aerospace Exploration Agency (JAXA) will develop the total system for positioning including on-board navigation equipment, the master control station (MCS), and several monitoring stations in and out of Japan. The National Institute of Information and Communications Technology, Japan (NICT) will develop time management system, which consists of on-board time transfer subsystem (TTS), (Time Comparison Unit (TCU) and Ku-band TX/RX) and related ground system such as time management stations (TMS). The configuration image of the time management system of QZSS is shown in Fig. 1.

2. Design of the Equipment

2.1. Mission of TTS

The block diagram of the on-board equipment for the positioning/navigation mission is shown in Fig. 2. The part in the red chain line is TTS and that in the green solid line is TCU.

*hamashin@nict.go.jp

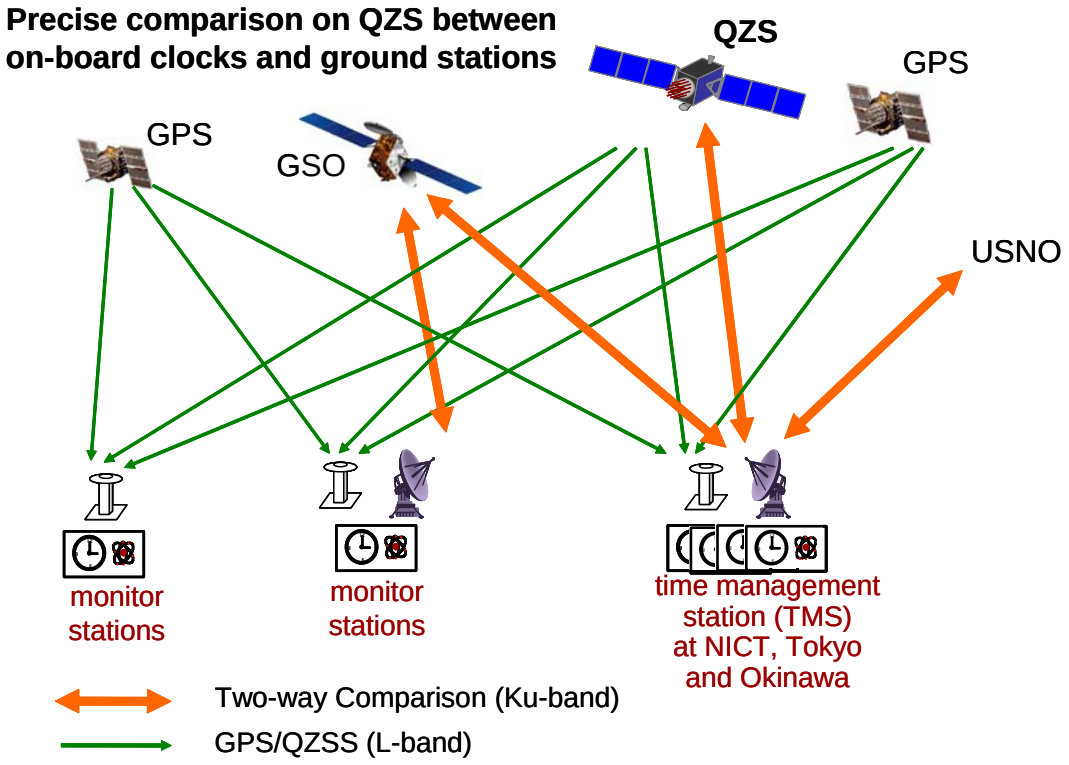

Figure 1. Configuration Image of Time Management System of QZSS

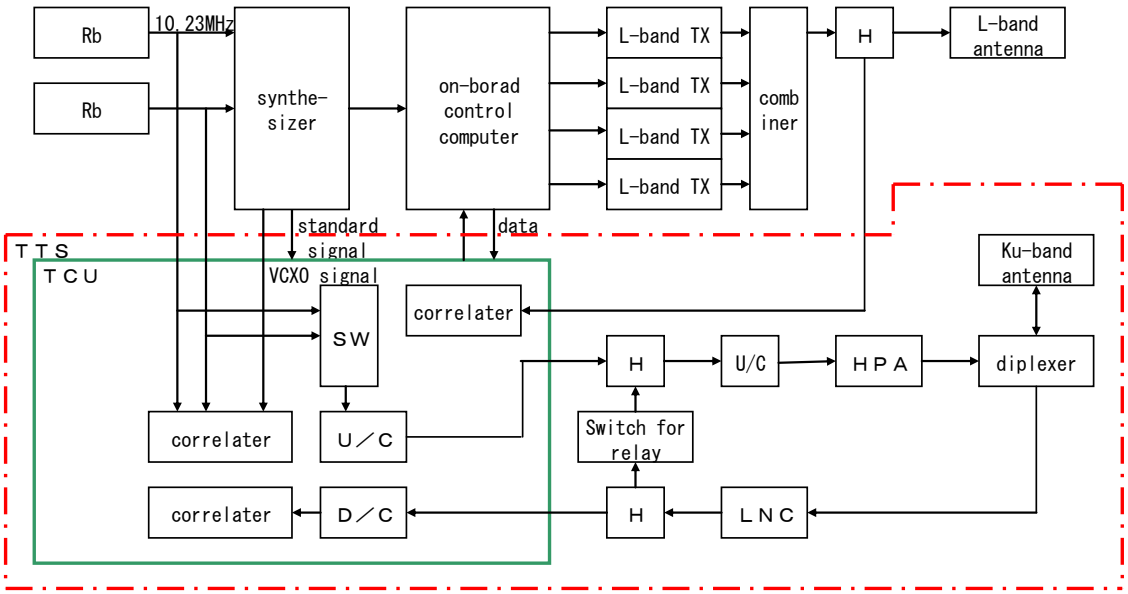

Figure 2. Block Diagram of the On-board Equipment for the Mission

TTS (inside the red chain line) is developed by NICT and discussed in this paper,
TTS: precise Time Transfer Subsystem TCU: Time Comparison Unit

TTS consists of a TCU and an RF part such as a Ku-band horn antenna, a low noise converter (LNC), an up converter (U/C), and a high power amplifier (HPA). The main functions of TTS are as follows;

(1) to measure the time differences between an on-board clock of a QZS and time of TMS with a precision better than 1 ns by using two-way technique in Ku-band.
(2) to modulate and superpose data such as telemetry on the Ku-band downlink signal and to demodulate downlinked data.
(3) to measure timing difference between on-board clocks (two Rb clocks and a VCXO)
(4) to carry out an IF instrumental calibration
(5) to measure the biases between L1, L2, and L5 signals.

Up to four channels are processed for satellite-to-ground time comparison. Typically two channels come from a TMS and one channel from another TMS, and one channel for another experiment such as the remote synchronization system using an on-board crystal oscillator (RESSOX)[2].

2.2. Time Management System

To attain a two-way QZS-to-TMS time comparison precision of 0.1 ns by using only code phase, we set the pseudo-random noise (PN) code rate as 10.23 Mcps, and the required C/No as 50 dBHz. The correlators used for QZS-to-TMS time comparison also have ability of carrier phase processing, though. The Ku-band antenna has a global beam and its minimum gain, when the QZS is at the perigee, is 16 dBi, and the maximum power of the HPA is over 4W. Based on a budget link assessment, 10W uplink power is enough for a 1.8m diameter antenna of a ground station. We would like to set TMS at Koganei, Tokyo (N35.5^{o}, E139.5^{o}) and at Okinawa (N26.5^{o}, E127.9^{o}). UTC(NICT), which QZSS time (QZSST) is based on, is maintained at Koganei using 18 Cs clocks, but a QZS is not visible when it is near the perigee. From Okinawa a QZS is visible for 24 hours. TMS Okinawa will be linked to TMS Koganei via TTS of the QZS, or by two-way satellite time and frequency transfer (TWSTFT) via a commercial Ku-band communication GSO satellite or via TTS.

QZSS is a complement system to GPS. The time offset between GPS time (GPST) and QZSST (GQTO) should be monitored precisely, and be broadcast to users via the navigation message of QZSS to assure the interoperability between both systems. So, we have an agreement with GPS as “The accuracy of the GQTO is aimed to be less than 3 ns rms over any 24-hour period, including calibration biases.” QZSST is defined at some point in the measurement system of TMS at Koganei and hard-wired to UTC(NICT), but will be defined as an ensemble time later. The primary method to get UTC(NICT)-GPST will be a utilization of GPS L-band receivers, but TWSTFT between NICT and USNO will also be carried out as an independent measurement. Since there is no common visible GSO satellite between NICT and USNO, we are going to have a relay station in between at Hawaii.

2.3. Data Superposition

As mentioned in 2.1.(1), we intended to superpose the navigation message and telecommand on the uplink Ku-band signal, and telemetry on the downlink at the first stage of the TTS design. Now the navigation message and most of the telemetry and telecommand signals have decided to be sent via an independent TT&C link, but still some signals related to TTS is sent by using this superposition function. Up to 2 kbps/ch data modulates the 10.23 Mcps PN code by binary phase shift keying (BPSK).

We studied some issues for actual operation. The most considerable problem is the effective power flux density (epfd) limit defined by the ITU-R Radio Regulations (RR). The

Ku-band signal of QZSS, which is regarded as a non-geostationary orbit (non-GSO) system in RR, is imposed a severe epfd limit to avoid interference to GSO satellite networks[3]. The Ku-band signal superimposes important data (e.g. navigation message was considered originally) but should have a cessation during a QZS crosses the equator. We can reduce the uplink channel from four to one, and can control the power to minimize the duration of the cessation. The minimum link loss at the worst case is assessed as 6 minutes 40 seconds for the uplink and 9 minutes for the downlink[4]. Though the time comparison between a QZS and TMS is not possible during the cessation, high performance Rb clock mitigates a deviation of the QZSS time; for example, in case the stability of the Rb clock is $2x10^{-13}$@1800sec, the deviation caused by a 30 minute cessation falls to just 0.36 ns. If an uninterrupted data link is required, a larger spread rate of data or a larger ground station antenna may be necessary.

2.4. Engineering Model (EM)

We finished the preliminary design review (PDR) of TTS on December 2004, and now we are carrying out performance tests and environmental tests of EM (see Fig. 3). Though some RF component is calibrated by using the function of the TTS, delay variation management is important for TTS. Careful selection of the components is carried out and on-board temperature monitoring will be performed to compensate those variations. Table 1 shows some major performance of the EM of the TTS. The gain and its flatness characteristics also met the required specifications.

Figure 3. Engineering Model (EM) of TCU

The critical design review (CDR) of TTS will be in early 2007.

Table 1. Major Performance of the Engineering Model of TTS

Mass		56.7 kg		
Power consumption		116.5 W		
HPA	delay variation*1	0.18 ns	delay deviation*2	0.24 ns
LNC	delay variation*1	0.21 ns	delay deviation*2	1.9 ns
UPC	delay variation*1	0.16 ns	delay deviation*2	0.1 ns

*1 for -20 to +60^{o}C *2 over 41 MHz bandwidth

Acknowledgments

We appreciate the associated engineers of JAXA and NEC TOSHIBA Space Systems Ltd. (NTS) for cooperating of the design and the tests of the system. This work is being carried out under the contract from Ministry of Internal Affairs and Communications (MIC).

References

[1] Hama, S., et al. 2004, ION GNSS 2004, D4-7, pp.1758-1763
[2] Iwata, T., et al., IGNSS symposium 2006
[3] ITU-R Radio Regulation ARTICLE 22
[4] Kimura, K., et al. 2006, 50th Space Science and Technology Conf, 3B04 (in Japanese).

Two-Way Satellite Time and Frequency Transfer with Long Baseline

Miho Fujieda* , Tadahiro Gotoh, Masanori Aida, Hideo Maeno and Jun Amagai

National Institute of Information and Communications Technology
4-2-1 Nukui-Kita, Koganei, Tokyo, 184-8795 JAPAN

Abstract

Two-Way Satellite Time and Frequency Transfer (TWSTFT) is prospective to enable precise time transfer between remote stations. National Institute of Information and Communications Technology (NICT) keeps two intercontinental TWSTFT links, which connect with Asia and Europe, and Asia and Australia. Diurnal variation is observed in them. From double difference between TWSTFT links, it proved that connection through two transponder showed diurnal component. On the other hand, there was not apparent diurnal variation in case of connection through one transponder.

1. Introduction

In Two-Way Satellite Time and Frequency Transfer (TWSTFT), paired earth stations transmit and receive pseudo-random-noise coded signal via communication satellite to exchange timing information [1]. Frequency for transmission is different from reception one, converted to reception one in onboad transponder and sent back to earth station. Because the transmission and reception paths are almost the same, the atmospheric and geometrical delays between the earth station and satellite are generally canceled. TWSTFT is consequently prospective to enable precise time transfer.

Time difference between site A and B, $T_A - T_B$ by TWSTFT is written as follows.

$$T_A - T_B \;=\; 0.5[(t_A - t_B) + (\tau_A - \tau_B) + I_{AB} + t^{AB}_{sagnac} + (dt_{B\to A} - dt_{A\to B})] \;, \quad (1)$$

where, t_i is signal reception time and τ_i is delay difference between transmission and reception paths in earth station. The lower subscript i means stations A and B. I_{AB} and t^{AB}_{sagnac} are delays due to the ionosphere and the Sagnac effect, respectively. Quantities, $dt_{A\to B}$ and $dt_{B\to A}$ represent delays of signals in satellite transponder which sent from A to B and from B to A. When cover area of communication satellite becomes larger, multiple transponders and antennas are usually used in communication of links with long baselines. In the case, signal paths for up and down links are slightly different. If uplink frequencies from A to B and from B to A are converted to downlink frequencies in the same transponder, the delays, $dt_{B\to A}$ and $dt_{A\to B}$, are almost canceled. In the case signal paths are asymmetric, for example, different transponders are used, the delays remain in the time-difference equation (1).

National Institute of Information and Communications Technology (NICT) keeps one inter-Asian and two intercontinental TWSTFT links [2], which connect with Physukalisch-Technische Bundesanstalt (PTB), National Measurement Institute (NMIA) and Asia. Multi-channel TWSTFT modem developed by NICT [3], called "NICT modem" hereafter, are used in those links. NICT and Korea Research Institute of Standards and Science (KRISS) join their intercontinental links as well as inter-Asian link. Their characteristics are summarized in Table 1. In the case we use Asia-Europe link via PAS-4,

*miho@nict.go.jp

uplink signals from NICT and KRISS are transmitted only to Europe, time transfer between NICT and KRISS cannot be performed simultaneously. The same is applicable for PAS-8. If we change uplink frequency for Asian beam of PAS-4 and PAS-8, time transfer between NICT and KRISS is possible, however.

Table 1. Characteristics of intercontinental TWSTFT links as well as inter-Asian link.

Satellite name	Paired stations	baseline length [km]	no. of transponder
JCSAT-1B	NICT - KRISS	1100	1
PAS-4	PTB - NICT	8300	2
	PTB - KRISS	7800	
PAS-8	NMIA - NICT	7300	2
	NMIA - KRISS	7600	

Diurnal variation in time transfer via PAS-4 are observed and we have studied the reason. Double differences are calculated in order to investigate characteristics of two links with long baseline, via PAS-4 and PAS-8. In this paper, we introduce time transfer results with both links and discuss instability briefly.

2. Double difference between GPS AV and TWSTFT

Figure 1 shows a time scale difference between KRISS and NICT and their modified Allan deviations by TWSTFT and GPS All-in-view (GPSAV) [4] between stations. TWSTFT data used in the data analysis are formatted following with recommendation ITU-R [5] and obtained per hour. GPS data are written in CCTF format and averaged per hour. Observation period is from Feb. 2006 to Oct. 2006. In the figure (a) and (b) show those for UTC(NICT)-UTC(KRIS), while (c), (d), (e) and (f) are the modified Allan deviations for UTC(NICT)-UTC(PTB), UTC(KRIS)-UTC(PTB), UTC(NICT)-UTC(AUS) and UTC(KRIS)-UTC(AUS), respectively. The link between NICT and KRISS is connected via JCSAT-1B. That among NICT, KRISS and NMIA is done via PAS-8 and that among NICT, KRISS and PTB is done via PAS-4. Short term stabilities measured by TWSTFT are superior than those of GPSAV. Regarding for long term stability, they are limited by time scale variation and equivalent for those of GPSAV. Figure 2 shows time stabilities of double difference, GPSAV-TWSTFT. In UTC(NICT)-UTC(KRIS) from TWSTFT data, apparent diurnal component is not seen. On the other hand, the time stabilities for the measurements via PAS-4 and via PAS-8 are worse than those via JCSAT-1b and show bumps around averaging time of 4×10^4 s in Figure 2 (b) and (c). Because the modified Allan deviation of TWSTFT and GPSAV are the same around 4×10^4 s in Figure 1 (c), (d), (e) and (f), both TWSTFT and GPSAV might contribute to their diurnal variations.

3. Double difference between TWSTFT links

3.1. Experiments

NICT modem has eight reception channels, which allows us to do time transfer with eight stations simultaneously. It is easy to calculate redundant time-scale difference using TWSTFT data by NICT modems. In order to investigate instability only due to TWSTFT link, we calculated redundant time-scale differences of UTC(NICT)-UTC(KRIS) using

data from JCSAT-1B, PAS-4 and PAS-8 links. The list and notation used below are shown in Table 2. Figure 3 shows modified Allan deviation of UTC(NICT)-UTC(KRIS)

Table 2. Data for redundant time scale difference of UTC(NICT)-UTC(KRIS). Site name A represents UTC(A).

Satellite name	Used data	Notation	Memo
JCSAT-1B	NICT-KRIS	Direct	1 transponder
JCSAT-1B	(NICT-TL)-(KRIS-TL)	via TL	1 transponder
PAS-4	(NICT-PTB)-(KRIS-PTB)	via PTB	2 transponders
PAS-8	(NICT-AUS)-(KRIS-AUS)	via NMIA	2 transponders

and time stability of double difference between "Direct" and redundant links. Since link noise increases in redundant links, modified Allan deviations become worse at shorter averaging times. Those over 10^5 s is limited by time scale variation and show good agreement. Figure 4 shows time-series plot of double differences between "Direct" and redundant links. It is clear that "via PAS-4" and "via PAS-8" have diurnal variation and degrade time stabilities in longer averaging time. Residuals of "Direct"-"via TL" show a property of a white phase noise with a small amplitude.

Regarding for PAS-4 and PAS-8, Asian area is covered by one transponder and antenna. Connections using them are named as "via direct PAS-4" and "via direct PAS-8". To investigate instability due to different earth stations, we performed time transfer within one transponder, "via direct PAS-4" and "via direct PAS-8", that is, data of UTC(NICT)-UTC(KRIS) were obtained by three direct connections via JCSAT-1B, PAS-4 and PAS-8 satellites. Figure 5 shows time-series plots and time stabilities of double difference between "via JCSAT-1B" and "via direct PAS-4", "via JCSAT-1B" and "via direct PAS-8". Data used in the double differences were observed at the same time and averaged every five minutes. These data shows us that the instabilities are smaller than those in the case using two transponders.

3.2. Discussion

Redundant time transfer data between A and B through site C are written as follows;

$$\begin{aligned} T_A - T_B &= (T_A - T_C) - (T_B - T_C) \\ &= 0.5[(t_A - t_C) - (t_B - t_C) + (\tau_A - \tau_C) - (\tau_B - \tau_C) \\ &- (dt_{A\to C} - dt_{C\to A}) + (dt_{B\to C} - dt_{C\to B}) \\ &+ I_{AC} - I_{BC} + t^{AC}_{sagnac} - t^{BC}_{sagnac}] \\ &= 0.5[(t_A - t_B) + (\tau_A - \tau_B) \\ &+ (I_{AC} - I_{BC}) + t^{AC}_{sagnac} - t^{BC}_{sagnac} \\ &- (dt_{A\to C} - dt_{C\to A}) + (dt_{B\to C} - dt_{C\to B})]. \end{aligned} \quad (2)$$

Total electron contents over site A and B are written as TEC_A and TEC_B, respectively. Up and down frequencies from A and B are represented as $f^u_A, f^d_A, f^u_B, f^d_B$, where ionospheric delay I is derived as follows [6];

$$I_{AB} = 1.345 \times 10^{-7}[TEC_B(\frac{1}{(f^u_B)^2} - \frac{1}{(f^d_B)^2}) - TEC_A(\frac{1}{(f^u_A)^2} - \frac{1}{(f^d_A)^2})] \ [s]. \quad (3)$$

If time transfers of A-B, B-C and C-A are performed with same uplink and downlink frequencies, I_{AB} is equal to $(I_{AC} - I_{BC})$.

Next, double difference of UTC(A)-UTC(B), Δ, between TW links, via JCSAT-1B and PAS-4 through site C is considered. Because time scale variation is removed, it is represented as follows;

$$\begin{aligned}\Delta &= 0.5[(\tau_A - \tau_B)_{JCSAT} - (\tau_A - \tau_B)_{PAS} \\ &+ (I_{AB})_{JCSAT} - (I_{AC} - I_{BC})_{PAS} \\ &+ (t^{AB}_{sagnac})_{JCSAT} - (t^{AC}_{sagnac} - t^{BC}_{sagnac})_{PAS} \\ &+ (dt_{B\to A} - dt_{A\to B})_{JCSAT} - [(-dt_{A\to C} + dt_{C\to A}) + (dt_{B\to C} - dt_{C\to B})_{PAS}]]. \quad (4)\end{aligned}$$

The instability due to delay variation in earth station was small as large as a few hundred ps [7], for the term in the first line of the equation (4) could be unconsidered. Using the Global Ionosphere Map (GIM) [8], we estimated the ionospheric delays from MJD 53710 to 53719 and from MJD 53767 to 53790. It found that mean amplitude of the delays became about 100 ps and the difference in the second line could be negligible. Delay due to the Sagnac effect was calculated using satellite orbit elements published by North American Aerospace Defense Command (NORAD) [9]. In the case of PAS-4 link, it sometimes reached at a half ns. The term in the third line means difference and its instability might be little.

The redundant time transfer data within one transponder showed the smallest instabilities. It is because observations were performed using the same earth stations and the variations of delay difference, τ were removed. In comparison with TWSTFT links via three direct connections, there were no large diurnal components in Δ, whose time stabilities were smaller than 80 ps. The results shows us that the instabilities due to the first line in the equation (4) were unconsidered. On the other hand, when we compared with TWSTFT links via direct connections using one transponder and via connections using two transponders, there were apparent diurnal variations. Since their all measurements did not perform simultaneously, we could not identify. The difference is whether the signal paths were asymmetric or not. Further investigation is required, specially about the term in the fourth line of equation (4).

4. Summary

NICT keeps two intercontinental TWSTFT links with long baseline via PAS-4 and PAS-8. In those links, we have observed diurnal variation. Double difference between GPSAV and TWSTFT, and redundant TWSTFT links were calculated to investigate the causes. Instability source was not identified so far. Regarding for PAS-4 and PAS-8, it was found that diurnal component existed in case that we calculated redundancy using connection through two transponders and clear diurnal component was none with usage of one transponder, however. Passage through two transponders or asymmetric path is usually required to establish of TWSTFT link with long baseline. Instability due to them should be studied more.

Acknowledgments

We would like to thank S. H. Yang from KRISS and D. Piester from PTB for their cooperation. We would like to express our gratitude to M. Hosokawa from NICT for his helpful advice.

References

[1] D. Kirchner, "Two-way satellite time and frequency transfer (TWSTFT): principle, implementation, and current performance", Rev. of Radio Science, Oxford University Press, pp. 27-44, 1999.

[2] Maeno, H. et al, "Establishment of a TWSTFT link between Asia and Europe connecting NICT and PTB", Proc. of EFTF2006, in press.

[3] Imae, M. et al, "Precise time and frequency transfer", J. Nat. Inst. Inf. Commun. Technol.-NICT, vol. 50 (1/2), pp. 105-112, 2003.

[4] Gotoh, T., "Improvement of GPS Time Link in Asia with All in View", Proc. of 2005 Joint IEEE International Frequency Control Symposium and PTTI Systems and Applications Meeting, pp. 707-711, 2005.

[5] RECOMMENDATION ITU-R TF.1153-2

[6] P. J. Teunissen and A. Kleusberg, "GPS Geodesy", 2nd edition, Sec. 15, Springer, 1998.

[7] Fujieda, M. et al, "Delay Difference Calibration of TWSTFT Earth Station", Conference Digest of CPEM2006, pp. 602-603, 2006.

[8] http://www.cx.unibe.ch/aiub/ionosphere.html.

[9] http://www.norad.mil/

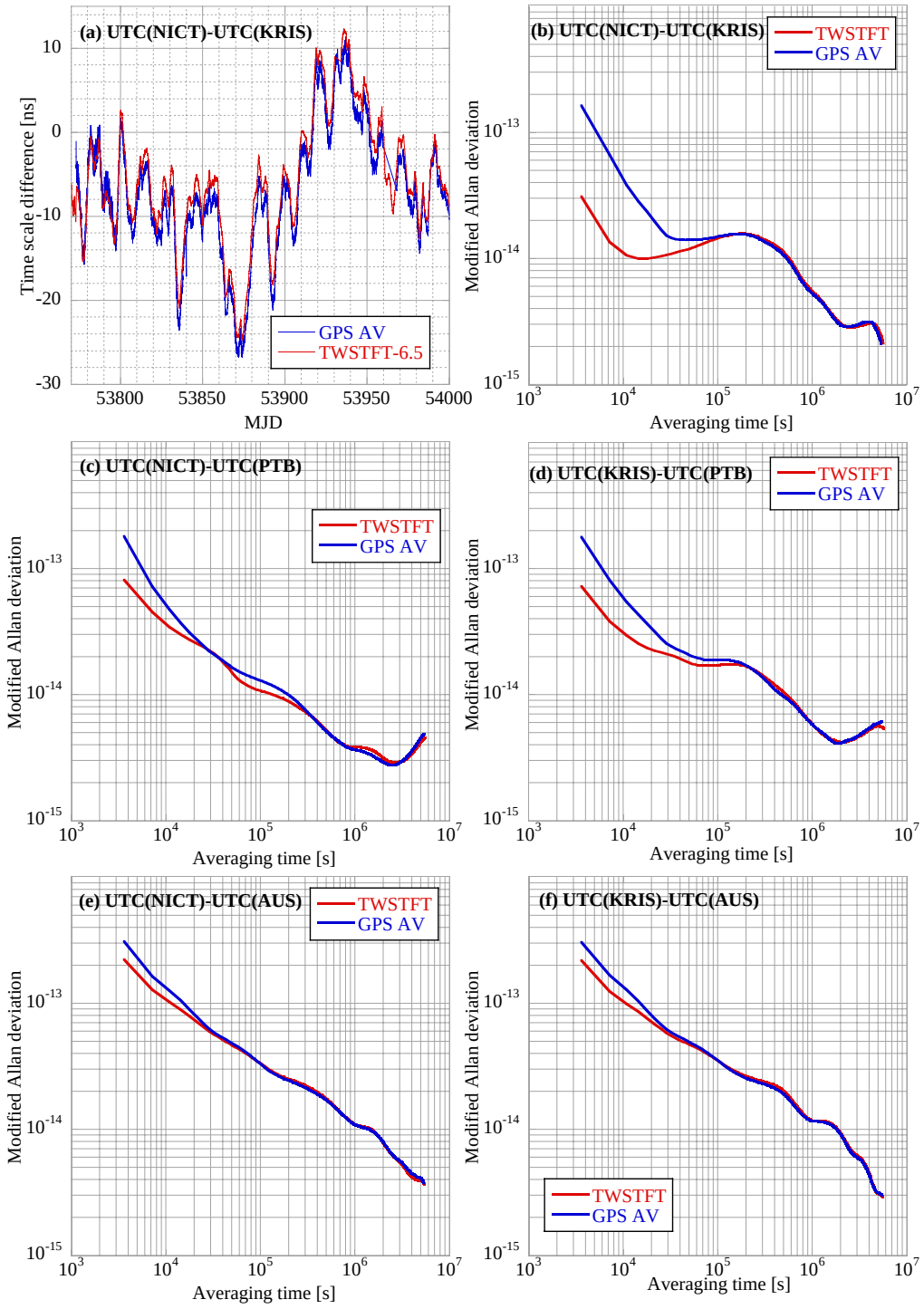

Figure 1. Time scale variation (a) and modified Allan deviation (b) of UTC(NICT)-UTC(KRIS) by TWSTFT and GPS All-in-View (GPSAV). Modified Allan deviations of UTC(NICT)-UTC(PTB) (c), UTC(KRIS)-UTC(PTB) (d), UTC(NICT)-UTC(AUS) (e) and UTC(KRIS)-UTC(AUS) (f). Their observation period is between 2006/2 and 2006/10.

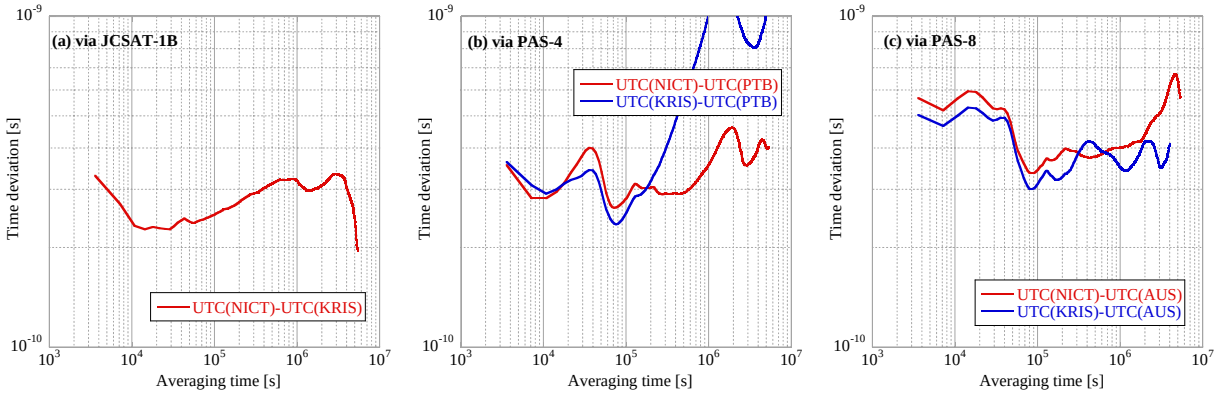

Figure 2. Time stability of double difference, GPSAV-TWSTFT. (a), (b) and (c) are GPSAV-TWSTFT via JCSAT-1B, GPSAV-TWSTFT via PAS-4 and GPSAV-TWSTFT via PAS-8, respectively. Their observation period is between 2006/2 and 2006/10.

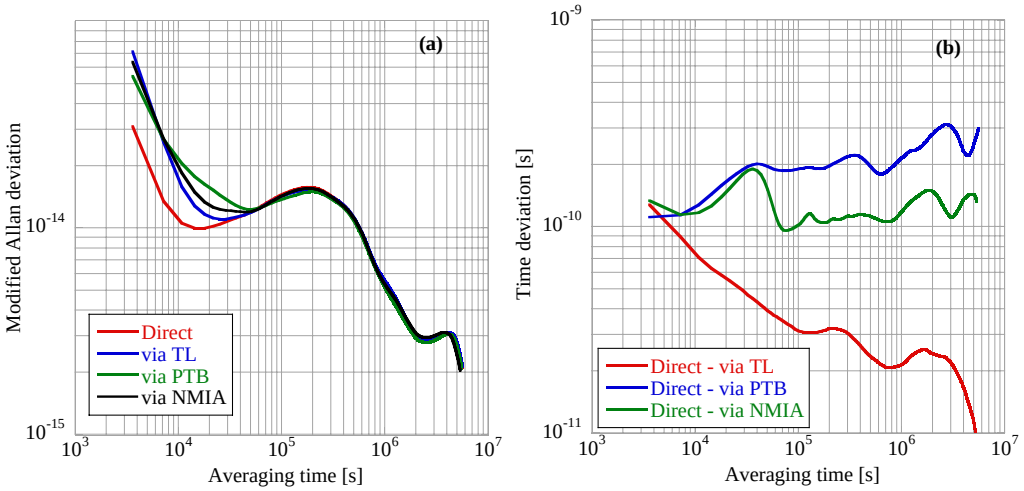

Figure 3. (a) Modified Allan deviations of UTC(NICT)-UTC(KRIS) and (b) Time stabilities of double differences between "Direct" and redundant time transfers of NICT-KRISS. Observation period is from 2006/2 to 2006/10.

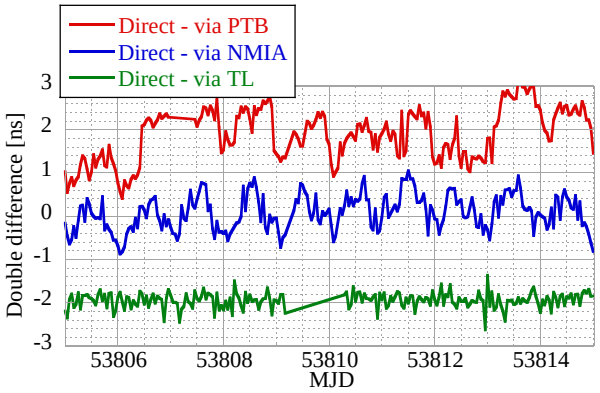

Figure 4. Double differences in time series between "Direct" and redundant time transfers of NICT-KRISS.

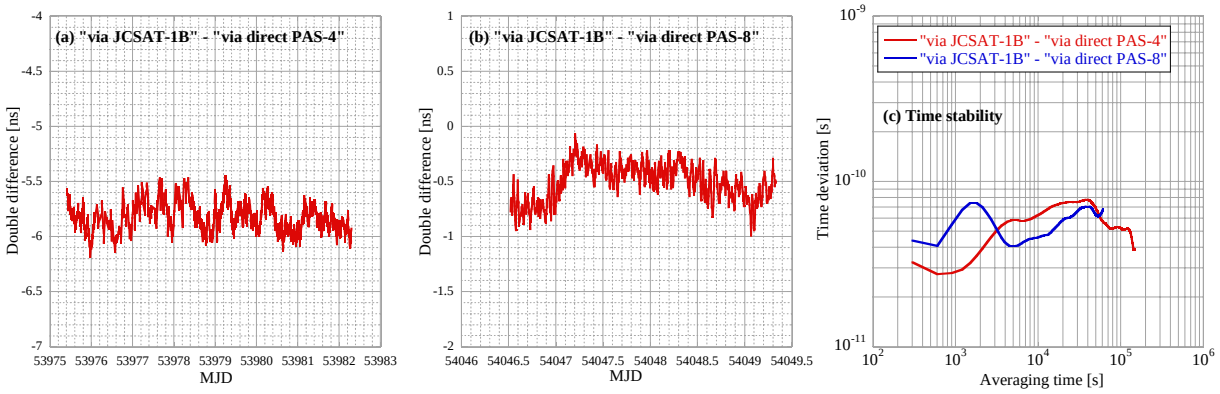

Figure 5. (a), (b) Double differences between "via JCSAT-1B" and "via direct PAS-4", "via JCSAT-1B" and "via direct PAS-8". (c) Their time stabilities. Data "via JCSAT-1B" and "via direct PAS-4" were obtained between 2006/8/28 and 2006/9/4. Those "via JCSAT-1B" and "via direct PAS-8" were done between 2006/11/7 and 2006/11/10.

Two-way Satellite Time and Frequency Transfer using a Pair of Pseudo Random Noises

Jun Amagai[1*]

[1] *National Institute of Information and Communications Technology*
4-2-1 Nukui-Kita, Koganei, Tokyo, 184-8795 JAPAN

Abstract

We plan to improve delay measurement precision of two-way satellite time and frequency transfer (TWSTFT) by introducing a pair of pseudo random noises (PRN's). Delay determination precision and required chip rate of PRN's are evaluated for this method and found that by using this method, we can improve the delay measurement precision by one order of magnitude even though the occupied band width is only 400 kHz. We carried out preliminary experiment and confirmed the effectiveness of this method.

1. Introduction

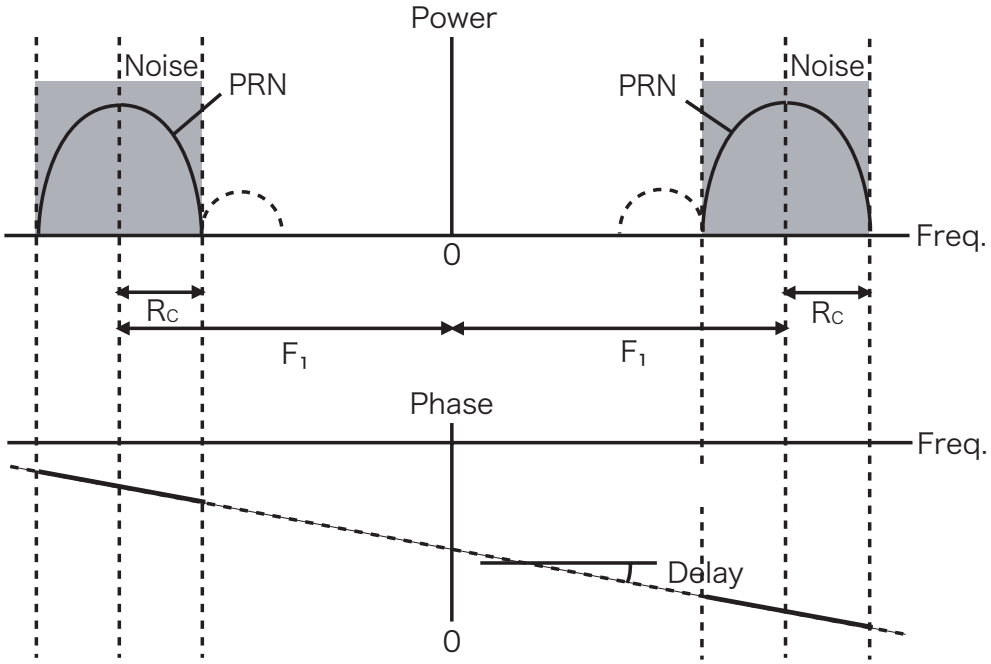

Figure 1. A pair of Pseudo Random Noises contaminated with noise. Power and phase of cross spectrum obtained by cross correlation of received signal and replica.

TWSTFT, in which the time that PRN takes to travel from one site to another is measured, is one of the most precise method to compare clocks in different locations. The

*amagai@nict.go.jp

measurement precision of conventional TWSTFT is less than 1 nsec with 1 sec integration and depends on the signal's bandwidth. The precision can thus be improved by increasing the chip rate of the PRN. However, this is problematic because of the high rental costs of the commercial communication satellites used to transfer the signals.

We can improve the measurement precision without increasing the occupied band width by introducing a pair of PRN's which is allocated separately in frequency space as binary offset carrier (BOC)[1]. We have evaluated the delay measurement precision with this method and have conducted a preliminary experiment.

2. Evaluation of delay measurement precision

As shown in Figure 1., we introduced a pair of PRN's; R_c [cps] is the chip rate of each PRN, and $2F_1$ [Hz] is the frequency spacing between them. This condition is almost the same as BOC(F_1, R_c). A filter with a bandwidth of $2R_c$ [Hz] is used to extract the main lobe spectral component of each PRN. Since group delay is defined as an inclination of the cross-spectral phase, which is obtained by cross correlating the received signal and the replica, the cross-spectral phase of the two PRN's should be on a line.

We calculated the delay measurement precision by estimating signal-to-noise ratio for each frequency component [2]. For the conditions where integration time T and C/N_0 for a PRN are given and $F_1 \gg R_c$, we can estimate the delay measurement precision by using

$$\sigma_\tau \approx \frac{1}{4\pi F_1 \sqrt{T\, C/N_0}} \tag{1}$$

Practically, inclination of the cross-spectral phase of each PRN should be on a line as previously mentioned, the frequency assignment should conform to

$$\frac{4F_1}{3R_c} < \sqrt{T\, C/N_0} \tag{2}$$

Using these formulae and assuming that C/N_0 of each PRN is 50 dBHz, that T is 1 sec, and that F_1 is 17 MHz (nearly half the bandwidth of a transponder on conventional communication satellites.), we estimated that the delay measurement precision, σ_τ and the required chip rate, R_c are about 15 psec and 100 kHz, respectively.

3. Preliminary experiment

To test the effectiveness of this method, we used a GPS simulator to generate a pair of PRN's, i.e. a PRN (R_c=1.023 MHz) converted using first a local 17 MHz signal and then a 70 MHz one (both generated by synthesizers). Figure 3. shows the system configuration of the experiment. The C/N_0 of each PRN was set to 50 dBHz. The PRN's were sampled respectively by A/D converters that was developed for Very long Baseline Interferometer (VLBI) [3]. Each sampled data was then correlated with the replica to determine group delay and the cross-spectral phase at the center frequency of each PRN. Using the difference in the cross-spectral-phases of the two PRN's, we determined the group delay with 34 MHz frequency separation. See Figure 3.

While stability in the short-term was almost as we expected (20 psec), the long-term stability was rather poorer; we saw an hourly drift that had an amplitude of about 100 psec. We have confirmed that this drift resulted from the drift of the local signal synthesizer used to generate 17 MHz signal. However, by using digital conversion to make a pair of PRN's as ordinary BOC, we can reduce the drift and thus improve the long-term stability.

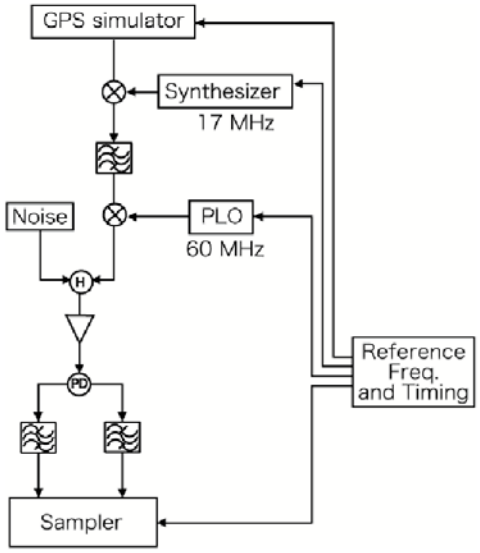

Figure 2. System configuration of preliminary experiment.

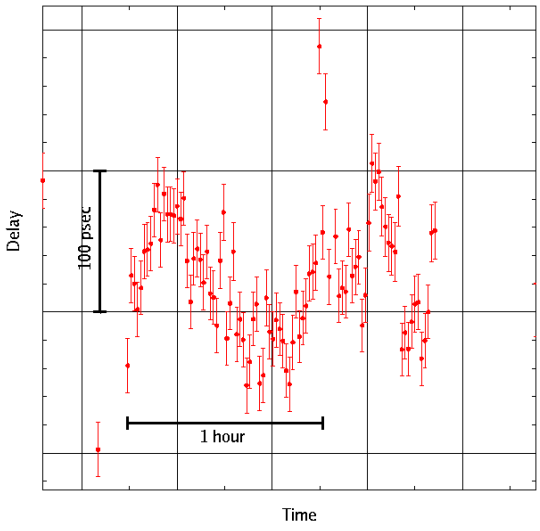

Figure 3. Result of preliminary experiment.

4. Conclusion

We proposed a new TWSTFT method in which a pair of PRN's are used. By using this method, we can improve the delay measurement precision by one order of magnitude even though the occupied band width is only 400 kHz, which is less than one-sixth the band width currently used (2.5 MHz).

References

[1] Betz, J., W. "Binary Offset Carrier Modulations for Radio navigation", Journal of The Institute of Navigation Vol. 48, No. 4, Winter 2001-2002
[2] Whitney, A. R., "Precision geodesy and astrometry via very-long-baseline interferometer", Ph. D. Thesis, M. I. T., 1974
[3] Kimura, M. et. al., "The implementation of the PC based Giga bit VLBI system", IVS CRL-TDC News, No. 21, pp31-33, 2002.

TWSTFT Network Status and Plans in the Pacific-Rim Region

Hideo Maeno*, Miho Fujieda, Masanori Aida, Yoshiyuki Shimizu,
Lam Quoc Tung, Ryo Tabichi, and Mizuhiko Hosokawa

National Institute of Information and Communications Technology
4-2-1 Nukuikita-machi, Koganei, Tokyo 184-8795 JAPAN

Abstract

NICT and major Time and Frequency institutes in the Pacific-Rim region, such as NMIJ of Japan, NMIA of Australia, NTSC of China, TL of Chinese Taipei, KRISS of Korea, and SPRING of Singapore, are cooperatively constructing a Two-Way Satellite Time and Frequency Transfer (TWSTFT) network in this region. To operate these links, we are using multi-channel modems (NICT modem) developed by NICT. Parallel with operating the links, NICT also carried out calibration trips using a portable station for NICT-TL, NICT-KRISS in the 2006. NICT also established a TWSTFT link with Europe between NICT and PTB in July 2005. This link is connected by the NICT modem via PAS-4 satellite. The time transfer is regularly performed and hourly data are reported to the BIPM. With purpose of constructing a world-around TWSTFT network, a link with USA has been experimentally started between NICT and USNO using a SATRE modem via VDB (Vandenberg) since April 2006. However, we plan to change the relay station to Hawaii.

1. Introduction

The National Institute of Information and Communications Technology（NICT）promotes to establish the observation network of the Two Way Satellite Transfer of Frequency and Time (TWSTFT) in the Asian and Pacific Rim in corporation with the Time and Frequency institutes in this region, such as the National Metrology Institute of Japan (NMIJ), the National Measurement Institute (AUS) in Australia, the National Time Service Center (NTSC) in China, the Telecommunication Laboratories (TL) in Taiwan, Korean Research Institute for Standards and Science (KRISS), the Standards, Productivity and Innovation Board (SG) in Singapore, Vandenberg (VDB) of USNO in USA and the Physikalisch-Technische Bundesanstalt (PTB) in Germany. The TWSTFT routine observations using JCSAT-B and PAS-8 satellites have been conducted on the baselines of NICT-NMIJ, NICT-TL, NICT-KRISS, NICT-NTSC, NICT-SG and NICT-AUS since May in 2005. In addition, NICT-PTB link via the PAS-4 satellite has been conducted since October in 2005 (Maeno et al. 2006, Jiang et al., 2006). We developed the new TWSTFT modem and we call it “NICT modem” (Imae et al. 2003). It is operated automatically by remote control. The Test observation of the NICT modem result was reported by takahashi et al. 2004. We have conducted Test observations using the SATRE modems in cooperation with VDB, AUS and TL.

*maeno@nict.go.jp

2. Network of TWSTFT in Asian and Pacific Rim

We have conducted the routine and test observations using NICT and SATRE modem. The network of TWSTFT is shown in figure 1.

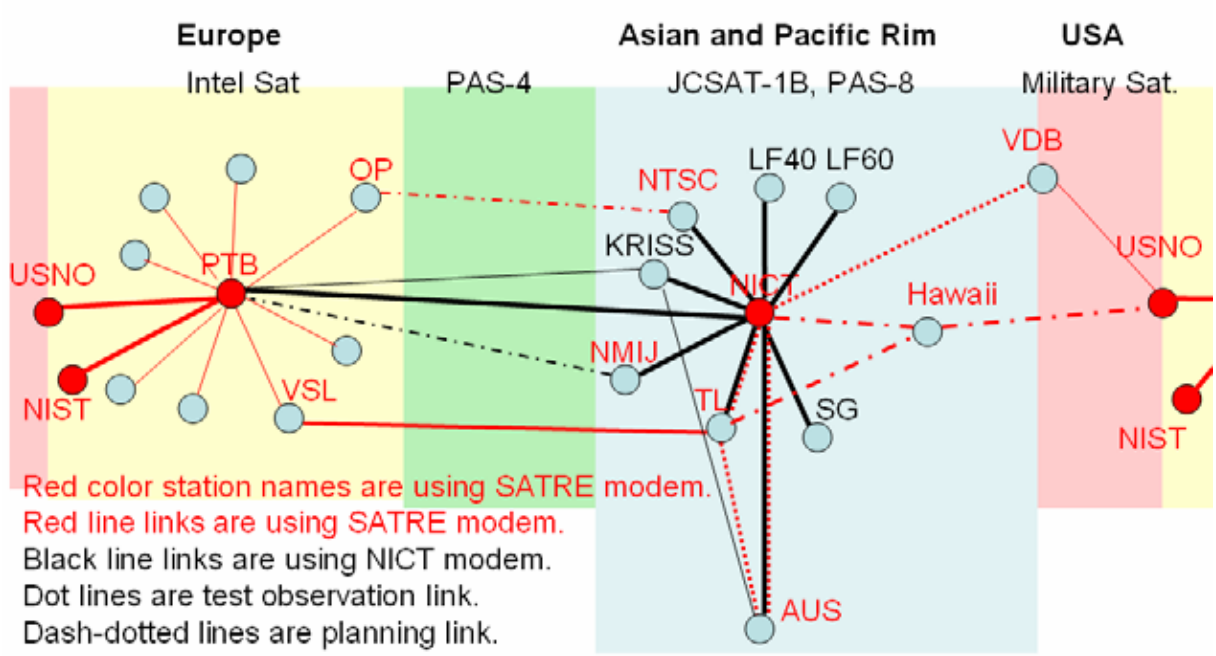

Figure 1. Network of TWSTFT in Asian and Pacific Rim

The three satellites, JCSAT, PAS-8 and PAS-4 are used. The used modems are two types. One is the NICT modem which is used for the routine observations of TWSTFT in the Asia and Pacific Rim. NICT modem is developed by NICT. This modem is available for multi-point simultaneous time transfers. The routine observations of the modem are conducted among NICT, NMIJ, NTSC, TL, AUS, KRIS, SG and PTB. The NICT modem is operated in automatic by the remote control from NICT. The routine observations are conducted 24 hours a day. First 5 minute raw data of each hour are averaged and converted into ITU-standard formats reported to BIPM. Data acquired from the SATRE modem are used for evaluation or experiment. Furthermore, we have also performed special observations via the PAS-8 satellite on the links of NICT-VDB since April 2006 and on NICT-AUS in May, 2006. Table 1 shows the modem and satellite in this region. In addition, NICT performed the portable station (Fujieda et al. 2006) trip by two domestic LF stations of Fukushima (LF40) in December, 2005, Kyushu (LF60) in September, 2006, TL in February, 2006 and KRISS in October, 2006. NMIJ-PTB and NTSC-OP links via the PAS-4 satellite are planning and will be available in the near future. NICT and TL are planning a relay station in Hawaii via the JCSAT-1B, in stead of direct link to VDB via the PAS-8. This plan will be started from July 2007.

3. Observation Systems in NICT

Table 1 shows Observation Systems in NICT. At the NICT head office in Tokyo, we have five systems for JCSAT-1B, PAS-8 and PAS-4 satellites used for International and Domestic Time-Transfer observations. Two other systems were also built for the real-time TWSFTF observations of the domestic Monitor of the LF Stations. All the TWSTFT systems are kept in the temperature-controlled room. Each LNA (Low Noise Amplifier) is installed in a temperature-controlled box near by the antenna, except for LNA units of the Domestic systems and the portable station.

Table 1. Observation Systems in NICT

Systems	Using satellite	Partner's stations	Modems	Antenna	Temp. cont.†
Asia, Hawaii	JCSAT-1B	NMIJ, NTSC, KRISS, TL, SG, Hawaii*	NICT, SATRE*	1.8 m	SSPA
Australia, USA	PAS-8 Aus Beam	KRISS, AUS, TL, VDB	NICT, SATRE	1.8 m	SSPA
Domestic	PAS-8 SE Asia Beam	LF Fukushima, LF Kyushu	NICT	1.8 m	SSPA, LNA
Europe	PAS-4	PTB, KRISS, NMIJ*	NICT, SATRE*	2.4 m	SSPA
Portable station	JCSAT-1B, PAS-8	JCSAT-1B, PAS-8 Station	NICT	1.2 m	SSPA, LNA, EO/OE+
LF Fukushima	PAS-8	NICT Tokyo	NICT	1.8 m x 2	SSPA
LF Kyushu	PAS-8	NICT Tokyo	NICT	1.8 m x 2	SSPA

*:planning, †:equipment without temperature control, +:Electric/Optical Converter

4. Routine observation results

Routine observation result shows one year data from November, 2005 to October, 2006. This chapter estimated the network of TWSTFT. Table 2 shows present status of each station and its modems used by the routine and test observations. As for them, the links under plan are also included. TWSTFT raw data are processed by averaging first 300 second of each hour data and GPSCV data are processed by one hour average.

4.1 Data acquisition rate

Regular observations are continuously performed per second using the NICT modem. The averaged first 300 second of each hour data is used for reporting to BIPM. Usually, observation is performed

continuously except for failure of equipment, a power failure or special observation. Data acquisition rate, it is defined as number of the data obtained with the number of the sum totals on the 365th by 24 times per day being comparatively alike. The number has been calculated in the period on October 31, 2006 since November 1, 2005. Table 3 shows the acquisition data number and acquisition rates [%]. An acquisition rate is 84.3% on an average. It would be not a bad result.

Table 2. The routine and test observation

Station	Routine (NICT Modem)	Test (SATRE modem)	Satellite
NICT(Japan)	✓	✓	JCSAT-1B, PAS-8 and PAS-4
NMIJ(Japan)	✓	✓*	JCSAT-1B and PAS-4*
AUS(Australia)	✓	✓	PAS-8
NTSC(China)	✓	✓	JCSAT-1B and PAS-4*
TL(Taiwan)	✓	✓	JCSAT-1B, PAS-8 and PAS-4
KRIS(Korea)	✓	×	JCSAT-1B, PAS-8 and PAS-4
SG(Singapore)	✓	×	JCSAT-1B
VDB(USNO, USA)	×	✓	PAS-8
PTB(Germany)	✓	✓*	PAS-4
Hawaii(USNO,USA) *	×	✓*	JCSAT-1B

✓:using, ×:not using, *:planning

Table 3. Data acquisition rate and intercomparison of routine observations

Baseline	Satellite	November 1, 2005- October 31, 2006		
		Acquisition data number	Acquisition rate [%]	Standard deviation TWSTFT-GPSCV [ns]
NICT-NMIJ	JCSAT-1B	7686 / 8760	87.7	2.5
NICT-AUS	PAS-8	7272 / 8760	83.0	13.7
NICT-NTSC	JCSAT-1B	7219 / 8760	82.4	4.7
NICT-TL	JCSAT-1B	7694 / 8760	87.8	1.4
NICT-SG	JCSAT-1B	5776 / 8760	65.9	7.3
NICT-KRIS	JCSAT-1B	7775 / 8760	88.8	4.5
NICT-PTB	PAS-4	7722 / 8760	88.2	5.7
Total		51144 / 61320	83.4	

4.2 Intercomparison of TWSTFT-GPSCV

Table 3 shows intercomparison of routine observations. Errors in the long period term are a few ns. We will continue evaluate whether the error becomes large in long period term. The standard deviation of TWSTFT-GPSCV(GPS common view) data is from 1.4 ns to 13.7 ns, which is mainly caused by the GPS errors. The TWSTFT data for NICT-TL is very good.

4.3 data and results

In Figure 2 the left figures show the change of the data of GPSCV data (Blue dots), Circular T data (Black circle), TWSTFT routine observation data by NICT modem (Red dots). In these figures, the last month data are lacked due to not having being uploaded by BIPM. The regular observation data of TWSTFT are acquired stably for more than one year. NICT-NTSC has the offset for about 20 ns in GPSCV. NICT-KRISS has the offset for about 10 ns in TWSTFT. The right figures show the frequency stability between TWSTFT data (red dots), GPSCV (Blue dots). These high quality data were acquired after NICT shifted its UTC source to the new system of DMTD, which adopted the Hydrogen-maser atomic clock from February 7, 2006. NMIJ, KRISS, NTSC and TL use the hydrogen master for their UTC sources. Other stations are using Cs atomic clock. The TWSTFT time comparison results of NICT with other stations are better than the ones of the GPSCV in the period of from hour to a few days. The Allan deviations of the stations with the Hydrogen master are less than $1x10^{-14}$ with the averaging time of $2x10^{4}$ seconds. A phase noise is shown by $P=\sigma_y \cdot \tau$ where σ_a is modified Allan deviation and τ is Averaging time. As for σ_y of NMIJ, KRISS, NTSC, and TL, τ is shown by $1/\tau$ to about $1x10^{-14}$. P was from 100 ps to 180 ps. P was from 250 ps to 1.5ns at the partner station of a long-distance baseline and using Cs. They show a good performance of the NICT modems.

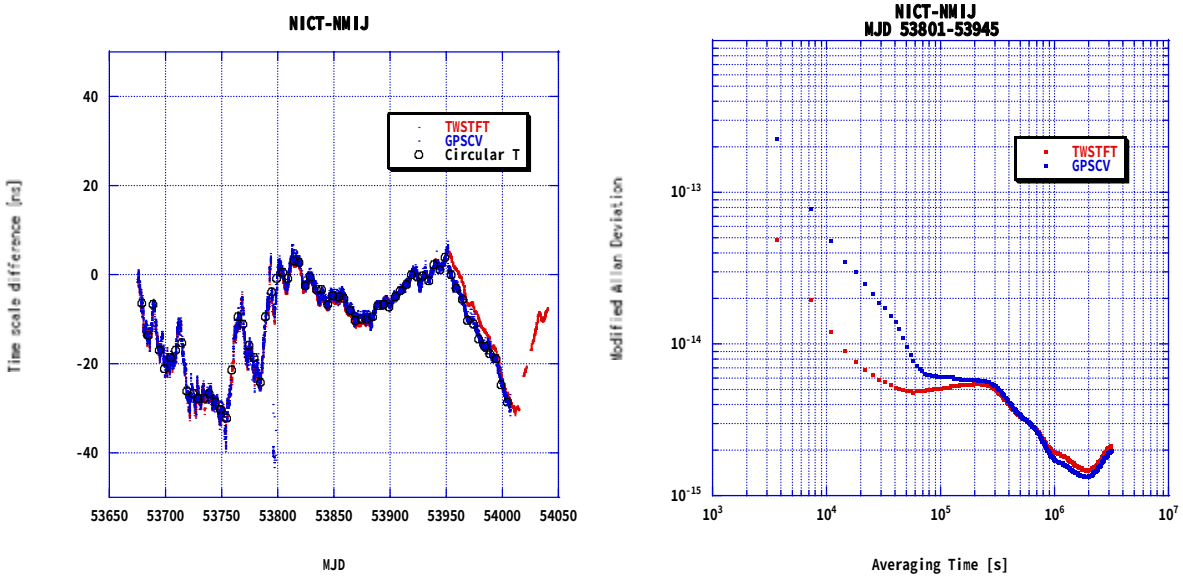

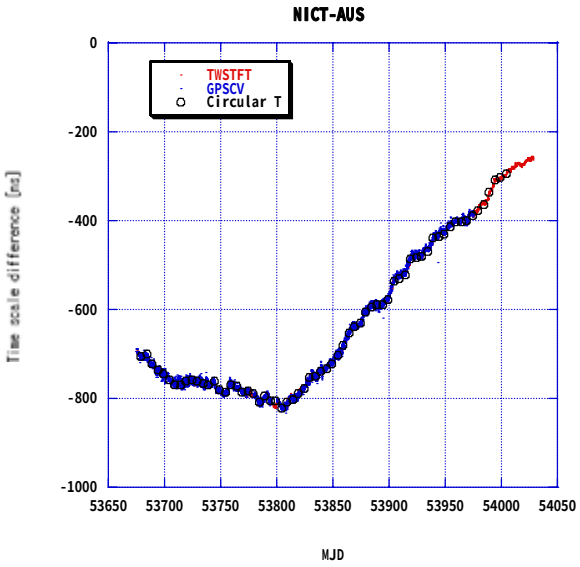
NICT-AUS
TWSTFT
GPSCV
Circular T
Time scale difference [ns]
MJD

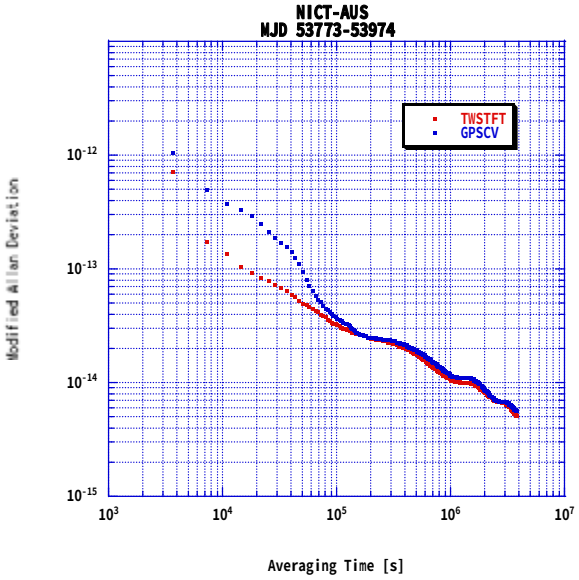
NICT-AUS
MJD 53773-53974
TWSTFT
GPSCV
Modified Allan Deviation
Averaging Time [s]

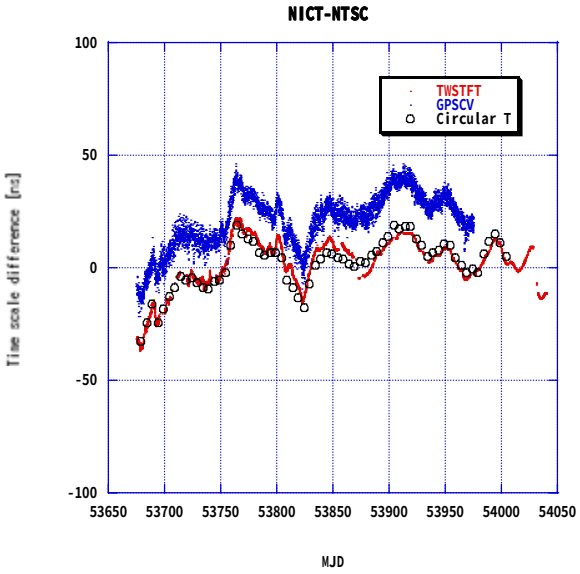
NICT-NTSC
TWSTFT
GPSCV
Circular T
Time scale difference [ns]
MJD

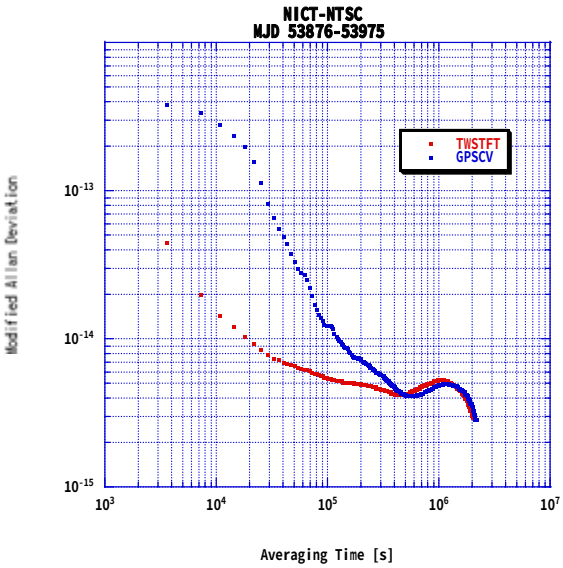
NICT-NTSC
MJD 53876-53975
TWSTFT
GPSCV
Modified Allan Deviation
Averaging Time [s]

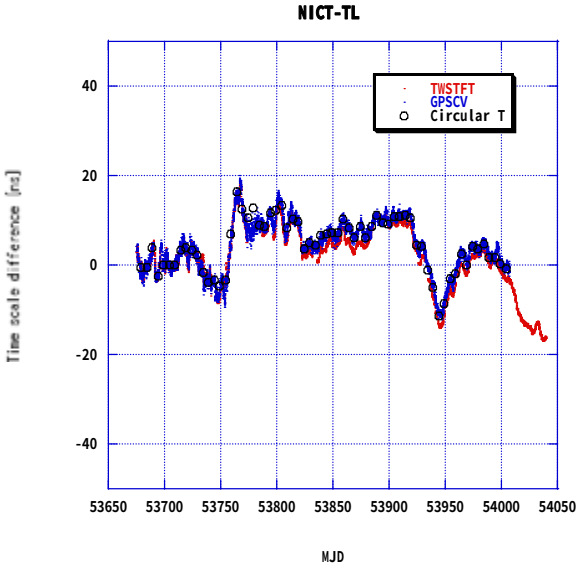
NICT-TL
TWSTFT
GPSCV
Circular T
Time scale difference [ns]
MJD

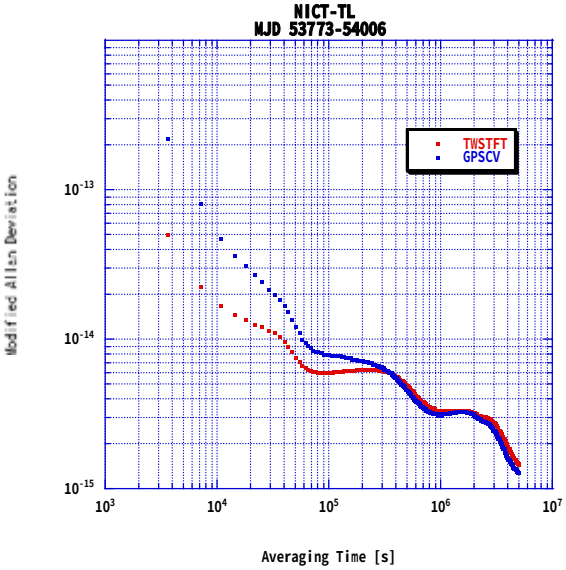
NICT-TL
MJD 53773-54006
TWSTFT
GPSCV
Modified Allan Deviation
Averaging Time [s]

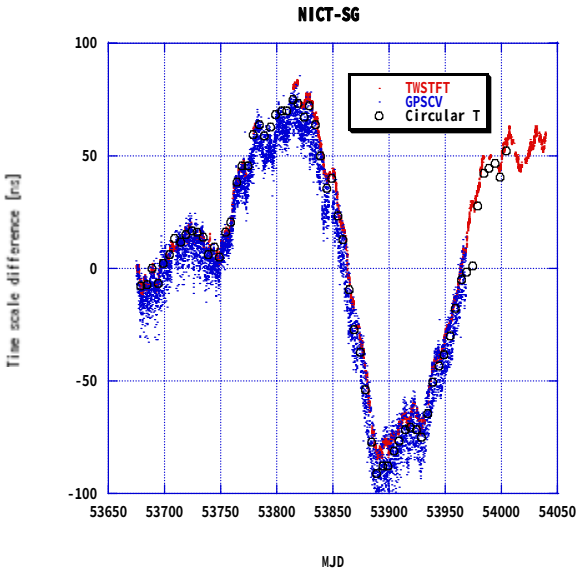
NICT-SG
TWSTFT
GPSCV
Circular T
Time scale difference [ns]
MJD

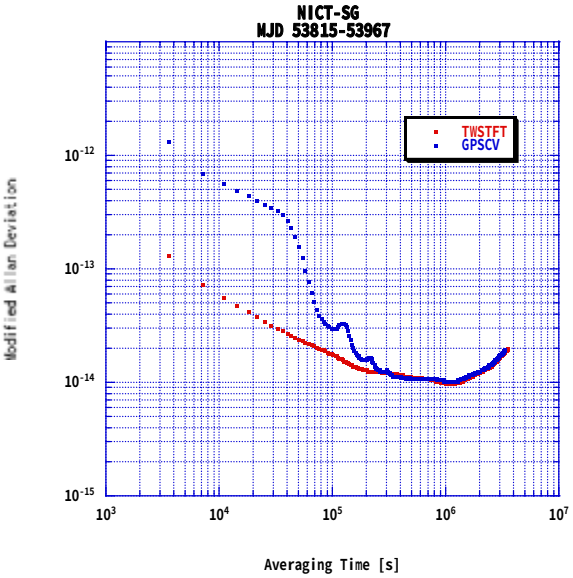
NICT-SG
MJD 53815-53967
TWSTFT
GPSCV
Modified Allan Deviation
Averaging Time [s]

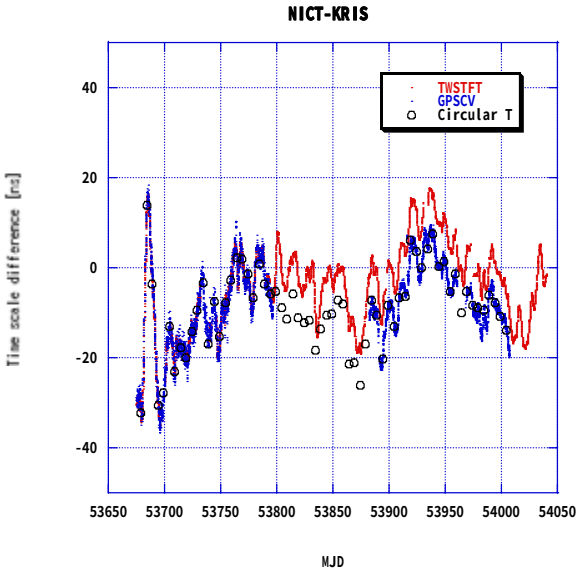
NICT-KRIS
TWSTFT
GPSCV
Circular T
Time scale difference [ns]
MJD

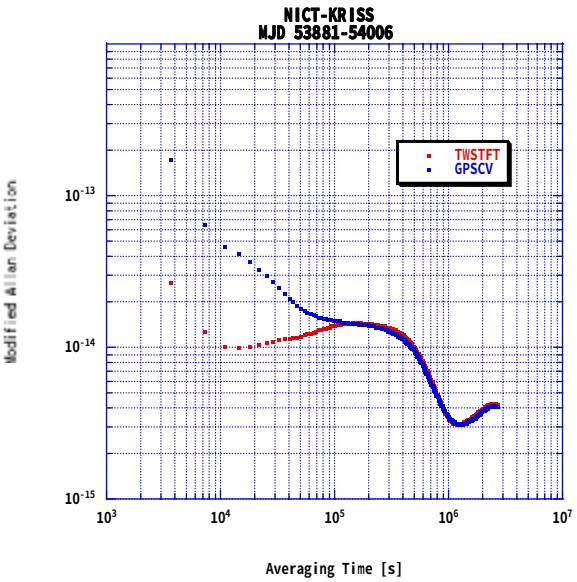
NICT-KRISS
MJD 53881-54006
TWSTFT
GPSCV
Modified Allan Deviation
Averaging Time [s]

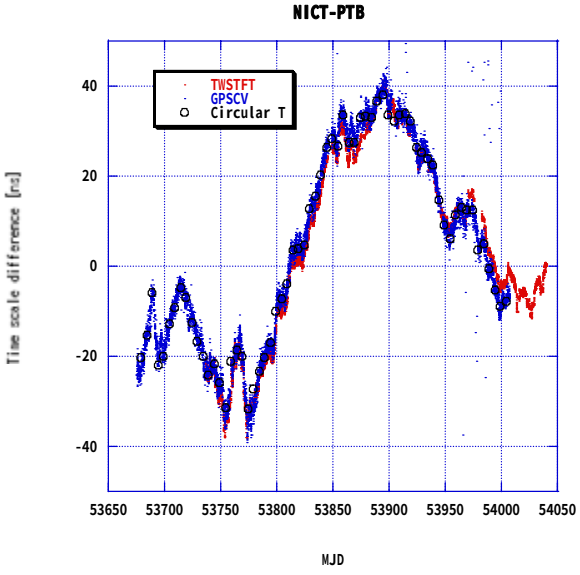
NICT-PTB
TWSTFT
GPSCV
Circular T
Time scale difference [ns]
MJD

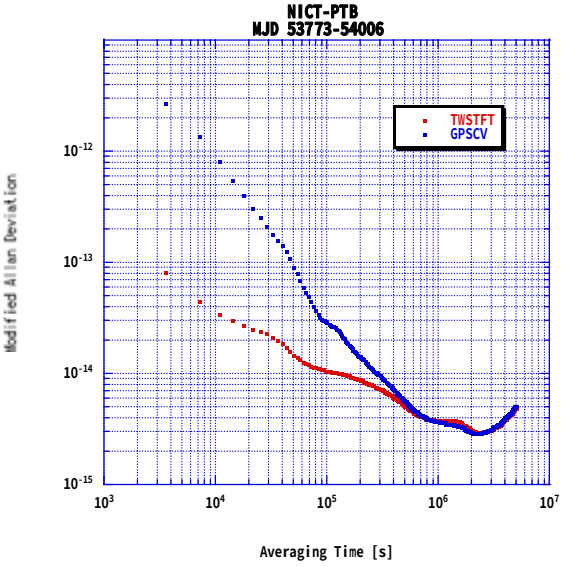
NICT-PTB
MJD 53773-54006
TWSTFT
GPSCV
Modified Allan Deviation
Averaging Time [s]

Figure 2 GPSCV data, Circular T data and TWSTFT routine observation data by NICT modem

5. Future plans

BIPM adopted GPS All in view for the status of Circular-T from October, 2006. Thereby, the link of each station of Asia-Pacific directly connects with PTB. The direct links of the Northern Asian institutes to PTB via PAS-4 satellite would be established in the near future. The beginning of 2007, NMIJ will be also linked with PTB. TL is presently linked with VSL using PAS-4 satellite with VSL. Therefore, linking to PTB will also be possible. NTSC has a plan to make a link with OP in next year.

6. Summary

We summarize our TWSTFT observations in the Asian and Pacific Rim as follows:

1) We cooperated and built the TWSTFT network by the NICT modem in the Asia-Pacific Rim.
2) We confirmed the quality of data acquired by the NICT modems.
3) PTB link has been operated as an important one for Asia to connect with Europe.

Acknowledgement

The TWSTFT network in the Asian and Pacific Rim has been kept in the collaboration with NMIJ, NTSC, KRISS, TL, SPRING, NMIA, USNO and PTB. We express our appreciation to all collaboration institutes and we hope to continue the TWSTFT observations in Asian and Pacific Rim.

References

Maeno H. Fujieda, M., Piester, D., Bauch, A., Aida, M., Tung, L.Q., Gotoh, T., and Takahashi, Y., “Establishment of a TWSTFT link between Asia and Europe connecting NICT and PTB”,2006, EFTF2006, in press.

Jiang, Z. and Petit, G., “BIPM first analysis of NICT-PTB TW link and comparison with GPS CV-AV P3 links BIPM”, 2006, TM144.

Imae, M., Suzuyama, T., Gotoh, T., Shibuya, Y., Nakagawa, F., Shimizu Y. and Kurihara, N., “Two Way Satellite Time and Frequency Transfer, Journal of the NICT”, 2003, Vol. 50, Numbers. 1/2, 125-133.

Takahashi, Y., Fujieda, N., Tung, L. Q., Tabuchi, R., Nakagawa, F., Maeno, H., Aida, M. and Suzuyama, T., ”TWSTFT Network Status and Plans in the Pacific-Rim Region”, 2004, Proc. ATF2004, 250-257

Fujieda, M., Aida, M., Maeno, H., Tung, L. Q. and Amagai, J., "Delay Difference Calibration of TWSTFT Earth station using Multi-channel modem", 2006, Digest of 2006 Conference on Precision Electromagnetic Measurements, 602-603.

Uncertainty of a frequency comparison when we use more than one real measurements

Dai Hyuk Yu[1], Taeg Yong Kwon[1], Ho Seong Lee[1], Marc Weiss[2], and Thomas E. Parker[2]

[1]*Korea Research Institute of Standards and Science*
1 Doryong, Yuseong, Daejeon 305-340, Korea

[2]*National Institute of Standards and Technology*
325 Broadway, Boulder, Colorado 80305, USA

Abstract

A general theory is presented for estimating the uncertainty of a frequency comparison in the presence of dead time and/or measurement interval offset. The uncertainties due to distributed dead time and lumped dead time with mixed power law noise type are calculated and compared. It is shown that use of distributed measurements of frequencies can greatly reduce the uncertainty as compared to that of lumped measurements.

1. Introduction

Operation of a laboratory built primary frequency standard continuously for tens of days is a difficult task. Thus dead time or measurement interval offset generally cannot be avoided when we compare the frequency of a primary frequency standard to that of a spatially remote standard or to International Atomic Time (TAI). This is also true for the same standard compared to itself at different times. Well known example is that there is always some time delay to know the time difference between UTC and UTC(NMI). This comparison process generally involves a stable but not necessarily accurate, secondary, or transfer, frequency standard such as a hydrogen maser, a maser ensemble, or TAI. A primary frequency standard measures the frequency of the transfer standard, and comparisons to other standards with dead time or to itself with a measurement interval offset depends on the stability of the transfer standard. High precision frequency comparison, therefore, needs accurate knowledge of the uncertainty caused by dead time and/or measurement interval offset.

Azoubib et al. presented a method of comparing the frequencies from several standards, or the same standard at different times with that of TAI [1]. They focused mainly on the frequency comparison with measurement interval offset, and each of the frequency measurements was assumed not to have dead time in it, or an unknown dead time. Douglas and Boulanger performed a similar analysis for dead time or measurement interval offset and presented a simple method to calculate the uncertainty due to a transfer process from one time interval to another [2]. Before this work, they developed a formalism to calculate the local oscillator's contribution to uncertainty of a cesium fountain running in a quasi continuous fashion [3]. This method was used for analysis of time scale work [4], frequency transfer uncertainty for hydrogen maser calibrated with a cesium fountain [5,6,7]. Examination of multiple calibration runs and drifting secondary frequency standard were also treated through these works. Parker et al. obtained an approximate solution that estimated uncertainty in the presence of uniformly distributed dead time [8].

In this paper, we present a simple method to extend the previous study [2] to calculate the uncertainty due to any form of dead time or measurement interval offset, and compare the differences between different configurations of dead time or measurement interval offset.

2. Theory

Assume the live frequency measurements in an interval A are performed N times with (N-1) dead times in betweens. We can calculate a weighted mean of the frequencies using all the live time measurements. The uncertainty to transfer the calculated frequency to another time interval B (which may contain all the live time measurements or has no overlap with them) should be calculated. The uncertainty U can be expressed as the mean-square difference between these two frequencies.

$$U^2 = \left\langle (\sum_{i=1}^{N} a_i y_i - y_T)^2 \right\rangle \tag{1}$$

where, y_i, a_i is i-th measured frequency and weight in the interval A, y_T is unknown 'true' frequency for an interval B. It can easily be shown that equation (1) can be simplified to equation (2). We assume that the signal is stationary and interchange of the order of the integration in calculating autocovariance gives the same value. This step allows the results of [2] to be extended to the case with distributed live measurements:

$$U^2 = \sum_{i=1}^{N} a_i \left\langle (y_i - y_T)^2 \right\rangle - \sum_{i=1}^{N} \sum_{j=i+1}^{N} a_i a_j \left\langle (y_i - y_j)^2 \right\rangle . \tag{2}$$

As shown in equation (2), the uncertainty variance is the weighted sum of variances of each live time interval to transfer to interval B, minus the weighted sum of covariance terms of all possible combinations between two live measurements. We get an analytical solution for the uncertainties $\left\langle (y_i - y_T)^2 \right\rangle$ or $\left\langle (y_i - y_j)^2 \right\rangle$ using the expressions found in [2]. Given any configurations of live measurements, weights a_i to minimize the uncertainty can be calculated by the Lagrangian multiplier method. For the specific case of white frequency modulation noise, it can be shown that only the total measurement live time matters and the weight of each measurement is proportional to the measurement interval, i.e. inversely proportional to Allan variance, as follows.

$$a_i = \tau_i / \sum_{j=1}^{N} \tau_j = (1/\sigma_y^2(\tau_i)) / \sum_{j=1}^{N} (1/\sigma_y^2(\tau_j)) \tag{3}$$

where, τ_i is i-th measurement interval. However, the optimum weights do not exactly follow equation (3) when there are other power law noise types.

3. Uncertainty due to the dead time

To compare the uncertainty due to lumped and distributed dead time, we consider a specific mixed noise type used in [8]. We assume interval B is 60 days and all the measurements are performed within interval B. All the live time is at the starting end of interval B for lumped dead time case, and live time and dead time are 1 day respectively and alternate from the starting end for distributed dead time case.

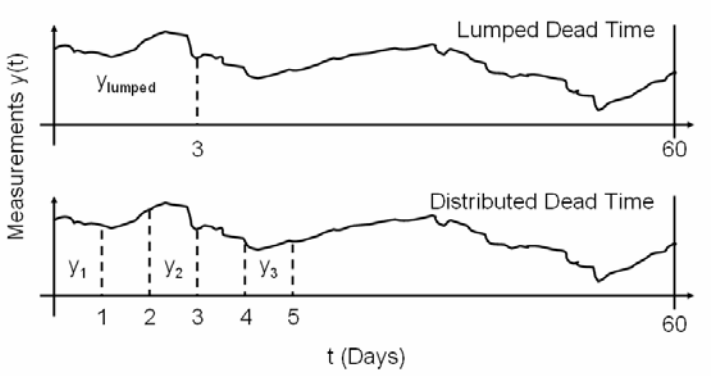

Figure 1. 3-day measurement example with lumped and distributed dead time around the starting end.

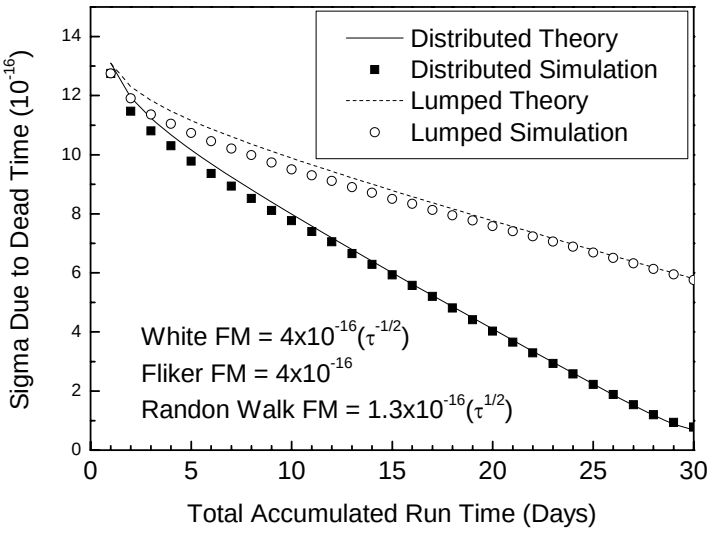

Figure 2. Fractional frequency uncertainty due to dead time in a 60 day evaluation interval (live time around the starting end).

A 3-day measurement example is shown in Figure 1. To test the theory, we generated an ensemble of 1000 simulated time series data sets with the given mixed noise type from above. We used a software (Stable 32) to generate the data sets and the noise generation is known to be based on the works by Kasdin and Walter [9], and Greenhall [10]. We calculated two different frequencies for a given total accumulated measurement time for each data set. One is an estimated frequency obtained by averaging the frequencies of live measurements, and the other is the "true" average frequency found from the end points of the data set. We obtained the variance by averaging the differences between the two frequencies squared for all simulated time series data sets. We also calculated the theoretical values from equation (2) and compared the simulated and theoretical variances. We tested the uncertainties due to lumped and distributed dead time. T. In figure 2, τ is expressed in days and the theoretical and simulated results are in good agreements showing that the theoretical approach is correct. The slight discrepancy between the analytical and "true" results in Figure 2 at low run time values is most

likely due to the difficulty in generating true simulated flicker frequency noise Also we should note that the uncertainty due to distributed dead time is always smaller than that due to lumped case as estimated in [8]. We also carried out similar comparisons for individual noise types.

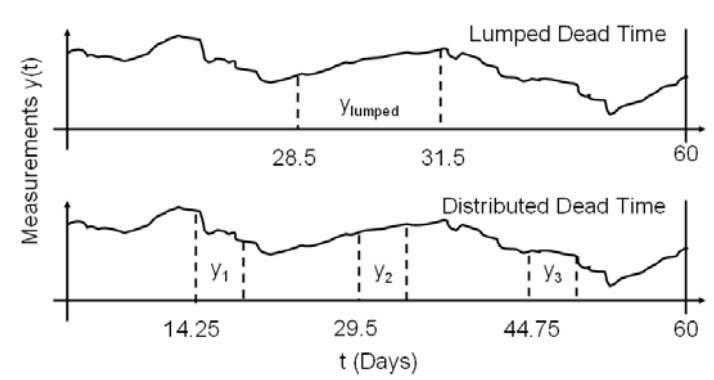

Figure 3. 3-day measurement example with lumped and distributed dead time around the center.

Figure 4. Fractional frequency uncertainty due to dead time in a 60 day evaluation interval (live time around the center).

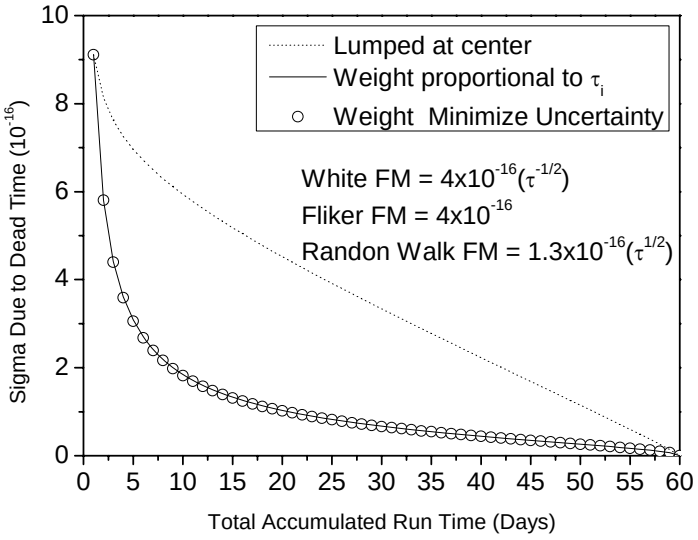

Since usually live measurements are centered in the middle of the reporting interval for the evaluation of a primary frequency standard, we compared the uncertainty due to lumped dead time centered at the 60 day interval and the distributed case of each 1 day live time distributed symmetrically with same dead time from the end and in betweens along the reporting interval. A 3-day measurement example is shown in Figure 3. The results are shown in Figure 4. The dotted line is for the lumped case, the solid line is for the distributed case with weights proportional to each separate live measurement interval. The circle points are for the distributed case with weight optimized to minimize the uncertainty. Weight optimization does

not reduce the uncertainty appreciably for the considered mixed noise type. This means that weight proportional to the interval is nearly optimum in practical applications. We should note that the difference between the lumped and distributed cases is appreciable and shows up to a 5 times decrease in distributed case.

4. Conclusion

We have developed a simple method to calculate the uncertainty of a frequency comparison in the presence of arbitrary configurations of dead time and measurement interval offset. The results show that given a real mixed noise type model, the uncertainty due to dead time for a given total accumulated run time can be reduced to less than one fifth with distributed measurements of frequencies compared to the lumped measurement. In other words, we can reduce the continuous running time of a frequency standard considerably with distributed measurements to obtain the same uncertainty as the lumped measurement case.

References

[1] J. Azoubib, M. Granveaud, and B. Guinot, "Estimation of the Scale Unit Duration of Time Scale," Metrologia, vol. 13, pp. 87-93, 1977.

[2] R. J. Douglas and J. -S. Boulanger, "Standard Uncertainty for Average Frequency Traceability," Proc. 11th European Frequency Time and Forum, pp. 345-349, 1997.

[3] R. J. Douglas and J. -S. Boulanger, "Local Oscillator Requirements for Timekeeping in the $10^{-14}\ \tau^{-1/2}$ Era," Proc. 1992 IEEE Int. Frequency Control Symposium, pp. 6-26, 1992.

[4] R. J. Douglas, J. -S. Boulanger and C. Jacques, "Accuracy Metrics for Judging Time Scale Algorithms," Proc. 25th Precise Time and Time Interval Meeting, pp 249-266, 1993.

[5] D. Morris, R. J. Douglas, and J. –S. Boulanger, "The Role of the Hydrogen Maser Frequency Transfer from Cesium Fountains," Jpn. J. Appl. Phys 33, pp 1659-1668.

[6] R. J. Douglas and J. -S. Boulanger, "Frequency Control of Hydrogen Masers Using High Accuracy Calibration," Proc. 1994 IEEE Int. Frequency Control Symposium, pp.695-708, 1994.

[7] R. J. Douglas and J. -S. Boulanger, "Mettafitting: Weight Optimization for Least-Square Fitting of PTTI Data," Proc. 26th Precise Time and Time Interval Meeting, pp 347-360, 1994.

[8] T. E. Parker, D. A. Howe and M. Weiss, "Accurate Frequency Comparison at the 1×10^{-15} Level," Proc. 1998 IEEE Int. Frequency Control Symposium, pp. 265-272, 1998.

[9] N. J. Kasdin and T. Walter, "Discrete Simulation of Power Law Noise," Proc. 1992 IEEE Int. Frequency Control Symposium, pp. 274-283, 1992.

[10] C. A. Greenhall, "FFT-Based Method for Simulating Flicker FM," Proc. 34th Precise Time and Time Interval Meeting, pp 481-489, 2002.

S. No.

Table of Contents

14. Optical Frequency Synthesis with a DBR Diode Laser Injection-Locked by Optical Frequency Comb
Sang Eon Park, Eok Bong Kim, Young-Ho Park, Dae-Su Yee, Taeg Yong Kwon, Chang Yong Park, Han Seb Moon and Tai Hyun Yoon

15. Performance Analysis Of an Internet Based UTC (SG) Dissemination System
Liu YanYing

16. Precise Estimation Of High-Speed Network Time-Transfer.
Tsukasa Iwama, Akihiro Kaneko, Akihiko Machizawa and Hiroshi Toriyama

17. Simple Time And Frequency Dissemination Method Using Optical Fiber Network
Masaki Amemiya, Michito Imae, Yasuhisa Fujii, Tomonari Suzuyama, Shin-Ichi Ohshima And Masaaki Susumu

18. Status Report Of Time & Frequency Activities At NMIJ/AIST
Shin-ichi Ohshima

19. Status Report of Time and Frequency Activities in NML–SIRIM, Malaysia
Dr. M. Nasir Z. Abidin, A. Sahar Omar, A. Rashid Z. Abidin and Md. Nor Md. Chik

20. Status Report Of Time And Frequency Activities At The Vietnam Metrology Institute
Nguyen Bang

21. Status Report on Time and Frequency Activities at KRISS
Taeg Yong Kwon, Dai-Hyuk Yu, Sang Eon Park, SooHeyong Lee, Sung Hoon Yang, Chang Bok Lee, Young Kyu Lee, Seung Woo Lee, Chang Yong Park, Won-Kyu Lee,and Ho Seong Lee

22. Status Report on Time and Frequency Standard Activities at ITDI
Manuel M. Ruiz

23. Time And Frequency Activities at the National Institute of Information and Communications Technology (NICT)
Mizuhiko Hosokawa, Kuniyasu Imamura, Yasuhiro Koyama, Hiroshi Toriyama, and Shin'ichi Hama

24. Time Management System of QZSS
Shin'ichi Hama, Yasuhiro Takahashi, Jun Amagai, Miho Fujieda, and Kazuhiro Kimura

25. Two-Way Satellite Time and Frequency Transfer with Long Baseline
Miho Fujieda , Tadahiro Gotoh, Masanori Aida, Hideo Maeno and Jun Amagai

26. Two-way Satellite Time and Frequency Transfer using a Pair of Pseudo Random Noises
Jun Amagai

27. TWSTFT Network Status and Plans in the Pacific-Rim Region
Hideo Maeno, Miho Fujieda, Masanori Aida, Yoshiyuki Shimizu, Lam Quoc Tung, Ryo Tabichi, and Mizuhiko Hosokawa

28. Uncertainty of a frequency comparison when we use more than one real measurements
Dai Hyuk Yu, Taeg Yong Kwon, Ho Seong Lee, Marc Weiss, and Thomas E. Parker

S. No.

Table of Contents

14. Optical Frequency Synthesis with a DBR Diode Laser Injection-Locked by Optical Frequency Comb
Sang Eon Park, Eok Bong Kim, Young-Ho Park, Dae-Su Yee, Taeg Yong Kwon, Chang Yong Park, Han Seb Moon and Tai Hyun Yoon

15. Performance Analysis Of an Internet Based UTC (SG) Dissemination System
Liu YanYing

16. Precise Estimation Of High-Speed Network Time-Transfer.
Tsukasa Iwama, Akihiro Kaneko, Akihiko Machizawa and Hiroshi Toriyama

17. Simple Time And Frequency Dissemination Method Using Optical Fiber Network
Masaki Amemiya, Michito Imae, Yasuhisa Fujii, Tomonari Suzuyama, Shin-Ichi Ohshima And Masaaki Susumu

18. Status Report Of Time & Frequency Activities At NMIJ/AIST
Shin-ichi Ohshima

19. Status Report of Time and Frequency Activities in NML–SIRIM, Malaysia
Dr. M. Nasir Z. Abidin, A. Sahar Omar, A. Rashid Z. Abidin and Md. Nor Md. Chik

20. Status Report Of Time And Frequency Activities At The Vietnam Metrology Institute
Nguyen Bang

21. Status Report on Time and Frequency Activities at KRISS
Taeg Yong Kwon, Dai-Hyuk Yu, Sang Eon Park, SooHeyong Lee, Sung Hoon Yang, Chang Bok Lee, Young Kyu Lee, Seung Woo Lee, Chang Yong Park, Won-Kyu Lee,and Ho Seong Lee

22. Status Report on Time and Frequency Standard Activities at ITDI
Manuel M. Ruiz

23. Time And Frequency Activities at the National Institute of Information and Communications Technology (NICT)
Mizuhiko Hosokawa, Kuniyasu Imamura, Yasuhiro Koyama, Hiroshi Toriyama, and Shin'ichi Hama

24. Time Management System of QZSS
Shin'ichi Hama, Yasuhiro Takahashi, Jun Amagai, Miho Fujieda, and Kazuhiro Kimura

25. Two-Way Satellite Time and Frequency Transfer with Long Baseline
Miho Fujieda , Tadahiro Gotoh, Masanori Aida, Hideo Maeno and Jun Amagai

26. Two-way Satellite Time and Frequency Transfer using a Pair of Pseudo Random Noises
Jun Amagai

27. TWSTFT Network Status and Plans in the Pacific-Rim Region
Hideo Maeno, Miho Fujieda, Masanori Aida, Yoshiyuki Shimizu, Lam Quoc Tung, Ryo Tabichi, and Mizuhiko Hosokawa

28. Uncertainty of a frequency comparison when we use more than one real measurements
Dai Hyuk Yu, Taeg Yong Kwon, Ho Seong Lee, Marc Weiss, and Thomas E. Parker

Preface

Asia Pacific Workshop on Time Frequency (ATF) is an important event for time and frequency community of Asia Pacific Region in the sense that during this event, experts in this field gather to present the related research activities, report the achievement of the respective countries and discuss the common issues. First timeATF2006 was held in New Delhi, India during December 11-13, 2006. It was quite well attended by the participants of countries of Asia Pacific region. More than 60 papers were presented in this workshop. These include seven invited talks in different aspects of time and frequency by the international experts in the related topics. Metrology society of India published a special issue on Time Frequency Metrology of its journal MAPAN covering most of the invited talks. This issue was released during this event and was distributed to all participants. A copy of this issue was also sent to other timing institutes of the world. In addition to this effort, a proceedings of ATF2006 in the form of a CD is being brought out. This proceedings contains 29 full papers.

I take this opportunity to express my heart-felt thanks to all the authors who put their best effort for submission of full papers. I am grateful to the members of SOC of ATF2006 for their valuable guidance not only in conducting ATF2006 but also for bringing out this CD. I am also thankful to Dr. Ashok Kumar of NPLI and his team for the efficient production of the CD.

P.Banerjee
Convenor, ATF2006